

University of Nottingham
UK | CHINA | MALAYSIA

Faculty of Medicine and Health Sciences
School of Medicine

ZEB1 Signalling in Endothelial Cell Heterogeneity

Joseph Louis Horder BSc, MRes

Thesis submitted to the University of Nottingham for the degree of Doctor of Philosophy (PhD)

March 2025

Signed:

Abstract

Endothelial cells (ECs) are at the core of vascular homeostasis, enabling angiogenesis, immune cell trafficking and barrier function. Zinc-finger E-box binding protein 1 (ZEB1) has recently emerged as a central regulator of EC plasticity, particularly through its roles in endothelial-to-mesenchymal transition (EndoMT) and vessel remodelling. Here, we test the hypothesis that ZEB1 expression dynamically modulates EC heterogeneity and specialisation during both developmental and pathological angiogenesis. Using siRNA knockdown (KD) and chromatin immunoprecipitation (ChIP)-seq in human umbilical vein endothelial cells (HUVECs), we show that ZEB1 broadly influences genes controlling cell adhesion, immune responses and tip-cell identity and cooperates with ETS and AP-1 transcription factors. Analyses of publicly available scRNA-seq datasets revealed ZEB1 enrichment in specialised EC subpopulations across multiple tissues, including venous-capillary ECs in the spleen, tip cells in the retina, tumour-associated ECs and floor ECs of the subcapsular sinus of the lymph node. Further analysis of myocardial infarction scRNA-seq data demonstrated that ZEB1 contributes to a partial EndoMT phenotype, wherein ECs retain some endothelial traits while acquiring mesenchymal characteristics. A text-mining approach further uncovered a proposed ZEB1 regulatory network in EndoMT. Finally, we demonstrate that adult induced ZEB1 knockout in adult retina ECs does not alter vascular area or number of ECs. Collectively, these findings position ZEB1 as a context-dependent modulator of ECs.

Authors Declaration

I declare that the work presented in this thesis was carried out during the registered period and granted extension at the University of Nottingham in accordance with the University Regulations and Code of Practice for Research Degree Programs. I confirm the results generated have not been submitted elsewhere for any other academic award. Except where acknowledged I confirm that the results demonstrated in this thesis "*ZEB1* Signalling in Endothelial Cell Heterogeneity" are my own.

Signed: 

Acknowledgements

I first want to thank my supervisory team Andy, Nigel, Alan and John for their strong support throughout this PhD. Each have gone above and beyond to give me every opportunity and have inspired me to pursue a career in science, for which I am truly grateful. I would also like to thank colleagues I have worked with over the years, including Nada, Kathryn, Zarah, Charles, George, Eva and Ashia for the laughs and conversation, both science based and not. I would like to acknowledge my partner, Vicky, for her unparalleled support throughout my entire University career. Most importantly I would like to thank Vicky for giving us our beautiful baby boy Oscar in my final year of the PhD. Although we had a difficult start as a family, we have managed to come through this year and be all the stronger for it. This thesis is for my son Oscar, his little smile kept me motivated throughout this past year.

Conferences and Publications

Conferences and awards

Gordon Research Conference – Understanding Endothelial Cell Diversity: Regulation and Regenerative Potential. Barcelona (2022). Poster: "RNA-seq to identify putative mechanistic differences and similarities between HUVECs and HDLECs"

Joint British Microvascular and Vascular Biology Society (BMVBS) and German Society for Microcirculation and Vascular Biology (GfMVB). Berlin (2022). Poster: "RNA-seq to identify putative mechanistic differences and similarities between HUVECs and HDLECs"

74th Annual Meeting of the British Microcirculation and Vascular Biology Society. Bristol (2024). Poster: "A data-mining approach to identify potential contributors to EndoMT" – **AWARD –** Best poster.

Other smaller conferences, workshops and seminars were attended, but not recorded here.

Publications

Tabrizi, Z.B. et al. (2021) 'Transcription Factor Control of Lymphatic Quiescence and Maturation of Lymphatic Neovessels in Development and Physiology', Frontiers in Physiology, 12. Available at: https://doi.org/10.3389/fphys.2021.672987.

Pinel, G.D. et al. (2022) 'Endothelial Cell RNA-Seq Data: Differential Expression and Functional Enrichment Analyses to Study Phenotypic Switching', in Angiogenesis. Humana, New York, NY, pp. 369–426. Available at: https://doi.org/10.1007/978-1-0716-2059-5_29.

Contributions to publications in writing

Other groups

"Pre-α-inhibitor and a novel polymer supports feeder-free reversion and expansion of naïve-like human pluripotent stem cells with increased efficiency" – contributed clustering analysis of 100's of RNA-seq and scRNA-seq datasets

"Effects of genes manipulation on vascular remodeling during adipose tissue expansion – a systematic review" – reviewed ~250 abstracts for consideration in the study

"BRD2 and BRD4 regulate transcriptional and metabolic adaptation to hypoxia to support tumour cell survival in triple-negative breast cancer (TNBC)" – Bulk RNA-seq of several conditions and knockdowns. ChIP-seq analysis of multiple histone and transcription factor data

Our lab group

"Modification of VE-cadherin signalling by ZEB1 in Lymphatic Endothelial Cells" – Bulk RNA-seq analysis

"Loss of Endothelial ZEB1 enhances neovascularisation but not inflammation during choroidal neovascularisation" – Bulk RNA-seq and scRNA-seq analyses

"A data-mining approach to identify potential contributors to EndoMT" – **First author**

Table of Contents

Abstract 2

Authors Declaration 3

Acknowledgements 4

Conferences and Publications 5

List of Figures 14

List of Abbreviations 18

Chapter 1: Introduction 19

1.1 Vasculature 19

1.1.1 Vascular structure and organisation 19

1.1.2 Functional roles of the vasculature 20

1.1.3 Vasculogenesis 22

1.1.4 Angiogenesis 25

1.2 Developmental angiogenesis 32

1.3 Pathological angiogenesis 33

1.4 Reparative angiogenesis 35

1.5 Endothelial-Mesenchymal Transition (EndoMT) 37

1.6 Zinc-finger E-box binding protein 1 (ZEB1) 42

1.7 Hypothesis and aims 46

Chapter 2: Materials and Methods 48

2.1 Methods to chapter 3 - ZEB1 knockdown via siRNA in HUVECs revealed a modulation of adhesion, angiogenesis and inflammation related processes and uncovered a predicted ZEB1 regulatory network 48

2.1.1 RNA-seq data analyses 49

2.1.2 Obtaining sets of genes of interest for cross-referencing with DEGs 51

2.2 Methods to chapter 4 - Comprehensive and unbiased analysis of ZEB1 binding patterns in HUVECs via ChIP-seq 51

2.2.1 Preprocessing of ZEB1 ChIP-seq data 51

2.2.2 ZEB1 ChIP-seq data replicate handling 53

2.2.3 Peak annotation and genomic distribution 53

2.2.4 Visualisation of signal enrichment 53

2.2.5 Motif analysis of ChIP-seq peaks 54

2.2.6 Functional enrichment analyses 54

2.2.7 Preprocessing of publicly available ERG HUVEC ChIP-seq data 55

2.2.8 Preprocessing of publicly available ZEB1 TNBC ChIP-seq data 55

2.2.9 Preprocessing of publicly available H3K4me1, H3K4me3 and H3K27ac HUVEC ChIP-seq data 56

2.2.10 Overlapping peaks analysis 56

2.2.11 Transcription factor cross reference 57

2.2.12 Overlap of RNA-seq and ChIP-seq data 57

2.3 Methods to chapter 5 - Analysis of publicly available endothelial cell scRNA-seq datasets revealed Zeb1 to be enriched in specialised endothelial subpopulations driving proliferative and immunoregulatory programs across diverse tissues 57

2.3.1 Publicly available single-cell transcriptome atlas of murine endothelial cells data processing 59

2.3.2 Publicly available P6 and P15 retina endothelial cell scRNA-seq dataset processing 59

2.3.3 Publicly available choroidal neovascularisation (CNV) endothelial cell scRNA-seq dataset processing 61

2.3.4 Publicly available mouse lung tumour endothelial cell scRNA-seq dataset processing 61

2.3.5 Publicly available human lymph node endothelial cell scRNA-seq dataset processing 62

2.4 Methods to chapter 6 - A combined scRNA-seq and text-mining approach elucidated putative functions of Zeb1 in partial EndoMT 62

2.4.1 Gathering raw sequencing data 62

2.4.2 Aligning raw sequencing data 63

2.4.3 scRNA-seq data preprocessing 63

2.4.4 Subsetting ECs from the dataset 64

2.4.5 Identifying EC phenotypes 64

2.4.6 Comparison of EndoMT signature with AlZaim et al (2024) 65

2.4.9 Trajectory analysis 66

2.4.10 ZEB1 expression analyses 67

2.4.11 Text mining 67

2.4.12 Network analyses 69

2.4.13 Comparison of text mining with bulk RNA-seq EndoMT publication 69

2.4.14 Text-mining functional enrichment analysis 69

2.5 Methods to chapter 7 - Adult inducible knockout of Zeb1 does not alter mouse retinal vascular area or endothelial cell number 70

2.5.1 Endothelial cell isolation from lung tissue 70

2.5.2 RNA extraction 71

2.5.3 Retina dissection 72

2.5.4 Retina antibody staining 72

2.5.5 Retina imaging 73

2.5.6 Retina image analysis 73

Chapter 3: ZEB1 knockdown via siRNA in HUVECs revealed a modulation of adhesion, angiogenesis and inflammation related processes and uncovered a predicted ZEB1 regulatory network 75

3.1 Introduction 75

3.2 Hypothesis and aim 77

3.3 Results 77

3.3.1 ZEB1 KD in HUVECs resulted in 296 differentially expressed genes including canonical tip endothelial cell and endothelial-to-mesenchymal transition markers .. 77

3.3.2 Network analysis of ZEB1 knockdown differentially expressed genes predicted a direct ZEB1 regulatory network including CXCR4 82

3.4 Discussion 85

Chapter 4: Comprehensive and unbiased analysis of ZEB1 binding patterns in HUVECs via ChIP-seq 88

4.1 Introduction 88

4.2 Hypothesis and aim 91

4.3 Results 92

4.3.1 ZEB1 ChIP-seq in HUVECs identified 12,577 significant peaks 77.7% of which were annotated to transcript promoter regions 92

4.3.2 Gene biotype assignment, TF identification and functional enrichment analyses of ZEB1 bound regions in HUVECs revealed a broad potential influence of ZEB1 on HUVEC behaviour 94

4.3.3 Motif analysis of peak summits of ZEB1 bound regions in HUVECs displayed an enrichment for ETS and AP-1 family binding motifs 97

4.3.4 A full genome scan for the presence of the ZEB1 motif and ZEB1 peak width analysis suggested our method of motif enrichment analysis may not be suitable to determine direct/indirect ZEB1 binding in our dataset 101

4.3.5 Comparison of ZEB1 HUVEC ChIP-seq with a publicly available ERG HUVEC ChIP-seq dataset revealed 47.4% of ZEB1 peaks to overlap with ERG peaks 103

4.3.6 Functional enrichment analysis of overlapping and ZEB1/ERG specific peaks identified a shared role of ZEB1 and ERG in binding to genes that regulate the cell cycle 106

4.3.7 Motif enrichment analysis of overlapping peaks did not show enrichment for the ZEB1 motif 109

4.3.8 Motif enrichment in ZEB1 unique peaks reveals an enrichment of the ZEB1 motif and potential binding redundancy with other TF motifs 110

4.3.9 Comparison of ZEB1 HUVEC ChIP-seq with a publicly available ZEB1 triple-negative breast cancer cell model ChIP-seq dataset identified 1685 overlapping peak regions related to junction, cell-matrix adhesion and cell polarity 112

4.3.10 Quality control and preprocessing of publicly available ENCODE data for H3K4me1, H3K4me3 and H3K27ac histone marks 115

4.3.11 ZEB1 binding overlaps primarily with active histone marks 116

4.3.12 ZEB1 direct binding associated primarily with promoters, with some overlap at enhancers 119

4.3.13 Co-binding of ZEB1 and ERG occurs primarily in active promoter regions 119

4.3.14 The top five significantly enriched ZEB1 ChIP-seq peaks in HUVECs annotated to REXO4, KCTD10, GAS8, LOC105372273 and ISY1-RAB43 are related to immunoregulation, angiogenesis and splicing 120

4.3.15 ZEB1 directly binds to endothelial and mesenchymal cell marker genes in HUVECs that are known to be regulated in EndoMT 123

4.3.16 ZEB1 directly binds to markers of proliferation and EC activation in HUVECs125

4.3.17 Integration of ZEB1 KD RNA-seq data in HUVECs revealed direct regulation by ZEB1 of five TFs, a histone deacetylase and other genes implicated in EndoMT and angiogenic processes 126

4.4 Discussion 129

Chapter 5: Analysis of publicly available endothelial cell scRNA-seq datasets revealed Zeb1 to be enriched in specialised endothelial subpopulations driving proliferative and immunoregulatory programs across diverse tissues 132

5.1 Introduction 132

5.2 Hypothesis and aim 133

5.3 Results 133

5.3.1 Zeb1 expression analysis across a scRNA-seq atlas of healthy murine tissue revealed Zeb1 to be preferentially expressed in spleen venous-capillary ECs. 133

5.3.2 Zeb1 expression was not significantly regulated upon quiescence entry in developing mouse retina vasculature 135

5.3.3 Zeb1 is upregulated in choroidal neovascularisation lesion endothelial cells and is predicted to orchestrate a proangiogenic transcriptional program 138

5.3.4 Zeb1 is enriched in tumour tip cells of a mouse lewis lung carcinoma model . 144

5.3.5 ZEB1 is upregulated in subcapsular sinus floor lymphatic endothelial cells of the lymph node and is implicated in immune regulation 148

5.4 Discussion 151

Chapter 6: A combined scRNA-seq and text-mining approach elucidated putative functions of Zeb1 in partial EndoMT 158

6.1 Introduction 158

6.2 Hypothesis and aim 162

6.3 Results 162

6.3.1 In-silico isolation of Cdh5+/Pecam1+ cells identified sub-populations expressing pericyte, mesenchymal and immune related genes 162

6.3.2 Expression analysis of EndoMT-related genes derived from literature identified EndoMT-like cell clusters 167

6.3.3 Generation of endothelial, mesenchymal and EndoMT scores identified venous ECs to be associated with an increased mesenchymal signature 169

6.3.4 Expression analysis of EndoMT-related genes across days post myocardial infarction found days 1-7 to upregulate EndoMT markers 171

6.3.5 Transcription factor analysis identified Zeb1 TF activity to be increased in EC+/MES+ cells and at days 1-7 post MI 174

6.3.6 Trajectory analysis suggests venous ECs to be a partial state along the EndoMT axis and did not identify Zeb1 expression to significantly change through EndoMT 177

6.3.7 Expression analysis of Zeb1 revealed angiogenic, proliferative and mesenchymal-like EC phenotypes show an increased proportion of cells to express Zeb1 compared to the most EC-like phenotype without a change in expression levels..... 180

6.3.8 In-silico KO of Zeb1 revealed perturbation of EndoMT-related genes and processes 182

6.3.9 Text-mining and network analysis of 421 abstracts identified 623 genes/proteins related to EndoMT and 22 core network hubs 184

6.3.10 Network analysis of 623 text-mined proteins revealed four highly connected clusters providing insight into protein network linked to specific processes..... 186

6.3.11 Text-mined network identified a predicted core Zeb1 interactome of EndoMT-related genes that contains 21 of 22 network hub proteins. 188

6.3.12 Cross-referencing text-mining with a publicly available bulk RNA-seq EndoMT dataset in different EC models revealed a central EndoMT core signature. 189

6.3.13 Comparison of text-mining extracted EndoMT related genes with HUVEC ZEB1 KD DEGs and ZEB1 HUVEC ChIP-seq peaks revealed a shared set of 16 genes..... 191

6.3.14 A publication related to EndoMT released after the text-mining analysis included results predicted by text-mining 192

6.4 Discussion..... 193

Chapter 7: Adult inducible knockout of Zeb1 does not alter mouse retinal vascular area or endothelial cell number 197

7.1 Introduction 197

7.2 Hypothesis and aim..... 199

7.3 Results 200

7.3.1 Adult induced Zeb1 KO via the iECKO model resulted in significant reduction of Zeb1 mRNA expression in murine lung Cd31^{+} cells specifically – results obtained by Kathryn Green 200

7.3.2 Adult induced Zeb1 KO did not significantly impact the vascular area or number of endothelial cell nuclei in adult mouse retina..... 202

7.4 Discussion 204

Chapter 8: Discussion..... 209

Appendix 219

Appendix 1. Supplementary methods to chapter 3 - ZEB1 knockdown via siRNA in HUVECs revealed a modulation of adhesion, angiogenesis and inflammation related processes and uncovered a predicted ZEB1 regulatory network 219

Appendix 1.1 Cell culture 219
Appendix 1.2 siRNA knockdown of ZEB1 220
Appendix 1.3 RNA extraction and sequencing 220
Appendix 2. Supplementary methods to chapter 4 - Comprehensive and unbiased analysis of ZEB1 binding patterns in HUVECs via ChIP-seq 220
Appendix 2.1 Cell culture 220
Appendix 2.2 ChIP (Chromatin-immunoprecipitation)-seq 221
Appendix 3. Supplementary methods to chapter 7 - Adult inducible knockout of Zeb1 does not alter mouse retinal vascular area or endothelial cell number 223
Appendix 3.1 Inducible endothelial cell knockout (iECKO) mouse model 223
Appendix 3.2 Tamoxifen-induced endothelial ZEB1 knockout (iECKO) in adult mice 224
Appendix 3.3 DNAse treatment 225
Appendix 3.4 cDNA synthesis 225
Appendix 3.5 Digital droplet PCR (ddPCR) 225
Appendix 3.6 Digital droplet PCR (ddPCR) data analysis 226
Appendix 4. Supplementary figures 226
Other works and Team Science 241
COVID-19 (and other) impact statements 245
References 246

List of Figures

Figure 1. VEGF, Notch and TGFB/BMP signalling mechanisms interact to maintain tip and stalk endothelial cell phenotypes in the angiogenic sprout. Figure from Li et al., (2019). 31

Figure 2. Overview of the scRNA-seq pipelines used for the analysis of publicly available datasets. 58

Table 1. Endothelial cell phenotype markers. 65

Table 2. Gene signatures for EndoMT derived from literature, EndoMT signature used by AlZaim et al., (2024) and endothelial-like. 66

Figure 3.1. ZEB1 knockdown in HUVECs resulted in 296 significantly differentially expressed genes including downregulation of tip cell markers UNC5B and CXCR4. 79

Figure 3.2. Functional enrichment analyses of DEGs identified pathways associated with adhesion, vasculature development and inflammation. 82

Figure 3.3. Network analysis of DEGs identified highly interconnected hub genes and a putative ZEB1 regulatory network. 84

Figure 4.1. Quality control of HUVEC ZEB1 ChIP-seq data identifies the optimal replicates for downstream analysis and an enrichment of ZEB1 ChIP-seq signal at peak regions compared to IgG control 93

Figure 4.2. Assignment of genes to peaks and binding locations of ZEB1 identified most ZEB1-bound regions to reside in promoter regions within 1kb of the TSS of protein-coding transcripts 95

Figure 4.3. Functional enrichment analysis identified a broad range of functions of ZEB1 bound genes and motif analysis of 200bp regions centered on ZEB1 ChIP-seq peak summits identified significant enrichment of ETS and AP-1 family binding motifs. 98

Figure 4.4. Distribution of ZEB1 HUVEC ChIP-seq peak widths identified a mean peak width of 1904 bp suggesting multiple ZEB1 binding sites in a given region. 102

Figure 4.5. Reanalysis of a HUVEC ERG ChIP-seq dataset revealed 47.4% of ZEB1 summit regions to overlap with ERG summit regions in HUVECs. 105

Figure 4.6. Functional enrichment analyses against the HALLMARKS, KEGG and GO Biological Process databases for ZEB1 and ERG overlapping, ZEB1 unique and ERG unique bound regions in HUVECs identified shared and individual cellular processes. 108

Figure 4.7. Motif enrichment analysis of overlapping ZEB1 and ERG bound regions did not identify the ZEB1 motif to be significantly enriched but the motif is still present within the overlapping peaks and known motif and De novo motif enrichment analysis of ZEB1 uniquely bound regions revealed a significantly enriched sequence motif that matched to the known ZEB1 binding motif and also matched highly to other TF binding motifs including SNAI1. 111

Figure 4.8. Reanalysis of a ZEB1 ChIP-seq dataset in MDA-MB-231 cells as a model of triple-negative breast cancer identified 13.4% of ZEB1 HUVEC binding sites overlapped with ZEB1 TNBC binding sites. 114

Figure 4.9. Reanalysis of histone marker peak datasets identified the majority of ZEB1 bound regions to reside within active promoter regions in HUVECs. 118

Figure 4.10. Integrated analysis of ZEB1 ChIP-seq and ZEB1 knockdown RNA-seq in HUVECs defined direct and indirect regulation by ZEB1. 127

Figure 5.1. scRNA-seq analysis of a publicly available EC atlas identified ZEB1 to be preferentially expressed in capillary-venous ECs within the spleen 134

Figure 5.2. scRNA-seq analysis of a publicly available retina EC dataset for p6 and p15 mice identified increased expression of Zeb1 in tip ECs. 137

Figure 5.3. scRNA-seq analysis of a publicly available murine EC choroidal neovascularization (CNV) dataset identified increased expression of Zeb1 in lesion ECs, particularly tip ECs. 139

Figure 5.4. In-silico KO of Zeb1 in CNV lesion ECs revealed differential regulation of AP-1 factors. 140

Figure 5.5. In-silico KO of Zeb1 in CNV lesion ECs predicted perturbation of 28 transcription factors, 20 of which were differentially expressed between lesion and non-lesion ECs and 6 were upregulated in tip cells compared to other EC phenotypes in the lesion. 142

Figure 5.6. Zeb1 is dynamically regulated across the cell cycle in CNV ECs. 143

Figure 5.7. scRNA-seq analysis of a publicly available murine lewis lung carcinoma dataset identified increased expression of Zeb1 tumour ECs. 145

Figure 5.8. In-silico KO of Zeb1 in tumour tip ECs revealed differential regulation of genes related to angiogenesis, cell cycle, matrix remodelling and EC identity. 147

Figure 5.9. scRNA-seq analysis of a publicly available human lymph node LEC dataset identified ZEB1 expression to be enriched in the floor LECs of the subcapsular sinus. 150

Figure 6.1. Reanalysis of a publicly available murine myocardial infarction scRNA-seq dataset identified 13 clusters of Cdh5+/Pecam1+ cells. 164

Figure 6.2. Annotation of Cdh5+/Pecam1+ cell clusters to EC phenotypes based on canonical marker genes. 167

Figure 6.3. Identification of EndoMT-like clusters based on an EndoMT signature derived from literature and comparison with a published EndoMT signature identified increased EndoMT-like expression in venous ECs. 169

Figure 6.4. Venous endothelial cells display endothelial and mesenchymal positive scores. 171

Figure 6.5. Days 1-7 post myocardial infarction (MI) exhibit increased expression of EndoMT-related genes. 173

Figure 6.6. Zeb1 transcriptional activity is increased in venous ECs, proliferating ECs, EC+/MES+ ECs and at days 1-7 post myocardial infarction (MI)..... 175

Figure 6.7. Trajectory analysis suggests venous ECs to be a partial state along the EndoMT axis at days 1-7 post myocardial infarction (MI). 179

Figure 6.8. The percent of cells expressing Zeb1 is increased in EC+/MES+ cells and in angiogenic ECs. 181

Figure 6.9. EndoMT-related genes were predicted to be perturbed in response to in-silico KO of Zeb1. 184

Figure 6.10. Network analysis of genes/proteins identified from text-mining of EndoMT-related abstracts retrieved from PubMed Central identified highly interconnected hub nodes that may modulate core EndoMT mechanisms. 185

Figure 6.11. MCODE analysis of the text-mined network identified 4 sub-clusters corresponding to specific processes. 188

Figure 6.12. Network of direct Zeb1 interactors involved 21 of 22 hub genes. 189

Figure 6.13. 108 genes overlap between text-mined EndoMT-related genes and DEGs identified from an EndoMT RNA-seq public dataset of 3 in-vitro EC models. 191

Figure 6.14. 16 genes overlap between text-mined EndoMT related genes, DEGs identified by ZEB1 KD RNA-seq analyses in chapter 3 and enriched peaks in ZEB1 HUVEC ChIP-seq in chapter 4..... 192

Figure 7.1. Significant reduction of ZEB1 mRNA expression in $CD31^+$ $ZEB1^{iECKO}$ cells. Data was analysed and figure created by Kathryn Green. 201

Figure 7.2. $CD31^+$ area, ERG nuclei counts and ERG nuclei per mm^2 of $CD31^+$ area of the adult mouse retina vasculature were not significantly altered between Cre- and Cre+ mice. 204

Figure 7.3. $CD31^+$ area of the superficial, intermediate and deep plexuses of the adult mouse retina vasculature were not significantly altered between Cre- and Cre+ mice. . 206

List of Abbreviations

Abbreviation	Description
ChIP-seq	Chromatin immunoprecipitation sequencing
CNV	Choroidal Neovascularisation
DEG(s)	Differentially Expressed Gene(s)
DR	Differentially regulated
EC(s)	Endothelial Cell(s)
EMT	Epithelial-Mesenchymal Transition
EndoMT	Endothelial-Mesenchymal Transition
GOBP	Gene Ontology Biological Process
HDLEC(s)	Human Dermal Lymphatic Endothelial Cell(s)
HUVEC(s)	Human Umbilical Vein Endothelial Cell(s)
iECKO	Inducible Endothelial Cell Specific Knockout
IF	Immunofluorescence
KD	Knockdown
KEGG	Kyoto Encyclopedia of Genes and Genomes
KO	Knockout
LEC(s)	Lymphatic Endothelial Cell(s)
log2FC	Log2 Fold Change
MI	Myocardial Infarction
NER	Named Entity Recognition
padj	Benjamini-Hochberg adjusted p-value
PPI	Protein-Protein Interaction
RNA	Ribonucleic acid
RNA-seq	RNA sequencing
scRNA-seq	Single cell RNA sequencing
siRNA	Short interfering RNA
TF(s)	Transcription factor(s)
t-SNE	t-distributed stochastic neighbour embedding
UMAP	Uniform Manifold Approximation and Projection

Chapter 1: Introduction

1.1 Vasculature

1.1.1 Vascular structure and organisation

The vascular system is composed of a highly specialised network of vessels that perform critical functions in delivering oxygen, nutrients, hormones and immune cells throughout the body, while also facilitating the removal of metabolic waste products (Aird, 2007; Potente, Gerhardt and Carmeliet, 2011). This system is typically organised into a hierarchy, in which a network of capillaries, venules, arterioles, veins and arteries form (Adams and Alitalo, 2007). At its core, this network relies on endothelial cells (ECs) that form a monolayer on the luminal surface of all blood (and lymphatic) vessels to orchestrate vascular homeostasis, regulate inflammation and maintain a selective barrier between the bloodstream and surrounding tissues (Brutsaert, 2003; Cahill and Redmond, 2016; Trimm and Red-Horse, 2023). The ECs display remarkable phenotypic heterogeneity and functional specialisation depending on the vessel type and organ location, making them central to both normal physiology and various pathophysiological states (Aird, 2012). The monolayer of typically flattened, polygonal cells attached to a thin basement membrane comprised primarily collagen IV, laminins and proteoglycans which provide structural support and also influence EC behaviour (Yurchenco, 2011). Cell-cell junctions such as tight junctions, adherens junctions and gap junctions mediate inter-endothelial adhesion, permeability and intercellular communication (Wallez and Huber, 2008; Dejana, Tournier-Lasserve and Weinstein, 2009). The luminal surface of endothelial cells is coated with the glycocalyx, a mesh of glycoproteins and proteoglycans involved in mechanotransduction and regulation of vascular permeability (Tarbell and Cancel, 2016). Also attached to the basement

membrane of arteries and veins is a layer of smooth muscle cells (SMCs) which control contraction and dilation of the vessels (Steucke *et al.*, 2015; Thomsen, Routhe and Moos, 2017; Leclech, Natale and Barakat, 2020). Capillaries on the other hand are supported with pericytes, providing stabilisation to the vessel (Bergers and Song, 2005).

1.1.2 Functional roles of the vasculature

The specialised architecture of the endothelium is critical for maintaining homeostasis, regulating vascular tone and modulating immune cell trafficking (Deanfield, Halcox and Rabelink, 2007; Jourde-Chiche *et al.*, 2019; Amersfoort, Eelen and Carmeliet, 2022). At the tissue level, capillaries form dense networks to maximise exchange capacity of oxygen, nutrients and signalling molecules to surrounding tissue (Poole *et al.*, 2013). Part of this process is perfusion and vasomotor tone, which is regulated by the secretion of vasoactive molecules by ECs (Sandoo *et al.*, 2010). These molecules include nitric oxide (NO), prostacyclin and endothelin-1 (Sandoo *et al.*, 2010). NO, synthesised by endothelial nitric oxide synthase (eNOS), is a particularly potent vasodilator that improves local blood flow and oxygen delivery under conditions of increased demand (Förstermann and Sessa, 2012). In contrast, endothelin-1 is a powerful vasoconstrictor (Félétou and Vanhoutte, 2006; Böhm and Pernow, 2007), highlighting the endothelium ability to maintain vascular homeostasis.

Beyond facilitating perfusion, the endothelium provides a selectively permeable barrier that regulates the exchange of solutes, fluids and immune cells between the bloodstream and interstitial tissues (Claesson-Welsh, Dejana and McDonald, 2021). This control of vascular permeability is vital for maintaining fluid balance and tissue homeostasis. In specialised vascular beds, such as those in the blood-brain barrier, endothelial tight junctions markedly restrict permeability, preserving neuronal function by shielding the

central nervous system from potentially harmful circulating factors (Abbott, Rönnbäck and Hansson, 2006). Disruption of the endothelial barrier is implicated in numerous pathological processes including ischaemia and cancer (Rodrigues and Granger, 2015).

The vasculature plays a pivotal role in regulating immune responses. During inflammation, ECs upregulate adhesion molecules such as intercellular adhesion molecule 1 (ICAM1) and vascular cell adhesion molecule 1 (VCAM1) that facilitate leukocyte adhesion and subsequent extravasation into the surrounding tissues (Pober and Sessa, 2007; Muller, 2011). This process is critical for immune surveillance and pathogen clearance. However, dysregulated endothelial activation can lead to chronic inflammation and contribute to the pathophysiology of conditions such as atherosclerosis and rheumatoid arthritis (Kadl and Leitinger, 2005; Castellon and Bogdanova, 2016).

ECs maintain a delicate balance between preventing blood loss (haemostasis) and avoiding unwarranted clot formation (thrombosis). Under physiological conditions, healthy endothelium expresses anticoagulant surface molecules and secretes platelet inhibitors (Aird, 2012). During pathology, dysfunctional ECs can shift to favour regulation of procoagulants, leading to exaggerated intravascular coagulation and fibrinolytic shutdown, inhibiting clot breakdown and can eventually lead to multiple organ failure in sepsis (Madoiwa, 2015). Moreover, aberrant clot formation (as caused by atherosclerosis/atheroma or embolism) within the vessel lumen can trigger pathological events such as myocardial infarction and stroke (Palasubramaniam, Wang and Peter, 2019). Conversely, when vascular integrity is compromised upon injury, the procoagulant regulation by ECs is beneficial, rapidly shifting to a prothrombotic state to prevent bleeding (Yau, Teoh and Verma, 2015), further emphasising the equilibrium that ECs control in maintaining a homeostatic state.

The vasculature contributes to organogenesis and regeneration. During embryonic development, blood vessels guide the spatial patterning of tissues and interact with resident progenitor cells (Adams and Alitalo, 2007). In adult tissues, ECs support regenerative processes by releasing paracrine signals that modulate stem cell niches and promote tissue repair following injury (Mirotsou *et al.*, 2011; Luk *et al.*, 2022). These interactions place ECs at the core of organ-specific microenvironments and functional recovery (De Bock, Cauwenberghs and Carmeliet, 2011).

The vasculature adapts continuously to fulfil the metabolic and function demands of tissues. Angiogenesis, defined as the growth of new blood vessels from pre-existing vasculature is fundamental to processes such as would healing, tissue regeneration and the female reproductive cycle (Carmeliet, 2003; Potente, Gerhardt and Carmeliet, 2011). ECs serve as key mediators of these processes by responding to angiogenic signals, notably vascular endothelial growth factor (VEGF) and migrating to form vascular sprouts (Lamalice, Le Boeuf and Huot, 2007). In pathological contexts, uncontrolled angiogenesis can support tumour growth and metastasis, rendering ECs and angiogenic pathways prime therapeutic targets in cancer (Ferrara and Adamis, 2016).

In order to uncover how the vasculature reacts to a changing microenvironment, understanding how the endothelial cells change behaviour during development is pivotal.

1.1.3 Vasculogenesis

Vasculogenesis is the *de-novo* formation of blood vessels from endothelial progenitor cells (EPCs), also termed angioblasts, primarily occurring during embryonic development (Risau, 1997; Patan, 2004). Unlike angiogenesis, where vessels form by sprouting or remodelling of pre-existing vasculature, vasculogenesis involves the assembly of endothelial

progenitors in regions devoid of pre-existing vessels (Coultas, Chawengsaksophak and Rossant, 2005). Historically, insights into vasculogenesis were gleaned from embryological studies showing blood islands in the yolk sac gave rise to primitive vascular structures, forming what is referred to as the primary/primitive capillary plexus (Flamme, Frölich and Risau, 1997; Carmeliet, 2003).

During embryogenesis, mesodermal progenitors become specified into hemangioblasts, which possess the potential to differentiate into both hematopoietic and endothelial lineages (Choi *et al.*, 1998; Carmeliet, 2003). These hemangioblasts give rise to more committed endothelial precursor cells or angioblasts, which begin expressing vascular endothelial growth factor receptor (VEGFR) family members (Flamme, Frölich and Risau, 1997; Coultas, Chawengsaksophak and Rossant, 2005).

At the molecular level, vascular endothelial growth factor (VEGF) and its receptors (VEGFR1/FLT1 and VEGFR2/FLK1/KDR) are principal drivers of vasculogenesis (Carmeliet, 2000). Indeed, experimental knockout models illustrate that the absence of either VEGF results in severe vascular defects and embryonic lethality (Ferrara, 2004). VEGF ligand-receptor engagement promotes angioblast proliferation, survival and directed migration toward sites where new vascular networks are assembled (Coultas, Chawengsaksophak and Rossant, 2005). Basic fibroblast growth factor (FGF2) also stimulates proliferation and migration of precursor cells, highlighting its importance in blood vessel formation (Yancopoulos *et al.*, 2000). On the transcriptional level, factors such as ETS-related genes including ETS variant transcription factor 2 (ETV2) coordinate the differentiation of mesodermal progenitors into ECs, with ETV2 mutant embryos lacking endothelial cell lineages rendering them nonviable (Ferdous *et al.*, 2009), indicating a fundamental basis of developing vasculature regulated by specific transcription factors (TFs). Other molecules,

including platelet-derived growth factor (PDGF) and angiopoietins, aid in vessel remodelling and the recruitment of pericytes or SMCs for stabilising nascent vascular structures (Risau, 1997; Jain, 2003).

The vasculogenesis process can be concisely described in four steps. First, mesodermal specification in which mesodermal cells are defined into hemangioblasts, bipotent progenitors for both hematopoietic and endothelial lineages (Choi *et al.*, 1998). Following this is angioblast formation, where hemangioblasts further refine towards angioblasts, losing hematopoietic potential (Risau and Flamme, 1995). Next is coalescence and tube formation during which angioblasts migrate, coalesce and form primitive vascular cords, which subsequently undergo lumenisation to yield the initial vascular plexus (Schmidt, Brixius and Bloch, 2007; Rai and Cross, 2014). During this time, ECs differentiate and line the initial vascular tubes and express canonical endothelial markers such as platelet and endothelial cell adhesion molecule (PECAM1/CD31) and VE-cadherin (CD144/CDH5) (Risau and Flamme, 1995). Finally, the primitive plexus matures via pruning, selective expansion and recruitment of pericytes or SMCs, guided by angiopoientin-Tie2 signalling and PDGF-PDGFR interactions (Jain, 2003; Herbert and Stainier, 2011a; Rai and Cross, 2014). Following vasculogenesis, the newly formed primitive vascular plexus undergoes a process of fate specification into arterial and venous vessels (Rai and Cross, 2014). One of the most pivotal regulatory axes involves notch signalling and its downstream effectors hes related family BHLH transcription factor with YRPW motif 1/2 (HEY1/2) which favour the adoption of an arterial phenotype (Zhong *et al.*, 2001). Conversely, lower notch activity by the nuclear receptor subfamily 2 group F member 2 (COUP-TFII) drives ECs towards a venous fate.

While vasculogenesis often refers to the *de-novo* formation of blood vessels during embryogenesis, accumulating evidence over the past three decades has suggested that

vasculogenesis can occur postnatally. The concept arose with the identification of EPCs in adult human peripheral blood, challenging the view that new vessel growth in adults occurred exclusively via angiogenesis (Asahara *et al.*, 1997). However, there has been controversy over the true identification of EPCs, with the initial identification deemed to consist of a mixed population of cells (Urbich and Dimmeler, 2004; Barber and Iruela-Arispe, 2006; Timmermans *et al.*, 2009). Recent studies have aimed to identify true EPC populations, where EPC has been used to describe a wide range of cell types and ultimately endothelial colony forming cells (ECFCs) being described as the true EPC (Medina *et al.*, 2010, 2017; O'Neill *et al.*, 2018; Blandinières *et al.*, 2023; Chambers *et al.*, 2025). Recent efforts to standardise the isolation of ECFCs have allowed for research to progress in the area of postnatal vasculogenesis, identifying ECFCs to have a putative role in angiogenesis and strong evidence for therapeutic potential in vascular diseases and injury (Reid *et al.*, 2018; Tan *et al.*, 2021; Zhang, Cannavicci and Kutryk, 2022; Blandinières *et al.*, 2023; Laan *et al.*, 2024; Liu *et al.*, 2024; Chambers *et al.*, 2025).

1.1.4 Angiogenesis

Angiogenesis is the process by which new blood vessels form from pre-existing vasculature, deriving from endothelial cells as opposed to progenitor cells as seen in vasculogenesis described above (Demir, Yaba and Huppertz, 2010). As with vasculogenesis, angiogenesis is essential for embryonic development, tissue repair and organ growth (Carmeliet and Jain, 2000). In adults, the tightly regulated process occurs mainly under specific physiological conditions such as wound healing and the menstrual cycle (Carmeliet, 2000). However, dysregulated angiogenesis contributes to numerous pathologies, including

cancer, chronic inflammation, cardiovascular diseases and diabetic retinopathy (Carmeliet, 2003).

Under normal conditions, ECs remain quiescent, supported by signals that maintain vessel integrity and prevent uncontrolled proliferation and display stable cell-cell junctions (Ouarné, Pena and Franco, 2021). Maintenance of quiescence is orchestrated by several pathways including hypoxia, VEGF, FGF, Wnt, Hedgehog, Angiopoietin, BMP and TGFB signalling (Potente, Gerhardt and Carmeliet, 2011; Ricard *et al.*, 2021). Quiescence is a reversible state, with an ability to shift to an activated phenotype in response to physiological and pathological processes including pregnancy, cancer and age-related macular degeneration (AMD) (Carmeliet and Jain, 2011; Potente and Mäkinen, 2017; Ouarné, Pena and Franco, 2021). Metabolism plays a pivotal role in controlling endothelial cell fate. During quiescence, cells rely on glycolysis for ATP production, which allows oxygen-rich blood to be reserved for surrounding tissues (De Bock *et al.*, 2013). When stimulated to become migratory tip cells, endothelial cells upregulate glycolytic enzymes, such as PFKFB3 to meet the energy demands of rapid proliferation and migration (Schoors *et al.*, 2014; Li, Sun and Carmeliet, 2019). Moreover, fatty acid oxidation control by notch signalling is implicated in the production of nucleotides, contributing to the increased demand for biomass in proliferating endothelial cells (Schoors *et al.*, 2015; Kalucka *et al.*, 2018). Changes in gene expression drive the transition between endothelial cell quiescence and activation. Transcription factors such as Kruppel-like factors (e.g., KLF2), ETS family members (e.g., ERG) and Forkhead box proteins (e.g., FOXO1) integrate signals from growth factors, shear stress and metabolic cues to modulate endothelial gene programs (Fish and Wythe, 2015; Wang *et al.*, 2015; Sangwung *et al.*, 2017; Andrade *et al.*, 2021; Harel *et al.*, 2021; Payne, Neal and De

Val, 2024). The shift of ECs in response to signalling pathways leading to a proangiogenic activation of ECs is often termed the angiogenic switch.

VEGF in the most potent and well characterised proangiogenic cytokine, acting mainly through VEGFR2 to stimulate endothelial cell proliferation, migration and survival (Schmidt, Brixius and Bloch, 2007). VEGF also increases vascular permeability, enabling plasma proteins to extravasate and provide a provisional matrix for endothelial cell migration (MAEDA, 2012; Claesson-Welsh, 2015). Hypoxia-inducible factor 1a (HIF1A) is a major transcriptional regulator of VEGF expression in response to low oxygen tension (Semenza, 2003). When VEGF binds to its receptors VEGFR1 and VEGFR2 on ECs, a cascade of intracellular signalling events promotes proliferation and migration (Adams and Alitalo, 2007). While VEGF is primarily known for its pro-angiogenic role, it has also been shown to exert anti-angiogenic effects through several mechanisms. First, the existence of isoforms, such as VEGF165b, which is an endogenous splice variant of VEGF-A, has been shown to bind to the VEGFR2 receptor but does not activate downstream pro-angiogenic signalling (Woolard *et al.*, 2004; Glass, Harper and Bates, 2006), inhibit tumour growth in mice (Rennel *et al.*, 2008), have an antiangiogenic effect in human obesity (Ngo *et al.*, 2014) and is abundant in peripheral arterial disease (PAD) (Chu *et al.*, 2016). Additionally, excessive microenvironmental concentrations of VEGF can lead to aberrant, dysfunctional vessel growth, such as haemangiomas, rather than stable, functional networks, reflecting an anti-angiogenic outcome through abnormal vessel remodelling (Ozawa *et al.*, 2004; von Degenfeld *et al.*, 2006; Wolff *et al.*, 2012; Mujagic *et al.*, 2013). Recently, arterial EC specification from capillary ECs (arteriogenesis) has been shown to be induced by fluid shear stress, during which the VEGFA-VEGFR2 signalling axis was declined, with VEGFA counteracting arterial fate specification (Cho *et al.*, 2024; Chen *et al.*, 2025). These recent

views of VEGF activity provide nuanced context to the angiogenic behaviour of VEGF, with specific contexts, such as arteriogenesis, requiring reduced levels of VEGF to operate. Along with VEGF, FGF2 is another important angiogenic factor that promotes endothelial cell proliferation and stimulates ECM degradation via protease induction (Davidson *et al.*, 2005; Gresham, Bahney and Leach, 2021). FGF proteins bind to FGF receptors (FGFRs), activating downstream signalling cascades including MAPK and PI3K-Akt that synergise with VEGF pathways to facilitate angiogenesis (Presta *et al.*, 2005). As active endothelial cells begin to migrate, they degrade and remodel the basement membrane and interstitial ECM (Rauff *et al.*, 2019). This process involves the upregulation of matrix metalloproteinases (MMPs), which cleave structural proteins like collagen and laminin (Egeblad and Werb, 2002). The controlled proteolysis of the ECM not only provides space for migrating cells but also releases bioactive fragments and growth factors bound to ECM components (Bergers and Benjamin, 2003).

Initiation of angiogenic sprouting involves the selection of a highly specialised phenotype of endothelial cells termed tip cells which form the forefront of the sprout (W. Chen *et al.*, 2019). These tip cells are highly migratory, extending filopodia that sense guidance cues in the microenvironment, following VEGF gradients (Gerhardt *et al.*, 2003). Notch signalling, mediated by Delta-like ligand 4 (Dll4) and the Notch receptors, plays a critical role in tip cell selection by limiting excessive sprouting, where tip cells express high levels of Dll4 to activate notch signalling in adjacent cells, pushing those into a stalk cell phenotype and maintaining a single leading tip cell (Adams and Alitalo, 2007; Hellström *et al.*, 2007; Pitulescu *et al.*, 2017; Lobov and Mikhailova, 2018; Akil *et al.*, 2021). Tip cells navigate towards guidance cues, including attractive signals (VEGF gradients) and repulsive signals (e.g., Slit-Robo, Semaphorin-Plexin) (Weitzman, Bayley and Naik, 2008; Adams and

Eichmann, 2010). The balance between these signals ensures a correct spatial organisation of vessel sprouts (Siemerink *et al.*, 2013). Endothelial cells thus exhibit a dynamic migratory phenotype, forming a network of newly sprouting vessels that eventually connect with neighbouring sprouts (Gerhardt, 2008). Following sprout extension, lumen formation allows blood flow through newly formed vessels (Herbert and Stainier, 2011b). Stalk cells located behind tip cells proliferate and form adherens junctions to stabilise the nascent vessel wall (Phng and Gerhardt, 2009). These cells maintain cell-cell adhesion, deposit basement membrane components and contribute to vascular elongation while ensuring that the lumen forms a continuous channel (Tung, Tattersall and Kitajewski, 2012; Choi and Chen, 2014; Y. Guo *et al.*, 2024). Vessel stabilisation requires the recruitment of mural cells (pericytes and vascular smooth muscle cells) that envelop the endothelial tube (Abraham *et al.*, 2008; Armulik, Genové and Betsholtz, 2011; Stratman *et al.*, 2017). Platelet derived growth factor-B (PDGFB) secreted by endothelial cells is a key signal that attracts pericytes to nascent vessels (Armulik, Genové and Betsholtz, 2011). Proper pericyte coverage is essential for maintaining endothelial quiescence, regulating blood pressure and preventing pathological vascular leakage (Gerhardt and Betsholtz, 2003). Not all new vessels persist. Excess, poorly perfused, or redundant vessels are pruned through apoptosis of endothelial cells or retraction of sprouts (Korn and Augustin, 2015; Watson, Grant and Coultas, 2017). This process refines the vascular network to match tissue demands. Factors such as blood flow shear stress, mechanical signals and notch activity can influence whether a developing branch stabilises or regresses (Franco *et al.*, 2015). Once the angiogenic drive subsides, ECs behind the stalk cells in the angiogenic sprout, termed phalanx cells, adopt a quiescent state and form the lining of the new mature vessel (De Smet *et al.*, 2009; Carmeliet and Jain, 2011; Siemerink *et al.*, 2013). Endothelial cells eventually adopt specialised arterial or venous

identities through coordinated signalling pathways (Corada, Morini and Dejana, 2014). Ephrin-B2 is strongly expressed in arterial endothelium, while EphB4 predominates in venous endothelium (Swift and Weinstein, 2009; Fang and Hirschi, 2019). Combined with the modulation of flow-induced cues (e.g., shear stress), these molecular signatures guide the specification and maintenance of arterial and venous vessel segments (Herbert and Stainier, 2011b).

Above we have provided an overview of sprouting angiogenesis. In the following we detail the specific signalling cascade that involves the VEGF, Notch and TGFB pathways within an angiogenic sprout (Ranchoux *et al.*, 2018; Y. Li *et al.*, 2019; Eelen *et al.*, 2020; Yoshitomi *et al.*, 2021; Laschke, Gu and Menger, 2022) (Fig. 1). An increase in VEGF-A in the EC microenvironment binds to VEGFR2 receptors on ECs, triggering an angiogenic switch that activates these cells (Ruhrberg *et al.*, 2002; Gerhardt *et al.*, 2003). This activation produces a tip cell that penetrates the basement membrane. The tip cell then migrates towards the VEGF-A gradient through VEGFR2 receptors on its filopodia. The VEGF-A/VEGFR2 interaction induces the expression of DLL4 in tip cells (Eelen *et al.*, 2020). DLL4 subsequently binds to and activates notch receptors on adjacent stalk cells (Yoshitomi *et al.*, 2021). Once activated, the notch receptor is cleaved, releasing the notch intracellular domain (NICD) which locates to the nucleus of the stalk cells (Y. Li *et al.*, 2019). There NICD drives the transcription of target genes, such as the TFs HEY1, HEY2 and HES1, that downregulate VEGFR2, VEGFR3 and DLL4 while upregulating VEGFR1 (Y. Li *et al.*, 2019). The decrease in VEGFR2 levels in stalk cells lowers their sensitivity to the VEGF-A signalling cascade, thereby preventing the shift to a tip cell and maintaining the stalk cell phenotype (Hellström *et al.*, 2007). In parallel, reduced DLL4 expression leads to diminished notch signalling in tip cells, preserving the presence of a single tip EC at the leading edge of the sprout (Hellström *et al.*, 2007), thus

describing the self-maintenance loop between tip and stalk ECs in angiogenic sprouts. VEGFR1 has lower kinase activity compared to VEGFR2 (Y. Li *et al.*, 2019). VEGFR1 bind VEGF-A with high affinity in stalk cells enabling it to compete with VEGFR2 and further reinforcing the stalk EC identity (Krueger *et al.*, 2011; Ho *et al.*, 2012). Finally, TGFB/BMP signalling activates SMAD1/5/8 through phosphorylation (Moya *et al.*, 2012; Y. Li *et al.*, 2019). The activated SMADs upregulate ID1-3 (inhibitor of DNA-binding proteins 1-3) and interact with the notch signalling pathway and downstream TFs to sustain the stalk cell phenotype (Moya *et al.*, 2012). Disruption to the mechanism described above can lead to excessive and aberrant sprouting through increased conversion of stalk cells into tip cells (Y. Li *et al.*, 2019).

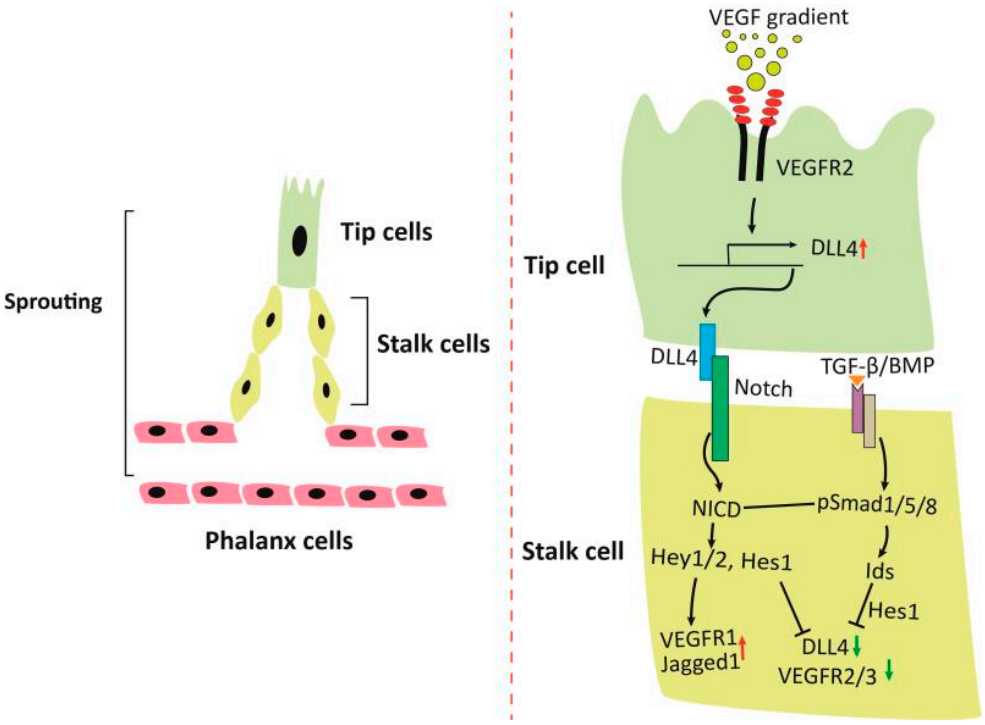


Figure 1. VEGF, Notch and TGFB/BMP signalling mechanisms interact to maintain tip and stalk endothelial cell phenotypes in the angiogenic sprout. Figure from Li et al., (2019).

Schematic summarising the major signalling cascades that regulate endothelial tip and stalk cell specification during sprouting angiogenesis. VEGF-VEGFR2 signalling promotes tip cell migration and filopodia extension, while Dll4-Notch restricts tip fate in neighbouring stalk cells to maintain a single tip cell within the angiogenic sprout. TGFB and BMP pathways maintain the stalk cell phenotype through SMAD1/5/8 activation.

1.2 Developmental angiogenesis

Angiogenesis is a fundamental process underlying both normal physiological development and a range of pathological conditions. During embryogenesis, angiogenesis refines the primary vascular plexus formed by vasculogenesis; in the adult, it supports tissue growth, regeneration, and wound repair under tightly regulated conditions (Carmeliet, 2003). However, dysregulated angiogenesis is also central to diseases such as cancer, ischemic disorders and retinopathies (Carmeliet and Jain, 2000; Gariano and Gardner, 2005; Crawford *et al.*, 2009).

In skeletal muscle, vascular expansion accompanies hypertrophy and increased metabolic demands (Egginton, 2009). Exercise-induced angiogenesis is regulated primarily by local hypoxia and shear stress, which elevate pro-angiogenic factors such a VEGF and FGF (Gustafsson and Kraus, 2001). This process enables more efficient oxygen and nutrient delivery, thereby optimising muscle performance (Kissane and Egginton, 2019; Ross *et al.*, 2023). Angiogenesis is also critical in the female reproductive cycle, especially in the ovarian follicle and corpus luteum, where cyclic neovascularisation occurs (Fraser and Duncan, 2005). The endothelium experiences recurrent episodes of proliferation, vascularisation and shedding, governed by hormonal fluctuations of oestrogen and progesterone (Girling and Rogers, 2009). Placental angiogenesis during pregnancy is likewise essential for proper foetal development and maternal-foetal nutrient exchange (Demir, Seval and Huppertz, 2007). Adipose tissue growth (adipogenesis) relies on adequate vascularisation and angiogenesis to supply expanding fat lobules with oxygen and nutrients, requiring a switch to an angiogenic phenotype (Cao, 2007). VEGF expression in adipocytes and stromal cells stimulates endothelial cell migration and vessel sprouting (Sung *et al.*, 2013). Dysregulation of adipose angiogenesis can contribute to metabolic disorders with insufficient vascularisation leading

to hypoxia and inflammation, whereas excessive angiogenesis may facilitate abnormal fat accumulation (Rutkowski, Davis and Scherer, 2009). Vascular integrity and the capacity for neovascularisation decline with advancing age (Moriya and Minamino, 2017; Hodges, Suarez-Martinez and Murfee, 2018; Xiao *et al.*, 2023). Endothelial progenitor cells, which can participate in vessel repair, demonstrate reduced number and function in older individuals (Williamson, Stringer and Alexander, 2012). This decline impairs wound healing and increases susceptibility to ischemic insults (Yang *et al.*, 2018). Oxidative stress, telomere shortening and chronic inflammation are thought to be significant contributors to the age-related deterioration of angiogenic potential (Donato *et al.*, 2015). Elucidating the molecular mechanisms of age-associated endothelial dysfunction remains a major research focus, with therapeutic potential for mitigating cardiovascular and neurodegenerative diseases (Guo *et al.*, 2022).

1.3 Pathological angiogenesis

While developmental angiogenesis serves crucial physiological functions, pathological angiogenesis arises when proangiogenic signals become dysregulated, leading to abnormal vessel growth and function (Dudley and Griffioen, 2023). This phenomenon underlies numerous diseases, ranging from cancer to ocular disorders.

Tumour progression in intimately linked to the ability of neoplastic cells to induce angiogenesis, described as the angiogenic switch (Hanahan and Folkman, 1996; Hanahan and Weinberg, 2011). Insufficient vascularisation prevents adequate blood flow and restricts tumour growth to just a few millimetres in diameter due to limited oxygen and nutrient diffusion (Hillen and Griffioen, 2007). Once cancer cells secrete high levels of VEGF, FGF and other angiogenic mediators, endothelial cells respond by sprouting new vessels that

infiltrate the tumour mass (Carmeliet and Jain, 2011). The vasculature of tumours is often disorganised, tortuous and permeable, lacking the hierarchical structure of normal vessels (Jain, 2005; Siemann, 2011). Endothelial cell proliferation and pericyte recruitment are erratic, resulting in leaky, poorly functional vessels that foster hypoxic regions within the tumour leading to a microenvironment that contributes to tumour heterogeneity and resistance to therapies (Armulik, Genové and Betsholtz, 2011; De Bock, Cauwenberghs and Carmeliet, 2011). Anti-angiogenic therapies, such as bevacizumab (an anti-VEGF antibody), can normalise the vasculature or deprive tumour cells of oxygen and nutrients (Lopes-Coelho *et al.*, 2021). However, resistance mechanisms frequently emerge, highlighting the complexity of tumour-endothelial interactions (Bergers and Hanahan, 2008).

Ischemic stroke occurs when cerebral blood flow is critically reduced to vessel occlusion, leading to neuronal death (Salaudeen *et al.*, 2024). Angiogenesis in the penumbra (the area surrounding the infarct core) is stimulated by local hypoxia, upregulating HIF1a, VEGF and other pro-angiogenic signals (He *et al.*, 2021; Xue *et al.*, 2025). While some spontaneous revascularisation occurs, it is often insufficient to fully restore blood supply (Esquiva, Grayston and Rosell, 2018; Rust, 2020; Fang, Wang and Miao, 2023). In the context of myocardial infarction, the infarcted region experiences necrosis and scar formation (Chalise, Becirovic-Agic and Lindsey, 2023). Atherosclerotic occlusions in peripheral vessels, commonly in the lower extremities, lead to peripheral artery disease (PAD) (Inampudi *et al.*, 2018). Ischemic tissue can upregulate VEGF, FGF and other cytokines that stimulate collateral vessel formation, however, advanced disease states can often exhibit insufficient or unstable neovascularisation, resulting in chronic pain, ulcers, and risk of amputation.

Diabetic retinopathy (DR) is a significant microvascular complication of diabetes mellitus and stands as a leading cause of preventable blindness worldwide (Cheung, Mitchell

and Wong, 2010). Chronic hyperglycaemia is the root of various pathophysiological changes in the retina, resulting in vascular dysfunction, neuronal cell damage and inflammation (Gardner *et al.*, 2000). A hallmark of DR, especially during the proliferative stages, is aberrant angiogenesis (Dudley and Griffioen, 2023). This neovascular process involves the excessive growth of fragile blood vessels originating from the retinal vasculature (Ji *et al.*, 2021). These newly formed vessels display increased vascular leakage, which can ultimately lead to vision loss (Nawaz *et al.*, 2019). Along with DR, age-related macular degeneration represents another vasculature-related pathology resulting from aberrant angiogenesis, but primarily affects the elderly (Heloterä and Kaarniranta, 2022).

The implications of angiogenesis within many pathologies emphasises the broad and essential functions of the process.

1.4 Reparative angiogenesis

In addition to the processes of developmental and pathological angiogenesis, reparative or regenerative angiogenesis describes a crucial physiological response aimed at restoring prefusion and tissue regeneration after injury or ischemia (Potente, Gerhardt and Carmeliet, 2011). Reparative angiogenesis is essential for healing and functional recovery in various contexts, including myocardial infarction, stroke, peripheral artery disease and cutaneous wounds . Unlike the often disorganised and leaky vasculature observed in pathological angiogenesis, reparative angiogenesis results in a functional, stable and efficient vascular network to replace damaged vessels and support tissue regeneration (DiPietro, 2016; Moradi *et al.*, 2022; Fang, Wang and Miao, 2023). Like other angiogenic process, reparative angiogenesis relies on endothelial cell activation, proliferation, migration and maturation, guided by a complex interplay of molecular signals and cellular actors described above (Eelen

et al., 2020; Shi *et al.*, 2023). While there are strong similarities between developmental and reparative angiogenesis at the molecular level, reparative angiogenesis is distinguished by its initiation in response to acute tissue damage (Tonnesen, Feng and Clark, 2000).

There has been debate surrounding the origin of new endothelial cells in vascular repair. Initially, postnatal vasculogenesis induced by circulating endothelial EPCs were proposed to contribute to neovascularisation in ischemic tissue (Asahara *et al.*, 1997; Urbich and Dimmeler, 2004). More recently, lineage tracing and parabiosis experiments have demonstrated that the predominant source for endothelial regeneration in large vessels is the local proliferation and migration of pre-existing, quiescent ECs flanking the site of injury (Carmeliet and Jain, 2011; Cooke and Losordo, 2015; Esquiva, Grayston and Rosell, 2018; McDonald *et al.*, 2018; Eelen *et al.*, 2020; Evans, Iruela-Arispe and Zhao, 2021). These ECs can rapidly re-enter the cell cycle in response to injury cues (McDonald *et al.*, 2018). While there is still some debate as to whether ECFCs are a source of *de-novo* ECs in reparative angiogenesis, it has been shown that ECFCs incorporate into neovessels and can function in a paracrine capacity at the site of injury, secreting a host of pro-angiogenic factors (e.g., VEGF, HGF, SDF-1) and extracellular vesicles that stimulate resident ECs, reduce apoptosis and support overall vascular remodelling (Mirotsou *et al.*, 2011; Silvestre, Smadja and Lévy, 2013; Hong *et al.*, 2016; Esquiva, Grayston and Rosell, 2018; O'Neill *et al.*, 2018; Evans, Iruela-Arispe and Zhao, 2021). Taken together, reparative angiogenesis may require a combination of both resident EC plasticity and contributions from progenitor cells.

Therapeutically, strategies to enhance reparative angiogenesis are under investigation for ischemic diseases (Martín-Bórnez *et al.*, 2023). Clinical approaches include delivery of growth factors, mobilisations of EPCs and transplantation of stem/progenitor cells with the aim of augmenting endogenous vascular repair (Silvestre, Smadja and Lévy, 2013). Although

challenges remain, particularly in patients with pathologies such as diabetes that impair vascular regeneration, along the aging process, targeting reparative angiogenesis holds promise for regenerative medicine (Lähteenvuo and Rosenzweig, 2012; Fadini *et al.*, 2020; Suh *et al.*, 2023; Xiao *et al.*, 2023; Huang *et al.*, 2025). Advances in understanding endothelial heterogeneity, plasticity and epigenetic regulation continue to reveal novel therapeutic targets in both pathological and reparative angiogenesis (Dejana, Hirschi and Simons, 2017; Potente and Carmeliet, 2017; Zhong *et al.*, 2025).

1.5 Endothelial-Mesenchymal Transition (EndoMT)

Endothelial-mesenchymal transition (EndoMT) is a complex, dynamic biological program wherein differentiated ECs lose their canonical endothelial characteristics and acquire mesenchymal or fibroblast-like traits and is a relatively recently recognised example of endothelial plasticity (Kovacic *et al.*, 2019; Piera-Velazquez and Jimenez, 2019). Throughout the transition, ECs shift morphology into an elongated spindle shape and begin to reflect characteristics associated with an active state, including loss of polarity and cell-cell junctions (Piera-Velazquez and Jimenez, 2019). During EndoMT, EC expression of CDH5, PECAM1 and von willebrand factor (VWF) is reduced, with a concomitant increase in alpha smooth muscle actin (aSMA), N-cadherin (CDH2), vimentin (VIM) and collagen I and III expression (Goumans, van Zonneveld and ten Dijke, 2008; Platel *et al.*, 2019). This phenotypic switch arises through a cascade of transcriptional signalling events that also drives cytoskeletal remodelling, reduced intercellular junctions and enhanced migratory potential (Potenta, Zeisberg and Kalluri, 2008; Ciszewski *et al.*, 2021). Originally characterised in embryonic cardiac cushion development (Markwald, Fitzharris and Smith, 1975; Eisenberg and Markwald, 1995), EndoMT has since been implicated in normal physiology, including vascular remodelling and

wound healing, and in diverse pathologies such as fibrosis, atherosclerosis, cancer progression and pulmonary arterial hypertension (Kovacic *et al.*, 2012, 2019; Souilhol *et al.*, 2018; Piera-Velazquez and Jimenez, 2019).

Initially identified as drivers of epithelial to mesenchymal transition (EMT), EndoMT is modulated by a suite of master transcription factors (TFs) that include Snail family transcriptional repressor 1 (SNAI1), Snail family transcriptional repressor 2 (SNAI2), Zinc finger E-box binding homeobox 1 (ZEB1), Zinc finger E-box binding homeobox 2 (ZEB2) and twist family BHLH transcription factor 1 (TWIST1) . While experimental and *in-silico* studies conclude that each of these TFs are involved to some extent during the EndoMT process, further study is required to uncover the precise mechanisms and interplay between the regulators, particularly the role of ZEB1 (Weinstein, Mendoza and Álvarez-Buylla, 2020; Fang, Hultgren and Hughes, 2021).

The spectrum of EndoMT is managed by a balance of signalling pathways. Transforming growth factor beta (TGFB) is widely considered a central inducer of EndoMT (Medici, Potenta and Kalluri, 2011; van Meeteren and ten Dijke, 2012; Pardali *et al.*, 2017). Activation of TGFB type I and II receptors leads to phosphorylation of SMAD2/3, which complex with SMAD4 and translocate to the nucleus, inducing the expression of several mesenchymal hallmarks, including serpin family E member 1 (SERPINE1) and collagen type I a 1 chain (COL1A1) (Sánchez-Duffhues, García de Vinuesa and ten Dijke, 2018). The TGFB pathway can also interact with other noncanonical SMAD independent signalling systems including p38, MAPK, ERK and RhoA (Zhang, 2009), processes that modulate EC junctions, migration and proliferation and may be involved in EndoMT (Abhinand *et al.*, 2016). Wnt signalling interacts with the TGFB pathway and has been implicated in EndoMT, with EndoMT induction derived from Wnt ligands resulted in a differentiation of ECs into SMCs and

pericytes in cardiac tissue (Chen *et al.*, 2016). Furthermore, AP1 factors are known to be activated in response to members of the Wnt pathway, albeit noncanonically, and may be involved in driving the EndoMT process (Sánchez-Duffhues, García de Vinuesa and ten Dijke, 2018) As with Wnt, NFKB, ET-1 and FGF signalling have also been shown to interact with the TGFB pathway, leading to a shift towards a mesenchymal like state (Fang, Hultgren and Hughes, 2021) and demonstrating EndoMT to be a complex process regulated through several biological avenues.

The EndoMT process is described as a continuum, in which complete transition results in ECs obtaining mesenchymal identity, whereas a partial state can occur where ECs retain expression of canonical EC features while acquiring mesenchymal traits (Welch-Reardon, Wu and Hughes, 2015). Recently, this partial state is proposed to be critical to sprouting angiogenesis, in which ECs adopt similar phenotypic characteristics to those undergoing EndoMT, such as increased mobility and a reduction in cell-cell junctions (Welch-Reardon, Wu and Hughes, 2015; Piera-Velazquez and Jimenez, 2019; Fang, Hultgren and Hughes, 2021). Within this process tip cells adopt a phenotype reminiscent of a more mesenchymal-like phenotype, whereas the trailing stalk cells retain increased EC phenotype maintaining cell contacts to form a new vessel, suggesting the angiogenic sprout to be a physical representation of the EndoMT process (Welch-Reardon, Wu and Hughes, 2015; Fang, Hultgren and Hughes, 2021). The mirrored processes and EC plasticity between sprouting angiogenesis and EndoMT prompted further research into partial EndoMT as key angiogenic process. Indeed, studies showed that during developmental and pathological sprouting angiogenesis, master EndoMT regulators SNAI1 and SNAI2 were upregulated (Parker *et al.*, 2004; Lu *et al.*, 2007; Hultgren *et al.*, 2020). Furthermore, loss of SNAI2 resulted in significant reduction of tumour growth through an impaired development of

tumour vasculature which is highly suggestive of SNAI2, and therefore EndoMT, being required for tumour angiogenesis (Hultgren *et al.*, 2020). Aside from regulation of master TFs, there is also overlap of signalling pathways between sprouting angiogenesis and EndoMT, with several of these described above. Notably, the TGBFB pathway influences the major proangiogenic VEGF signalling process through canonical SMAD targeting and noncanonical PI3K/AKT, MAPK, ERK and JNK/AP1 systems, including a positive feedback loop between VEGF and TGFB1 through PI3K/AKT (Li *et al.*, 2005; Ma *et al.*, 2020; Fang, Hultgren and Hughes, 2021). The striking similarities of regulation and exhibited phenotype between sprouting angiogenesis and EndoMT is highly suggestive of a partial EndoMT state within vascular growth. Furthermore, the balance of signalling within EndoMT and a partial state result in a reversible process, with ECs retaining the ability to return to an EC state after initial activation (Fang, Hultgren and Hughes, 2021; Krishnamoorthi *et al.*, 2022; Yoshimatsu and Watabe, 2022). The reversibility of the process allows ECs to gain a mesenchymal-like phenotype to respond to different molecular cues under specific microenvironments, both pathological and developmental, reflecting the flexibility of the process and ECs (Fang, Hultgren and Hughes, 2021). Indeed, a recent scRNA-seq study identified ECs to exhibit mesenchymal gene expression in response to acute myocardial infarction, before returning to a standard EC state (Tombor *et al.*, 2021). Along these lines, we could consider ECs in an EndoMT position to be a distinct EC phenotype which can be detected by scRNA-seq, allowing for future research into the process at an increased resolution. Furthermore, an *in-vitro* assay of EndoMT reversibility was developed that demonstrated induction of the process via Nω-nitro-L-arginine methyl ester hydrochloride (L-NAME) and angiotensin II (Ang II) in HUVECs was reversible upon removing the stimuli (Krishnamoorthi *et al.*, 2022). The reversibility of EndoMT specifically, as opposed to EndoMT as an overall process, has recently

been implicated as playing a role in pathologies including cancer, atherosclerosis and cardiovascular diseases, highlighting the importance of the inherent plasticity of the process (Clere, Renault and Corre, 2020; Hall *et al.*, 2024; Qian *et al.*, 2025; You *et al.*, 2025; Zhang *et al.*, 2025). While the mechanisms behind the reversibility of EndoMT are not fully understood, experimentation into the reversibility of EndoMT can provide insights into the therapeutic potential of targeting this process or targeting the adaptive phenotypes that arise (Fang, Hultgren and Hughes, 2021; Qian *et al.*, 2025).

EndoMT is an essential process in development. A well-studied example occurs in the developing heart valves, during which ECs lining the endocardium undergo EndoMT, migrate into the cardiac jelly and differentiate into mesenchymal cells that form atrioventricular cushions and valve leaflets (Markwald, Fitzharris and Smith, 1975; Eisenberg and Markwald, 1995; Armstrong and Bischoff, 2004). Perturbations in these signalling gradients, such as TGFB, BMP and notch, can lead to congenital heart defects (Person, Klewer and Runyan, 2005; Gong *et al.*, 2017). Beyond the heart, EndoMT also appears in the forming pulmonary vasculature (Piera-Velazquez and Jimenez, 2019), indicating that endothelial plasticity underlies multiple embryonic morphogenetic events. When dysregulated, EndoMT contributes to several pathologies, including fibrosis, atherosclerosis, pulmonary hypertension, diabetic retinopathy and cancer in which persistent EC destabilisation and EndoMT induce a dysfunctional endothelium (Potenta, Zeisberg and Kalluri, 2008; Welch-Reardon, Wu and Hughes, 2015; Souilhol *et al.*, 2018; Sánchez-Duffhues, García de Vinuesa and ten Dijke, 2018; Piera-Velazquez and Jimenez, 2019; Fang, Hultgren and Hughes, 2021; Peng *et al.*, 2022). The sheer number of pathological implications of EndoMT, both partially and full, and considering the reversibility of the process present EndoMT as an attractive area for therapeutic development. Of particular interest is exploration into the specific roles of

the proposed master transcription factors of EndoMT, including ZEB1 (Weinstein, Mendoza and Álvarez-Buylla, 2020; Fang, Hultgren and Hughes, 2021). Indeed, endothelial ZEB1 has been shown to promote angiogenesis during bone formation (Fu, Lv, *et al.*, 2020), which we can hypothesise involves partial EndoMT.

1.6 Zinc-finger E-box binding protein 1 (ZEB1)

Zinc-finger E-box binding protein 1 (ZEB1) comprises 1117 amino acids and features two C2H2-type zinc finger (ZF) clusters, one towards the N-terminus and the other at the C-terminus, separated by a central homeodomain (Wu *et al.*, 2020). The ZF clusters bind specific E-box or E-box-like motifs (5'-CACCTG-3') within target gene promoters, whereas the central homeodomain does not directly bind DNA (Comijn *et al.*, 2001; Drápela *et al.*, 2020). Flanking the homeodomain are functional protein-binding domains responsible for interactions with co-repressors and co-activators, including a carboxyl terminal binding protein domain (CBD) that is responsible for recruiting histone deacetylases (HDACs) as a co-repressor (Caramel, Ligier and Puisieux, 2018; Farfán *et al.*, 2018). The structure of ZEB1 also includes smad-binding (SBD) and p300/CREB-binding protein associated factor (p300/PCAF) binding domains, allowing for transcriptional activation and crosstalk with TGFB signalling (Postigo *et al.*, 2003; Drápela *et al.*, 2020). The presence of these domains in the structure of ZEB1 highlights the dual role of ZEB1 as both a repressor and activator of gene expression.

Potentially the most notable post-transcriptional regulator of ZEB1 is the microRNA (miRNA) 200 family (miR-200) which forms a reciprocal feedback loop with ZEB1 in which ZEB1 suppresses miR-200 family expression, whose family members then prevent ZEB1 mRNA translation (Brabletz and Brabletz, 2010). Importantly, it has been shown that ZEB1 regulates the notch pathway in cancer cells through this miR-200 relationship (Brabletz *et*

al., 2011). Along with miR-200, ZEB1 regulation is modulated by various pathways that are also highly relevant to angiogenesis and EndoMT, including TGFB, Wnt, NFKB and PI3K/AKT (Drápela *et al.*, 2020; Lu *et al.*, 2022). While being regulated by TGFB, ZEB1 has also been shown to induce transcription of genes that respond to the TGFB pathway (Caramel, Ligier and Puisieux, 2018), suggesting a regulation of TGFB consequences by ZEB1, further implicating the TF in angiogenic and EndoMT processes. In line with this, experiments surrounding ZEB1 in breast cancer revealed ZEB1 upregulated VEGF, stimulating angiogenesis (Liu *et al.*, 2016). The molecular mechanism behind VEGFA transcription by ZEB1 involved recruitment of Sp1 transcription factor (SP1) to the promoter of VEGFA through PI3K and p38 processes (Liu *et al.*, 2016). Interestingly, the interaction between ZEB1 and SP1 is also implicated in corneal fibrosis, in which SP1 induction by ZEB1 led to EndoMT through binding of SP1 binding sites in the promoters of EndoMT-related genes COL1A1, FN1 and VIM (Lee *et al.*, 2020).

ZEB1 is extensively studied in oncogenesis, particularly in the promotion of metastasis and tumour progression (Vandewalle, Van Roy and Berx, 2009; Caramel, Ligier and Puisieux, 2018; Perez-Oquendo and Gibbons, 2022; Durand *et al.*, 2024). By repressing E-cadherin (CDH1) and epithelial cell adhesion molecule (EPCAM), ZEB1 fosters the loss of epithelial polarity resulting in enhanced cell motility and invasiveness (Vannier *et al.*, 2013; Lu *et al.*, 2022). The downregulation of CDH1 is an example of the repressive behaviour of the ZEB1 structure, where ZEB1 directly binds to the promoter of CDH1 while recruiting histone deacetylases to inhibit transcription (Aghdassi *et al.*, 2012). ZEB1 also promotes the maintenance of cancer cell stemness, a tumour cell phenotype that protects cancer cells against DNA damage, through inhibiting miR-200 (Wellner *et al.*, 2009). Indeed, it has been shown that ZEB1 increased homologous recombination-mediated DNA damage repair,

implicating ZEB1 in chemoresistance (Zhang *et al.*, 2018). Phenotypic plasticity of cancer cells is also known to be largely regulated by ZEB1 preferentially over SNAI1 and SNAI2, further inducing tumour metastasis (Krebs *et al.*, 2017). A hallmark of cancer progression is increased proliferation. A link between ZEB1 and the cell cycle has been identified, where ZEB1 was found to shift roles from a chromatin bound protein in interphase to a microtubule associated protein during mitosis in various *in-vitro* cancer cell models (Fouani *et al.*, 2020), suggesting a direct role of ZEB1 in proliferation. In addition, EC specific deletion of ZEB1 in mouse cancer models revealed reduced tumour angiogenesis and a drive towards tumour vascular normalisation, primarily through TGFB signalling repression (Fu, Li, *et al.*, 2020). High ZEB1 expression often correlates with poor prognosis in an array of malignancies (Zhang, Sun and Ma, 2015; L. Li *et al.*, 2019; Lu *et al.*, 2022). Indeed, a meta-analysis study across 1616 patients focussing on solid tumours revealed that increased ZEB1 expression was associated with significantly worse overall survival (B. Chen *et al.*, 2019). Although a known driver of cancer, ZEB1 remains a difficult target for treatment, conveying a key role in the therapeutic resistance of cancers against multiple therapies (Lu *et al.*, 2022). Beyond its direct effects on cancer cells, ZEB1 can promote tumour angiogenesis by inducing proangiogenic cytokines, such as VEGF mentioned above, to further support tumour angiogenesis and growth (Liu *et al.*, 2016; Zeng *et al.*, 2023). Together, the multiple roles of ZEB1 in cancer convey the multifaceted nature of the TF as a player in several aspects of tumour progression opposed to regulated a single, defined process.

ZEB1 is less well studied in ECs, but recent findings are establishing ZEB1 as an important EC TF. EC-specific knockout (KO) of ZEB1 reduced vascularisation within human and mouse bone, suggesting ZEB1 is a driver of angiogenesis in bone formation (Fu, Lv, *et al.*, 2020). Mechanistically, it was identified that deletion of ZEB1 epigenetically repressed

Dll4/notch signalling, indicating an activation of the proangiogenic pathway by ZEB1 (Fu, Lv, *et al.*, 2020). Moreover, ZEB1 was shown to reverse osteoporosis in mice (Fu, Lv, *et al.*, 2020) placing ZEB1 as a promising candidate for treatment of osteoporosis. Posterior polymorphous corneal dystrophy (PPCD) is an inherited disorder in which the endothelium of the cornea displays increased oedema and is replaced by multi-layered epithelial-like cells (Fung *et al.*, 2021). ZEB1 gene mutation is implicated in the disorder, with approximately 30% of disorder instances reflecting a monoallelic mutation (Frausto *et al.*, 2019; Guier *et al.*, 2025). CRISPR-Cas9 ZEB1 KO within corneal endothelial cells (CEnCs) led ECs to undergo an epithelial-like transition, reflecting the PPCD phenotype and showing increased CEnC apoptosis and barrier function (Frausto *et al.*, 2019), demonstrating the ability of ZEB1 to regulate EC plasticity. Further studies of the corneal endothelium identified ZEB1 to promote EC proliferation and corneal neovascularisation (Jin *et al.*, 2020). The same study revealed homozygous KO of ZEB1 to disrupt embryonic mouse lung vasculogenesis and ZEB1 deletion to reduce mouse retinal microvascular EC proliferation with no effect on VEGF expression (Jin *et al.*, 2020). This led to the conclusion that ZEB1 regulates neovascularisation in cornea independently of VEGF signalling (Jin *et al.*, 2020). In addition, ZEB1 and SNAI1 were shown to be upregulated in corneal ECs in Fuchs endothelial corneal dystrophy and acted through TGFB signalling to induce excessive extracellular matrix (ECM) production, specifically of proteins COL1A1 and fibronectin (FN1) (Okumura *et al.*, 2015). ZEB1 has also been shown to upregulate VEGF signalling in human dermal microvascular endothelial cells during wound healing, displaying a proangiogenic role (Lan *et al.*, 2022). The ability of ZEB1 to induce proangiogenic effects both dependently and independently of VEGF is again indicative of the adaptive capabilities of the TF. In contrast to the proangiogenic effects displayed by ZEB1 in tumour and corneal models, a recent study of the mouse retina revealed ZEB1 to be

upregulated during quiescence entry of developing vasculature (Yu *et al.*, 2022). Indeed, KO of ZEB1 in retinal ECs disrupted normal vessel stabilisation in the developing retina, resulting in excessive vascular sprouting and deformities (Yu *et al.*, 2022). Mechanistically, the study showed ZEB1 to repress negative modulators of the Wnt/B-catenin-FOXO1 axis, suggesting ZEB1 activates the Wnt pathway in ECs to stimulate quiescence entry (Yu *et al.*, 2022). The contradictory roles of ZEB1 within ECs and vasculature strongly suggest that ZEB1 function is highly dependent on context, whether that be at a pathological, developmental or microenvironment level.

1.7 Hypothesis and aims

ZEB1 emerges from the literature as a crucial regulator of endothelial plasticity, influencing pathways such as EndoMT and angiogenesis. By modulating both pro and anti angiogenic signals, ZEB1 can shape how endothelial cells respond to developmental cues and pathological stressors, inducing a heterogeneity amongst ECs of the vasculature. This prompted the following hypothesis, which this thesis seeks to address:

Hypothesis

Endothelial *ZEB1* expression is dynamic during angiogenesis and contributes to EC heterogeneity by modulating gene expression programs that drive endothelial cell specialization and plasticity. This regulation may play a critical role in cellular responses to normal development and physiological stress, such as myocardial infarction, contributing to the adaptive or maladaptive remodelling of ECs in vascular processes.

We will test the hypothesis by achieving the following aims:

Aim 1: Determine potential direct and indirect gene regulatory pathways activated by ZEB1 in different EC populations in vitro using a combination of RNA-seq and ChIP-seq approaches and analysis pipelines.

Aim 2: Characterise the heterogeneity of ZEB1 expression across EC phenotypes via scRNA-seq in multiple models of developmental and pathological angiogenesis.

Aim 3: Investigate a potential role of ZEB1 in EndoMT through scRNA-seq analysis of a myocardial infarction dataset and generate a predictive ZEB1/EndoMT signature from text-mining.

Aim 4: Determine the functional impact of ZEB1 loss on adult vascular phenotype using *in-vivo* genetic models of ZEB1 deletion in the mouse retina.

Chapter 2: Materials and Methods

The first instance of tools/packages used will be cited and referenced. Any subsequent mention of the tool assumes the same version unless stated otherwise. This was done to improve readability of the methods. Analyses in R (R Core Team, 2024) were performed under R version 4.3.3 “Angel Food Cake”.

Computational resources

The downloading and aligning of raw sequencing data was performed with a 3.60GHz 16-CPU Intel(R) core(TM) i9-9900K CPU with 128Gb RAM under Ubuntu version 20.04.2 LTS (Focal Fossa) as was *in-silico* KO simulations in scRNA-seq data (Osorio *et al.*, 2022) (more below). Downstream analysis of aligned data was performed with a MacBook Pro 2019 2.3GHz 8-Core Intel Core i9 with 16Gb RAM under MacOS Monterey.

Code availability

All code is available at https://github.com/JHorder/thesis_analyses.

2.1 Methods to chapter 3 - ZEB1 knockdown via siRNA in HUVECs revealed a modulation of adhesion, angiogenesis and inflammation related processes and uncovered a predicted ZEB1 regulatory network

Samples were generated for RNA-seq prior to joining the lab group. I was responsible for processing raw FASTQ files, generating results and forming further hypotheses. This process was also used to co-first author a methods and workflow publication (Pinel *et al.*, 2022) (https://github.com/vasc-bioinf/rnaseq_exp). Methods for HUVEC culture, ZEB1 siRNA knockdown, RNA extraction, and RNA sequencing are provided in Appendix 1.

2.1.1 RNA-seq data analyses

Read quality and adapter content were assessed with FASTQC (v0.11.9) (Andrews, 2010). Reads were trimmed of adapters and quality filtered using cutadapt (v3.6) (Martin, 2011) to a minimum quality 20 (-q 20) and a minimum read length of 1 (--minimum-length 1) in a paired-end manner before reanalysis with FASTQC. Subsequent alignment of trimmed, paired-end reads was performed using STAR (v2.7.9) (Dobin *et al.*, 2013) to the reference genome GRCh38 (primary assembly, release 107, https://ftp.ensembl.org/pub/release-107/fasta/homo_sapiens/dna/). Alignment files were output from STAR in sorted BAM format. Qualimap (v2.2.1) (Okonechnikov, Conesa and García-Alcalde, 2016) was used to assess alignment statistics. Aligned reads were quantified using featureCounts (v2.0.0) (Liao, Smyth and Shi, 2014). Read normalisation and identification of significantly (Benjamini-Hochberg adjusted p-value <0.05) differentially expressed genes (DEGs) was carried out with DESeq2 (v1.42.1) (Love, Huber and Anders, 2014). Conversion of gene naming convention from Ensembl to HGNC symbol was done with biomaRt (v2.58.2) (Durinck *et al.*, 2009) but it is important to note that the ensembl ID was used for all analyses, converting only for readability of results. Data for PCA plotting was transformed via regularised log transformation and plot using PCAtools (v2.14.0) (Blighe and Lun, 2024). ComplexHeatmap (v2.18.0) (Gu, 2022) was used to cluster and generate heatmap plots of genes of interest, Functional enrichment analyses against Gene Ontology Biological Process (GOBP) database (Ashburner *et al.*, 2000; The Gene Ontology Consortium *et al.*, 2023) via the GO.db annotation package within Bioconductor (v3.18) released October 2023, and Kyoto Encyclopedia of Genes and Genomes (KEGG) (Kanehisa and Goto, 2000; Kanehisa, 2019; Kanehisa *et al.*, 2023) database (v108.1) released October 2023, was done with

clusterProfiler (v4.10.1) (Yu *et al.*, 2012) and *clusterProfiler::simplify()* function was used to remove redundancy within the GOBP results with a similarity cutoff of 0.7. A custom background reference (universe) list of genes was used for functional enrichment analyses that consisted of only genes whose expression were detected in HUVECs by excluding genes that showed zero counts across all samples. This was done in an attempt to remove biases within the analyses that may be induced through using the entire genome as the background (Hansen *et al.*, 2011; Lindholm *et al.*, 2014; Timmons, Szkop and Gallagher, 2015; Simillion *et al.*, 2017). The rationale for this filtering step is that including genes with zero expression, which therefore may not be biologically relevant in the specific context, may impact the enrichment results by being included in the statistical model leading to potentially misleading conclusions about overrepresented biological processes. By restricting the background to expressed genes, the enrichment analysis is closer to actual the transcriptional landscape of the context, in this case HUVECs, thereby reducing the risk of false enrichment due to potentially irrelevant genomic background (Hansen *et al.*, 2011; Lindholm *et al.*, 2014; Timmons, Szkop and Gallagher, 2015; Simillion *et al.*, 2017). Network analyses were performed with Cytoscape (v3.9.1) (Shannon *et al.*, 2003) and the following Cytoscape plugins; Protein-Protein interaction network was generated with stringApp (v1.6.0) (Doncheva *et al.*, 2019) (minimum confidence score 0.4), hub genes identified by connectivity (degree) through cytoHubba (v0.1) (Chin *et al.*, 2014) and regulons predicted with iRegulon (v1.3) (Janky *et al.*, 2014). Plots were generated with the ggplot2 (v3.5.1) package (Wickham, 2009).

2.1.2 Obtaining sets of genes of interest for cross-referencing with DEGs

A comprehensive list of human transcription factors (TFs) was obtained from Lambert *et al.,* 2018. Splicing-related genes were identified from (Marques-Coelho *et al.*, 2021). Tip-cell related genes from (del Toro *et al.*, 2010; Goveia *et al.*, 2020; Zarkada *et al.*, 2021). EndoMT-related genes from several sources including scRNA-seq publications (Mintet *et al.*, 2015, 2015; Z. Li *et al.*, 2019; Tombor *et al.*, 2021; Ren *et al.*, 2023).

2.2 Methods to chapter 4 - Comprehensive and unbiased analysis of ZEB1 binding patterns in HUVECs via ChIP-seq

Details of the chromatin immunoprecipitation and sequencing methods are provided in Appendix 2.

2.2.1 Preprocessing of ZEB1 ChIP-seq data

The raw fastq files were subjected to initial quality control with FASTQC (v0.11.9) (Andrews, 2010) along with adapter identification. Cutadapt (v3.6) (Martin, 2011) was used to trim the reads of the identified Illumina Universal adapter AGATCGGAAGAG and to filter low quality reads with a minimum phred score of 20 to retain reads with a high precision of base call. Indexing of the human reference genome (GRCh38 primary assembly release 107) and subsequent alignment of the trimmed reads was performed with Bowtie2 (v2.4.1) (Langmead and Salzberg, 2012) in a paired manner. Qualimap (v2.2.1) (Okonechnikov, Conesa and García-Alcalde, 2016) was used to assess alignment statistics. The resulting SAM files from alignment were sorted, indexed and converted to BAM format with Samtools (v1.20) (Danecek *et al.*, 2021) *view*. Following this, the IgG control files were merged with

Samtools *merge* to generate a master control BAM file for downstream applications. Duplicated reads were marked and removed with Sambamba (v0.7.1) (Tarasov *et al.*, 2015) *markdup* while unmapped and multimapped reads were removed with the *view* function of Sambamba, specifying *-F "[XS] == null and not unmapped"* where [XS] is a tag used by Bowtie2 during alignment to signify the secondary alignment score, thereby indicating that a read with an [XS] tag is multimapping. The result was a BAM file containing only uniquely mapping reads and was confirmed using Samtools to view the BAM files. Reads that aligned to blacklisted regions of the genome, those that are known to produce artifacts and noise in ChIP-seq experiments introducing a bias, were removed with Bedtools (v2.30.0) (Quinlan and Hall, 2010; Quinlan, 2014) *intersect*. The blacklist region was downloaded from http://mitra.stanford.edu/kundaje/akundaje/release/blacklists/hg38-human/. Qualimap was used to assess read statistics post filtering and the *plotFingerprint* command of deepTools (v3.5.1) (Ramírez *et al.*, 2016) was used to plot enrichment profiles of the BAM files. Peaks were called with MACS2 (v2.2.7.1) (Zhang *et al.*, 2008) individually on ZEB1 replicates against the combined control file. As we used paired-end data the MACS2 argument -f BAMPE was used which skips the peak model building step of peak calling. The output .narrowPeak files were sorted by the -log10(p-value) column via *sort -k8,8nr*. ChIP-seq quality assessment was analysed with the ChIPQC (v1.38.0) (Carroll *et al.*, 2014) R package. To identify the presence of multimapped reads Samtools was used in conjunction with ripgrep (rg) on the command line to check for the presence of [XS] tags in reads with the following command structure: *samtools view -h BAMfile.bam | rg -c "XS:"* before and after filtering.

2.2.2 ZEB1 ChIP-seq data replicate handling

Replicate handling was performed by applying the Irreproducible Discovery Rate (IDR) tool (Li *et al.*, 2011) following the ENCODE ChIP-seq pipeline (https://github.com/ENCODE-DCC/chip-seq-pipeline2). This method statistically assesses peak reproducibility and is limited to two replicates. Quality metrics for each replicate were obtained with ChIPQC and deepTools *plotFingerprint* to evaluate enrichment, with the two replicates with the highest enrichment profiles selected for IDR analysis. As described in the IDR documentation, peaks were called with MACS2 with a relaxed p-value cut off of 1e-3. IDR was run with the default parameters and reproducible peaks passing the IDR cut off of 0.05 were extracted using the command *awk '{if($5 >= 540) print $0}*.

2.2.3 Peak annotation and genomic distribution

The R package ChIPseeker (v1.38.0) (Yu, Wang and He, 2015) was used to annotate peaks to transcripts and genes using the *annotatePeak* function, specifying the argument *level = "transcript"* or *"gene"* respectively, with the remaining default parameters. Promoter regions were defined as +/-1000bp from the transcription start site (TSS). ChIPseeker was also used to determine the genomic distribution of peaks and AnnotationDbi (v1.64.1) (Hervé Pagès *et al.*, 2023) was used to identify the gene biotype.

2.2.4 Visualisation of signal enrichment

BigWig files were generated using the *bamCoverage* function of deepTools with the normalisation method of bins per million (BPM) with a bin size of 20. In order to focus on the peak summits, we used a custom R script to identify the peak summit from the IDR output

file and created 2000 bp regions (+/- 1000bp from the peak summit) for input to plot the signal distance from peak summit. *computeMatrix reference-point* and *computeMatrix scale-regions* of deepTools were used to generate data matrices focused on the centre (peak summit) and whole gene length respectively. Finally, heatmaps of the data were plot using the *plotHeatmap* function. BigWig files were visualised in IGV viewer to assess regions of interest. Signalling track plots were produced using Gviz (v1.46.1) (Hahne and Ivanek, 2016) in R. Publicly available HUVEC data in BigWig format from ENCODE were also loaded into the IGV web app for visualisation, including DNase-seq (accession: ENCFF305BCB) to identify TSS/sites of open chromatin and H3K27me3 (accession: ECNFF616JNZ) for repressed regions.

2.2.5 Motif analysis of ChIP-seq peaks

The *findMotifsGenome* function of HOMER (v3.12) (Heinz *et al.*, 2010) was used to identify enriched motifs within the significant peaks using the same genome used for alignment. A custom R script was used to identify the peak summits from the IDR output file and created 200 bp regions (+/- 100bp from the peak summit) and was used as input for motif enrichment. Genome-wide prediction of TF motif locations were identified with the *scanMotifGenomeWide* function of HOMER. UpSet plots were generated in R using the UpSetR (v1.4.0) (Nils Gehlenborg, 2019) package.

2.2.6 Functional enrichment analyses

Functional enrichment analysis against the Gene Ontology Biological Process ontology (GOBP) (Ashburner *et al.*, 2000; The Gene Ontology Consortium *et al.*, 2023) via the GO.db annotation package within Bioconductor (v3.18) released October 2023, Kyoto

Encyclopedia of Genes and Genomes (KEGG) (Kanehisa and Goto, 2000; Kanehisa, 2019; Kanehisa *et al.*, 2023) database (v108.1) released October 2023 and HALLMARKS database via the msigdbr (v7.5.1) CRAN package released March 2022 was performed with clusterProfiler (v4.10.1) (Yu *et al.*, 2012). The *clusterProfiler::simply()* function was used to remove redundancy within the GOBP results with a similarity cutoff of 0.7.

2.2.7 Preprocessing of publicly available ERG HUVEC ChIP-seq data

Raw FASTQ files were downloaded from the Sequence Read Archive (SRA) with SRA Toolkit (v3.1.1) (https://github.com/ncbi/sra-tools) *prefetch* and *fasterq-dump* commands for runs SRR8428506 (ERG ChIP) and SRR8428507 (input) datasets. This data had a single library layout (i.e. not paired-end) and the original publication (Kalna *et al.*, 2019) did not generate replicates for the ChIP or input control. We followed the overall workflow of preprocessing as previously described but with modifications to handle the single-end data and lack of replicates. Briefly, we ensured that the correct parameters were used to handle single-end data and we removed the handling of peak replicates, since there were none, and continued with the peaks identified from the MACS2 peak calling output.

2.2.8 Preprocessing of publicly available ZEB1 TNBC ChIP-seq data

Raw FASTQ files were downloaded from ArrayExpress accession E-MTAB-8258 via an ftp script. This data had a paired library layout and consisted of 2 replicates for the ChIP and 2 for the input control. Since this dataset is paired-end and had 2 replicates for each condition we followed the workflow used to preprocess our original data as previously described.

2.2.9 Preprocessing of publicly available H3K4me1, H3K4me3 and H3K27ac HUVEC ChIP-seq data

Raw FASTQ files were downloaded from ENCODE for H3K4me1 (accession: ENCSR000AKL), H3K4me3 (accession: ENCSR578QSO), H3K27ac (accession: ENCSR000ALB) and the input control that was used for all 3 experiments (accession: ENCSR000ALG). The input control consisted of 3 fastq files of technical replicates that were concatenated post trimming. H3K4me1 consisted of 3 replicates, whereas H3K4me3 and H3K27ac had 2. Since H3K4me1 gives broad marks, peak calling with MACS2 was performed with the broad function. For H3K4me3 and H3K27ac the narrow peak calling function was applied. The replicate alignment files were pooled and peaks called on the single merged BAM file. Since all samples were single-end data we adjusted parameters accordingly.

2.2.10 Overlapping peaks analysis

To identify overlapping peaks between ZEB1 and ERG HUVEC ChIP-seq data and ZEB1 HUVEC and ZEB1 TNBC data we extracted the peak summit data from IDR analysis for ZEB1 data and MACS2 peak calling for ERG data and employed the *closest* function of Bedtools to identify all peaks in which the summits positions were no more than 200bp apart (i.e. +/-200bp from peak summit). Venn diagrams were drawn using the eulerr (v7.0.2) (J Larsson, 2024) R package and the overlap p-value was calculated by a permutation test using the *peakPermTest* from the ChIPpeakAnno (v3.36.1) (Zhu *et al.*, 2010) R package. The background pool of potential binding sites used in the permutation test was downloaded from https://hgdownload.soe.ucsc.edu/goldenPath/hg38/encRegTfbsClustered/ and the permutation number was set to 500. The overlap between ZEB1 HUVEC and histone data

was performed on the 400bp region around ZEB1 peak summits and the full histone peak using the *intersect* command of Bedtools.

2.2.11 Transcription factor cross reference

A comprehensive list of human transcription factors was obtained from Lambert *et al.,* 2018 and was cross referenced with significant peaks identified from IDR analysis with R.

2.2.12 Overlap of RNA-seq and ChIP-seq data

R was used to compare DEGs of HUVEC ZEB1 KD RNA-seq data previously generated with the annotated peaks with the ChIP-seq data to identify overlapping and unique gene lists.

2.3 Methods to chapter 5 - Analysis of publicly available endothelial cell scRNA-seq datasets revealed Zeb1 to be enriched in specialised endothelial subpopulations driving proliferative and immunoregulatory programs across diverse tissues

All scRNA-seq analyses were performed with Seurat (v5.1.0) (Hao *et al.*, 2024). UMAPs, featureplots, dotplots and clustered dotplots of gene expression across clusters were generated with scCustomize (v2.1.2) (Marsh, 2021) using the *DimPlot_scCustom()*, *FeaturePlot_scCustom()*, *DotPlot_scCustom()* and *Clustered_DotPlot()* functions respectively.

Several of the published datasets used in this chapter provided t-SNE or UMAP dimensions alongside counts data, which allowed processing of the Seurat objects to remove

cells that were filtered out in the original publication and reproduce dimensionality reduction plots. This was particularly useful to increase reproducibility, as attempts to repeat analyses of several different published scRNA-seq datasets based on accompanying methods often yielded varying results, even with robust attempts to use matching tool and package versions with strictly maintained environments and virtual machines (VM).

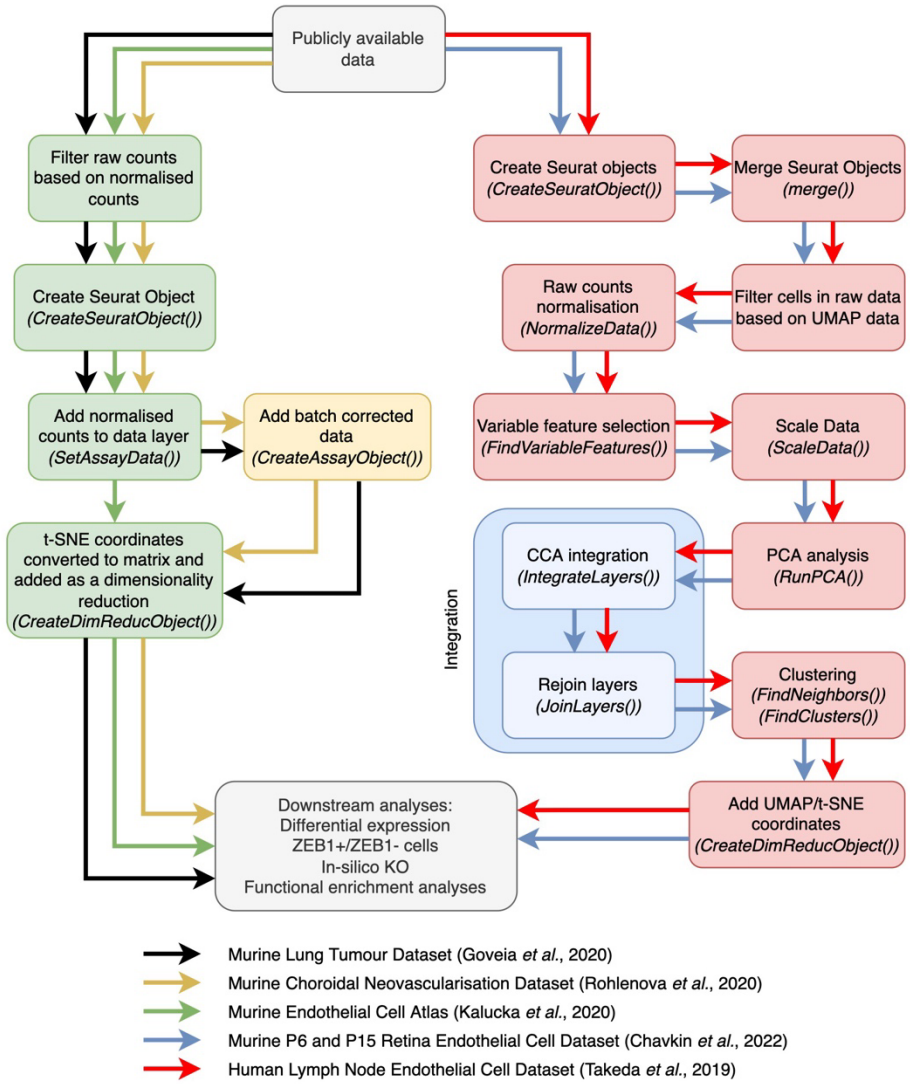


Figure 2. ***Overview of the scRNA-seq pipelines used for the analysis of publicly available datasets.***

Workflow outlining the major computational steps in the scRNA-seq analysis applied in this thesis: data acquisition, quality control, normalisation , feature selection, clustering, integration, t-SNE/UMAP plotting and downstream analyses.

2.3.1 Publicly available single-cell transcriptome atlas of murine endothelial cells data processing

Raw counts, normalised counts, metadata and t-SNE dimension data of the endothelial cell atlas were downloaded from the EC atlas (https://carmelietlab.sites.vib.be/en/software-tools) (Kalucka *et al.*, 2020). Raw counts were filtered to include only the cells present in the normalised counts data which reflect those that remained post filtering from the original publication (Kalucka *et al.*, 2020). A Seurat object was generated from the filtered raw data with the *CreateSeuratObject()* function. Normalised counts were added to the "data" layer of the object with the *SetAssayData()* function. T-SNE coordinates were converted into a matrix and added as a dimensionality reduction to the Seurat object using *CreateDimReducObject()*. Normalised counts and t-SNE data for spleen EC scRNA-seq data was also extracted from the EC atlas (https://carmelietlab.sites.vib.be/en/software-tools) (Kalucka *et al.*, 2020). This generated a reproducible example of the data present on the EC atlas webserver (https://carmelietlab.sites.vib.be/en/software-tools) (Kalucka *et al.*, 2020).

2.3.2 Publicly available P6 and P15 retina endothelial cell scRNA-seq dataset processing

Raw counts data were obtained from the NCBI GEO database with accession number GSE169039 (Chavkin *et al.*, 2022). Individual Seurat objects for p6 and p15 data were created with *CreateSeuratObject()* and were subsequently merged with *merge()*. The UMAP co-ordinates provided by Chavkin *et al.,* (2022) were used to filter the Seurat objects to include only the cells that were retained in the original analysis (Chavkin *et al.*, 2022). The data were

then subjected to normalisation, variable feature identification, data scaling and PCA analysis with *NormalizeData()*, *FindVariableFeatures()*, *ScaleData()*, and *RunPCA()* respectively. Integration was performed using the CCA method with *IntegrateLayers()* before rejoining the layers in the Seurat object with *JoinLayers()*. Clustering was performed on the first 13 dimensions with a resolution of 0.5 using the *FindNeighbors()* and *FindClusters()* arguments. UMAP co-ordinates were added, ensuring correct cell to cell data matching. Cell phenotype was assigned based on the meta data provided by (Chavkin *et al.*, 2022) to match the original publication, but we remained critical of the markers that were used and performed our own unbiased checks (blind to the UMAP visualisation of clusters). Cluster markers and p6/p15 markers were identified with *FindAllMarkers()* while markers of individual phenotypes between p6 and p15 were found with *FindMarkers()*. We assigned cells to Zeb1 expression status by specifying cells with expression levels > 0 to be Zeb1+ and 0 expression to be Zeb1-. Differential expression analysis between Zeb1+ and Zeb1- cells was calculated with *FindMarkers()*. Virtual *in-silico* KO of Zeb1 was performed with the scTenifoldKNK package (v1.0.2) (Osorio *et al.*, 2022) function *ScTenifoldKNK()* specifying qc = TRUE on the raw scRNA-seq data matrix of tip cells only. Features were filtered to include those with a mean expression of > 0.1 and ribosomal/mitochondrial genes were removed prior to *in-silico* KO. Visualisation of the *in-silico* KO results was inspired by (Guduric-Fuchs *et al.*, 2024). Functional enrichment analyses against GOBP and KEGG databases (see section 2.1.1 for versions) was done with clusterProfiler and *clusterProfiler::simplify()* function was used to remove redundancy within the GOBP results with a similarity cutoff of 0.7. Volcano plots were generated with ggplot2 .

2.3.3 Publicly available choroidal neovascularisation (CNV) endothelial cell scRNA-seq dataset processing

The raw, normalised and batch-corrected counts accompanying a published CNV scRNA-seq dataset (Rohlenova *et al.*, 2020) were downloaded from the Murine ECTax (https://carmelietlab.sites.vib.be/en/software-tools) along with t-SNE co-ordinates and cell phenotype assignments. The preprocessing was largely the same as for 2.3.1, except batch-corrected counts were provided and added as an assay with *CreateAssayObject()*. *In-silico* KO of Zeb1 was performed in lesion ECs only. A comprehensive list of mouse TFs for cross-referencing was obtained from https://esbl.nhlbi.nih.gov/Databases/KSBP2/Targets/Lists/TranscriptionFactors/ . Data and plots of Zeb1 expression throughout the cell cycle was obtained from the scCycle tool (https://carmelietlab.sites.vib.be/en/software-tools).

2.3.4 Publicly available mouse lung tumour endothelial cell scRNA-seq dataset processing

The raw, normalised and batch-corrected counts accompanying a published murine lewis lung carcinoma scRNA-seq dataset (Goveia *et al.*, 2020) were downloaded from the Lung tumor ECTax (https://carmelietlab.sites.vib.be/en/software-tools). The analysis followed section 2.3.3, except marker identification analysis was tailored to the phenotypes in this dataset and *in-silico* KO of Zeb1 was performed in tip cells of the tumour ECs only (untreated).

2.3.5 Publicly available human lymph node endothelial cell scRNA-seq dataset processing

The aligned scRNA-seq data in barcodes, features and matrix files for the 6 samples of a lymph node scRNA-seq dataset (Takeda *et al.*, 2019) were downloaded from the NCBI GEO database under accession code GSE124494. Processing was similar to 2.3.2. Briefly, each sample was coerced into a Seurat object and all 6 objects were merged. The merged Seurat object was normalised and variable features identified. The data was then scaled while regressing on percentage of mitochondrial and ribosomal genes as well as the total UMI count as per the original publication (Takeda *et al.*, 2019). PCA analysis was run before integration of the data with the CCA methods and layers rejoined. Following the methodology of the publication, clustering was performed with the first 30 dimensions with a resolution of 0.5. After filtering contaminating clusters (see section 5.3.5), the subset Seurat object was re-scaled and clustered with the same parameters and UMAP dimensions calculated with *RunUMAP()*. *In-silico* KO of ZEB1 was carried out in LEC II cell phenotype only (see section 5.3.5).

2.4 Methods to chapter 6 - A combined scRNA-seq and text-mining approach elucidated putative functions of Zeb1 in partial EndoMT

2.4.1 Gathering raw sequencing data

Raw sequencing data was downloaded from ArrayExpress: E-MTAB-7895 (Forte *et al.*, 2020) via ftp with a script provided by ArrayExpress. The ftp script was executed with the following command: *nohup cat ./E-MTAB-7895-unix-ftp.txt | sh > ftp_files.log &*

2.4.2 Aligning raw sequencing data

Cellranger *(v7.0.1)* ('10XGenomics/cellranger', 2024) *count()* function was run on samples MF17010, MF17013, MF17014, MF17015, MF17016, MF17017, MF17018 to align against the refdata-gex-mm10-2020-A reference transcriptome. The aligned, filtered matrices were taken forward for further analysis.

2.4.3 scRNA-seq data preprocessing

ScRNA-seq analysis were carried out under R *(v4.3.3)*. The filtered aligned matrices for each sample were loaded with Seurat (*v5.1.0*) (Hao *et al.*, 2024). The *Read10X()* function was used to read in the matrices and Seurat objects were created with the *CreateSeuratObject()* function. The individual Seurat objects were merged with the *merge()* function. For this analysis, the samples were not integrated as this would attempt to reduce the differences observed between timepoints and the UMAP visualisation of clusters did not reveal separation based on timepoint. This was also reflected in the original publication (Forte *et al.*, 2020) and another publication in which the original dataset was reanalysed (Tombor *et al.*, 2021). The layers were rejoined using the *JoinLayers()* function for quality control. We filtered genes that had an RNA count of > 18,000 and filtered cells that expressed < 400 and > 4500 features and a mitochondrial gene expression proportion of > 10%. Data were normalised with the *NormalizeData()* object with the "LogNormalize" method and a scale factor of 10,000. Next, variable features were identified using *FindVariableFeatures()* and data scaled using *ScaleData()*, regressing on the mitochondrial gene percentage. PCA was calculated with *RunPCA()*. Subsequently, the first 10 PCA dimensions were used to calculate Neighbours and Clusters with *FindNeighbours()* and *FindClusters()* respectively with a resolution of 0.6. UMAP was calculated with *RunUMAP()* with 10 dimensions.

2.4.4 Subsetting ECs from the dataset

The scCustomize *(v2.1.2)* (Marsh, 2021) package was used to visualise UMAP, Feature plots and Clustered dot plots via *DimPlot_scCustom()*, *FeaturePlot_scCustom()* and *Clustered_DotPlot()* functions respectively. The Seurat object was subset for ECs based on Pecam1+/Cdh5+ expression and the standard preprocessing workflow described above was run to perform reclustering.

2.4.5 Identifying EC phenotypes

Automated cell type assignment of ECs was performed with ScType (Ianevski, Giri and Aittokallio, 2022) specifying "Heart" as the tissue of interest. Cardiac EC phenotypes were annotated based on marker genes (Table 1) identified from a published single-cell atlas of murine endothelial cells (Kalucka *et al.*, 2020) and cardiac EC scRNA-seq focussed studies (McCracken *et al.*, 2022; Z. Liu *et al.*, 2023; Long *et al.*, 2023). EndoMT related genes were identified from scRNA-seq publications (Z. Li *et al.*, 2019; Tombor *et al.*, 2021; Ren *et al.*, 2023; Wälchli *et al.*, 2024) and non scRNA-seq (Mintet *et al.*, 2015) (Table 1) as per section 2.1.5. Angiogenic EC markers were collated from the above, as well as other scRNA-seq EC studies (Goveia *et al.*, 2020; Rohlenova *et al.*, 2020) (Table 1). Differential expression analysis of the phenotype marker genes across clusters was performed with *FindAllMarkers()*. Module scores of each phenotype were calculated with the *AddModuleScore()* function of Seurat.

***Table 1**. Endothelial cell phenotype markers.*

EC phenotype	Markers
Capillary	*Car4, Hspa1a, Rgcc, Cd36*
Arterial	*Fbln5, Gja4, Gja5, Stmn2*
Venous	*Cfh, Ptgs1, Mgp, Vcam1*
Proliferating	*Mki67, Top2a*
Angiogenic	*Apln, Tmsb10, Cldn5, Lxn, Pgf, Pfn1, Fscn1, Actb, Actg1, Adm, Aplnr, Mcam, Lama4, Foxo1, Lrg1, Plvap, Col4a2, Trp53i11, Col15a1, Col4a1*
Pericyte	*Vtn, Abcc9, Pdgfrb*

2.4.6 Comparison of EndoMT signature with AlZaim et al (2024)

Module scores of the EndoMT related genes (EndoMT signature) extracted from literature described above and the EndoMT signature used by AlZaim *et al.,* (2024) (Table 2) were calculated with *AddModuleScore()*. Endothelial and mesenchymal scores were calculated for each cell through computing average RNA-seq z-scores for endothelial markers and mesenchymal markers (Malagoli Tagliazucchi *et al.*, 2023; AlZaim *et al.*, 2024). EndoMT scores were calculated by subtracting the average endothelial marker gene z-scores from the average mesenchymal z-scores (Malagoli Tagliazucchi *et al.*, 2023; AlZaim *et al.*, 2024). These analyses were heavily inspired by AlZaim *et al.,* (2024).

Table 2. Gene signatures for EndoMT derived from literature, EndoMT signature used by AlZaim et al., (2024) and endothelial-like.

Signature	Genes
Our EndoMT (mesenchymal) signature	*Acta2, Acvrl1, Apoe, Atxn1, Bgn, Bmpr1a, Bmpr2,Cd44, Cdkn1a, Cnn1, Col1a1, Col1a2, Col3a1, Col5a2, Col8a1, Ctnnb1, Dcn, Edn1, Eln, Enpp2, Fn1, Gsk3b, Hey1, Hey2, Icam1, Lum, Mfap4, Mfap5, Mgp, Mmp14, Mmp2, Mmp9, Nog, Notch3, Pdgfra, Pdgfrb, Plaur, Postn, Rgs5, S100a4, Sele, Selp, Serpine1, Smad1, Smad3, Smad5, Smad7, Smtn,Snai1, Snai2, Tagln, Tgfb1, Tgfb2, Tgfbr2, Thbd, Thy1, Timp1, Tnc, Tnr, Tnxb, Tpm2, Vcam1, Vim, Zeb2*
AlZaim *et al.*, (2024) mesenchymal (EndoMT)	*Acta2, Fap, S100a4, Aifm2, Col1a1, Col3a1, Twist1, Zeb2, Snai1, Snai2, Smad2, Smad3, Smad4, Yap1, Kdm4b, Mapk8, Mapk14, Tgfb1, Tgfb2, Tgfb3, Tgfbr1*
Endothelial	*Pecam1, Cdh5, Vwf*

2.4.8 Transcription factor activity analysis

Transcription factor activity analysis was carried out with the R package decoupleR (v2.9.7) (Badia-i-Mompel *et al.*, 2022) against the CollecTRI resource (Müller-Dott *et al.*, 2023) as per the reference manual (https://saezlab.github.io/decoupleR/articles/tf_sc.html). These analyses were inspired by AlZaim *et al.,* (2024).

2.4.9 Trajectory analysis

Trajectory analysis was performed with Monocle3 (v1.3.7) (Cao *et al.*, 2019), understanding the potential limitations of graph-based analyses (Chari and Pachter, 2023). Cells at days 1-7 post myocardial infarction were isolated from the data and subjected to reclustering. The Seurat object was converted into a cell data set object with the *as.cell_data_set()* function. Subsequent processing with Monocle3 followed the reference

manual. Briefly, the *estimate_size_factors()*, *cluster_cells()*, *learn_graph()* and *order_cells()* functions were used in that order. Prior to *order_cells()*, we calculated the earliest principal node to be the most endothelial-like cluster based on expression of endothelial markers *Pecam1* and *Cdh5*, which was Capillary1 (see results section). This cluster was denoted as the root (start) of the trajectory, since EndoMT is a transition originating from endothelial cells with a relative increase in EC marker expression (Platel *et al.*, 2019). Separate proliferating and EndoMT trajectories were selected with *choose_graph_segments()* by selecting the start and end points of the trajectories. The flow of functions described above was applied to each separate trajectory and the resulting pseudotime data was added to the original Seurat object as metadata to plot for visualisation. The *graph_test()* function was used to identify genes whose expression changed significantly across pseudotime.

2.4.10 ZEB1 expression analyses

Average expression and percent of cells expressing was calculated with the *AverageExpression()* and *Percent_Expressing()* functions of Seurat. Zeb1+ and Zeb1- DE analysis was performed as described in section 2.3.2 for all ECs in the data (not split by days post myocardial infarction). *In-silico* KO of Zeb1 for all ECs in the dataset was performed as described in section 2.3.2. Functional enrichment analyses were performed as described in section 2.3.2.

2.4.11 Text mining

Articles were retrieved from the PubMed Central database utilising the Entrez (Sayers, 2022; Kans, 2024) package in a custom Python *(v3.8.3)* script in line with copyright

rules and terms of use. *"(endMT[AB] OR endoMT[AB]) AND open access[filter]", mindate = "2013", maxdate = "2024"* was used as a search term to retrieve papers in XML format between 2013 and 2024 that mention endMT or endoMT in the abstract. The results presented are from running the code specifically on 25th April 2024, therefore articles within the PubMed Central database deposited after this date are not included in the analysis. The open access filter was specified to perform text-mining analyses within copyright rules. The retrieved publications were filtered to retain only research articles, excluding reviews etc. The abstracts of the returned research articles were used for subsequent text mining analysis.

Initially, custom python code was written to iterate through abstracts and extract gene/protein names based on a dictionary collated from several sources. However, there are several considerations with this approach including dealing with synonyms, naming across species and conversion into a standard naming convention. To improve efficiency, abstracts were subjected to named entity recognition (NER) via the Tagger (Jensen, 2016, 2024) tool to extract protein names and collapse synonyms to a preferred naming convention. This was performed under an OpenSUSE Leap *(v15.5)* virtual machine through VirtualBox *(v7.0)* software and required some troubleshooting with compiling. Tagger (Jensen, 2016, 2024) was run following the documentation detailed in the GitHub repository (Jensen, 2024). It was understood that scRNA-seq naming of features is at the gene level while this text-mining approach is at the protein name level. Results were carefully validated taking this into consideration.

2.4.12 Network analyses

Network analyses were performed with Cytoscape *(v3.9.1)* (Shannon *et al.*, 2003). The retrieved protein names in Ensembl format (ENSP) were input into the stringApp *(v1.6.0)* (Doncheva *et al.*, 2019) to generate a protein-protein interaction (PPI) network with a minimum confidence score of 0.4. Hub genes were identified from the network via 5 algorithms implemented in the cytoHubba *(v0.1)* (Chin *et al.*, 2014) app: Degree, Radiality, Closeness, MNC and MCC. The results from each algorithm were combined to obtain a final list of unique hub proteins. MCODE *(v2.0.0)* (Bader and Hogue, 2003) was then used to identify sub clusters within the network with an MCODE score of ≥ 5. A direct ZEB1 network was generated through selecting undirected first neighbour nodes of ZEB1.

2.4.13 Comparison of text mining with bulk RNA-seq EndoMT publication

DEGs were extracted from the supplementary of a bulk RNA-seq EndoMT publication (Bronson, Lyu and Xiong, 2023) and cross referenced with the text-mined list of genes/proteins. Venn diagram was generated with InteractiVenn (Heberle *et al.*, 2015).

2.4.14 Text-mining functional enrichment analysis

Functional enrichment analysis for the text-mining results was carried out with the same methodology described for the scRNA-seq analysis, although dotplots associated with the MCODE clustering were generated with a previous version of clusterProfiler (v4.8.0) and will be updated in future to align with the rest of the thesis.

2.5 Methods to chapter 7 - Adult inducible knockout of Zeb1 does not alter mouse retinal vascular area or endothelial cell number

Full experimental details for the inducible endothelial-specific Zeb1 knockout mouse model, tamoxifen administration, cDNA synthesis, digital droplet PCR and associated data analysis are provided in Appendix 3.

2.5.1 Endothelial cell isolation from lung tissue

Primary murine endothelial cells were isolated from the lungs of $ZEB1^{fl/fl}$ Cdh5 Cre-$ERT2^{+/-}$ and $ZEB1^{fl/fl}$ Cdh5 Cre-$ERT2^{-/-}$ mice following Tamoxifen induction as outlined above. Mice were euthanised via cervical dislocation and death confirmed by permanent disruption of blood flow. Lung tissues were then processed using the Miltenyi Lung Dissociation Kit. Whole lungs were dissected out, rinsed 4-5 times in ice-cold PBS to remove blood, then transferred in basal endothelial cell media (Promocell). The tissue was finely minced and incubated with the lung dissociation kit enzyme mix (Miltenyi) at 37°C for 2 hours with intermittent agitation to facilitate digestion. The resulting cell suspension was passed through 70µm and 30µm smart strainers (Miltenyi) and combined with 2.5mL of PEB sorting buffer, generating a single-cell suspension. After digestion, total cells were counted using a haemocytometer. 10% of the total cell suspension was set aside, pelleted at 300xg, the supernatant discarded and the pellet stored at -80°C for subsequent RNA extraction as the input fraction. The remaining cells were pelleted at 100xg, the supernatant discarded and the pellet resuspended in CD31 microbeads (Miltenyi) at 10µL of beads plus 90µL of PEB sorting buffer per 10^7 cells. This mixture was rotated end-to-end at 4°C for 30 minutes before being pelleted at 100xg at 4°C, resuspended in 500µL of PEB per 10^7 cells and transferred to

LS columns positioned in a Miltenyi magnet primed with 3mL of PEB. The columns were washed three times with 3mL of PEB and the flow-through was collected as the $CD31^-$ fraction. The column was then removed from the magnet and 3mL of PEB was applied with the plunger to elute the $CD31^+$ fraction. Finally, both $CD31^-$ and $CD31^+$ fractions were pelleted at 300xg, the supernatant discarded and the pellets stored at -80°C for subsequent RNA or protein extractions.

2.5.2 RNA extraction

Unless otherwise specified, total RNA was isolated using the QIAGEN RNeasy kit. Briefly, cell pellets were resuspended in 350µL of RLT buffer mixed with 350µL of 70% ethanol and transferred onto a QI-shredder column. The column was centrifuged at 8000xg for 15 seconds, after which the flow-through was discarded. Next, the column was washed by adding 700µL of RW1 buffer, followed by centrifugation at 8000xg for 15 seconds and discarding the flow-through. A volume of 500µL RPE buffer was applied to the column, centrifuged at 8000xg for 15 seconds, and the flow-through was discarded. This rinse step was repeated using another 500µL of RPE buffer, with centrifugation extended to 2 minutes. To dry the membrane, the column was centrifuged without any additional buffer at 16,000xg for one minute. RNA was eluted by adding 30µL of RNase-free water directly to the column, followed by centrifugation at 8000xg for one minute. Concentration and purity of the RNA were assessed using a NanoDrop™ (ThermoFisher Scientific) and samples were stored at −80°C.

2.5.3 Retina dissection

Retina were dissected from whole eyes taken from ZEB1$^{fl/fl}$ Cdh5 Cre-ERT2$^{+/-}$ and ZEB1$^{fl/fl}$ Cdh5 Cre-ERT2$^{-/-}$ following Tamoxifen induction as outlined above. Both retina per mouse were processed with the best quality image of the pair being used in analysis, resulting in one retina per mouse.

2.5.4 Retina antibody staining

Retina were washed in PBS for two hours, changing to fresh PBS every 15 minutes at room temperature in a 96 well plate on a rocking platform. Permeabilisation-blocking buffer (PBB) (PBS, 4% bovine serum albumin (BSA), 0.5% Triton-X) was added to the tissue and kept on a rocking platform at 4°C for two hours to prevent non-specific binding of antibodies. Primary antibodies were prepared in PBB at the following concentrations just before use: 1:100 Cd31 (550274, BD Pharmingen), 1:100 Erg (ab92513, abcam). The PBB was removed from the tissue and 70µL of the primary antibody solution was added to each retina and incubated at 4°C for 2 nights on a rocking platform. Following this the tissue was washed in PBS-X (PBS, 0.5% Triton-X) for 4 hours changing to fresh PBS-X every 30 minutes at RT on a rocking platform. The second antibody solution was prepared just before use with the following concentrations: 1:500 Donkey Anti-Rat Alexa Fluor 488 (A21208, Thermo Fischer Sci.), 1:500 Goat Anti-Rabbit Alexa Fluor 555 (A21428, Thermo Fisher Sci.). The PBB was removed and 100µL of the secondary antibody solution was added to each retina and incubated at 4°C for 2 nights on a rocking platform. Samples were protected from light by wrapping in tin foil. After 2 nights the tissue was washed in PBS-X for 4 hours, changing to fresh PBS-X every 30 minutes at RT on a rocking platform. Following this, the retina were mounted flat on superfrost glass slides by making four cuts to create a petal shape. Two drops

of fluoroshield were placed on each retina and the cover slip was positioned and sealed with nail varnish. The mounted slides were left to cure overnight protected from light at 4°C.

2.5.5 Retina imaging

Retina were imaged via confocal microscopy and optimised settings as a 5*5 tile scan taken at 20x magnification centred on the optic nerve with Z-stack taken at 2.5µm steps, resulting in a .lif file containing a Z-stack for each sample.

2.5.6 Retina image analysis

Image analysis was carried out via FIJI (ImageJ) v2.1.0/1.53c (Schindelin *et al.*, 2012) in a blind manner, with genotype only known once analysis for all samples was complete. Tissue area in mm^2 was measured through creating a maximum intensity Z-stack, converting the scale to mm, measuring the entire area of the image followed by using the wand tool to subtract the non-tissue area (including any stain blotches) from the total image area to give tissue area in mm^2. Cd31+ area in mm^2 was determined by splitting the colour channels of the maximum intensity Z-stack, selecting the Cd31+ channel, auto adjusting the brightness/contrast, subtracting the background via the rolling ball radius method at 50.0 pixels, further auto brightness/contrast adjustment, removing noise using the median filter at 2.0 pixels and auto thresholding the image with the Li method. The threshold area was then measured in mm^2. Cd31+ area was normalised to tissue area by calculating the Cd31+ area mm^2/mm^2 tissue area. The number of Erg+ nuclei was performed by selecting the Erg+ channel of the image maximum intensity Z-stack, applying auto brightness/contrast adjustment, subtracting the background through the rolling ball radius process set to 50.0

pixels, auto threshold detection via the Li method, performing the watershed process to split any groups of threshold areas into individual particles and the number of particles weas analysed with particle sizes between 5-Infinity micron^2 in order to avoid detection of individual pixel noise. The number of Erg+ nuclei was normalised to the ERG+ nuclei/mm^2 tissue area.

Analysis of the vascular plexus of the retina was done by selecting three regions of interest between macro-vessels, each 225µm x 225µm and split into the individual layers by scrolling through the Z-stack and extracting the relevant Z-slices for each plexus. The quantification of Cd31 area was the same as described above.

Both manual and automated thresholding methods were evaluated and found to produce consistent results. Image analysis for each retina was repeated on three separate days, and mean values were used to minimise user bias.

The data collected from the FIJI analysis workflow described above were processed in GraphPad Prism v9.2.0 (https://www.graphpad.com/). The data are represented as columns and plot as a scatter plot with bar, displaying the value for each sample and the mean with Standard Deviation (SD). Statistical analyses to determine significance were performed using two-tailed unpaired t-test with a significance threshold of $P < 0.05$.

Chapter 3: ZEB1 knockdown via siRNA in HUVECs revealed a modulation of adhesion, angiogenesis and inflammation related processes and uncovered a predicted ZEB1 regulatory network

3.1 Introduction

Endothelial cells (ECs) are key mediators of vascular homeostasis, serving critical roles in angiogenesis, barrier function and inflammation throughout development and disease (Augustin and Koh, 2024). The transcription factor ZEB1 has been extensively studied in the context of epithelial-to-mesenchymal transition (EMT), where it orchestrates cellular reprogramming and a shift in phenotype (Zhang, Sun and Ma, 2015). During this process, epithelial cells express mesenchymal markers and lose epithelial markers along with a reduction in adhesive behaviour, becoming increasingly invasive and migratory (Nieto *et al.*, 2016). Recent studies, however, have increasingly implicated ZEB1 in endothelial biology, suggesting that it may similarly regulate endothelial plasticity and influence angiogenic processes (Drápela *et al.*, 2020; Lan *et al.*, 2022). Endothelial-to-mesenchymal transition (EndoMT) is a processes analogous to EMT, in which endothelial cells lose their identity and shift towards a mesenchymal-like state. Indeed, as with EMT, inflammation, loss of cell polarity and adhesion and an increase in a motile, migratory-like state are observed during EndoMT (Cho *et al.*, 2018; Peng *et al.*, 2022; Singh *et al.*, 2024). By association, ZEB1 has been implicated as a driver of EndoMT (Fang, Hultgren and Hughes, 2021). However, a recent RNA-seq study that stimulated endoMT in primary human pulmonary microvascular endothelial cells (HPMVECs), primary human aortic endothelial cells (HAECs) and primary human umbilical vein endothelial cells (HUVECs) through TGFB1 and IL1B stimulation (both

of which are canonical inducers of endoMT) did not identify ZEB1 to be differentially expressed (Bronson, Lyu and Xiong, 2023), suggesting the role that ZEB1 may play in EndoMT is perhaps context specific, with the exact mechanisms remaining to be understood.

Previous RNA-seq studies have found ZEB1 to regulate inflammation pathways and phenotypes in models of breast cancer through inducing expression of inflammatory cytokines IL6 and IL8 (Katsura *et al.*, 2017). Furthermore, ZEB1 has also been shown to induce alternative splicing of fibroblast growth factor receptors through downregulation of epithelial splicing regulatory proteins (ESRPs) (Horiguchi *et al.*, 2012). RNA-seq analyses of ZEB1 in glioblastoma stem cells identified regulators of invasion and migration to be activated by ZEB1 expression (Rosmaninho *et al.*, 2018). ZEB1 was also found to stimulate angiogenesis in breast cancer cells, with siRNA knockdown (KD) of ZEB1 reducing capillary tube formation in HUVECs (Liu *et al.*, 2016). These current studies surrounding ZEB1 RNA-seq reveal a multifaceted role of ZEB1, in particular at the cross-talk between endothelial cells and tumour progression and the pro-angiogenic phenotype in ECs.

To further dissect the regulatory landscape governed by ZEB1 in endothelial cells, we employed siRNA-mediated knockdown (KD) of ZEB1 in human umbilical vein endothelial cells (HUVECs) followed by bulk RNA sequencing (RNA-seq). This approach enabled a comprehensive analysis of the transcriptomic alterations induced by ZEB1 reduction, highlighting differentially expressed genes (DEGs) associated with cell adhesion, inflammatory responses and EndoMT. The study further integrates functional enrichment and network analyses to predict regulatory interactions and identify downstream effectors of ZEB1 which are implicated in angiogenic and immune pathways.

Here, we present a detailed characterisation of the transcriptomic landscape following ZEB1 KD in HUVECs, elucidating a putative regulatory network that positions ZEB1

as a central modulator of endothelial cell function. Our findings provide insights into the mechanisms through which ZEB1 may influence vascular development and pathology, setting the stage for future studies aimed at understanding the interplay between endothelial identity, angiogenesis and inflammation. Such information will be critical to fully interpret subsequent experimental chapters in this thesis.

3.2 Hypothesis and aim

Hypothesis: *ZEB1* KD via siRNA in HUVECs will result in the differential expression of angiogenesis related genes and pathways.

The hypothesis was tested through applying RNA-seq analysis techniques to address the following aim:

Aim: To assess the transcriptomic consequences of *ZEB1* knockdown in HUVECs with a focus on identifying key regulatory pathways, network features and potential downstream effectors.

3.3 Results

3.3.1 ZEB1 KD in HUVECs resulted in 296 differentially expressed genes including canonical tip endothelial cell and endothelial-to-mesenchymal transition markers

In order to elucidate the regulatory mechanisms of ZEB1 in endothelial cells, we performed knockdown (KD) of ZEB1 in HUVECs via siRNA. We first assessed the efficiency of ZEB1 KD and found significant downregulation of ZEB1 (log2FC = -0.59, adjusted p-value =

7.84E-12) (Fig 3.1B). In addition, confirmation at the protein level by western blot identified a 51% KD (performed by Kathryn Green, not shown here). Principal component analysis did not identify the ZEB1 KD to be the principal source of variation between the samples, likely confounded by the HUVEC_control_3 sample (Fig 3.1A). It did however contribute to 26.09% of the overall variation. We performed downstream analyses being critical of this observation and are currently repeating the experiment.

Subsequent RNA-seq analysis identified 296 differentially expressed genes (DEGs) with 194 upregulated and 102 downregulated genes following ZEB1 KD (Fig 3.1C). We did not apply a log2FC threshold and significance was determined by an adjusted p-value threshold (padj < 0.05). The log2FC threshold was not applied since 296 significant DEGs is a manageable number and further filtering was not required to focus on a subset of DEGs, aiming instead to capture and analyse all significant expression changes upon ZEB1 KD. Among the top upregulated DEGs identified by both significance and log2FC was LLGL2 (Fig 3.1D), a gene that encodes a polarity protein that has been shown to be required for branching morphogenesis during placental development (Sripathy, Lee and Vasioukhin, 2011). Furthermore, ZEB1 repressed LLGL2 in colorectal cancer cells (Spaderna *et al.*, 2008) in agreement with the observed upregulation upon ZEB1 KD in HUVECs. GRB7 was also a highly upregulated DEG (Fig 3.1D). Importantly, GRB7 is associated with a pro-angiogenic state and knockdown of GRB7 in HUVECs resulted in reduced proliferation, migration, invasion and tube formation (Xu *et al.*, 2021). Significant upregulation of GRB7 upon ZEB1 KD in HUVECs shown here suggests that ZEB1 may supress key pro-angiogenic

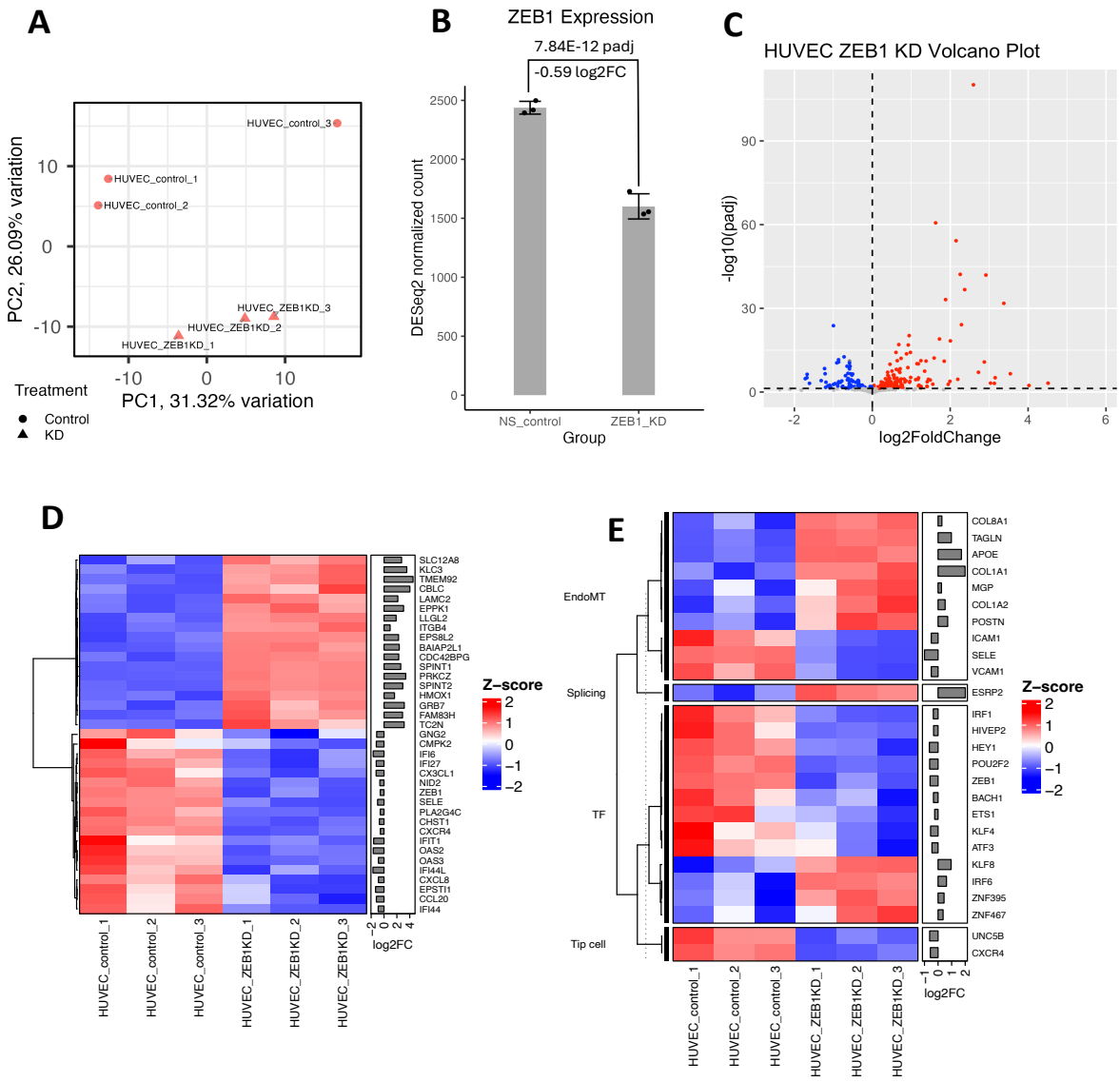


Figure 3.1. ***ZEB1 knockdown in HUVECs resulted in 296 significantly differentially expressed genes including downregulation of tip cell markers UNC5B and CXCR4.***

(A) Principal component analysis (PCA) showed clear separation between non silenced control (Control) and ZEB1 siRNA knockdown (KD), but identified ZEB1 KD to not be the principal cause (PC1) of variation between samples.

(B) Mean DESeq2 normalised counts of ZEB1 in non-silenced (NS_control) and ZEB1 KD (ZEB1_KD) (n=3 per group) revealed a significant KD of ZEB1. The standard deviation is shown and p-value was adjusted with the default Benjamini-Hochberg method within DESeq2.

(C) Volcano plot displaying the regulation of the 296 significant differentially expressed genes (DEGs). 194 genes were upregulated and 102 were downregulated, represented by red and blue dots respectively. Differential expression was determined with an adjusted p-value < 0.05.

(D) Heatmap displaying the scaled expression of the top upregulated and downregulated genes identified by both significance and fold change (i.e. those with the lowest adjusted p-values and the greatest absolute fold changes). Log2FC of the genes is shown as a bar chart.

(E) Heatmap displaying the scaled expression of genes related to EndoMT, splicing, Transcription factors (TFs) and tip EC markers. Log2FC of the genes is shown as a bar chart.

processes. Within the top downregulated DEGs were multiple genes related to immune and inflammation processes (IFI6, IFI27, CX3CL1, IFIT1, OAS2, OAS3, IFI44L) (Fig 3.1D), suggesting that ZEB1 KD significantly modulates the immune response in HUVECs and that un-perturbed ZEB1 expression may act to sustain inflammatory and immune response genes in endothelial cells.

Since ZEB1 is a known regulator of epithelial-to-mesenchymal transition (EMT), we investigated the potential regulation of genes related to endothelial-to-mesenchymal transition (EndoMT) in response to ZEB1 KD in HUVECs. Indeed, we identified differential expression of 10 EndoMT-related genes (Fig 3.1E) from a curated list of genes derived from relevant literature (see methods section 2.1.5). Within the 10 genes, known mesenchymal markers TAGLN, COL1A1 and COL1A2 were upregulated (Fig 3.1E), indicating reduced ZEB1 expression is associated with an increased mesenchymal-like phenotype and that ZEB1 might contribute to maintain EC identity by suppressing mesenchymal genes. Downregulated EndoMT-related genes included leukocyte adhesion molecules ICAM1, VCAM1 and SELE (Fig 3.1E) which display reduced expression in ECs that have progressed through EndoMT (Alvandi and Bischoff, 2021). Thus, ZEB1 KD appears to shift HUVECs towards a pro-EndoMT-like phenotype.

Within the most significantly downregulated genes was CXCR4, a canonical marker of tip endothelial cells (Li *et al.*, 2021). This prompted us to probe the dataset for other known tip cell markers UNC5B, DLL4, ESM1 and CD34 (Geudens and Gerhardt, 2011), revealing UNC5B to also be downregulated upon ZEB1 KD in HUVECs (Fig 3.1E). The significant reduction of tip-cell associated genes in response to ZEB1 KD is indicative of the ability of ZEB1 to regulate genes that are markers of specific EC phenotypes, suggesting a putative role for ZEB1 in modulating EC heterogeneity. Specifically, reduction of ZEB1 leading to reduced

tip cell gene expression is highly suggestive of ZEB1 expression being required in pro-angiogenic EC phenotypes.

To continue utilising the RNA-seq dataset to shape an overview of ZEB1 regulatory mechanisms, we investigated the regulation of transcription factors (TFs) as a consequence of ZEB1 KD. We identified four TFs to be upregulated by ZEB1 KD: ZNF467, ZNF395, IRF6 and KLF8 and nine to be downregulated: IRF1, HIVEP2, HEY1, POU2F2, ZEB1, BACH1, ETS1, KLF4, and ATF3 (Fig 3.1E). The regulation of TFs by ZEB1 within HUVECs implies ZEB1 mediates a larger regulatory network within ECs. Finally, ZEB1 KD resulted in the downregulation of ESRP2 (epithelial splicing regulatory protein 2) (Fig 3.1E), suggesting ZEB1 is involved in splicing within ECs.

To annotate the DEGs to larger biological processes, we employed functional enrichment analyses against the Gene Ontology (GO) and KEGG databases. GO analysis revealed significant enrichment of processes related to adhesion, endothelial/vessel development and inflammation (Fig 3.2A), supporting the observations from DEGs alone. Interestingly, GO terms specifying the regulation of vascular permeability and angiogenesis involved in wound healing (Fig 3.2A) indicate a role of ZEB1 in response to pathological angiogenesis, of which vascular permeability can be a characteristic (Wautier and Wautier, 2022). In addition, genes relating to lymph node development were also differentially regulated (Fig 3.2A), supporting the notion that ZEB1 is relevant to EC phenotype specificity. KEGG pathway analysis further validated these findings, highlighting the significance of inflammatory and cell adhesion pathways following ZEB1 KD (Fig 3.2B).

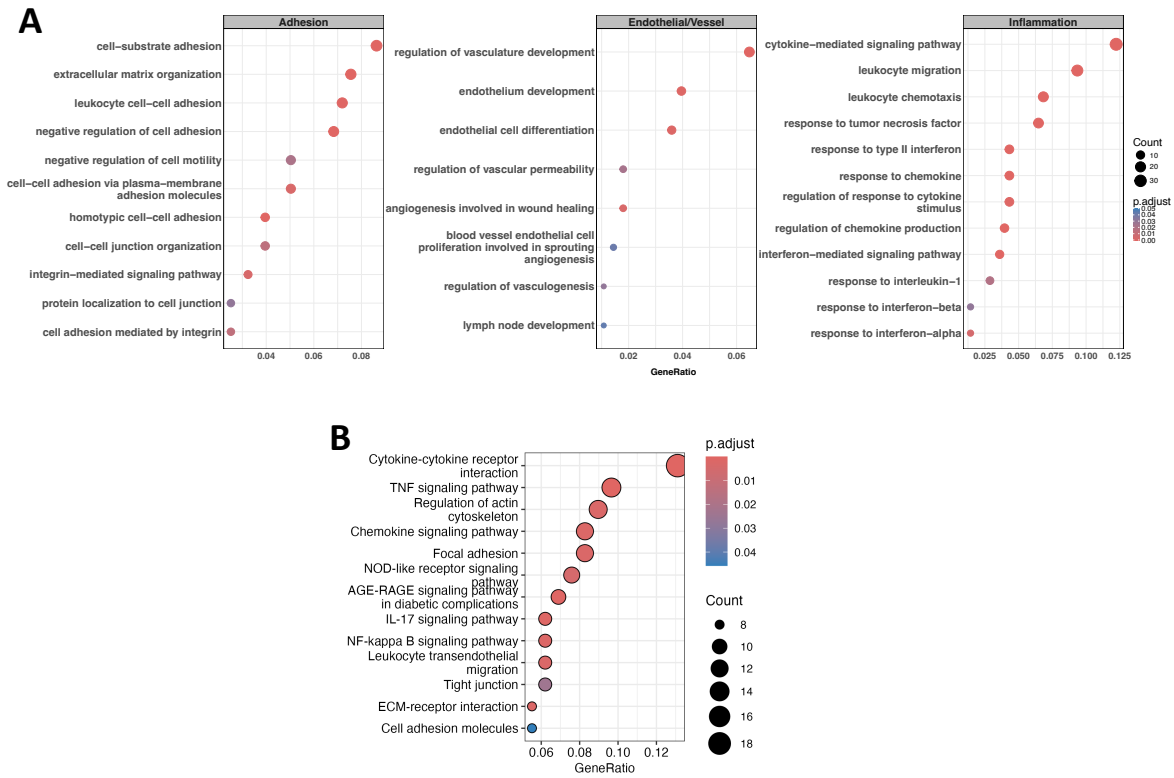


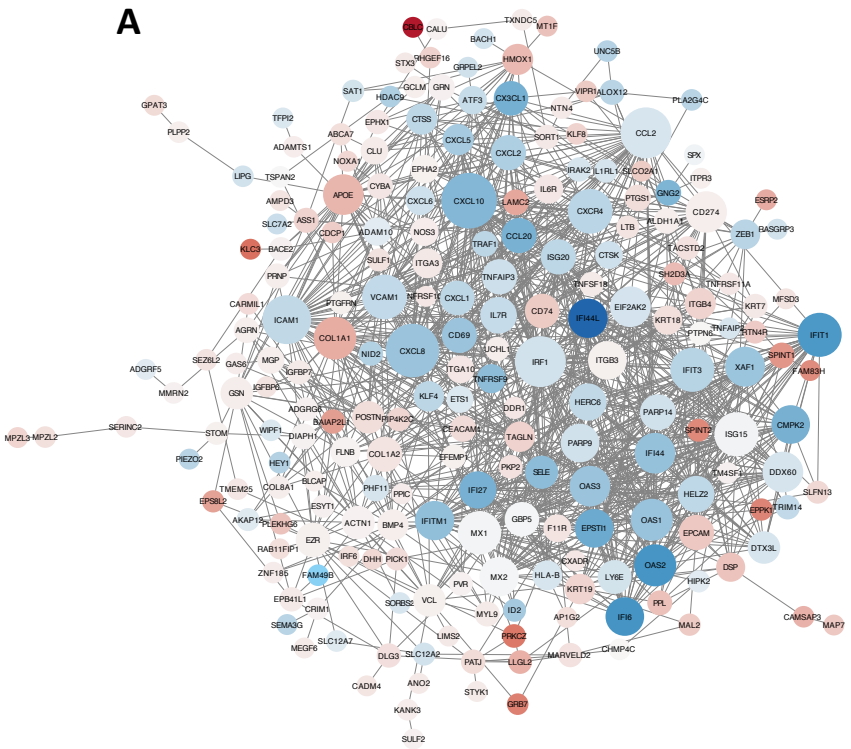
Figure 3.2. ***Functional enrichment analyses of DEGs identified pathways associated with adhesion, vasculature development and inflammation.***

(A) Gene Ontology (GO) functional enrichment analysis of all DEGs revealed enrichment of biological processes related to adhesion, vasculature development and inflammation.

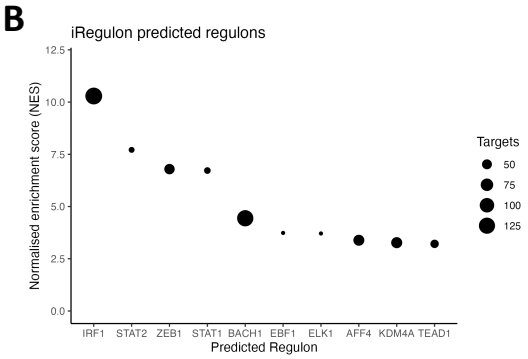
(B) KEGG pathway functional enrichment analysis corroborated the gene ontology results. Dot size indicates the number of DEGs associated with the GO term/KEGG pathway and colour represents adjusted p-value. The GeneRatio of the x-axis refers to the ratio *k/n* where *k* is the number of DEGs that overlap with the GO term/KEGG pathway and *n* is the total number of DEGs, indicating the proportion of total DEGs that is related to a GO term/KEGG pathway.

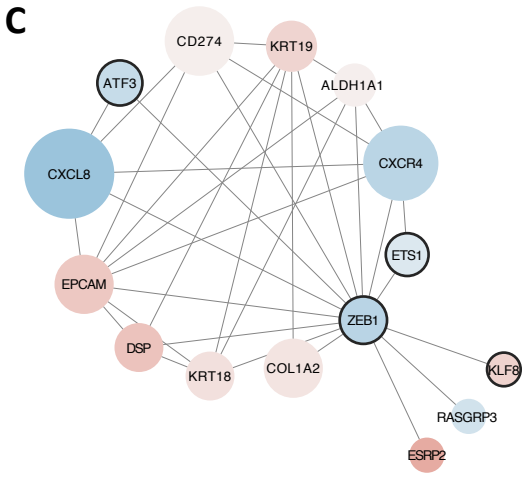
3.3.2 Network analysis of ZEB1 knockdown differentially expressed genes predicted a direct ZEB1 regulatory network including CXCR4

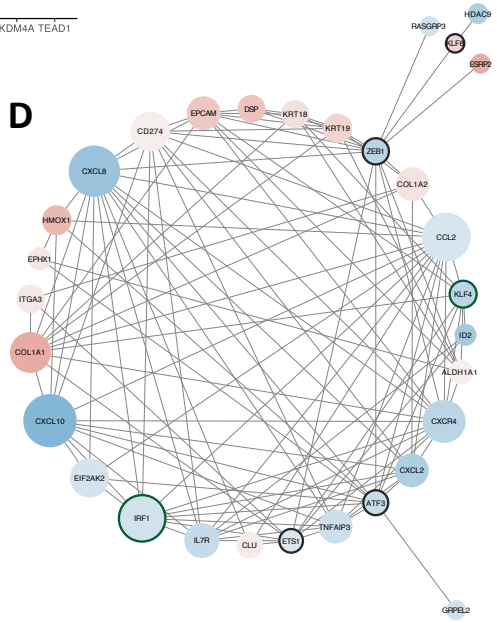
Given the transcriptional alterations observed following ZEB1 KD, we conducted a protein-protein interaction (PPI) network analysis to uncover predicted underlying connectivity among DEGs and to better understand the mechanisms through which ZEB1 influences endothelial cell function. The resulting network consisted of 218 DEGs after removing singlets and sub networks with < 4 nodes (Fig 3.3A). Within the network we



	Gene	Log2FC	Degree
Upregulated hub DEGs	COL1A1	1.9930355	33
	CD274	0.25863986	31
	APOE	1.72452968	30
	ITGB3	0.22755968	27
	EPCAM	1.25380799	22
	COL1A2	0.52092139	22
	CD74	1.17372337	21
	EZR	0.22941426	21
	ACTN1	0.17116621	19
	POSTN	0.70653278	18
Downregulated hub DEGs	CXCL10	-1.0839875	52
	CXCL8	-0.867223	49
	CCL2	-0.2971505	45
	IRF1	-0.3523118	45
	ICAM1	-0.5044011	42
	VCAM1	-0.5007973	36
	CXCR4	-0.5712262	36
	ISG15	-0.0524478	35
	IFIT3	-0.5960956	35
	IFIT1	-1.6126426	35







<u>Figure 3.3.</u> Network analysis of DEGs identified highly interconnected hub genes and a putative ZEB1 regulatory network.

(A) STRING PPI network of the remaining 218 DEGs following ZEB1 KD in HUVECs after removing singlets and subnetworks with < 4 nodes. Nodes represent proteinsand edges between nodes represent predicted interactions from the STRING database The size of the node corresponds to degree value (number of connections). The colour is scaled, with upregulated DEGs in red and downregulated DEGs in blue. The corresponding table lists hub genes which show the greatest number of connections (degree) in the network.

(B) iRegulon analysis of the network in (A) predicted transcription factors that may play a regulatory role within the network, indicating a potential cooperation between ZEB1 and the identified TFs. The top 10 predicted regulons by normalized enriched score (NES) are shown.

(C) The direct neighbours of ZEB1 within the main network in (A). Transcription factors are shown with a black border.

(D) Expanded ZEB1 regulatory network incorporating the direct neighbours of the transcription factors identified in (C), shown in (D) with a black border. Newly identified transcription factors are bordered in green.

identified hub nodes, those with the most connections (degree) and often represent key regulators whose central role can influence the stability and function of molecular pathways in the network. The top 10 DEGs with the highest connectivity were all downregulated and included IRF1, ICAM1, VCAM1 and CXCR4 (Fig 3.3A). Expanding the identification of hub nodes to upregulated DEGs identified COL1A1 to display the highest connectivity (Fig 3.3A).

To shed further light on the regulatory mechanisms within the DEG network, we applied iRegulon analysis to identify potential regulons of the DEGs detected upon ZEB1 KD. The regulon analysis identified 10 TFs with the potential to regulate DEGs in the network: IRF1, STAT2, ZEB1, STAT1, BACH1, EBF1, ELK1, AFF4, KDM4A and TEAD1 (Fig 3.3B). IRF1 showed the greatest enrichment (Fig 3.3B), suggesting ZEB1 and IRF1 can induce shared patterns of gene regulation in HUVECs.

Focusing on ZEB1, we inferred a ZEB1 interaction network through nodes that are predicted to directly interact with ZEB1, resulting in a network of 15 genes that may form the regulatory core of ZEB1 behaviour in HUVECs (Fig 3.3C). ZEB1 was predicted to directly

interact with CXCR4, further alluding to the requirement of ZEB1 to maintain expression of EC phenotype specific genes (Fig 3.3C). CXCL8, the DEG with the second highest connectivity (Fig 3.3A), was also directly connected to ZEB1 and has been shown to promote angiogenesis in ovarian tumours as well as recently being implicated in EndoMT (Ji *et al.*, 2023), providing further evidence for the role of ZEB1 in EndoMT and angiogenesis. COL1A2 was also within the network (Fig 3.3C), in agreement with ZEB1 potentially directly regulating EndoMT. The previously identified splicing factor ESRP2 is also predicted to interact with ZEB1 (Fig 3.3C), suggesting ZEB1 can directly regulate splicing within HUVECs. Importantly, ZEB1 formed direct connections with three TFs; ATF3, ETS1 and KLF8, foreshadowing a large TF regulatory with ZEB1 at the centre. Indeed, identifying DEGs that form direct interactions with ZEB1, ATF3, ETS1 and KLF8 inferred a larger regulatory network mediated by ZEB1 (Fig 3.3D) that may form the core of ZEB1 regulatory behaviour in HUVECs. Interestingly, IRF1 and KL4 were also contained in this network (Fig 3.3D), further alluding to the mechanisms through which ZEB1 acts within ECs.

3.4 Discussion

RNA-seq analyses of ZEB1 KD in HUVECs demonstrated ZEB1 to exert broad regulatory effects in ECs, impacting critical biological processes such as EndoMT, inflammation, cell adhesion and angiogenesis. The successful KD of ZEB1 significantly altered the expression of 296 genes, notably increasing the expression of genes associated with mesenchymal characteristics while concurrently reducing the expression of inflammatory and adhesion-related genes. Regulation of genes involved in extracellular matrix composition and signalling pathways suggested potential mechanistic roles for ZEB1 in maintaining endothelial cell structural integrity and response to environmental cues. Furthermore,

regulation of immune-related genes highlights the broader role of ZEB1 in immunomodulatory potential in ECs, suggesting a dual role in barrier function and immune cell recruitment. In addition, ZEB1 KD was found to regulate genes known to be canonical markers of tip cells, suggesting ZEB1 to play a role in EC phenotype specificity and the control of a pro-angiogenic state. These observations were supported by functional enrichment analysis revealing pathways and processes related to ECM, cell adhesion, angiogenesis and inflammation. While the enrichment of several biological themes may suggest an expansive role of ZEB1 in HUVECs, each of the observed processes are involved in the overall function of ECs and angiogenesis, suggesting ZEB1 to be a master regulator of several aspects to EC behaviour. Network analysis reinforced the initial observations, with highly interconnected DEGs involved in adhesion and cytokine signalling predicted to play a central role in HUVEC response to ZEB1 KD. Furthermore, the predicted regulons indicate that the transcriptional response induced by ZEB1 KD is reminiscent of the transcriptional profiles of other TFs, from which functions can be applied to ZEB1. For example, the enrichment of IRF1 as a regulon predicted to govern the DEG network derived from ZEB1 KD can suggest ZEB1 to carry out a similar function to that of IRF1. The direct ZEB1 interactome and the expanded network of TF interconnections highlight multiple potential regulatory mechanisms in which ZEB1 may act as a central modulator.

Overall, our findings provide insight into the regulatory roles of ZEB1 in endothelial biology, emphasising its potential involvement in endothelial plasticity, inflammatory modulation and vascular homeostasis as well as strengthening the notion that ZEB1 is a regulator of EndoMT. Further studies are warranted to elucidate the precise mechanistic roles of identified TFs, particularly IRF1, in mediating the functional impacts of ZEB1. Furthermore, the RNA-seq analyses here will need to be coupled with further angiogenic in-

vitro assays to observe phenotypic responses to ZEB1 KD. As discussed in the introduction, there are several functional steps to angiogenesis, models to which exist at the in-vitro level including sprout, migration, adhesion and tube formation assays (Arnaoutova and Kleinman, 2010; Tahergorabi and Khazaei, 2012; Rahman *et al.*, 2020; Laschke, Gu and Menger, 2022). A combination of these assays should be carried out in order to cover several aspects of angiogenesis, as each experiment addresses one facet. These will be performed in future to generate a more comprehensive overview of the potential role of ZEB1 in angiogenesis.

Chapter 4: Comprehensive and unbiased analysis of ZEB1 binding patterns in HUVECs via ChIP-seq

4.1 Introduction

The development of chromatin immunoprecipitation followed by high-throughput sequencing (ChIP-seq) has revolutionised the study of transcription factor (TF) binding and histone modifications, providing an unbiased and genome-wide approach to mapping protein-DNA interactions. Originally developed to analyse histone modifications, ChIP-seq has since been widely adapted for TF studies, offering insights into gene regulation by identifying binding sites across the genome (Barski et al., 2007; Robertson et al., 2007; Furey, 2012). Unlike earlier approaches such as ChIP-PCR, which is limited to predefined regions and requires a priori knowledge of binding sites and can technically prove difficult. Although ChIP-PCR remains a viable method to validate specific ChIP-seq results. ChIP-seq allows for the discovery of novel binding sites and regulatory elements (Park, 2009). Despite these advantages, ChIP-seq primarily identifies TF occupancy rather than direct transcriptional regulation, necessitating complementary functional assays to infer the biological significance of binding events including additional validation methods such as ChIP-qPCR, electrophoretic mobility shift assays (EMSAs) and luciferase reporter assays which are often employed to confirm specific interactions and assess their regulatory impact (Levitsky et al., 2014; Zhang et al., 2015; Kim and Dekker, 2018; Qiu et al., 2023). Furthermore, integrating ChIP-seq data with transcriptomic data, such as RNA-seq or single-cell RNA-seq (scRNA-seq) can help determine whether TF binding correlates with gene expression changes and identify direct and indirect regulation (Jiang and Mortazavi, 2018; Muhammad et al., 2019; Höllbacher et al., 2020; Ramos, Felty and Roy, 2020). While a powerful tool to gain an understanding of the DNA binding behaviour of TFs, careful validation and understanding of potential bias

within ChIP-seq data is required to avoid reporting false positive/negative results (Meyer and Liu, 2014).

ChIP-seq provides critical insights into TF-mediated gene regulation by identifying promoter and enhancer binding sites, co-factor interactions and chromatin modifications associated with transcriptional activity (Whyte et al., 2013). While TF binding is often enriched at gene promoters, many regulatory events occur at distal enhancers which interact with promoters through chromatin looping (Bulger and Groudine, 2011). Computational approaches, such as motif enrichment analysis and chromatin state annotation are widely used to classify ChIP-seq peaks and predict functional outcomes (Zhu et al., 2010; Machanick and Bailey, 2011; Ernst and Kellis, 2012). Alternative methods for studying TF binding include DNase-seq and ATAC-seq which map open chromatin regions rather than direct TF occupancy (Buenrostro et al., 2013). Additionally, CUT&RUN and CUT&TAG have emerged as low-input alternatives to ChIP-seq, offering improved sensitivity for mapping TF binding with reduced sequencing depth requirements (Skene and Henikoff, 2017; Kaya-Okur et al., 2019). However, even with the advent of newer techniques ChIP-seq remains a viable and commonly used method for identifying TF-DNA interactions on a genome-wide scale.

As previously discussed, ZEB1 is a zinc finger E-box binding TF that plays a key role in cellular plasticity and is known to be a driver of epithelial-to-mesenchymal transition (EMT). ChIP-seq studies in cancer models have identified thousands of ZEB1 binding sites, predominantly in promoter and enhancer regions, suggesting a broad role in transcriptional regulation (Feldker et al., 2020). In breast cancer, ZEB1 has been shown to regulate genes involved in invasion and metastasis by binding to promoter regions of EMT-associated genes (Katsura et al., 2017). Furthermore, ZEB1 has been shown to alter the epigenetic landscape of colorectal cancer cells (Lindner et al., 2020). Despite extensive characterisation in

epithelial and cancerous contexts, relatively little is known about ZEB1 DNA binding in endothelial cells. Given its involvement in EMT, ZEB1 has been hypothesised to play a role in endothelial-to-mesenchymal transition (EndoMT) and regulate endothelial identity and vascular function by targeting key endothelial transcriptional programs (Fu, Lv, *et al.*, 2020; Yu *et al.*, 2022). Indeed, deletion of ZEB1 in skeletal ECs has been shown to reduce histone acetylation at the promoters of Dll4 and Notch1, displaying an epigenetic regulation of the notch signalling pathway. Despite this, the research surrounding the genome-wide binding of ZEB1 in endothelial cells (ECs) remains sparse.

To investigate the genome-wide binding patterns of ZEB1 in vascular ECs, we performed ChIP-seq in human umbilical vein endothelial cells (HUVECs). Previous studies in HUVECs have demonstrated that endothelial TFs such as ERG and ETS factors bind extensively to promoter and enhancer regions to regulate vascular identity (Kalna et al., 2019). Our study aimed to determine the binding patters and preferences of ZEB1 in HUVECs and to explore its potential interactions with other TFs. Furthermore, integration of ZEB1 ChIP-seq data with histone modification profiles from publicly available datasets was used to assess whether ZEB1 binding occurs at active regulatory regions in HUVECs. Active enhancer regions are typically marked by H3K4me1 and H3K27ac, whereas active promoters are characterised by H3K4me3 and H3K27ac (Pekowska et al., 2011). By comparing ZEB1 ChIP-seq data with publicly available histone datasets, we aim to identify potential regulatory elements associated with ZEB1 binding in an attempt to uncover the epigenetic mechanisms through which ZEB1 may regulate fundamental EC processes, including angiogenesis and EndoMT.

Despite its strengths, ChIP-seq has inherent limitations. Antibody specificity, sequencing depth and peak-calling stringency can affect data interpretation, leading to false positives or false negative binding events (Landt et al., 2012). Additionally, ChIP-seq does not

distinguish between direct and indirect TF binding. Further co-immunoprecipitation experiments or TF knockdown approaches can aid in determining whether ZEB1 binds directly to DNA or interacts with other TFs to mediate regulatory effects. Hence, we apply the ChIP-seq data presented here to the RNA-seq data in the previous chapter.

This chapter presents a comprehensive analysis of ZEB1 binding in HUVECs through ChIP-seq, highlighting its preferential localisation at promoter regions and its potential role in gene regulation. By comparing ZEB1 binding patterns in ECs with those observed in other cell types we provide insights into its function in vascular biology. Through motif enrichment, histone modification analysis, functional annotation and integrating with the RNA-seq data from chapter 3, this study contributes to our understanding of ZEB1 as a transcriptional regulator in endothelial cells.

4.2 Hypothesis and aim

Hypothesis: *ZEB1* can directly and indirectly regulate genes related to angiogenesis and EndoMT in HUVECs.

The hypothesis was tested through integrating ChIP-seq and RNA-seq analysis techniques to address the following aim:

Aim: To define genome-wide *ZEB1* binding sites in ECs and integrate this data with gene expression profiles to reveal regulatory targets.

Due to the nature of how results are presented in this chapter and the fact that our computational analyses were constantly optimised throughout, some discussion points are integrated within the results to expand on findings where relevant.

4.3 Results

4.3.1 ZEB1 ChIP-seq in HUVECs identified 12,577 significant peaks 77.7% of which were annotated to transcript promoter regions

To investigate the genome-wide binding patterns of ZEB1, we performed ChIP-seq using HUVECs as an EC model. Quality control of the ChIP-seq data identified ZEB1 ChIP-seq replicates 1 and 2 to display the greatest signal enrichment and were subsequently used for IDR and downstream analyses (Fig 4.1A-C). Binding was identified at 12,577 regions of the genome across 10,505 genes in which reads are enriched compared to the IgG control (Fig 4.1D). To corroborate this number of binding sites we reviewed the literature for ZEB1 ChIP-seq experiments and found that ZEB1 has been shown to bind to 12,617 sites in a triple negative breast cancer cell line (Feldker et al., 2020) and 14,811 in a human basal-type breast cancer cell line (Katsura et al., 2017). Further visualisation of the ChIP-seq data showed that the majority of ZEB1 ChIP signal was bound to the region -1000bp to the TSS of genes with very little enrichment after the TSS (Fig 4.2A,B). This was supported by peak annotation analysis revealing 77.7% of the peaks to lie in the promoter region of transcripts, suggesting that ZEB1 preferentially binds to regions of HUVEC DNA that may have a direct role in regulation (Fig 4.2C). We also annotated peaks at the gene level and found that 62.24% were assigned to promoter regions, with 12.8% at the 5` UTR. This result suggested that the majority of ZEB1 binding is at the promoter of the transcript/gene, while some binding sites occur at other sites in the gene body.

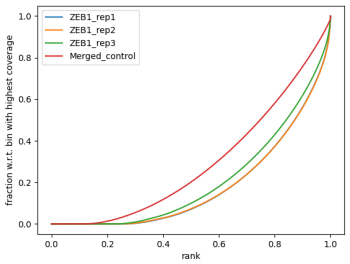
A

	Pre-filtering				Post-filtering			
	Merged control	ZEB1 ChIP replicate 1	ZEB1 ChIP replicate 2	ZEB1 ChIP replicate 3	Merged control	ZEB1 ChIP replicate 1	ZEB1 ChIP replicate 2	ZEB1 ChIP replicate 3
Number of reads	242,501,818	81,869,696	79,863,934	79,767,078	115,231,927	41,041,078	43,802,142	36,434,700
Mapped reads	191,433,811 / 78.94%	65,136,809 / 79.56%	68,595,486 / 85.89%	60,486,217 / 75.83%	115,231,927 / 100%	41,041,078 / 100%	43,802,142 / 100%	36,434,700 / 100%
Unmapped reads	51,068,007 / 21.06%	16,732,887 / 20.44%	11,268,448 / 14.11%	19,280,861 / 24.17%	0 / 0%	0 / 0%	0 / 0%	0 / 0%
Duplicated reads (estimated)	43,427,452 / 35.3%	14,164,074 / 31.44%	14,932,079 / 31.5%	13,872,826 / 34.05%	5,129,735 / 6.82%	1,403,890 / 4.86%	1,897,675 / 6.17%	1,192,013 / 4.77%
Duplication rate	32.27%	32.11%	32.22%	35.19%	6.16%	4.61%	5.91%	4.71%
Multimapped reads	31,746,130	7,514,099	7,997,566	7,241,944	0	0	0	0

B

ID	Tissue	Factor	Condition	Replicate	Reads	Dup%	ReadL	FragL	RelCC	SSD	RiP%
A1		ZEB1		1	41036675	0	138	277	2.2	0.61	18
A2		ZEB1		2	43797900	0	139	279	1.5	0.65	19
A3		ZEB1		3	36431666	0	141	283	1.6	0.48	12
Control	NA	NA	NA	NA	115192341	0	142	285	1.2	0.46	NA

C



D

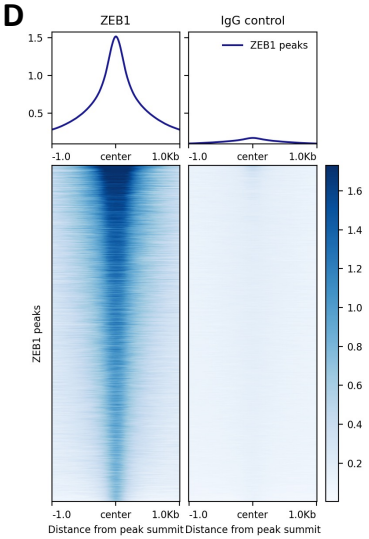


Figure 4.1. ***Quality control of HUVEC ZEB1 ChIP-seq data identifies the optimal replicates for downstream analysis and an enrichment of ZEB1 ChIP-seq signal at peak regions compared to IgG control.***

(A) Quality control metrics for the ZEB1 ChIP-seq data identified by Qualimap and basic command-line arguments (see Methods) to confirm the filtering of reads.

(B) ChIP-QC quality control to identify signal to noise ratio to select the optimal replicates for IDR replicate handling analysis. Dup% = duplicated reads percentage. ReadL = mean read length. FragL = mean fragment length. RelCC and SSD are quality control metrics described by the ENCODE consortium in which a higher value indicates greater ChIP enrichment. RiP% = percentage of reads in peaks, which can be used as an indication of signal-noise ratio. The difference in duplication rate % between A and B is a result of using multiple QC tools. Total removal of duplicates was confirmed within the BAM files via duplicate marking as described in section 2.2.3

(C) Fingerprint plot to show the sufficient enrichment of ChIP signal replicates to distinguish from background signal in which the further the shift to the right from the control, the greater the enrichment. Replicates 1 and 2 show greatest enrichment. Replicate 1 (blue) is overlapped by the line for replicate 2 (orange).

(D) Heatmap of ZEB1 and IgG ChIP-seq signals against the significant ZEB1 ChIP-seq peaks centered on the peak summits. The ZEB1 ChIP-seq signal is enriched at these sites, whereas the IgG control is not.

4.3.2 Gene biotype assignment, TF identification and functional enrichment analyses of ZEB1 bound regions in HUVECs revealed a broad potential influence of ZEB1 on HUVEC behaviour

In order to further assess the binding of ZEB1, we assigned transcript biotypes (e.g., protein coding, lincRNA, etc) to the enriched peaks (Fig 4.2D). 64.4% were protein-coding transcripts, indicating 35.6% of bound transcripts are not protein-coding and included antisense (3.1%) and lincRNA (2.9%) transcripts. This finding indicated that ZEB1 does not bind solely to protein-coding transcripts, but also to non-protein-coding regions whose role may serve other aspects of HUVEC and EC functions. Furthermore, 13.3% of bound regions were annotated to an unassigned biotype. These regions may warrant pursued experimentation and could putatively shed further light on the behaviour of ZEB1 in HUVECs, but we also understand this could be a limitation of the tool and inputs used for annotation. Antisense transcripts have the potential to regulate gene expression (Pelechano and Steinmetz, 2013). For example, long non-coding antisense transcript of GATA6 has been shown to interact with the epigenetic regulator LOXL2 to regulate endothelial gene expression and promote EndoMT (Neumann et al., 2018). It stands to reason that binding of antisense transcript genes by ZEB1 in HUVECs could have an impact on several aspects of EC behaviour and could be an avenue for further hypothesis generation. This can also be applied to long intergenic non-coding RNAs (lincRNA).

In addition to potential regulation of antisense and lincRNA molecules by ZEB1 suggesting other potential directions to explore, we identified transcription factors within the enriched ZEB1 HUVEC ChIP-seq peaks by cross referencing with a detailed list of 1639 human TFs (Lambert et al., 2018), acknowledging gene synonyms. We identified 773 TF genes to contain a significantly enriched ChIP-seq peak, suggesting ZEB1 might induce a wide

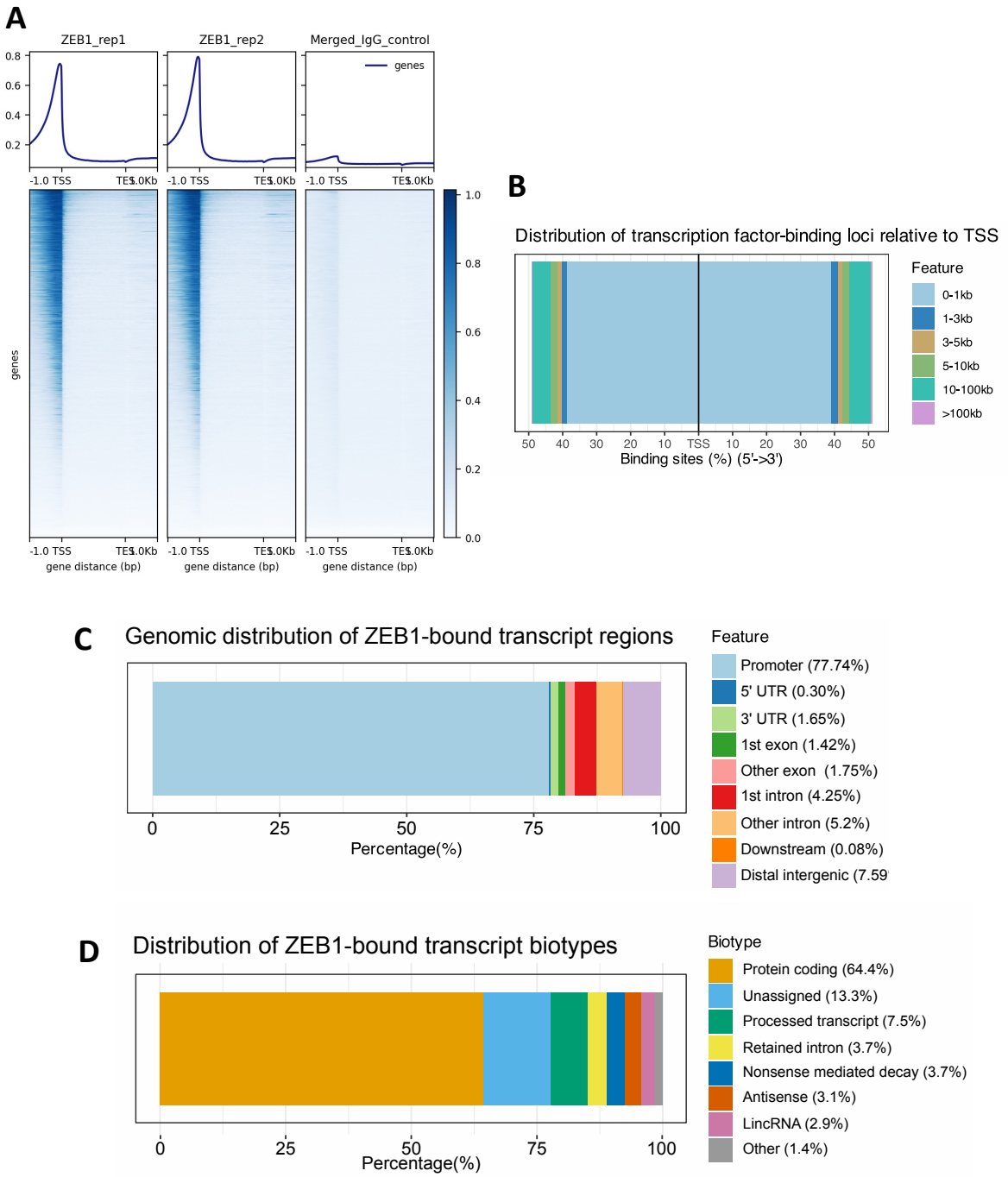


Figure 4.2. Assignment of genes to peaks and binding locations of ZEB1 identified most ZEB1-bound regions to reside in promoter regions within 1kb of the TSS of protein-coding transcripts.

(A) Heatmap of the individual replicates of ZEB1 ChIP-seq and IgG signals against all genes in the hg38 genome. The full gene length is shown. The enrichment is observed within 1kb of the TSS with little enrichment along the gene length.

(B) Distribution of ZEB1 binding relative to the TSS revealed ~80% of ZEB1 binding to be within 1kb of the TSS.

(C) Transcript-level annotation of ZEB1 peaks identified 77.74% of peaks to bind to the promoter region of transcripts.

(D) Biotype annotation of ZEB1-bound transcripts revealed 64.4% to be protein coding transcripts.

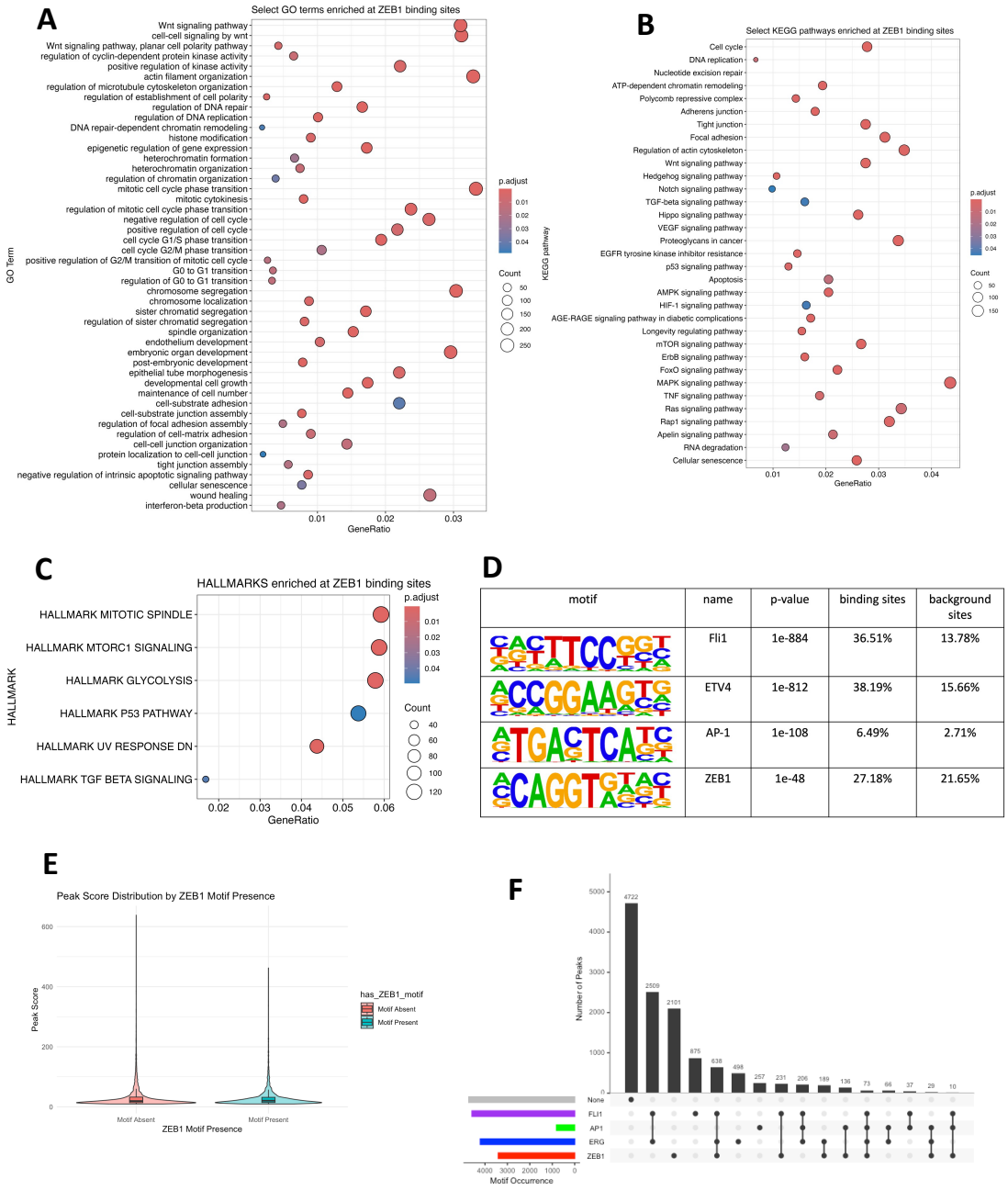
signalling cascade in HUVECs through the binding, and potential regulation, of TFs themselves. Interestingly a signal peak is enriched at the promoter of ZEB1 itself (Appendix 4.1A), indicative of potential self-regulation. Furthermore, the same peak was assigned to ZEB1-AS1 and overlaps the promoter regions of both ZEB1 and ZEB1-AS1 genes (Appendix 4.1A). The binding of ZEB1 to the ZEB1-AS1 gene promoter could indicate the putative regulation of ZEB1 itself via the antisense sequence. Auto-antisense regulation has previously been demonstrated in prostate cancer cells where ZEB1-AS1 expression promoted ZEB1 expression (Su et al., 2017). ZEB1-AS1 has also been identified in various malignancies (Ghafouri-Fard et al., 2023) in which angiogenesis is known to be a key process. Following further studies to validate this observation, if ZEB1 can regulate ZEB1-AS1 through direct binding to the promoter region in HUVECs, we can hypothesise that ZEB1 plays an angiogenic role through binding and potential regulation of the expression of ZEB1-AS1 in tumour vasculature.

In order to gain an overview of the function of genes/transcripts bound by ZEB1 we performed functional enrichment analyses against the Gene Ontology Biological Processes (GO BP), KEGG and HALLMARKs databases for the enriched peaks (Fig. 4.3A-C). GO BP analyses identified 305 significant terms related to 15 categories; cell signalling and regulation, Intracellular transport and organelle organisation, cytoskeleton and cell morphogenesis, protein modification and processing, transcriptional and epigenetic regulation, RNA processing and translation, cell cycle and proliferation, cellular stress and metabolic responses, development and differentiation, cell growth and junction assembly, organelle and vesicular processes, metabolism and biosynthetic processes, apoptosis and cell death, cellular senescence and regeneration, immune stress and responses. KEGG analysis revealed pathways enriched in the cell cycle, DNA replication and junctional

adhesion. Furthermore, several specific signalling cascades were enriched including Wnt, Notch, Hippo, TGF-beta and FoxO. The HALLMARKs analysis identified mitotic spindle and TGF-beta signalling in line with the GO BP and KEGG results. The HALLMARKs results also included glycolysis, suggesting a role of ZEB1 in the binding of genes related to metabolism. The broad range of enriched GO terms, KEGG pathways and HALLMARKs associated with genes bound by ZEB1 highlights its potential downstream influence on multiple aspects of HUVEC behaviour.

4.3.3 Motif analysis of peak summits of ZEB1 bound regions in HUVECs displayed an enrichment for ETS and AP-1 family binding motifs

To further investigate the binding mechanism of ZEB1 we performed motif enrichment analysis to identify TF motifs that are overrepresented within ZEB1 peaks. Known motif analysis focused on the 200bp region around the summit of the enriched ZEB1 ChIP-seq peaks identified four major motifs. The top three motif families were represented by Fli1 (ETS family), ETV4 (ETS family, which includes ERG) and AP-1 (bZIP family) with the motifs found in 36.51%, 38.19% and 6.49% of peak summit regions respectively (Fig 4.3D), implicating these factors in the ZEB1 regulatory network. These results indicate a potential interaction between ZEB1 and ETS transcription factors in endothelial cells, consistent with the role of ETS factors in maintaining endothelial identity. The fourth motif was the ZEB1 motif which was enriched in 27.18% of the 200bp peak target sequences compared to 21.65% of background sequences. While a significant result, a greater enrichment for the ZEB1 motif may be expected. Indeed, other ZEB1 ChIP-seq datasets identified 38.49% of target and 9.57% of background to display the ZEB1 motif in a melanoma cell line (Durand et al., 2024) and 68.0% in target and 28.9% in background in a triple negative breast cancer cell



<u>Figure 4.3.</u> Functional enrichment analysis identified a broad range of functions of ZEB1 bound genes and motif analysis of 200bp regions centered on ZEB1 ChIP-seq peak summits identified significant enrichment of ETS and AP-1 family binding motifs.

(A) Dotplot of enriched Gene Ontology Biological Processes terms enriched at ZEB1 binding sites organised by term relation. Enriched processes included cell cycle, proliferation and junction assembly.

(B) Dotplot of enriched KEGG pathways enriched at ZEB1 binding sites included signalling pathways related to angiogenesis including Notch, TGFB and VEGF.

(C) Dotplot of enriched HALLMARKS at ZEB1 binding sites.

(D) The top 4 non-redundant binding motifs enriched in 200bp regions of ZEB1 ChIP-seq peaks centred on peak summits.

(E) Violin plot to show the comparison of the distribution of peak enrichment score for 200bp ZEB1 peak summit regions with and without the ZEB1 motif. Presence of ZEB1 motif was not observed to be correlated with higher peak enrichment scores.

(F) UpSet plot displaying the overlap of the top 4 non-redundant binding motifs presences in 200bp ZEB1 peak summit regions.

line (Feldker et al., 2020). The lower percentage of ZEB1 motif in HUVECs compared to other datasets could indicate ZEB1 to be indirectly bound to the majority of peaks with potential facilitation through interaction with other TFs or cofactors such as Fli1, ETV4 and the AP-1 family identified above. It could also suggest that the ZEB1 motif lies further away from the peak summit and that the 200bp region of motif enrichment should be extended. However, this is counterintuitive to the behaviour of TFs in ChIP-seq data, in which a narrow peak is to be expected. There are other bioinformatics reasons to consider. For example, an increase in stringency of peak calling may reduce the potential false-positive peaks from the results, or application of a cut-off to the strength of ChIP-seq signal in peaks. A different approach to handling of peak replicates could also be taken. For example, pooling of all replicates after careful validation of individual replicates to ensure there were no significant difference or poor quality replicates before pooling. While a useful method to capture all signal in the experiment, the resolution that individual replicates provides is lost. Another approach is the use of Bedtools to find the intersect of peaks. This is a common approach, however it can result in high numbers of false positive and false negative results (Yang *et al.,* 2014). R packages GenomicRanges (Lawrence *et al.,* 2013) or DiffBind (R Stark and G Brown, 2011) can be used to identify consensus peak regions that are present in 2/3 or 3/3 of replicates. While these approaches are valid, they lack the benefit of a statistical model to apply significance values to the peaks. Experimentally, there may be cause to investigate the specificity of the antibody used, or validation of the results through cross-referencing the data of multiple ZEB1 antibodies. To further investigate the percentage of peak summits with the ZEB1 motif we plotted the correlation between peak enrichment score and presence of ZEB1 motif (Fig 4.3E). We did not identify any correlation with strength of enrichment to the

presence of the ZEB1 motif, suggesting that indirect binding by ZEB1 did not exhibit a lower enrichment score compared to direct binding.

Continuing with the current motif analysis, we extracted the peaks in which the summit regions displayed any combination of ZEB1, ERG, FLI1 and AP-1 motifs (Fig 4.3F). In this case we opted to use the ERG motif as opposed to the representative ETV4 of the motif family that included ERG due to its known essential role in ECs (Birdsey *et al.*, 2015). The ERG motif showed 33.56% of target ZEB1 peak summits to contain the motif against 14.35% of background sequences. Interestingly, the majority of ZEB1 peak summits did not contain any of the four enriched motifs (Fig 4.3F). The second most common occurrence was the combination of FLI1 and ERG motifs. Both of these TFs belong to the same ETS family with similar motifs and so this is perhaps not surprising. 2101 ZEB1 peaks displayed only the ZEB1 motif, indicating direct ZEB1 binding. 638 peak summits contained ZEB1, ERG and FLI1 motifs, suggesting direct binding of ZEB1 with a potential co-binding of FLI1 and ERG. 498 peaks summits contained an ERG motif without a ZEB1 motif. In this instance, this may be indicative of ZEB1 indirectly binding to the genomic regions through ERG. Furthermore, we saw 257 peak summits displaying the AP-1 motif only, suggesting indirect ZEB1 binding through AP-1 TFs. Interestingly, 206 ZEB1 peak summits displayed the presence of FLI1, ERG and AP1 motifs but no ZEB1 motif. Here, ZEB1 may be indirectly binding to genes via any of these TFs and may even form a complex given all motifs are within 200bp of the ZEB1 peak summit. 189 peak summits contained the ZEB1 and ERG motif, while 136 contained the ZEB1 and AP1 motif, suggesting regions where ZEB1 directly binds and is also potentially co-bound with either ERG or AP1 TFs. Furthermore, 73 peak summits contained all 4 motifs, again indicating a potential co-binding complex but with ZEB1 directly binding. The quantification of peak

summits expressing motifs detailed here alludes to the direct and indirect binding patterns that ZEB1 can exhibit, with potential co-binding with other TFs.

4.3.4 A full genome scan for the presence of the ZEB1 motif and ZEB1 peak width analysis suggested our method of motif enrichment analysis may not be suitable to determine direct/indirect ZEB1 binding in our dataset

To further validate the indirect binding of ZEB1 we scanned the entire genome to predict instances of the ZEB1 motif, resulting in 2,823,600 ZEB1 motif locations. In comparison, we also identified 2,175,645 ERG and 1,008,183 AP-1 motif regions since these were enriched in our motif analysis of ZEB1 peaks. The limitation to the current approach of motif enrichment analysis is the focus on 200bp regions surrounding the peak summits. Some of the ZEB1 binding peaks are wide, indicating that ZEB1 can bind in several locations in a single peak. Indeed, the mean peak width was 1904bp (Fig 4.4). While the summit of a peak is typically the indication of the location of TF binding, if the data shows wider peaks that do not have a clear singular summit, then there may be several areas of ZEB1 binding. Furthermore, peak summits are extracted from the IDR peak replicate analysis which generates a merged peak summit as opposed to using the summits from the individual replicates derived from peak calling. If the two replicates share summit positions that are close together, then the merged summit from IDR will be at this region. However, in the case of peak replicates having summit positions that are further apart the IDR summit will fall between the two, which may cause false positive or negative overlaps with a ZEB1 motif and be incorrectly detected as a direct or indirect binding site. Since ZEB1 gives an average peak width of 1904bp we can speculate that ZEB1 may be binding at clusters of binding sites along with isolated singlet binding sites at narrower peaks. Given we know the read and fragment

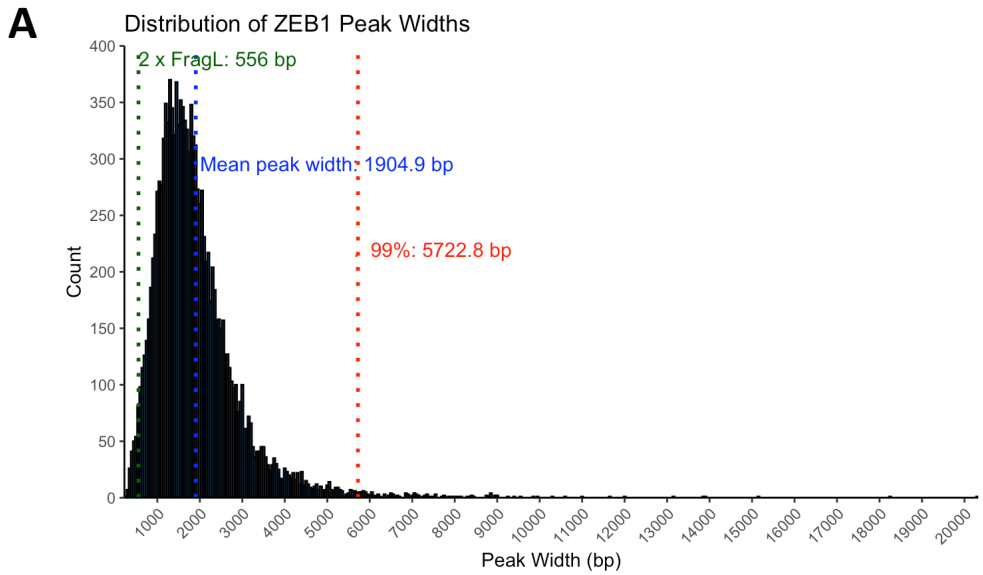


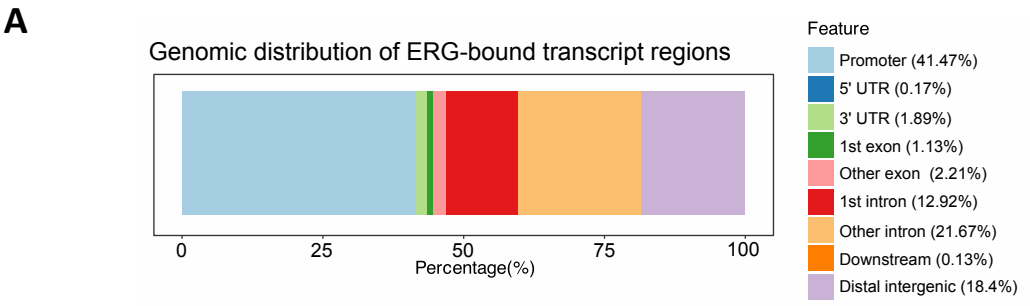
***Figure 4.4.* Distribution of ZEB1 HUVEC ChIP-seq peak widths identified a mean peak width of 1904 bp suggesting multiple ZEB1 binding sites in a given region.**
Distribution of ZEB1 peak widths identified from IDR analysis. The dotted green line signifies 2x the average fragment length of the ChIP-seq dataset in which a single ZEB1 binding motif can be present, the blue is the mean peak width and the red is the 99th peak width percentile.

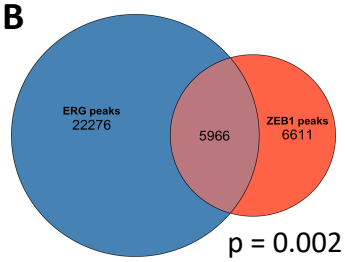
lengths of our dataset, we could calculate peaks that are likely single or clustered ZEB1 binding sites and categorise the peaks into these groups, as has been done in other ChIP-seq experiments (Matsuda et al., 2017). As per the calculation in Matsuda et al., 2017, 2 x the mean fragment length of our dataset (2 x 278bp) gives 556 bp, suggesting peaks with a width of ~600bp would indicate a single ZEB1 binding site where peak widths above this suggest multiple ZEB1 binding sites within short genomic intervals. For the purposes of this thesis we did not pursue these analyses, however the width of ZEB1 peak regions can raise several hypotheses, including; 1) ZEB1 binding sites are not isolated but occur in clusters within regulatory regions, leading to broader peaks due to cooperative or redundant binding events. 2) ZEB1 binds to chromatin across large enhancer or promoter regions rather than at discrete sites. 3) ZEB1 co-binds with other TFs in a complex resulting in ChIP-seq peaks that span multiple adjacent binding events rather than a single isolated motif. 4) ZEB1 is enriched at super-enhancer regions which are characterised by broad ChIP-seq peaks (Kalna et al.,

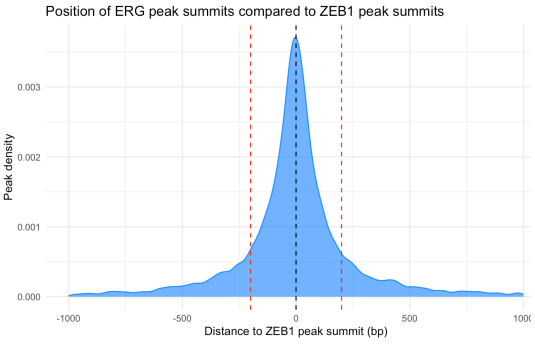
2019). Rather than relying on standard motif enrichment analysis to determine direct or indirect binding of ZEB1, the nature of the analysis pipeline and the width of the ZEB1 peaks would potentially benefit from an intersect analysis of full ZEB1 peaks and identified locations of the ZEB1 motif by genome scanning to identify ZEB1 binding regions that contain the motif, as opposed to only 200bp regions around a peak summit. Furthermore, manual validation of direct/indirect binding can be predicted for specific genes by visualisation of signalling tracks and motif locations in a genome viewer. Examples of manual validation include the ZEB1 peak at the active promoter of the Metal Regulatory Transcription Factor MTF1 (Appendix 4.1B). This peak does not overlap with an identified ZEB1 motif, however it does overlap with an ERG peak suggesting that ZEB1 may indirectly bind the active promoter of MTF1 via co-binding with ERG. Furthermore, ZEB1 binds at the active promoter of SART1 (Appendix 4.1C) but also does not exhibit a ZEB1 motif however it does contain an ERG motif and overlaps with and ERG peak. In this instance ZEB1 appears to co-bind with ERG to indirectly bind to SART1.

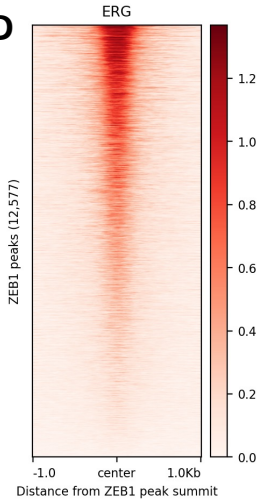
4.3.5 Comparison of ZEB1 HUVEC ChIP-seq with a publicly available ERG HUVEC ChIP-seq dataset revealed 47.4% of ZEB1 peaks to overlap with ERG peaks

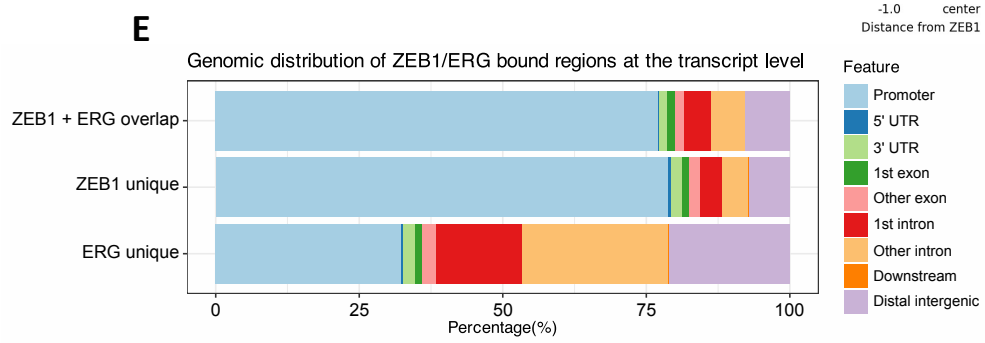
Since the ETS family motif, specifically ERG, was enriched in the ZEB1 peaks suggestive of co-binding of ERG and ZEB1 at the same genomic sites, we reanalysed a publicly available ERG HUVEC ChIP-seq dataset (Kalna et al., 2019) for validation. We identified 28,242 genomic regions bound by ERG, 41.47% of which were bound to promoter regions of transcripts and 28.7% bound to the promoter at the gene level (Fig 4.5A-B). We investigated the overlap between ZEB1 and ERG ChIP-seq peaks and found 5966 ERG peaks (21.1% of all significant ERG peaks) with summit positions within 200bp of ZEB1 peak summits (Fig 4.5C-

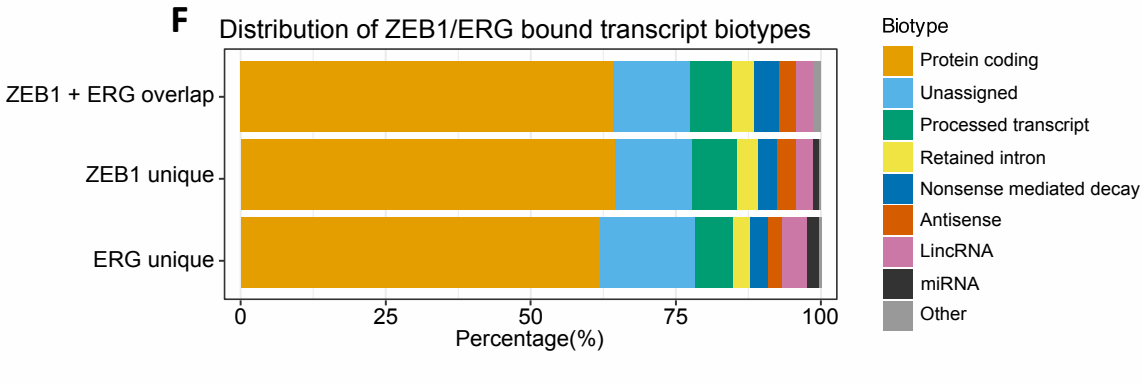

A
Genomic distribution of ERG-bound transcript regions
0
25
50
75
100
Percentage(%)
Feature
Promoter (41.47%)
5' UTR (0.17%)
3' UTR (1.89%)
1st exon (1.13%)
Other exon (2.21%)
1st intron (12.92%)
Other intron (21.67%)
Downstream (0.13%)
Distal intergenic (18.4%)


B
ERG peaks
22276
5966
ZEB1 peaks
6611
p = 0.002


C
Position of ERG peak summits compared to ZEB1 peak summits
Peak density
0.003
0.002
0.001
0.000
-1000
-500
0
500
Distance to ZEB1 peak summit (bp)


D
ERG
ZEB1 peaks (12,577)
1.2
1.0
0.8
0.6
0.4
0.2
0.0
-1.0
center
1.0Kb
Distance from ZEB1 peak summit


E
Genomic distribution of ZEB1/ERG bound regions at the transcript level
ZEB1 + ERG overlap
ZEB1 unique
ERG unique
0
25
50
75
100
Percentage(%)
Feature
Promoter
5' UTR
3' UTR
1st exon
Other exon
1st intron
Other intron
Downstream
Distal intergenic


F
Distribution of ZEB1/ERG bound transcript biotypes
ZEB1 + ERG overlap
ZEB1 unique
ERG unique
0
25
50
75
100
Percentage(%)
Biotype
Protein coding
Unassigned
Processed transcript
Retained intron
Nonsense mediated decay
Antisense
LincRNA
miRNA
Other

<u>Figure 4.5.</u> Reanalysis of a HUVEC ERG ChIP-seq dataset revealed 47.4% of ZEB1 summit regions to overlap with ERG summit regions in HUVECs.

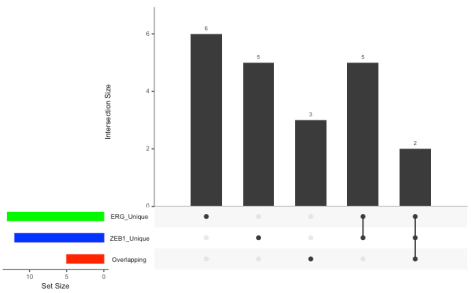
(A) Transcript-level annotation of ERG peaks identified 41.47% of peaks to bind to the promoter region of transcripts.
(B) Overlap between ERG and ZEB1 peaks in HUVECs. P-value was calculated by permutation test as described in Methods.
(C) Density of ERG peak summit distances to the ZEB1 peak summit. The 400bp region (+/-200bp) centred on the ZEB1 peak summit is denoted by the two dashed red lines. ERG peaks that fell within the 400bp ZEB1 peak summit region were those described as overlapping ZEB1 peaks.
(D) Heatmap displaying the ERG ChIP-seq enrichment centred on the ZEB1 peak summit positions.
(E) Transcript-level annotation of ZEB1 and ERG overlapping peaks, ZEB1 unique peaks and ERG unique peaks identified 77.07% of overlapping ZEB1 and ERG peaks, 78.88% of ZEB1 unique peaks and 32.42% of ERG unique peaks to bind to the promoter region of transcripts.
(F) Biotype annotation of overlapping and unique peak sets revealed ~63% to be bound to protein coding transcripts.

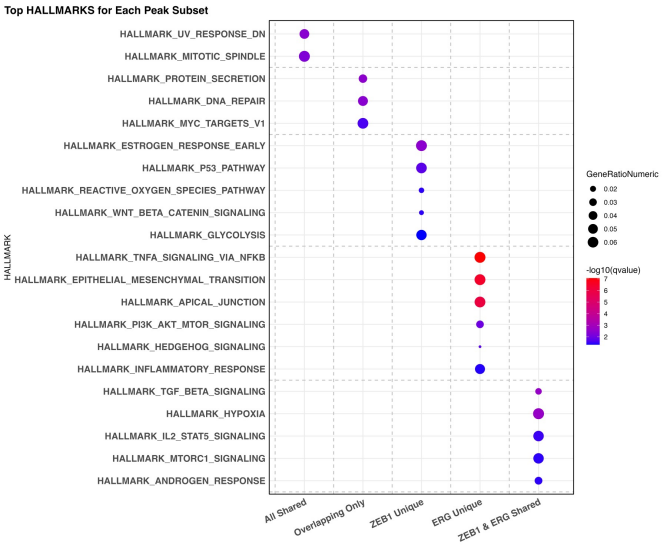
D), suggesting ERG peaks summits coincide with ZEB1 peaks summits and a strong co-binding relationship between ZEB1 and ERG in HUVECs. In addition, ERG ChIP-seq signal was enriched around sites of ZEB1 binding (Fig 4.5E). Furthermore the 5966 ZEB1 peaks with adjacent ERG summits accounted for 47.4% of all significant ZEB1 peaks (Fig 4.5C), indicating that almost half of ZEB1 binding in HUVECs displays a potential co-binding with ERG. From this, we can hypothesise that ERG plays a key role in the behaviour of ZEB1 as a TF in HUVECs. The genomic regions of binding of peaks that overlap and are specific to each transcript identified the majority (~78%) of overlapping and ZEB1 unique peaks to be assigned to the promoter regions of transcripts (Fig 4.5F, H). Conversely, the ERG only peaks showed 32.42% of peaks bound to the promoter of transcripts, with 21% binding to intergenic regions and the majority of the remaining peaks binding at intragenic regions (Fig 4.5J). This suggested that ZEB1 and ERG co-bind preferentially at the promoter regions of transcripts as opposed to intra and inter genic regions. However, this was likely to be expected with the majority of ZEB1 peaks binding at the promoter of transcripts. Transcript biotype assignment of

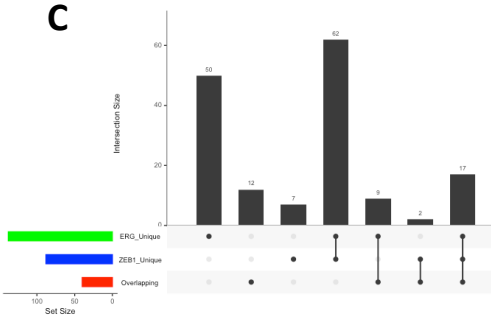
overlapping and TF specific peaks identified ~63% of bound transcripts to be protein coding (Fig 4.5G, I, K).

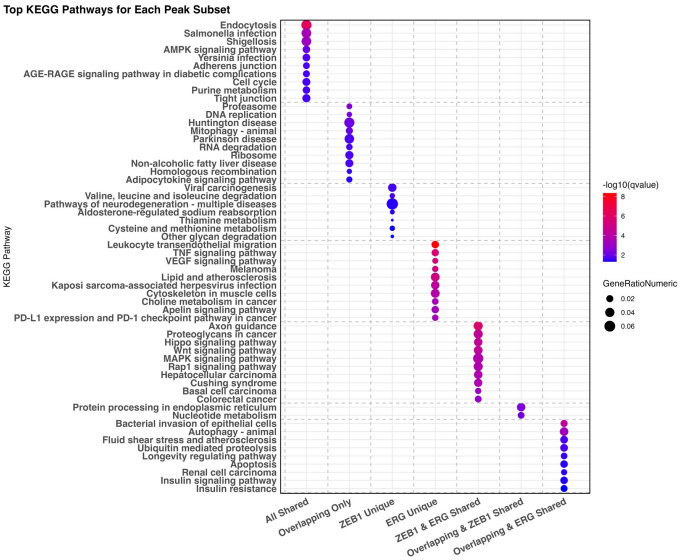
4.3.6 Functional enrichment analysis of overlapping and ZEB1/ERG specific peaks identified a shared role of ZEB1 and ERG in binding to genes that regulate the cell cycle

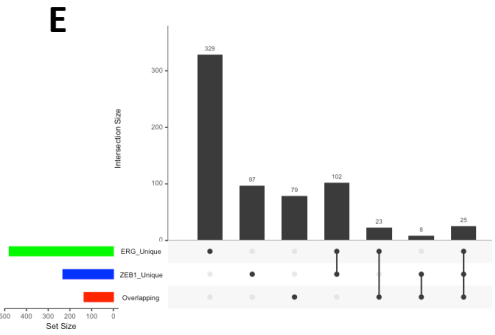
To investigate whether overlapping and ZEB1/ERG specific peaks contributed to separate biological functions we extracted the ZEB1 peaks that overlap ERG peaks, ZEB1 unique peaks and ERG unique peaks and carried out functional enrichment analyses to identify common and unique results (Fig 4.6A-F). Analyses against the HALLMARKS database (Fig 4.6A,B) identified mitotic spindle to be significantly enriched in overlapping, ZEB1 only and ERG only peaks, suggesting that ZEB1 and ERG can bind to different genes involved at the mitotic spindle, with some mitotic spindle related genes co-bound by both ZEB1 and ERG. HALLMARKS enriched in the overlapping peaks only identified genes co-bound by ZEB1 and ERG to play a role in protein secretion, DNA repair and MYC targets. ZEB1 unique peak targets were enriched for the p53 pathway and Wnt Beta Catenin signalling, suggesting a role of ZEB1 in these pathways. ERG unique peaks bound to genes enriched for TNFA signalling, PI3K-Akt signalling and Hedgehog signalling, indicating a role of ERG within key signalling pathways in ECs. Furthermore, ERG unique HALLMARKS included apical junction related bound genes. EMT was also enriched in ERG only peaks, but surprisingly not in ZEB1 only peaks. Genes bound by ZEB1 and genes bound by ERG separately showed enrichment of TGFB and IL2 signalling, suggesting each TF plays a role in the same inflammation related pathways but do not necessarily co-bind the genes involved. Additionally, hypoxia was enriched in both ZEB1 unique and ERG unique peaks, again displaying a potentially non-overlapping role of ZEB1 and ERG in hypoxia. KEGG pathway analysis (Fig 4.6C,D) identified


A
Intersection Size
ERG_Unique
ZEB1_Unique
Overlapping
Set Size


B
Top HALLMARKS for Each Peak Subset
HALLMARK_UV_RESPONSE_DN
HALLMARK_MITOTIC_SPINDLE
HALLMARK_PROTEIN_SECRETION
HALLMARK_DNA_REPAIR
HALLMARK_MYC_TARGETS_V1
HALLMARK_ESTROGEN_RESPONSE_EARLY
HALLMARK_P53_PATHWAY
HALLMARK_REACTIVE_OXYGEN_SPECIES_PATHWAY
HALLMARK_WNT_BETA_CATENIN_SIGNALING
HALLMARK_GLYCOLYSIS
HALLMARK_TNFA_SIGNALING_VIA_NFKB
HALLMARK_EPITHELIAL_MESENCHYMAL_TRANSITION
HALLMARK_APICAL_JUNCTION
HALLMARK_PI3K_AKT_MTOR_SIGNALING
HALLMARK_HEDGEHOG_SIGNALING
HALLMARK_INFLAMMATORY_RESPONSE
HALLMARK_TGF_BETA_SIGNALING
HALLMARK_HYPOXIA
HALLMARK_IL2_STAT5_SIGNALING
HALLMARK_MTORC1_SIGNALING
HALLMARK_ANDROGEN_RESPONSE
HALLMARK
All Shared
Overlapping Only
ZEB1 Unique
ERG Unique
ZEB1 & ERG Shared
GeneRatioNumeric
-log10(qvalue)


C
Intersection Size
ERG_Unique
ZEB1_Unique
Overlapping
Set Size


D
Top KEGG Pathways for Each Peak Subset
Endocytosis
Salmonella infection
Shigellosis
AMPK signaling pathway
Yersinia infection
Adherens junction
AGE-RAGE signaling pathway in diabetic complications
Cell cycle
Purine metabolism
Tight junction
Proteasome
DNA replication
Huntington disease
Mitophagy - animal
Parkinson disease
RNA degradation
Ribosome
Non-alcoholic fatty liver disease
Homologous recombination
Adipocytokine signaling pathway
Viral carcinogenesis
Valine, leucine and isoleucine degradation
Pathways of neurodegeneration - multiple diseases
Aldosterone-regulated sodium reabsorption
Thiamine metabolism
Cysteine and methionine metabolism
Other glycan degradation
Leukocyte transendothelial migration
TNF signaling pathway
VEGF signaling pathway
Melanoma
Lipid and atherosclerosis
Kaposi sarcoma-associated herpesvirus infection
Cytoskeleton in muscle cells
Choline metabolism in cancer
Apelin signaling pathway
PD-L1 expression and PD-1 checkpoint pathway in cancer
Axon guidance
Proteoglycans in cancer
Hippo signaling pathway
Wnt signaling pathway
MAPK signaling pathway
Rap1 signaling pathway
Hepatocellular carcinoma
Cushing syndrome
Basal cell carcinoma
Colorectal cancer
Protein processing in endoplasmic reticulum
Nucleotide metabolism
Bacterial invasion of epithelial cells
Autophagy - animal
Fluid shear stress and atherosclerosis
Ubiquitin mediated proteolysis
Longevity regulating pathway
Apoptosis
Renal cell carcinoma
Insulin signaling pathway
Insulin resistance
KEGG Pathway
All Shared
Overlapping Only
ZEB1 Unique
ERG Unique
ZEB1 & ERG Shared
Overlapping & ZEB1 Shared
Overlapping & ERG Shared
-log10(qvalue)
GeneRatioNumeric


E
Intersection Size
ERG_Unique
ZEB1_Unique
Overlapping
Set Size

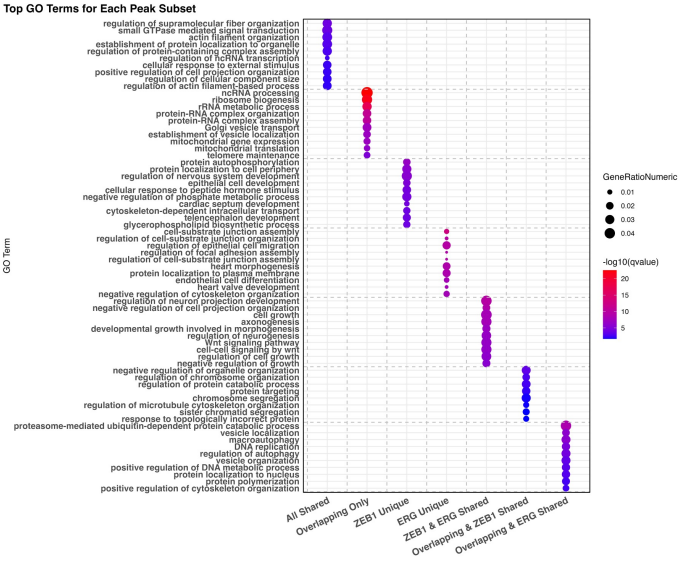

F
Top GO Terms for Each Peak Subset
regulation of supramolecular fiber organization
small GTPase mediated signal transduction
actin filament organization
establishment of protein localization to organelle
regulation of protein-containing complex assembly
regulation of ncRNA transcription
cellular response to external stimulus
positive regulation of cell projection organization
regulation of cellular component size
regulation of actin filament-based process
ncRNA processing
ribosome biogenesis
RNA metabolic process
protein-RNA complex organization
protein-RNA complex assembly
Golgi vesicle transport
establishment of vesicle localization
mitochondrial gene expression
mitochondrial translation
telomere maintenance
protein autophosphorylation
protein localization to cell periphery
regulation of nervous system development
epithelial cell development
cellular response to peptide hormone stimulus
negative regulation of phosphate metabolic process
cardiac septum development
cytoskeleton-dependent intracellular transport
telencephalon development
glycerophospholipid biosynthetic process
cell-substrate junction assembly
regulation of cell-substrate junction organization
regulation of epithelial cell migration
regulation of focal adhesion assembly
regulation of cell-substrate junction assembly
heart morphogenesis
protein localization to plasma membrane
endothelial cell differentiation
heart valve development
negative regulation of cytoskeleton organization
regulation of neuron projection development
negative regulation of cell projection organization
cell growth
axonogenesis
developmental growth involved in morphogenesis
regulation of neurogenesis
Wnt signaling pathway
cell-cell signaling by wnt
regulation of cell growth
negative regulation of growth
negative regulation of organelle organization
regulation of chromosome organization
regulation of protein catabolic process
protein targeting
chromosome segregation
regulation of microtubule cytoskeleton organization
sister chromatid segregation
response to topologically incorrect protein
proteasome-mediated ubiquitin-dependent protein catabolic process
vesicle localization
macroautophagy
DNA replication
regulation of autophagy
vesicle organization
positive regulation of DNA metabolic process
protein localization to nucleus
protein polymerization
positive regulation of cytoskeleton organization
GO Term
All Shared
Overlapping Only
ZEB1 Unique
ERG Unique
ZEB1 & ERG Shared
Overlapping & ZEB1 Shared
Overlapping & ERG Shared
GeneRatioNumeric
-log10(qvalue)

***Figure 4.6.* Functional enrichment analyses against the HALLMARKS, KEGG and GO Biological Process databases for ZEB1 and ERG overlapping, ZEB1 unique and ERG unique bound regions in HUVECs identified shared and individual cellular processes.**

(A-B) UpSet and Dotplot showing the overlap of HALLMARKS enrichment between overlapping and unique peak sets.

(C-D) UpSet and Dotplot showing the overlap of KEGG pathway enrichment between overlapping and unique peak sets.

(E-F) UpSet and Dotplot showing the overlap of GO BP enrichment between overlapping and unique peak sets.

adherens and tight junction pathways to be enriched in all peak subsets, suggesting ZEB1 and ERG co-bind genes related to the junctions as well as binding to genes uniquely. Furthermore, the cell cycle was enriched in all peak subsets along with the AGE-RAGE signalling pathway. ZEB1 and ERG overlapping peaks (co-bound) displayed an enrichment of the DNA replication pathway along with proteasome, RNA degradation and Ribosome pathways. ZEB1 unique peaks were related to metabolism and glycan degradation. ERG unique peaks were involved in TNF and VEGF signalling pathways along with apelin. Also, ERG peaks showed an enrichment of genes related to the cytoskeleton in muscle cells. Interestingly, genes bound by ZEB1 and ERG separately identified several signalling pathways; Hippo, Wnt, MAPK and Rap1. The Hippo pathway contains AP-1 factors, the motif of which was significantly enriched in the ZEB1 peaks. The enrichment of these pathways bound by both ZEB1 and ERG uniquely, but not co-bound, indicates an individual regulation of these pathways by ZEB1 and ERG. We could hypothesise that both ZEB1 and ERG are required for the regulation of these pathways and that KO of both ZEB1 and ERG could inhibit the signalling activity. GO BP analysis (Fig 4.6.E,F) identified all peak subsets to be enriched for regulation of cell projection organisation and a response to external stimulus, processes that are key in ECs and angiogenesis. The ZEB1 and ERG co-bound peaks were enriched for RNA and protein related processes in line with the KEGG pathway results. Mitochondrial related processes were also enriched along with telomere maintenance. The peaks unique to ZEB1

were enriched for metabolism and development related processes. The peaks unique to ERG were enriched for junction and adhesion related GO terms. GO terms enriched by both ZEB1 unique and ERG unique peaks included cell projection and axonogenesis related terms. Furthermore, Wnt signalling and cell growth were also enriched. Co-bound ZEB1 and ERG peaks and ZEB1 unique peaks were both enriched for GO terms related to chromosome organisation and segregation and microtubule cytoskeleton organisation suggesting ZEB1 to play a role in the cell cycle, with some involved genes also co-bound by ERG. The increase in number of pathways/terms in ERG only peaks is a reflection of the greater number of ERG only bound regions compared to ZEB1 only. This simple comparison of terms needs to be considered carefully as many terms/pathways may consist of similar lists of genes but have slightly different term names and so cannot be considered a definite comparison of biological function, but it can provide a level of insight. Taken together, these functional enrichment results identified both shared and distinct biological roles for ZEB1 and ERG bound regions in HUVECs, with co-bound predominately associated with RNA processing, DNA replication and cell cycle regulation, while ZEB1 uniquely bound regions suggested a role of ZEB1 in metabolic and developmental pathways with ERG uniquely bound regions related to adhesion and key signalling pathways. The functional enrichment highlights the potential cooperative and independent functions of ZEB1 and ERG in EC regulation, warranting further investigation into their context-specific gene regulatory mechanisms.

4.3.7 Motif enrichment analysis of overlapping peaks did not show enrichment for the ZEB1 motif

To validate the co-binding of ZEB1 and ERG, we performed motif enrichment analysis on the ZEB1 peaks that overlap with ERG peaks (Fig 4.7A). As expected, the ERG motif was

present in 53% of overlapping peaks. The AP-1 motif was also significantly enriched and was present in 8.78% of overlapping peaks. Strikingly, the ZEB1 motif was not significantly enriched, suggesting ZEB1 is not directly binding to genomic regions in the peaks that overlap with ERG peaks. While the ZEB1 motif was not significantly enriched, the ZEB1 motif may still be present in some of the peaks. To investigate this, we extracted the ZEB1 peaks that have the presence of a ZEB1 motif and cross-referenced this with the overlapping ZEB1 and ERG peaks to identify a list of ZEB1 peaks that co-bind with ERG and have the ZEB1 motif present. This revealed 19.43% (1159) of the 5966 overlapping ZEB1 and ERG peaks to have a ZEB1 motif present (Fig 4.7B), indicating ZEB1 can directly bind to ~20% of these genomic regions and indirectly binds to ~80%. For further experimentation, we could perform ZEB1 ChIP-seq on HUVECs with ERG KO and determine which of the ZEB1 and ERG overlapping peaks are still bound by ZEB1.

4.3.8 Motif enrichment in ZEB1 unique peaks reveals an enrichment of the ZEB1 motif and potential binding redundancy with other TF motifs

We next performed motif analysis on the ZEB1 unique peaks to assess whether the proportion of direct ZEB1 binding was increased in peaks only bound by ZEB1 and not ERG. Indeed, the ZEB1 motif was significantly enriched and identified in 34.14% of peaks (Fig 4.7C). There appeared to be sequence redundancy amongst the known motif results with several motifs sharing a similar sequence to the ZEB1 motif. To explore this, we examined the de novo motif enrichment results for ZEB1 unique peaks (Fig 4.7D). This approach scans the input sequences for enriched sequence repeats and then finds the best matches to known TF motifs as opposed to scanning for known motif sequences. De novo motif analysis identified the significantly enriched sequence 3-NNNKBYACCTGN present in 34.03% of

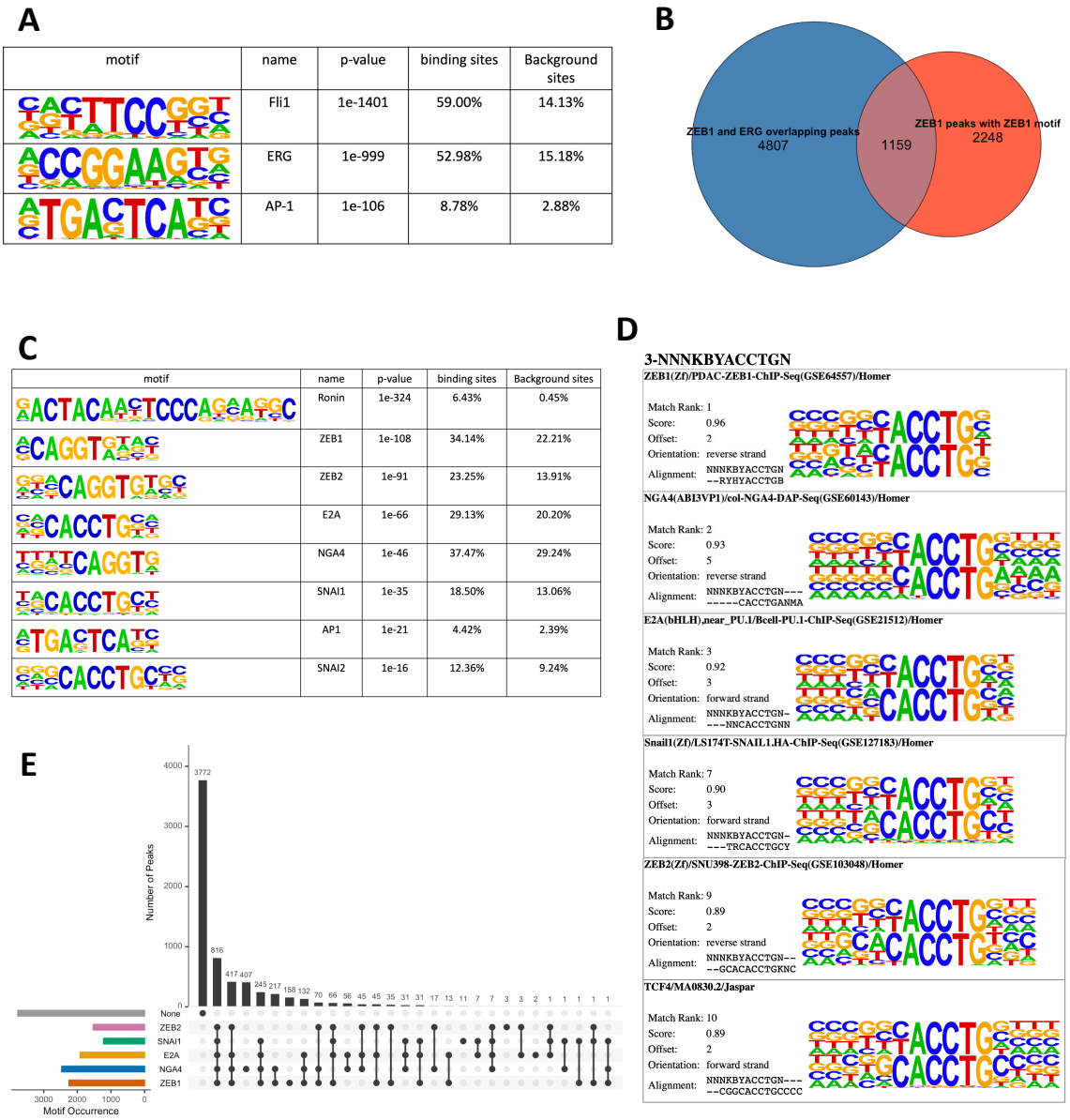


***Figure 4.7.* Motif enrichment analysis of overlapping ZEB1 and ERG bound regions did not identify the ZEB1 motif to be significantly enriched but the motif is still present within the overlapping peaks and known motif and De novo motif enrichment analysis of ZEB1 uniquely bound regions revealed a significantly enriched sequence motif that matched to the known ZEB1 binding motif and also matched highly to other TF binding motifs including SNAI1.**

(A) The top 3 non-redundant binding motifs enriched in the 200bp regions of ZEB1 ChIP-seq peaks centred on peak summits that overlap with ERG peak summit binding regions.

(B) Venn diagram showing the number of overlapping ZEB1 and ERG peak summit regions that contain a ZEB1 motif.

(C) Known motif analysis of ZEB1 uniquely bound regions identified the significant enrichment of the ZEB1 binding motif.

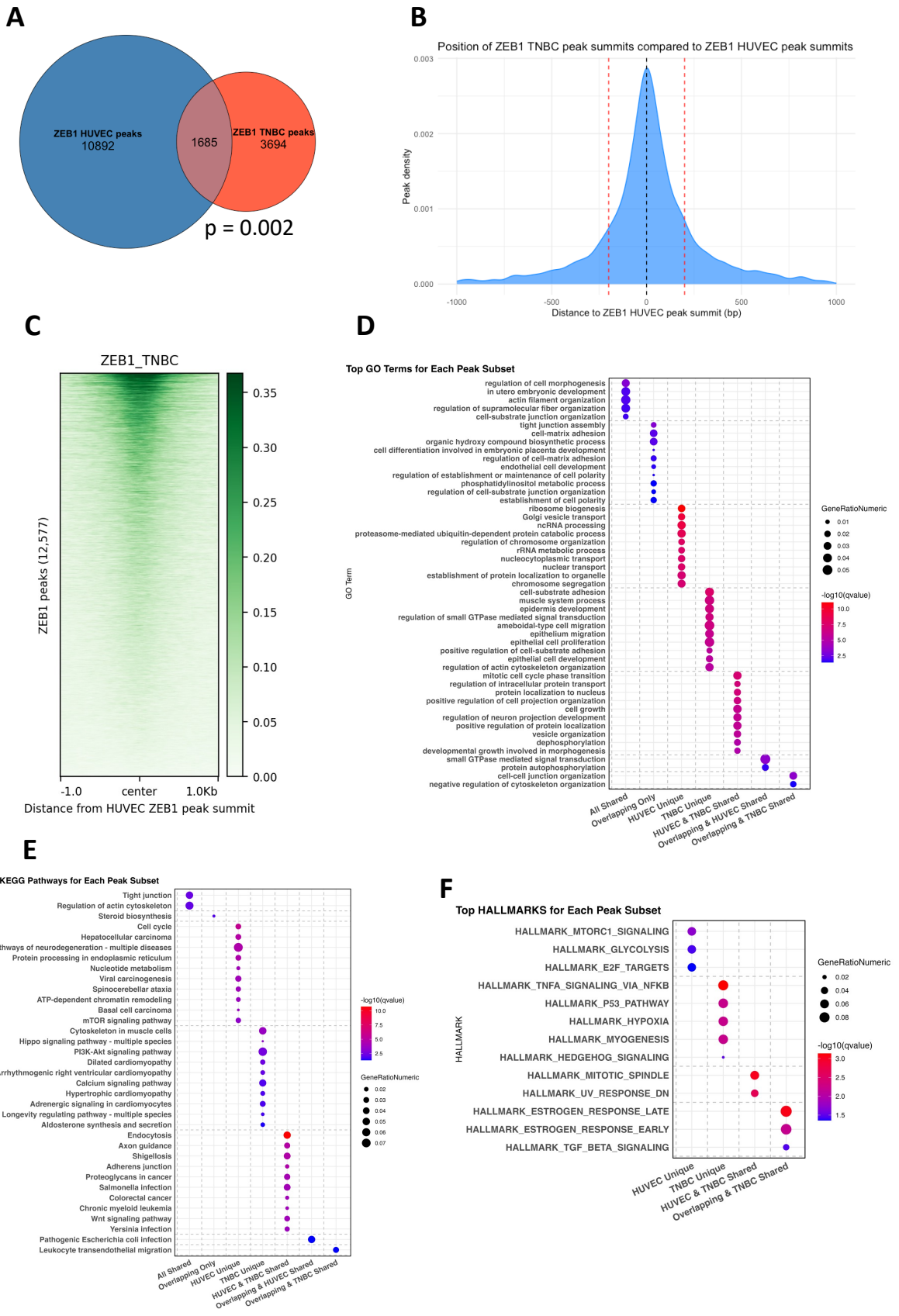
(D) *De novo* motif analysis identified the sequence 3-NNNKBYACCTGN to be significantly enriched in the ZEB1 unique binding regions with the highest match being against the ZEB1 binding motif, but with other strong matches against NGA4, E2A, SNAI1, ZEB2 and TCF4. The "Score" denotes the match strength, with 1 being a perfect match.

(E) UpSet plot displaying the overlap of enriched motifs in the ZEB1 uniquely bound regions.

sequences to match to the ZEB1 motif. We also explored the other TF motif matches to the enriched sequence with a match score > 0.85 (1 being a perfect match) and found that 3-NNNKBYACCTGN also matched NGA4, E2A, SNAI1, ZEB2 and TCF4 known TF motifs (Fig 4.7D). Identifying the ZEB1 unique peaks which contain ZEB1, NGA4, E2A, SNAI1 and ZEB2 motifs revealed 57% of the peaks to not contain any of these motifs (Fig 4.7E). As noted in the motif enrichment results, 34% contained the ZEB1 motif. Interestingly, 12.3% of peaks contained all 5 motifs. The redundancy between sequences and the high match scores between the enriched sequence motif in ZEB1 unique peaks and several TFs, with ZEB1 being the highest, suggests that ZEB1 may also be able to bind to motifs that are canonically assigned to other TFs. Further exploration into this would shed light on the direct and indirect binding behaviour of ZEB1, with the current analyses presented here discussing the binding of ZEB1 to be limited to the presence/lack of the canonical ZEB1 motif. For example, if ZEB1 can bind to the NGA4 motif, discovering ERG peaks that contain this motif could propose the hypothesis that ZEB1 co-binds with ERG at certain genomic regions through the direct binding to genes via the NGA4 motif. This was not followed up in this thesis.

4.3.9 Comparison of ZEB1 HUVEC ChIP-seq with a publicly available ZEB1 triple-negative breast cancer cell model ChIP-seq dataset identified 1685 overlapping peak regions related to junction, cell-matrix adhesion and cell polarity

To investigate the specific binding patterns of ZEB1 in HUVECs, we reanalysed a publicly available ZEB1 ChIP-seq dataset performed in MDA-MB-231 cells, a model of triple negative breast cancer (TNBC) (Feldker et al., 2020). Interestingly, our analysis pipeline discovered 5379 significant peaks compared to 12,617 in the original publication. While the analysis pipelines are similar, the original authors used a more relaxed MACS2 p-value cutoff


A
ZEB1 HUVEC peaks
10892
1685
ZEB1 TNBC peaks
3694
p = 0.002
B
Position of ZEB1 TNBC peak summits compared to ZEB1 HUVEC peak summits
Peak density
Distance to ZEB1 HUVEC peak summit (bp)
C
ZEB1_TNBC
ZEB1 peaks (12,577)
-1.0
center
1.0Kb
Distance from HUVEC ZEB1 peak summit
D
Top GO Terms for Each Peak Subset
GO Term
GeneRatioNumeric
-log10(qvalue)
All Shared
Overlapping Only
HUVEC Unique
TNBC Unique
HUVEC & TNBC Shared
Overlapping & HUVEC Shared
Overlapping & TNBC Shared
E
Top KEGG Pathways for Each Peak Subset
KEGG Pathway
F
Top HALLMARKS for Each Peak Subset
HALLMARK

<u>Figure 4.8.</u> Reanalysis of a ZEB1 ChIP-seq dataset in MDA-MB-231 cells as a model of triple-negative breast cancer identified 13.4% of ZEB1 HUVEC binding sites overlapped with ZEB1 TNBC binding sites.

(A) Overlap between ZEB1 HUVEC and ZEB1 TNBC peaks. P-value was calculated by permutation test as described in section 5.2 Methods.
(B) Density of ZEB1 TNBC peak summit distances to the ZEB1 HUVEC peak summit. The 400bp region (+/- 200bp) centred on the ZEB1 HUVEC peak summit is denoted by the two dashed red lines. ZEB1 TNBC peaks that fell within the 400bp ZEB1 HUVEC peak summit region were those described as overlapping peaks.
(C) Heatmap displaying the ZEB1 TNBC ChIP-seq enrichment centred on the ZEB1 HUVEC peak summit positions.
(D) Dotplot showing the overlap of GO BP enrichment between overlapping and unique peak sets.
(E) Dotplot showing the overlap of KEGG pathway enrichment between overlapping and unique peak sets.
(F) Dotplot showing the overlap of HALLMARKS enrichment between overlapping and unique peak sets.

of 1e-2 to call peaks for input to IDR. We used 1e-3 (which is still considered relaxed) to match our original analysis of ZEB1 ChIP-seq in HUVECs to increase comparability of datasets. Indeed, running MACS2 with a p-value cutoff of 1e-2 for the ZEB1 TNBC ChIP-seq data before IDR analysis identified 7893 significant peaks, which is still less than the original authors identified. This highlights the requirement for careful validation of input parameters in bioinformatics analyses as subtle changes can result in different results. Furthermore, the need for complete transparency in the methods of bioinformatics analyses, perhaps through the provision of all commands and scripts used in publications, is essential for the reproducibility of results. In these analyses, we continued with the 5379 significant peaks detected using our analysis pipeline. To assess overlap between the HUVEC and TNBC ZEB1 ChIP-seq peaks we employed the same procedure as the ERG HUVEC comparison in which peaks of the two datasets were considered overlapping if the summits were within 200bp of each other, resulting in 1685 overlapping peaks (Fig 4.8A,B). The ZEB1 TNBC signal enrichment at ZEB1 HUVEC peak summits revealed an enrichment within +/-1000 bp of the peak summit with a slight increase towards the centre of the summit (Fig 4.8C). This revealed

that ZEB1 binds in different genomic locations in different cell types and may change function based on the cellular environment. Furthermore, different cell types may have differing sites of accessible chromatin which inherently will result in different areas for ZEB1 to bind. In this instance, ZEB1 could have a different transcriptional effect in endothelial cells compared to TNBC cells. Indeed, functional enrichment analysis identified genes annotated to overlapping peaks to be associated with tight junction, cell-matrix adhesion and cell polarity while HUVEC unique peaks related to chromosome organisation and MTOR signalling and TNBC unique peaks enriched for epithelial cell development and hypoxia. Interestingly, HUVEC and TNBC uniquely bound ZEB1 regions share enrichment of terms associated with mitosis, cell growth, adherens junctions and Wnt signalling, suggesting ZEB1 may be involved in regulating these processes but binds to different genes in the signalling pathways dependent on the cell type.

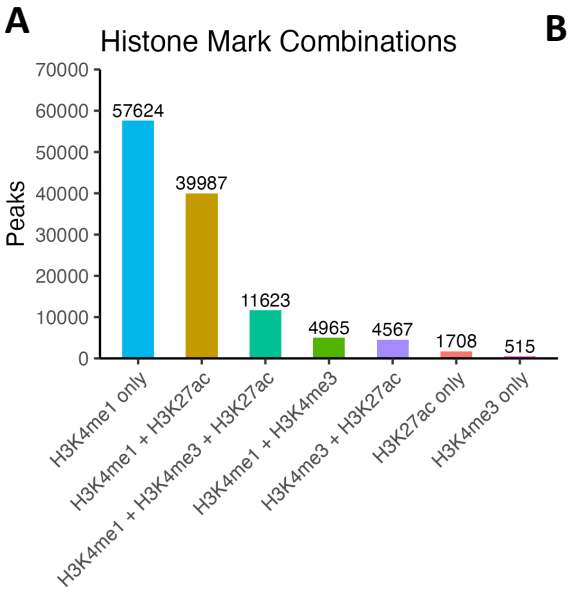
4.3.10 Quality control and preprocessing of publicly available ENCODE data for H3K4me1, H3K4me3 and H3K27ac histone marks

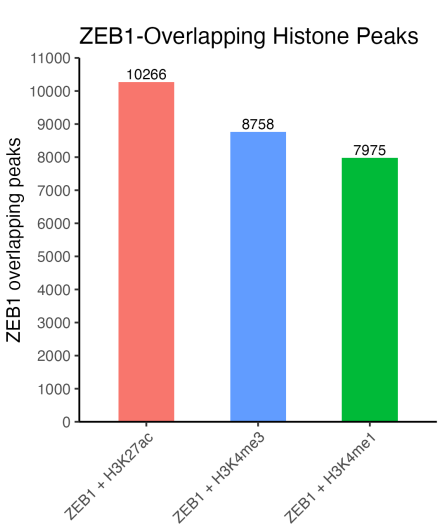
To investigate the presence of ZEB1 peaks within promoters and enhancers we reanalysed publicly available histone data for H3K4me1 (enhancer region marker), H3K4me3 (promoter region marker) and H3K27ac (active region marker) from ENCODE (see methods for accession IDs). Upon quality control of the FASTQ files it was noticed that the majority of the files show many reads with bases of poor quality. We removed bases of poor quality which reduced the number of counts. As an example, the raw fastq file of H3K4me1 replicate 1 contained 1,100,622,240 bp and 30,572,840 reads. Of these, 266,808,038 bp (24.2% of total bp) and 23,578,326 reads (77.1% of total reads) passed QC. We continued with the analysis but understanding the potential impacts of poor-quality sequencing data on downstream analyses. Furthermore, the poor quality displayed in some of the samples

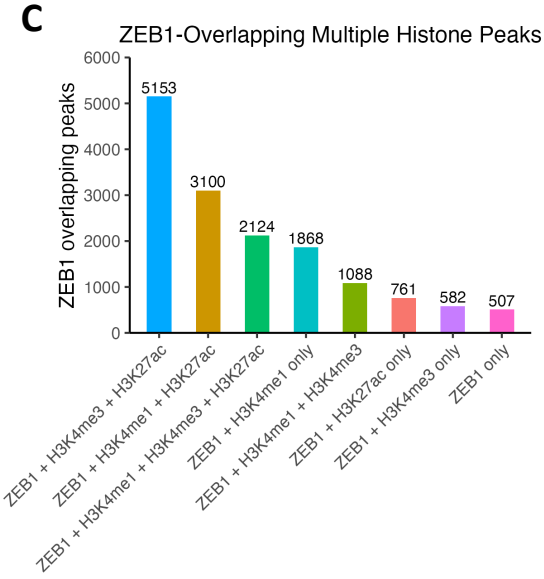
further validates the approach of merging BAM files prior to peak calling to maximise signal, as described in methods, since some replicates are of poor quality and could result in false negative peaks.

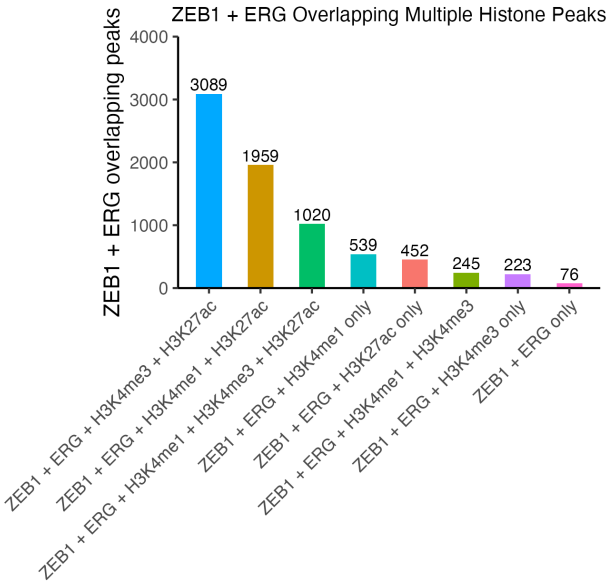
4.3.11 ZEB1 binding overlaps primarily with active histone marks

Peak calling identified 105,086, 18,550 and 49,247 peaks for H3K4me1, H3K4me3 and H3K27ac histone marks respectively. 39,987 peaks displayed overlap between H3K4me1 and H3K27ac denoting active enhancer regions in HUVECs, 4965 peaks were overlapping for H3K4me3 and H3K27ac identifying active promoter regions, and 11,623 regions overlapped H3K4me1, H3K4me3 and H3K27ac suggesting active regions with adjacent enhancer/promoters (Fig. 4.9A). To investigate the overlap between ZEB1 and histone mark peaks we extracted the 400bp region around the ZEB1 peak summits (as previously described when overlapping with ERG peaks) and intersected these regions against the full histone peaks. We used the full histone peaks as opposed to reduced regions as the broader peaks give a less established summit to calculate a distance from and may result in false negative overlaps. Interestingly, 10,266 of the 12,577 ZEB1 peaks summit regions overlapped a H3K27ac peak (Fig 4.9B), which is often used to signify active regulatory elements of the genome, suggesting that the majority of ZEB1 bound regions are sites of active regulation activity while 2,311 ZEB1 bound regions are not at active sites. To pursue this analysis, we would reanalyse HUVEC ChIP-seq data for the repressive histone mark H3K27me3 and DNase-seq data to identify whether the ZEB1 peaks not bound to active sites are associated with repressed/poised enhancers/promoters or non-accessible chromatin sites, but for the purposes of this thesis we utilised publicly available BigWig signalling tracks for visualisation of these marks and did not call peaks. 8758 ZEB1 summit regions were associated with the









E

ZEB1 Overlapping Multiple Histone Peaks ZEB1 Motif Presence			
Peak subset	Total overlapping peaks	Peaks with ZEB1 motif	%
ZEB1 + H3K4me3 + H3K27ac	5153	884	17.2
ZEB1 + H3K4me1 + H3K27ac	3100	847	27.3
ZEB1 + H3K4me1 + H3K4me3 + H3K27ac	2124	580	27.3

F

ZEB1 + ERG Overlapping Multiple Histone Peaks ZEB1 Motif Presence			
Peak subset	Total overlapping peaks	Peaks with ZEB1 motif	%
ZEB1 + ERG + H3K4me3 + H3K27ac	3089	426	13.8
ZEB1 + ERG + H3K4me1 + H3K27ac	1959	439	22.4
ZEB1 + ERG + H3K4me1 + H3K4me3 + H3K27ac	1020	206	20.2

<u>Figure 4.9.</u> Reanalysis of histone marker peak datasets identified the majority of ZEB1 bound regions to reside within active promoter regions in HUVECs.

(A) Quantification of histone marker peaks within HUVECs.
(B) Quantification of 400bp ZEB1 peak summit regions that overlap histone marker peaks.
(C) Combinations of overlapping ZEB1 and histone marker peaks
(D) Combinations of overlapping ZEB1 and ERG peaks that overlap histone marker peaks.
(E) Proportion of overlapping ZEB1 and histone peaks that have the presence of a ZEB1 motif.
(F) Proportion of overlapping ZEB1, ERG and histone peaks that have the presence of a ZEB1 motif.

promoter histone marker H3K4me3 and 7975 overlapped H3K4me1 peaks (Fig 4.9B) indicating enhancer regions, suggesting that ZEB1 may regulate gene transcription directly at promoters while also playing a role as a transcription effector by binding to enhancer elements, possibly recruiting other co-factors previously discussed. It is important to note that the total of the ZEB1 overlapping peaks is greater than the number of ZEB1 peaks. This is due to the fact that the overlapping peaks are not mutually exclusive. We intersected the peaks which overlap histone marks to identify regions of multiple histone and ZEB1 binding (Fig 4.9C). The greatest number of ZEB1 summits overlapping histone marks was 5153 overlapping with H3K4me3 and H3K27ac (no H3K4me1), which revealed ZEB1 to bind to active promoter regions and is indicative of direct gene regulation. However, 3100 ZEB1 peak summits overlapped H3K4me1 and H3K27ac peaks (no H3K4me3) which shows a binding to active enhancer regions. Furthermore 2124 ZEB1 peaks overlapped all 3 histone marks which could suggest a dynamic function of ZEB1 between enhancers and promoters at these regions. However, H3K4me3 has been shown to also be associated with active enhancers and not exclusively promoters (Pekowska et al., 2011), albeit in T-cells.

4.3.12 ZEB1 direct binding associated primarily with promoters, with some overlap at enhancers

We focused our analysis on the ZEB1 and histone mark overlaps that exhibit a H3K27ac peak and performed motif analysis on these peak sets to assess whether direct or indirect ZEB1 binding is associated with active promoters or enhancers. The ZEB1 motif was only significantly enriched in the ZEB1 overlap with all 3 histone marks and was present in 27.50% (584/2124) of overlapping regions suggesting that most direct binding of ZEB1 at active sites occurs at adjacent enhancers and promoters as opposed to active promoters or active enhancers alone. As described above, we also cross-referenced all ZEB1 peak summit regions that were identified to have the ZEB1 motif present with our histone overlapping peak subsets to quantify the number of peaks with the ZEB1 motif regardless of enrichment results (Fig 4.9E). We identified 27.3% (580/2124) regions overlapping ZEB1, H3K4me1, H3K4me3 and H3K27ac, 27.3% (847/3100) regions overlapping ZEB1, H3K4me1 and H3K27ac and 17.2% (884/5153) regions overlapping ZEB1, H3K4me3 and H3K27ac with the ZEB1 motif present. These results suggest that direct ZEB1 binding shows greater association with active promoters than active enhancers, although the majority of peaks display likely indirect ZEB1 binding due the lack of predicted ZEB1 motif within the called peak region.

4.3.13 Co-binding of ZEB1 and ERG occurs primarily in active promoter regions

We also applied the histone marker overlap analysis to peaks common to ZEB1 and ERG. The co-binding regions of ZEB1 and ERG are largely located in active regions denoted by H3K27ac (Fig 4.9D). Furthermore, the ZEB1 and ERG overlapping peaks are mostly associated with active promoter regions, agreeing with the genomic region annotation previously discussed (Fig 4.5F). In addition, overlapping ZEB1 and ERG peaks also bound in

active enhancer and overlapping active promoter/enhancer regions. Of these overlaps, 22.4% (439/1959) ZEB1 + ERG + H3K4me1 + H3K27ac, 13.8% (426/3089) ZEB1 + ERG + H3K4me3 + H3K27ac peaks and 20.2% (206/1020) ZEB1 + ERG + H3K4me1 + H3K4me3 + H3K27ac had the ZEB1 motif to indicate direct binding (Fig 4.9. F). These results suggest that co-binding of ZEB1 and ERG is mostly found in active promoter regions and may form a complex to drive transcription of co-bound genes and that the direct binding of ZEB1 at ERG co-bound regions most likely occurs primarily at promoter regions.

4.3.14 The top five significantly enriched ZEB1 ChIP-seq peaks in HUVECs annotated to REXO4, KCTD10, GAS8, LOC105372273 and ISY1-RAB43 are related to immunoregulation, angiogenesis and splicing

In order to analyse the mechanism of ZEB1 binding in HUVECs at regions with the greatest ChIP-seq enrichment we identified the top five most enriched peaks by p-value and visualised the sequencing data alongside the reanalysed publicly available ERG and histone data. The top five peaks were annotated to genes REXO4 (REX4 homolog), KCTD10 (potassium channel tetramerization domain containing 10), GAS8 (growth arrest specific 8), LOC105372273 (uncharacterized LOC105372273) and ISY1-RAB43 (ISY1-RAB43 readthrough) (Appendix 4.1 D-H). ZEB1 ChIP-seq peaks reside in active promoter regions of genes REXO4, KCTD10, and ISY1-RAB43. It is important to note that while the peak annotation identified a peak at the ISY1-RAB43 readthrough, this is simply because of the transcript it was annotated to spans these two genes. However, the peak also resides at the promoter of transcripts encoding ISY1 alone. Since without further experimentation we cannot confirm which transcript ZEB1 is binding to, and there is a small increase in ZEB1 signal at the RAB43 promoter also, we decided to continue with the peak assignment as ISY1

alone. Interestingly, the ZEB1 peak at REXO4 does not overlap with a predicted ZEB1 motif, suggesting indirect binding. Furthermore, there is an ERG peak that overlaps ERG motifs and the ZEB1 peak, alluding to ZEB1 indirectly binding to the promoter of REXO4 via co-binding with ERG. The peak at GAS8 lies in a region of open chromatin further along the gene with no obvious enhancer, promoter or active signal but displays the presence of many predicted ZEB1 binding motifs in a relatively small genomic region, suggesting a cluster of direct ZEB1 binding. LOC105372273 is an uncharacterised region of the genome that appears to reside in the gene DOCK6. The peak assigned here did not show any signal other than ZEB1 and a slight increase in DNase-seq signal and displays a cluster of condensed predicted ZEB1 motifs similar to GAS8. These results suggested that ZEB1 can have different behaviours of regulation from direct binding at the promoters of genes to binding to regions of open chromatin further along the gene length, perhaps for co-regulation in complex with other TFs or cofactors. These results also highlighted the importance of critically assessing the assignment of peaks to genes, as GAS8 for example is annotated to the promoter, but it is the promoter of a specific transcript (ENST00000569558.5) that is not protein coding. In future we may amend the peak assignment method to assign to the nearest gene as discussed in the method section. It also highlights the need to be critical of peak assignment in publications and to not simply rely on the percentage of peaks assigned to genomic region (e.g. 77.7% of peaks assigned to promoter regions in the ZEB1 HUVEC dataset).

The functions of REXO4 in endothelial cells is not clear, but the protein has been implicated in hepatocellular carcinoma in which it was linked to tumour-infiltrating macrophages and NK cells and was suggested to play an immunoregulatory role (Chen *et al.*, 2021; Ruan *et al.*, 2021). Since immune-EC crosstalk is essential in vascular function and angiogenesis, we might speculate that ZEB1 binding to the REXO4 gene may regulate these

immune processes through REXO4 expression. KCTD10 has been shown to be involved in vascular development and pathologies in several tissues (Hu *et al.*, 2014; Ren *et al.*, 2014; Angrisani *et al.*, 2021; Feng, Wang and Wang, 2022; Cheng *et al.*, 2024). Briefly, inhibition of KCTD10 was shown to affect diabetic retinopathy through potential inhibition of angiogenesis (Feng, Wang and Wang, 2022) and is involved, perhaps critically, in heart, blood vessel, brain and cardiovascular system and notch signalling in embryonic development (Hu *et al.*, 2014; Ren *et al.*, 2014; Cheng *et al.*, 2024). Potential regulation of this gene by ZEB1 suggests that ZEB1 may also play a key role in the development of vasculature and ultimately regulate key signalling pathways. Little could be found regarding GAS8 and endothelial cells. However, GAS6, another member of the growth arrest specific protein family, has been suggested to play a role in the regulation of angiogenesis (Lei *et al.*, 2020) through which we could speculate a similar function for GAS8. LOC105372273/DOCK6 has been shown to modulate EC migration, vascular smooth muscle differentiation and pericyte recruitment, suggesting a key role in vascular development and pathology (Benson and Southgate, 2021). Furthermore, DOCK6 has been shown to be implicated in the TGF-B signalling pathway (Benson and Southgate, 2021) which is known to play an important role in vascular processes including vascular homeostasis and EndoMT. An enriched ZEB1 signal was also identified at DOCK4 (not shown here), another member of the DOCK family, which upon knockdown by siRNA has been shown to lead to a decrease in the development of branching vessels, indicating that DOCK4 is required for vessel sprouting along with tubule development and EC adhesion (Abraham *et al.*, 2015). ZEB1 binding at DOCK proteins suggests ZEB1 influences important aspects of EC behaviour and angiogenesis. ISY1 is a splicing factor and has been shown to be expressed in retinal vascular endothelial cells (Bharadwaj *et al.*, 2013) as well as being related to angiogenesis in diabetes (Su *et al.*, 2024). Indeed, ZEB1 is known to partly

mediate processes such as Epithelial-Mesenchymal Transition (EMT), during which extensive alternative splicing occurs and ZEB1 expression itself has been shown to repress epithelial splicing regulatory protein 1 (ESRP1) (Larsen *et al.*, 2016; Maturi *et al.*, 2018). The potential regulation of splicing machinery by ZEB1 suggests ZEB1 may regulate alternative splicing in HUVECs and would benefit from further exploration.

4.3.15 ZEB1 directly binds to endothelial and mesenchymal cell marker genes in HUVECs that are known to be regulated in EndoMT

We examined the binding of ZEB1 to genes that are used as markers of ECs including PECAM1, CDH5, PROX1 and ERG (Appendix 4.1 I-L) where PROX1 is used as a marker for lymphatic ECs and is a driver of EC differentiation into lymphatic ECs. ZEB1 was found to directly bind to PECAM1 at the active promoter as well as several active enhancer regions along the gene length, suggesting a key role in the regulation of PECAM1. Similar binding behaviour was observed at the CDH5 gene, with ZEB1 directly binding at both the active promoter and active enhancer elements including an active enhancer adjacent to the active promoter. ZEB1 bound PROX1 at the active promoter and at an enhancer element upstream of the promoter that displayed an increase in the H3K27me3 signal, suggesting a potentially repressed/poised enhancer. ZEB1 directly bound ERG at active enhancer regions downstream of the promoter, but did not bind the promoter itself, suggesting ZEB1 may play a regulatory role through distal elements rather that directly initiating transcription. The binding of ZEB1 to key EC genes suggests that ZEB1 may play a role in the basic function of ECs and may regulate genes that maintain EC identity. From these observations we can hypothesise that ZEB1 binds and may regulate EC genes that maintain EC identity and plays a role in processes in which loss/gain of endothelial marker genes is observed, such as

EndoMT. Indeed, we probed the bound ZEB1 regions in HUVECs for mesenchymal markers CDH2, VIM and ACTA2 (Appendix 4.1 M-O) that are known to increase their expression during the shift towards a mesenchymal-like phenotype in EndoMT (Yoshimatsu and Watabe, 2022). We found ZEB1 to be directly bound to CDH2 at the active promoter as well as a region downstream of the promoter that displayed a cluster of predicted ZEB1 motifs and was not associated with a histone mark. ZEB1 was also directly bound at the promoter of ACTA2. While a reproducible peak was not identified for ZEB1 at the VIM promoter, there was an increase in ChIP signal compared to the IgG control suggesting some level of binding. The binding of ZEB1 to endothelial and mesenchymal marker genes whose expression is dynamic in the EndoMT process suggests ZEB1 may play a role in the shifting of endothelial phenotype into a transient mesenchymal state.

To further investigate the potential of ZEB1 being a factor in EndoMT we assessed the binding of ZEB1 to the genes of known EMT/EndoMT drivers. We found reproducible peaks at the promoters of SNAI1, TWIST2 and ZEB2 (Appendix 4.1 P-R), but not SNAI2 and TWIST1. Interestingly, the ZEB1 bound promoter region of TWIST2 did not display a H3K27ac signal signifying an active region, but did exhibit an increase in the H3K27me3 repression signal, suggesting that this is a repressed promoter in HUVECs and may be poised for transcriptional activity, perhaps to induce EndoMT in response to required stimuli. The binding of ZEB1 at this region may indicate a potential role of ZEB1 in the repression of this promoter region, therefore playing a regulatory role of EndoMT. ZEB1 was also found to bind to an active enhancer region downstream of the repressed promoter of TWIST2.

Taken together, these findings suggest that ZEB1 occupies a central regulatory position in balancing the expression of genes critical for endothelial identity with those required for a mesenchymal phenotype.

4.3.16 ZEB1 directly binds to markers of proliferation and EC activation in HUVECs

Since functional enrichment analysis for ZEB1 bound regions identified the cell cycle process we evaluated the binding profile of ZEB1 to key cell cycle genes MKI67 and CDC45 (Appendix 4.1 S,T) and observed ZEB1 to bind to the active promoter region of both, indicative of direct role of ZEB1 in HUVEC proliferation. Furthermore, ZEB1 was bound to the active promoter of DLL4 (Appendix 4.1 U), the gene product of which regulates angiogenesis (Pitulescu *et al.*, 2017). There was an enriched ChIP signal at the active promoter of NOTCH1 (Appendix 4.1 V), shown to regulate EC phenotype (Mack and Iruela-Arispe, 2018), and active enhancer regions along the gene length. DLL4 and NOTCH1 are involved in EC sprouts and tip cells during angiogenesis and the binding of ZEB1 to the promoter of these genes suggests a role of ZEB1 in angiogenesis. Since FOXO1 has been shown to be required for vessel sprouting and defining a tip cell phenotype (Miyamura *et al.*, 2024) we also probed the ZEB1 ChIP-seq data for binding to FOXO1. We found ZEB1 to bind to the active promoter of FOXO1 (Appendix 4.1 W). Furthermore, Notch signalling and FOXO1 has been shown to play a role in establishing and maintaining EC quiescence (Wilhelm *et al.*, 2016; Ren, 2018; Andrade *et al.*, 2021; Sun *et al.*, 2021), suggesting that ZEB1 may play a role in EC quiescence through binding to FOXO1 and NOTCH1. These results suggest that ZEB1 may be involved in angiogenesis and the stalk/tip EC cross-talk as well as maintaining a level of quiescence.

4.3.17 Integration of ZEB1 KD RNA-seq data in HUVECs revealed direct regulation by ZEB1 of five TFs, a histone deacetylase and other genes implicated in EndoMT and angiogenic processes

To identify direct and indirect regulation by ZEB1 in HUVECs, we integrated the ZEB1 HUVEC ChIP-seq data with differentially expressed genes (DEGs) obtained from ZEB1 knockdown (KD) RNA-seq analyses. Of the 296 DEGs, 170 were found to be bound by ZEB1 across 223 peaks (Fig 4.10A). Of these, 147 had promoter-bound peaks (±1 kb from the TSS), with 114 genes upregulated (thus repressed by ZEB1) and 33 genes downregulated (thus activated by ZEB1) upon ZEB1 KD (Fig 4.10A). To gain insight into the functional impact of these directly regulated genes, we performed functional enrichment analyses of both activated and repressed DEGs. In total, 51 Gene Ontology (GO) terms were significantly enriched, encompassing processes such as cell–cell adhesion, cytoskeleton organization, endothelial cell migration, cell polarity, endothelial/vascular development, endothelial cell differentiation, angiogenesis, and vascular permeability (Fig 4.10. B). KEGG pathway analysis further highlighted two pathways related to cytoskeleton regulation (Fig 4.10. C) and HALLMARKS analysis revealed an enrichment for genes involved in interferon alpha and gamma responses (Fig 4.10. D). While the endothelial nature of HUVECs may predispose these findings toward vascular processes, the results nonetheless emphasise a central regulatory role for ZEB1 in core endothelial biology.

We identified five TFs as direct ZEB1 targets: KLF4 (KLF transcription factor 4), ATF3 (activating transcription factor 3), IRF1 (interferon regulatory factor 1), BACH1 (BTB domain and CNC homolog 1) and ZNF395 (zinc finger protein 395). KLF4, ATF3, IRF1, and BACH1 were activated by ZEB1, whereas ZNF395 was repressed. KLF4 is essential for maintaining endothelial and vascular identity in adult mice and regulates key endothelial genes

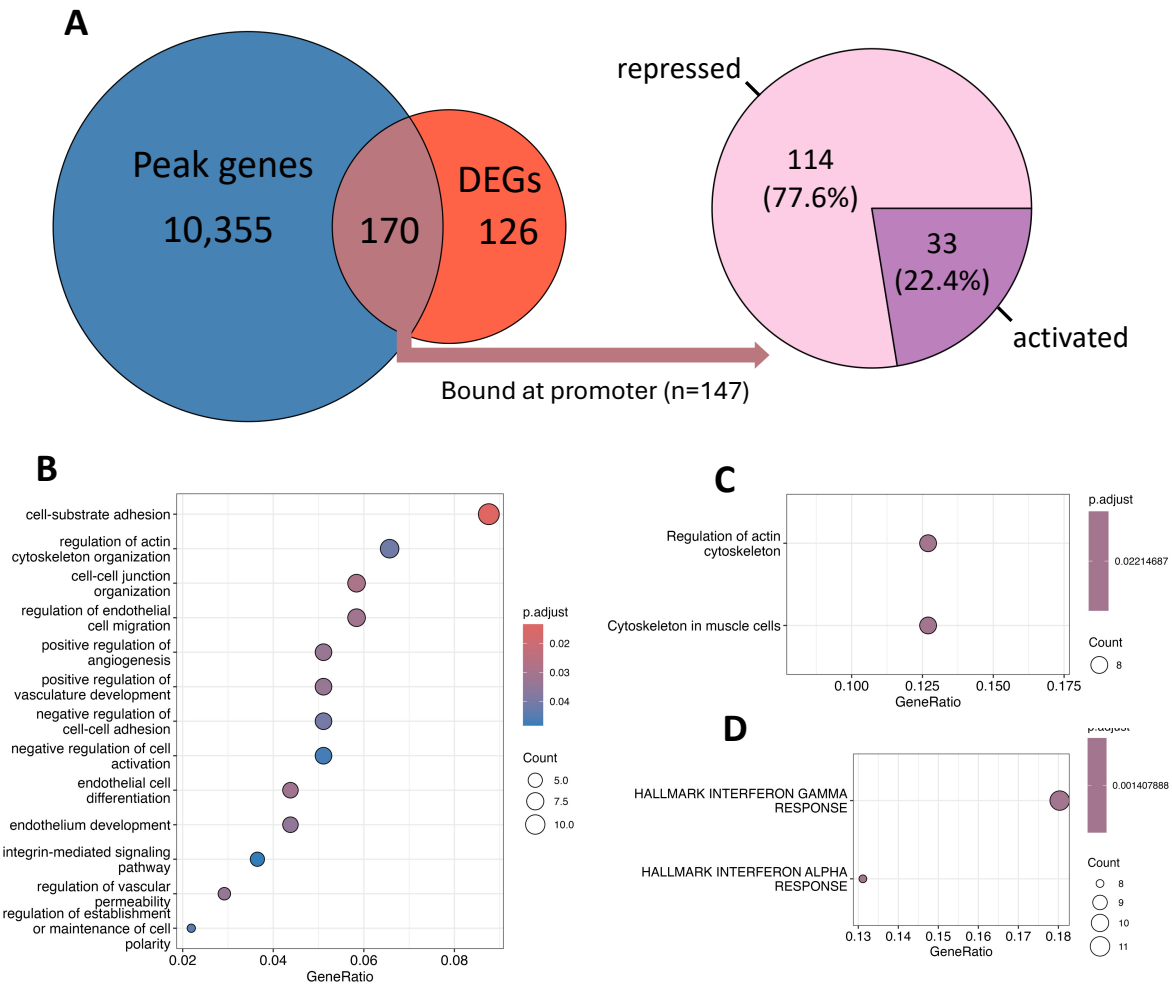


Figure 4.10. ***Integrated analysis of ZEB1 ChIP-seq and ZEB1 knockdown RNA-seq in HUVECs defined direct and indirect regulation by ZEB1.***

(A) Venn diagram reflecting the overlap between the DEGs identified by RNA-seq and the genes assigned to enriched ChIP-seq peaks to. Overlapping genes were deemed to be directly regulated by ZEB1, whereas DEGs not identified in the ChIP-seq peaks were indirect. Overlapping genes with peaks annotated to the promoter were subset into repressed and activated genes, where repressed are upregulated in the presence of ZEB1 knockdown and activated are downregulated.

(B) Dotplot of selected GO terms identified from functional enrichment analysis of genes directly regulated by ZEB1.

(C) Dotplot of KEGG pathways identified from functional enrichment analysis of genes directly regulated by ZEB1.

(D) Dotplot of HALLMARKS identified from functional enrichment analysis of genes directly regulated by ZEB1.

(Sangwung *et al.*, 2017; Sweet *et al.*, 2023). It can also activate enhancers to modulate endothelial gene expression (Moonen *et al.*, 2022). ATF3 binds to the promoter of TGFB2 in HUVECs to facilitate EndoMT (Hong *et al.*, 2020), is required for the vascular response to lung injury and alveolar regeneration (Niethamer *et al.*, 2023), primes muscle ECs for

angiogenesis (Fan *et al.*, 2021) and promotes angiogenesis and vessel repair after oxygen-induced retinopathy in mouse retina (Ueda *et al.*, 2025). IRF1, by contrast, exerts an anti-angiogenic effect in HUVECs and inhibits lung endothelial regeneration after injury (Lee *et al.*, 2008; Chen *et al.*, 2023). BACH1 represses endothelial cell (EC) proliferation, migration, and angiogenesis, triggering cell cycle arrest and apoptosis (Wang *et al.*, 2016). Deletion of BACH1 in ECs was shown to reduce the expression of endothelial adhesion molecules ICAM1 and VCAM1 and knockdown in HUVECs inhibited monocyte-endothelial adhesion (Jia *et al.*, 2022). BACH1 also suppresses ischemia-induced angiogenesis, potentially via Wnt signalling (Jiang *et al.*, 2020; Yusoff *et al.*, 2021) and has been implicated in mediating EndoMT (Li *et al.*, 2022; Meng *et al.*, 2023). Although less is known about ZNF395 in ECs, it has been associated with cancer and glioma progression (Jordanovski *et al.*, 2013; Xiao *et al.*, 2022). Notably, ZEB1's activation of TFs with both pro- and anti-angiogenic properties suggests it may maintain a quiescent vasculature while also serving as a pivotal switch between opposing angiogenic states. Moreover, the direct regulation of multiple TFs implies a broader controlling role for ZEB1 within the endothelial transcriptional network, warranting further integrative analyses of TF-specific ChIP-seq and RNA-seq data.

We also found that ZEB1 activates histone deacetylase 9 (HDAC9), which removes acetyl groups from histones and thereby represses transcription. This discovery opens avenues for investigating how ZEB1 may exert epigenetic control in HUVECs. Endothelial-specific knockout of HDAC9 has been found to reduce EndoMT in murine atherosclerosis models, indicating HDAC9's role in promoting EndoMT (Lecce *et al.*, 2021). Silencing HDAC9 inhibits endothelial sprouting in vitro and diminishes vessel growth in Matrigel plug assays and zebrafish, while HDAC9 deletion impairs retinal vessel outgrowth and blood flow

recovery after hindlimb ischemia (Kaluza *et al.*, 2013). Thus, ZEB1-driven HDAC9 expression may mediate both proangiogenic and EndoMT pathways in endothelial cells.

In addition, we identified the endothelial adhesion molecule ICAM1 as being activated by ZEB1, whereas EPCAM1 was repressed. Although EndoMT can reduce ICAM1 expression (Alvandi and Bischoff, 2021), these findings highlight a nuanced regulatory landscape in which ZEB1 differentially modulates adhesion molecules. We also found that ZEB1 activates CXCR4 and UNC5B, both of which are enriched in endothelial tip cells and are involved in vascular branching and angiogenesis (Strasser, Kaminker and Tessier-Lavigne, 2010; Unoki *et al.*, 2010; Noels *et al.*, 2014; Xu *et al.*, 2017; Li *et al.*, 2021; Pradella *et al.*, 2021; Furtado *et al.*, 2023; Cano *et al.*, 2024; Raza *et al.*, 2024). Collectively, these data suggest that ZEB1 can govern tip cell behaviour during angiogenesis and supports a model in which ZEB1 orchestrates multiple pathways—ranging from chromatin remodelling to transcription factor activation—to regulate endothelial cell function and fate.

4.4 Discussion

Our ChIP-seq analysis in HUVECs identified regions of ZEB1-DNA binding with a strong enrichment in promoter regions, suggesting that ZEB1 primarily targets gene promoters to influence transcriptional regulation. A substantial portion of the bound regions were associated with active chromatin marks, further supporting a role for ZEB1 at regions of transcription. Moreover, motif analysis revealed an enrichment for ETS (e.g. ERG) and AP-1 family motifs in ZEB1 bound regions, indicating ZEB1 may operate in conjunction with other TFs to establish regulatory networks in HUVECs. The preferential localisation of ZEB1 binding at promoter regions of protein-coding genes, along with its presence at noncoding transcripts such as lincRNAs and antisense RNAs, highlights its potentially multifaceted role

in regulating HUVEC function. Our data not only align with previous findings in cancer models but also extends these observations to ECs, implicating ZEB1 in processes such as endothelial identity maintenance, proliferation and EndoMT. The co-binding with ERG, a well-known endothelial TF, suggests that ZEB1 may contribute to a cooperative regulatory mechanism that alters the expression of genes crucial to vascular homeostasis and angiogenesis.

Furthermore, the integration of our ChIP-seq data with RNA-seq from a ZEB1 knockdown experiment implied a direct regulatory role for ZEB1 in modulating genes involved in endothelial function, proliferation, and EndoMT. However, given the complexity of transcriptional networks, future studies should consider higher-resolution approaches (e.g. single-cell RNA-seq or ATAC-seq) to dissect cell-to-cell variability and to further elucidate the interplay between chromatin accessibility and TF binding. In addition, incorporating three-dimensional chromatin conformation assays (such as Hi-C) could reveal enhancer-promoter interactions that refine our understanding of how ZEB1 and its co-factors orchestrate gene regulation over long genomic distances.

To build upon the findings presented in this chapter, several avenues for further investigation would be considered. Complementary assays such as CRISPR-mediated gene perturbation or TF knockdown experiments could validate whether the binding of ZEB1 is direct or indirect. Additionally, given the enrichment of ETS and AP-1 motifs, future studies should explore the potential interactions between ZEB1 and other TFs like ERG, using techniques such as co-immunoprecipitation or sequential ChIP experiments to provide deeper insights into these cooperative regulatory complexes. Moreover, our comparison of ZEB1 binding in HUVECs versus publicly available cancer cell model datasets emphasises the context-dependent nature of transcriptional regulation, suggesting that further comparative

analyses across different cell types or disease models may reveal novel insights into the dynamic role of ZEB1 in diverse biological contexts.

In conclusion, our comprehensive ChIP-seq analysis suggested that ZEB1 may be a key regulator of endothelial gene expression, predominantly binding at active promoter regions and likely acting in concert with other TFs to modulate vascular function. While questions remain, our findings provide a foundation for further exploration of the role of ZEB1 in endothelial biology and its broader implications in vascular health and disease. Continued integration of genomic, epigenomic and functional studies will be essential for unravelling the complex regulatory networks orchestrated by ZEB1.

Chapter 5: Analysis of publicly available endothelial cell scRNA-seq datasets revealed Zeb1 to be enriched in specialised endothelial subpopulations driving proliferative and immunoregulatory programs across diverse tissues

5.1 Introduction

Single cell RNA-sequencing (scRNA-seq) has revolutionised the study of endothelial biology by enabling the profiling of tens of thousands of ECs, allowing a granular view of tissue and phenotype specific transcriptional signatures and the diversity amongst them (Kalucka *et al.*, 2020; Kharchenko, 2021). Using this approach, the identification of both known and novel EC subpopulations is facilitated by clustering algorithms, which can often reveal previously unrecognised cellular states, transitions and relationships (Rohlenova *et al.*, 2020). Crucially, scRNA-seq can allow researchers to pinpoint expression patterns of key transcription factors (TFs) across subpopulations, associating those patterns to potential functional roles (Paik *et al.*, 2020; Koenig *et al.*, 2022; Ren *et al.*, 2023). In parallel, computational tools have emerged to infer gene regulatory networks and predict how perturbations might influence downstream targets (Osorio *et al.*, 2020, 2022).

In this chapter we present analyses probing ZEB1 expression in ECs from multiple publicly available scRNA-seq datasets, encompassing healthy and pathological states in murine and human systems. By combining differential expression, *in-silico* knockout (KO) modelling and functional enrichment analyses, this study aims to clarify the core endothelial processes regulated by ZEB1 and elucidate any phenotype-specific expression. By examining ZEB1 expression across diverse tissues and pathologies, the chapter highlights the

multifaceted nature of ZEB1, providing a foundation to understand the role of ZEB1 within endothelial heterogeneity and function.

5.2 Hypothesis and aim

Hypothesis: *ZEB1* expression is heterogenous between different EC phenotypes across developmental and pathological conditions and regulates angiogenic genes and pathways.

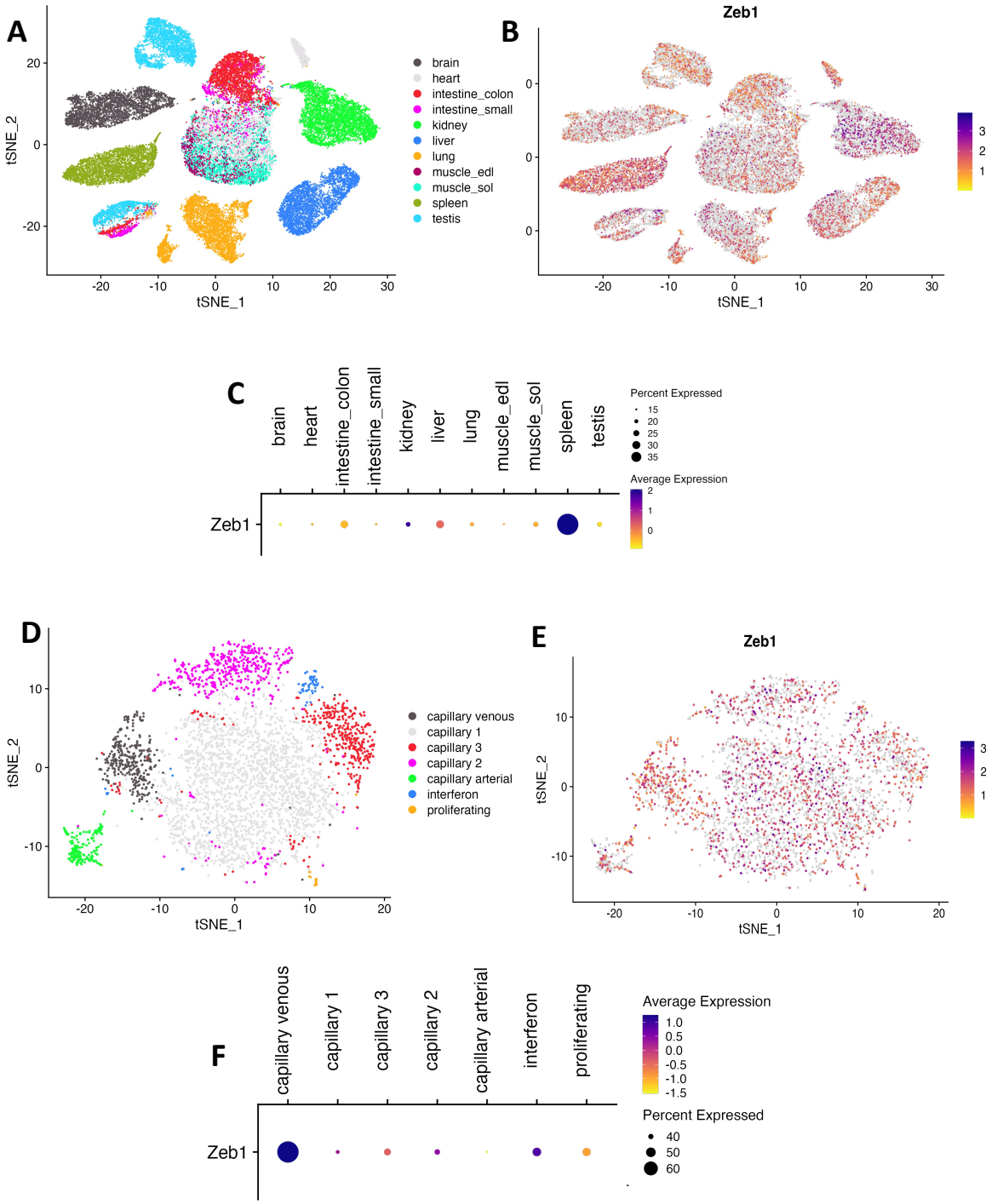
The hypothesis was tested through scRNA-seq analysis techniques of publicly available dataset to address the following aim:

Aim: To explore the contextual heterogeneity of *ZEB1* expression in ECs across diverse organ systems and angiogenic contexts using multiple scRNA-seq datasets.

5.3 Results

5.3.1 Zeb1 expression analysis across a scRNA-seq atlas of healthy murine tissue revealed Zeb1 to be preferentially expressed in spleen venous-capillary ECs.

To develop a general overview of Zeb1 expression we probed a publicly available endothelial cell scRNA-seq atlas of healthy murine endothelial cells across different tissues (Kalucka *et al.*, 2020). We found Zeb1 to be a marker for spleen ECs, displaying an increased expression compared to other tissue types (Fig 5.1A-C). Furthermore, 37.6% of spleen ECs expressed Zeb1, with all other tissue ECs expressing Zeb1 from 12.8% (extensor digitorum longus (EDL) skeletal muscle ECs) to 20.22% (liver ECs). These results indicated that under healthy conditions Zeb1 is preferentially expressed in spleen ECs compared to other tissue



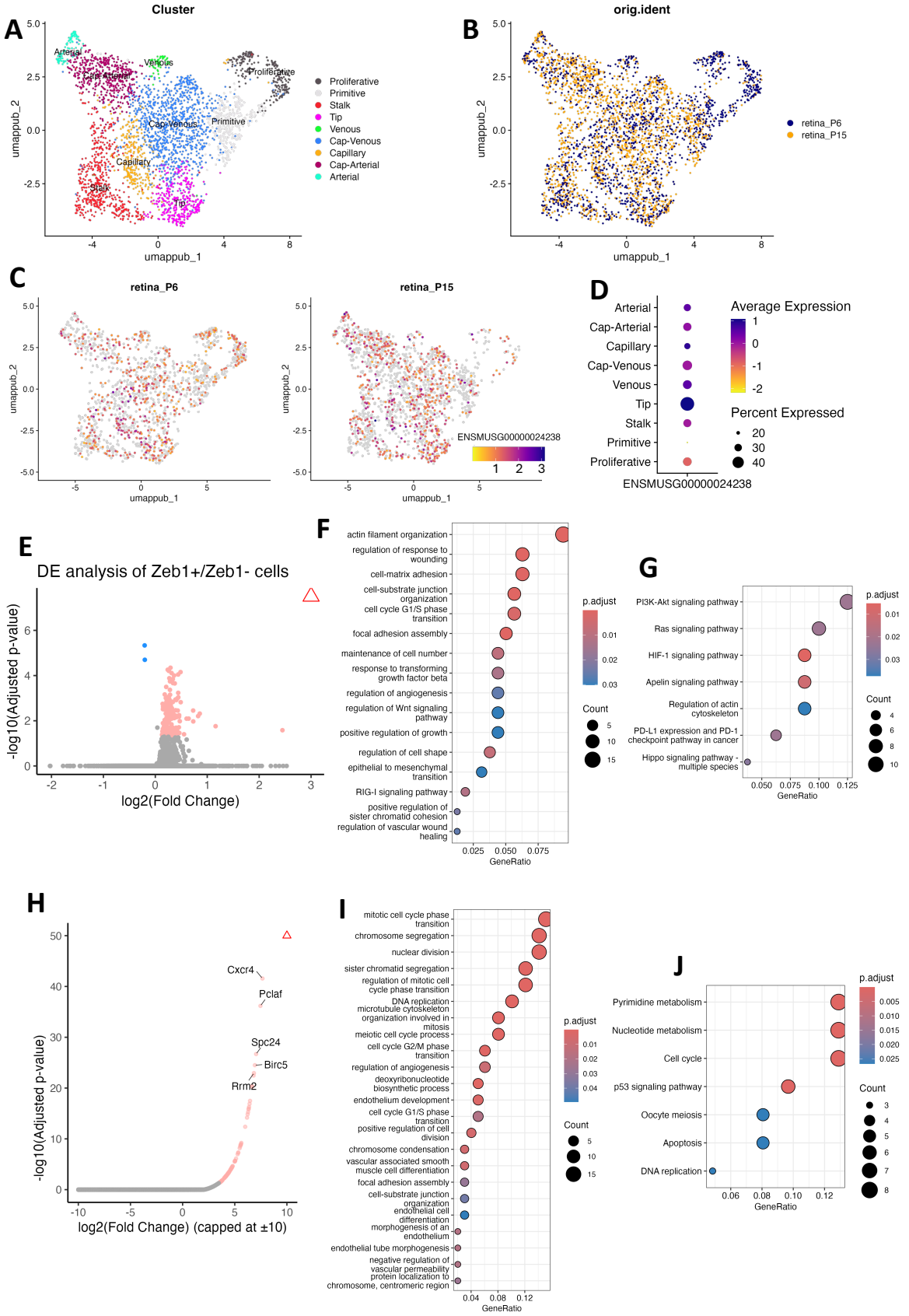
<u>Figure 5.1.</u> scRNA-seq analysis of a publicly available EC atlas identified ZEB1 to be preferentially expressed in capillary-venous ECs within the spleen

(A) t-SNE plot of ECs within tissues of the EC atlas.
(B) Feature of ZEB1 expression showed expression in every tissue of the EC atlas.
(C) Dotplot displaying the average expression and percent of cells expressing ZEB1 for each tissue type revealed increased expression in spleen ECs.
(D) t-SNE plot of the EC phenotypes within the spleen.
(E) Featureplot of ZEB1 showed expression across all spleen EC phenotypes.
(F) Dotplot for spleen EC phenotypes identified ZEB1 to show greatest expression and highest proportion of cells expressing ZEB1 in capillary-venous spleen ECs.

ECs in mice, potentially being required in EC behaviour in response to the spleen environment and function. Subsetting on spleen ECs identified Zeb1 to show highest expression in venous-capillary and interferon phenotypes and the lowest in arterial-capillary and proliferating (Fig 5.1D-E). Furthermore, spleen venous-capillary ECs showed the greatest proportion of cells to express Zeb1 at 61.5%, with other phenotypes ranging from arterial-capillary (31.3%) to interferon (41.4%). These results show that within the spleen Zeb1 is preferentially expressed in venous-capillary and interferon spleen EC phenotypes in healthy tissue.

5.3.2 Zeb1 expression was not significantly regulated upon quiescence entry in developing mouse retina vasculature

Since Zeb1 has been shown by qPCR to increase in expression during quiescence entry in retina ECs (Yu *et al.*, 2022), we decided to further investigate the expression of Zeb1 throughout retina development at the single-cell level by probing a publicly available retina EC scRNA-seq dataset of p6 and p15 mice (Chavkin *et al.*, 2022). To maintain comparability with the dataset we utilised the UMAP dimensions and cell type assignment provided by the original authors, retaining the same cells in the dataset. We found Zeb1 to be expressed in each EC phenotype and was significantly upregulated in tip cells compared to all other ECs (Fig 5.2A-D). Differential expression between p6 and p15 ECs did not identify Zeb1 to be significantly differentially expressed. We also probed for differential expression of Zeb1 for each EC phenotype between age (e.g. p6 tip cells vs p15 tip cells) and did not identify any differential expression. The results suggested that Zeb1 is upregulated in tip cells, but expression does not significantly change between p6 and p15, in contrast to previous work (Yu *et al.*, 2022).


A
Cluster
Arterial
Venous
Cap-Arterial
Proliferative
Cap-Venous
Primitive
Capillary
Stalk
Tip
Proliferative
Primitive
Stalk
Tip
Venous
Cap-Venous
Capillary
Cap-Arterial
Arterial
umappub_1
umappub_2
B
orig.ident
retina_P6
retina_P15
C
retina_P6
retina_P15
ENSMUSG00000024238
D
Arterial
Cap-Arterial
Capillary
Cap-Venous
Venous
Tip
Stalk
Primitive
Proliferative
ENSMUSG00000024238
Average Expression
Percent Expressed
E
DE analysis of Zeb1+/Zeb1- cells
-log10(Adjusted p-value)
log2(Fold Change)
F
actin filament organization
regulation of response to wounding
cell-matrix adhesion
cell-substrate junction organization
cell cycle G1/S phase transition
focal adhesion assembly
maintenance of cell number
response to transforming growth factor beta
regulation of angiogenesis
regulation of Wnt signaling pathway
positive regulation of growth
regulation of cell shape
epithelial to mesenchymal transition
RIG-I signaling pathway
positive regulation of sister chromatid cohesion
regulation of vascular wound healing
GeneRatio
p.adjust
Count
G
PI3K-Akt signaling pathway
Ras signaling pathway
HIF-1 signaling pathway
Apelin signaling pathway
Regulation of actin cytoskeleton
PD-L1 expression and PD-1 checkpoint pathway in cancer
Hippo signaling pathway - multiple species
GeneRatio
p.adjust
Count
H
Cxcr4
Pclaf
Spc24
Birc5
Rrm2
-log10(Adjusted p-value)
log2(Fold Change) (capped at ±10)
I
mitotic cell cycle phase transition
chromosome segregation
nuclear division
sister chromatid segregation
regulation of mitotic cell cycle phase transition
DNA replication
microtubule cytoskeleton organization involved in mitosis
meiotic cell cycle process
cell cycle G2/M phase transition
regulation of angiogenesis
deoxyribonucleotide biosynthetic process
endothelium development
cell cycle G1/S phase transition
positive regulation of cell division
chromosome condensation
vascular associated smooth muscle cell differentiation
focal adhesion assembly
cell-substrate junction organization
endothelial cell differentiation
morphogenesis of an endothelium
endothelial tube morphogenesis
negative regulation of vascular permeability
protein localization to chromosome, centromeric region
GeneRatio
p.adjust
Count
J
Pyrimidine metabolism
Nucleotide metabolism
Cell cycle
p53 signaling pathway
Oocyte meiosis
Apoptosis
DNA replication
GeneRatio
p.adjust
Count

<u>Figure 5.2.</u> scRNA-seq analysis of a publicly available retina EC dataset for p6 and p15 mice identified increased expression of Zeb1 in tip ECs.

(A) UMAP plotting visualising the cells and EC clusters in the dataset.
(B) UMAP plot splits by age of mice. P6 cells are shown in blue and p15 in yellow. The proliferating cluster is almost lost in p15 ECs.
(C) Featureplot of Zeb1 (ENSMUSG00000024238) expression split by age of mice showed expression of Zeb1 at both p6 and p15.
(D) Dotplot of Zeb1 (ENSMUSG00000024238) average expression and percent of cells expressing Zeb1 identified Zeb1 to be enriched in tip cells, with both the highest expression and the greatest proportion of cells expressing Zeb1.
(E) Volcano plot of Zeb1+/Zeb1- differentially expressed genes identified predominately upregulation of genes in Zeb+ cells, revealing a set of genes to be potentially regulated by Zeb1 and suggests Zeb1 to be an activator TF in the developing retina. Significantly upregulated genes are in red, downregulated in blue and not significant in grey. Zeb1 is represented as a triangle.
(F) Functional enrichment analysis against the Gene Ontology database for Zeb1 DEGs identified GO terms relating to adhesion and cell cycle.
(G) KEGG pathway functional enrichment identified several specific signalling pathways enriched in Zeb1+/- DEGs including PI3K-Akt and HIF-1.
(H) Differentially regulated genes predicted by *in-silico* knockout of Zeb1 by scTenifoldKNK. Highlighted are the top differentially regulated genes with Cxcr4, a tip cell marker, redicted to be the most perturbed. Zeb1 is represented as a triangle. Significantly regulated genes are plot in red and non-significant in grey.
(I) Functional enrichment analysis against the Gene Ontology database for significantly regulated genes upon Zeb1 *in-silico* KO identified GO terms relating to adhesion and cell cycle.
(J) KEGG pathway functional enrichment identified cell cycle and DNA replication pathways enriched in Zeb1 differentially regulated genes.

To further investigate Zeb1 in retinal ECs we performed differential expression between Zeb1+ and Zeb1- cells identifying 165 significant DEGs (Fig 5.2E). Subsequent functional enrichment analysis identified significant GO terms related to cell-matrix, cell-junction, angiogenesis, epithelial-to-mesenchymal transition and cell cycle (Fig 5.2F), suggesting Zeb1 may be involved in these processes in retinal ECs. Furthermore, KEGG pathway analysis identified PI3K-Akt, Ras, HIF-1, Apelin and hippo signalling pathways to be significantly enriched in the Zeb1 DEGs (Fig 5.2G), highlighting potential cascades influenced by Zeb1. We applied an *in-silico* KO of Zeb1 across all ECs in the dataset to predict genes that are regulated by Zeb1 within retinal ECs. This analysis identified 104 genes predicted to be perturbed by Zeb1 KO, including Cxcr4, a marker of tip ECs, and Pclaf, Spc24, Birc5 and Rrm2

which are involved in proliferation and DNA repair (Fig 5.2F). GO and KEGG analysis of the predicted perturbed genes identified pathways related to the cell cycle and DNA replication (Fig 5.2I-J).

These results indicate Zeb1 to not be differentially expressed between p6 and p15 retina ECs, suggesting Zeb1 expression is not altered throughout retinal development. However, Zeb1 was differentially upregulated in tip ECs, suggesting Zeb1 expression is highest in the pro-angiogenic EC phenotype. Furthermore, Zeb1 KO predicted Zeb1 to be involved in the cell cycle and DNA replication processes.

5.3.3 Zeb1 is upregulated in choroidal neovascularisation lesion endothelial cells and is predicted to orchestrate a proangiogenic transcriptional program

To evaluate whether we see a similar behaviour of Zeb1 in a pathological context, we applied scRNA-seq analyses to a publicly available dataset of choroidal neovascularisation (CNV) (Rohlenova *et al.*, 2020). We utilised the raw, normalised and batch corrected counts along with t-SNE dimension provided by the authors to ensure our analysis is comparable to the original publication. t-SNE projection identified a clear population of ECs present within the CNV condition, but not the healthy, which are deemed lesion ECs and was enriched for specialised EC phenotypes including tip, proliferating, neophalanx, immature and CNV transitioning ECs (Fig 5.3A-B). It is important to note that we also used the same cell annotation as the original publication after critically assessing clusters with canonical markers ourselves. We next examined Zeb1 expression across all cells and found Zeb1 to be detected in most phenotypes but showed an increased signal in the lesion ECs, specifically tip and proliferating phenotypes (Fig 5.3C-D). Indeed, differential expression analysis

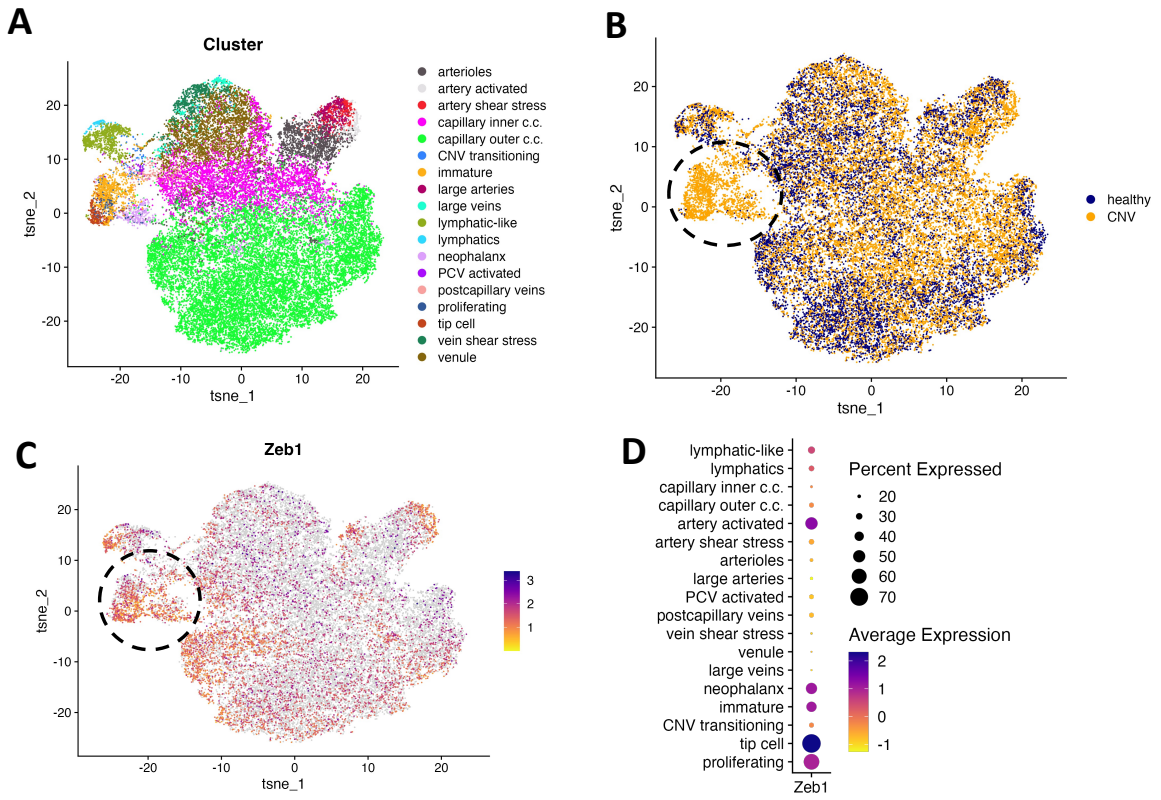
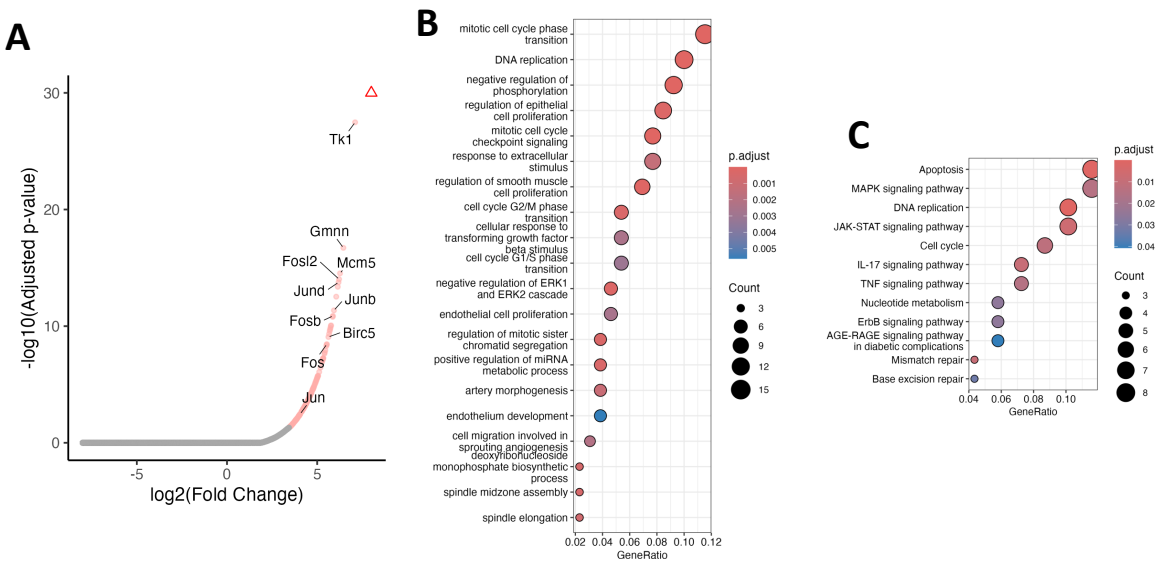


Figure 5.3. ***scRNA-seq analysis of a publicly available murine EC choroidal neovascularization (CNV) dataset identified increased expression of Zeb1 in lesion ECs, particularly tip ECs.***

(A) t-SNE of the EC phenotypes within the dataset.
(B) t-SNE coloured by condition with healthy ECs in blue and CNV ECs in yellow. Circled is a population of ECs only present in the CNV data, corresponding to lesion ECs.
(C) Featureplot of Zeb1 expression across all cells showed condensed expression in CNV lesion ECs. Lesion ECs are circled.
(D) Dotplot showing average expression and percent of cells expressing Zeb1 across EC phenotypes revealed and enrichment in lesion EC phenotypes, particularly tip cells, which showed the highest expression and greatest proportion of cells expressing Zeb1.

identified Zeb1 to be significantly upregulated in the lesion ECs compared to non-lesion ECs, suggesting Zeb1 may be upregulated in choroidal neovascularisation.

To further dissect the role of Zeb1, we performed an *in-silico* KO of Zeb1 within lesion ECs using scTenifoldKNK (Osorio *et al.*, 2022) to predict differentially regulated (DR) genes. 133 genes were predicted to be perturbed, including cell cycle and DNA-replication genes Tk1, Gmnn, Mcm5 and Birc5 as well as AP-1 factors amongst the most significantly altered (Fig 5.4A). Functional enrichment analysis revealed that these DR genes were significantly associated with pathways involved in cell cycle regulation, DNA replication and



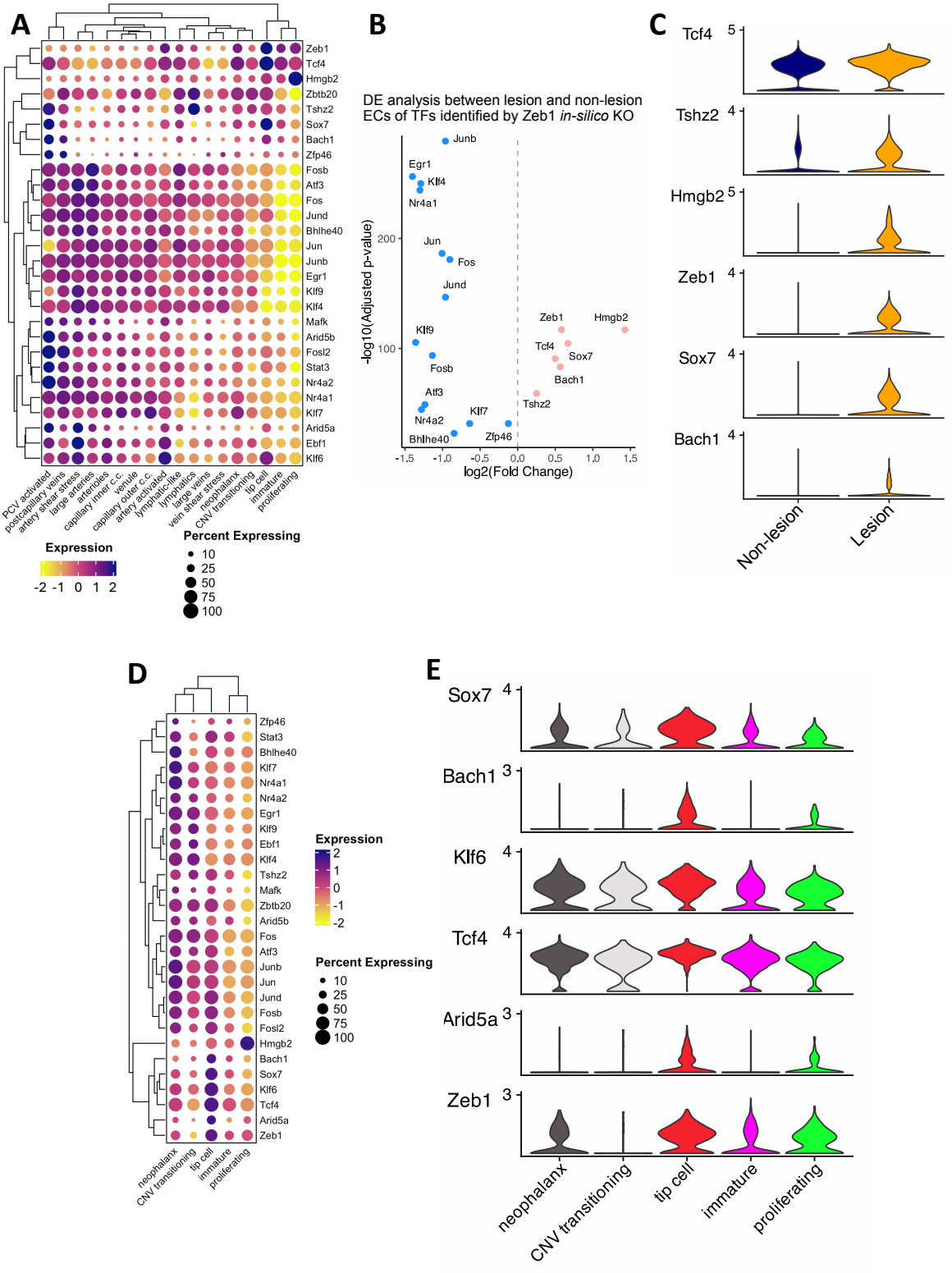
<u>Figure 5.4.</u> In-silico KO of Zeb1 in CNV lesion ECs revealed differential regulation of AP-1 factors.

(A) Differentially regulated (DR) genes predicted by *in-silico* Zeb1 KO in lesion ECs. Labelled are the most DR genes as well as AP-1 factors. Significant DR genes are in red, non-significant in grey. Zeb1 is represented as a red triangle.

(B) Dotplot of the significantly enriched GO terms identified by functional enrichment analysis of the significant DR genes revealed regulation of cell cycle.

(C) Dotplot of KEGG pathways enriched from DR genes identified cell cycle and immune related processes.

epithelial/mesenchymal transition-related processes (Fig 5.4B). Virtual Zeb1 KO also impacted signalling pathways important for cell survival and proliferation, as indicated by enrichment in apoptosis, MAPK signalling, JAK-STAT signalling and cell cycle pathways as well as inflammation pathways denoted by IL-17 and TNF signalling (Fig 5.4C). Closer examination of the DR genes identified 28 TFs predicted to be perturbed upon Zeb1 KO (Fig 5.5A). Differential expression analysis between lesion and non-lesion ECs revealed 20 of the DR TFs to be differentially expressed, with 6 upregulated in lesion ECs and 14 downregulated (Fig 5.5B). The downregulated TFs perturbed by *in-silico* Zeb1 KO in lesion ECs included AP-1 and factors and Klf4/7/9, suggesting reduced expression of these TFs during angiogenic repair. The 6 upregulated TFs included Zeb1, Hmgb2, Tcf4, Sox7, Bach1 and Tshz2, indicating these TFs to be required for regenerative angiogenesis in response to injury. Furthermore, the


A
Zeb1
Tcf4
Hmgb2
Zbtb20
Tshz2
Sox7
Bach1
Zfp46
Fosb
Atf3
Fos
Jund
Bhlhe40
Jun
Junb
Egr1
Klf9
Klf4
Mafk
Arid5b
Fosl2
Stat3
Nr4a2
Nr4a1
Klf7
Arid5a
Ebf1
Klf6
PCV activated
postcapillary veins
artery shear stress
large arteries
arterioles
capillary inner c.c.
venule
capillary outer c.c.
artery activated
lymphatic-like
lymphatics
large veins
vein shear stress
neophalanx
CNV transitioning
tip cell
immature
proliferating
Expression
-2 -1 0 1 2
Percent Expressing
10
25
50
75
100
B
DE analysis between lesion and non-lesion
ECs of TFs identified by Zeb1 in-silico KO
-log10(Adjusted p-value)
log2(Fold Change)
C
Tcf4
Tshz2
Hmgb2
Zeb1
Sox7
Bach1
Non-lesion
Lesion
D
Expression
Percent Expressing
E
Sox7
Bach1
Klf6
Tcf4
Arid5a
Zeb1
neophalanx
CNV transitioning
tip cell
immature
proliferating

<u>Figure 5.5.</u> In-silico KO of Zeb1 in CNV lesion ECs predicted perturbation of 28 transcription factors, 20 of which were differentially expressed between lesion and non-lesion ECs and 6 were upregulated in tip cells compared to other EC phenotypes in the lesion.

(A) Dotplot of the 28 transcription factors (TFs) that were predicted to be differentially regulated upon *in-silico* Zeb1 KO across all EC phenotypes. Zeb1, Tcf4 and Sox7 showed increased expression in tip cells.
(B) Differential expression analysis between lesion and non-lesion ECs of the 28 TFs predicted to be regulated by Zeb1 KO identified 6 upregulated and 14 downregulated TFs in lesion ECs. Zeb1, Hmgb2, Tcf4, Sox7, Bach1 and Tshz2 were upregulated, while AP-1 and Klf family factors were downregulated.
(C) Violin plots showing the expression of the upregulated TFs in (B). Tshz2, Hmgb2, Zeb1, Sox7 and Bach1 show a greater proportion of lesion ECs to express these TFs compared to non-lesion ECs, suggesting these TFs to regulated lesion EC related processes. Tcf4 is expressed in both lesion and non-lesion ECs, suggesting a requirement for overall EC function, but expression levels are elevated in lesion ECs.
(D) Dotplot of the 28 TFs that were predicted to be perturbed upon Zeb1 KO in lesion EC phenotypes only.
(E) Violin plot of the 6 TFs perturbed by *in-silico* Zeb1 KO that are upregulated in tip cells compared to other lesion EC phenotypes, including Sox7, Bach1, Klf6, Tcf4, Arid5a and Zeb1. Potential regulation of these TFs that are upregulated in tip ECs by Zeb1 suggests Zeb1 may impact a transcriptional network in tip cells within the lesion environment.

predicted regulation of these TFs by Zeb1 highlights a putative role of Zeb1 in coordinating the expression of TFs which are regulated in the angiogenic response of lesion ECs in CNV. Since we performed the *in-silico* KO on the lesion ECs only, we investigated the expression of the 28 TFs solely in the lesion ECs (Fig 5.5D). A distinct cluster consisting of Bach1, Sox7, Klf6, Tcf4, Arid5a and Zeb1 showed increased expression in tip cells compared to other lesion ECs, suggesting a potential TF regulatory network in tip cells that was predicted to be perturbed upon loss of Zeb1. Differential expression analysis between lesion EC phenotypes identified 6 of the 28 TFs predicted to be perturbed by Zeb1 to be upregulated in tip cells specifically (Fig 5.5E), including Sox7, Bach1, Klf6, Tcf4, Arid5a and Zeb1, indicating a requirement of these TFs in tip cell function in the CNV lesion. Predicted perturbance of these upregulated TFs by Zeb1 is suggestive of Zeb1 modulating a regulatory network in tip cells during angiogenesis. As Zeb1 was shown to also be expressed in proliferating ECs of the lesion (Fig 5.5E), we evaluated Zeb1 across the cell cycle phases in CNV (Fig 5.6). Indeed, it was

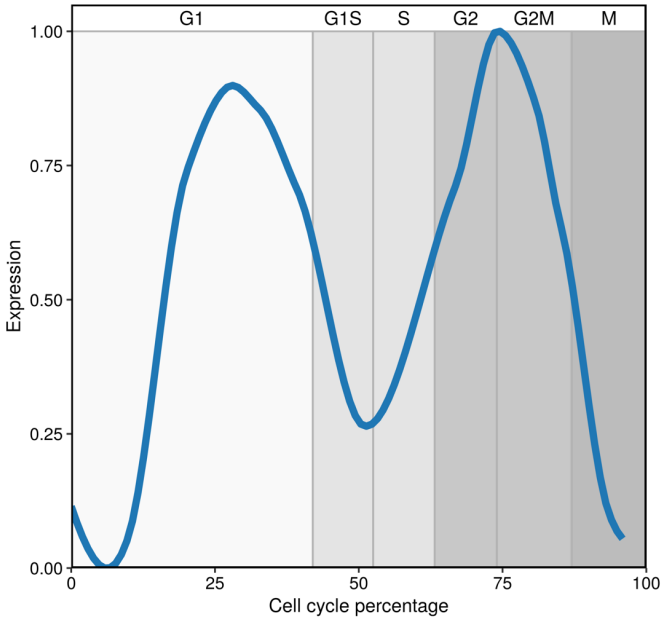


Figure 5.6. Zeb1 is dynamically regulated across the cell cycle in CNV ECs.
The expression levels of Zeb1 shown as a line graph across phases of the cell cycle. The expression of Zeb1 peaks at G1 and G2 stages and is reduced in early G1, and G1S/S, and M, suggesting expression of Zeb1 is cell cycle regulated, or Zeb1 may play a role in cell cycle control at the G1 and G2 phases of the cell cycle in proliferating ECs. Data from scCycle tool (see methods).

demonstrated that Zeb1 expression rises in late G1, drops at G1S and peaks at the G2/G2M transition before reducing through the M stage (Fig 5.4F,G), supporting a cell cycle-dependent role of Zeb1 in endothelial proliferation, or Zeb1 to be a modulator of the cell cycle, potentially acting as a control to progressing through the stages. The dynamic expression of Zeb1 throughout the cell cycle could reflect a role of Zeb1 in the highly proliferative stalk cells in the angiogenic sprout in the CNV lesion and in conjunction with a predicted tip cell role, suggests Zeb1 is a key regulator of the angiogenic sprout.

5.3.4 Zeb1 is enriched in tumour tip cells of a mouse lewis lung carcinoma model

Continuing the analysis of Zeb1 in pathology, we utilised a publicly available scRNA-seq dataset of endothelial cells extracted from a Lewis lung carcinoma orthotopic lung tumour model in mice as well as non-tumour ECs (Goveia *et al.*, 2020). As before, we used the cluster assignment and t-SNE coordinates provided by the original publication to increase comparability. Plotting the data revealed 16 clusters including activated artery, arteries, breach cell, capillaries type I, capillaries type II, immature, interferon, large veins, lymphatics, neophalanx, postcapillary veins, pre-breach cell, proliferating, TEC capillaries, tip cell, and vein (Fig 5.7A). When cells were split according to condition, non-tumour ECs (NEC), tumour ECs (TEC), and TECs treated with PTK787 (VEGFR tyrosine kinase inhibitor) or DC101 (an anti-VEGF agent as a VEGFR2 antibody), distinct distributions and enrichments of these clusters were apparent (Fig 5.7B). In particular, certain clusters such as tip, proliferating and TEC capillaries were predominant in the tumour environment.

Zeb1 was shown to be broadly expressed in multiple EC phenotypes but notably higher in subsets of TECs (Fig 5.7C,D). While Zeb1 could be detected in all EC phenotypes, its abundance and the percentage of Zeb1 positive cells varied markedly. Clusters associated with tumour ECs and more angiogenic phenotypes such as tip, proliferating, neophalanx, immature, interferon and postcapillary vein ECs showed a higher proportion of Zeb1 positive cells, with tip cells displaying increased expression (Fig 5.7D). Differential expression analysis of Zeb1 across all clusters further confirmed that Zeb1 expression was significantly upregulated in tip and neophlanx ECs (Fig 5.7E). While differential expression analysis indicated that proliferating, immature and post-capillary veins displayed significant downregulation of Zeb1, the increased proportion of Zeb1 expressing cells in those cell populations indicate Zeb1 to be required for function (Fig 5.7D,E). Zeb1 was not found to be

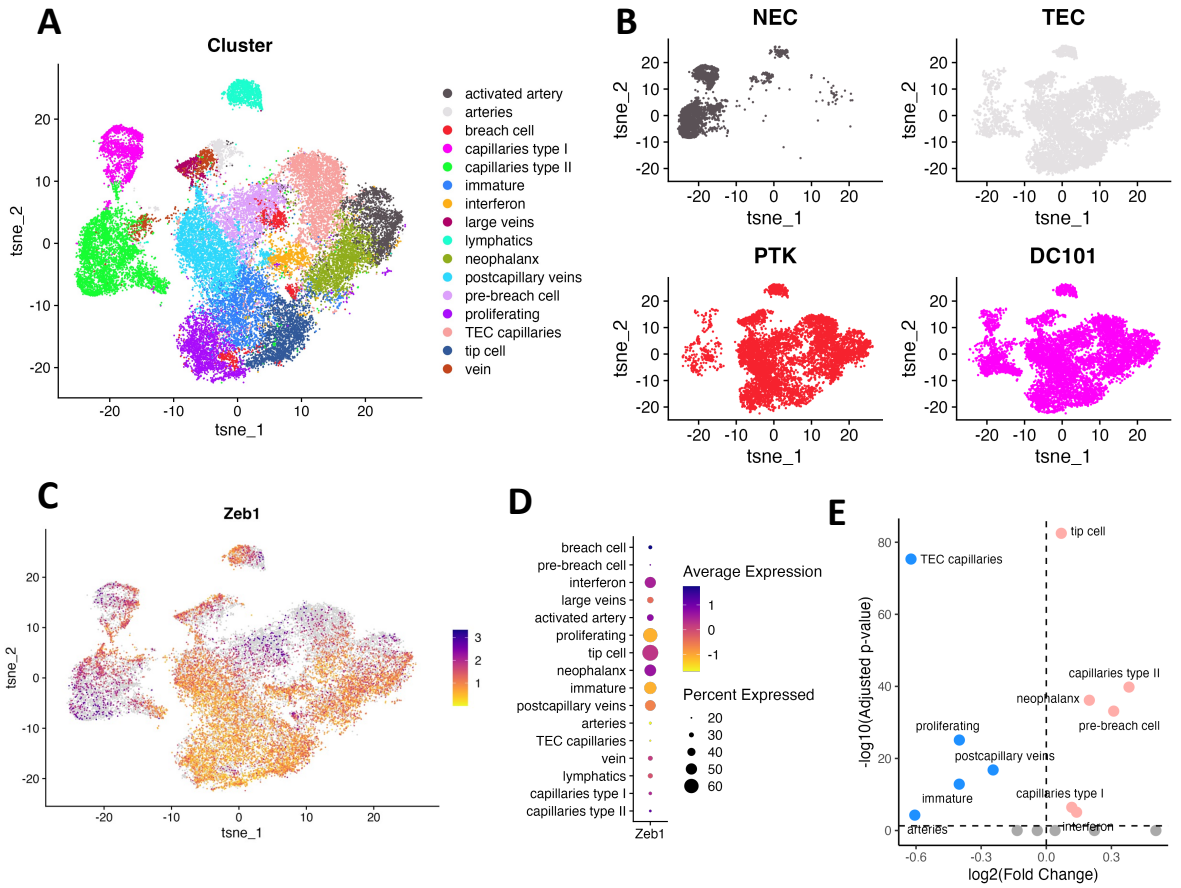


Figure 5.7. ***scRNA-seq analysis of a publicly available murine lewis lung carcinoma dataset identified increased expression of Zeb1 tumour ECs.***

(A) t-SNE of the EC phenotypes within the dataset.

(B) t-SNE split by condition. NEC = non-tumour ECs, TEC = tumour ECs, PTK = PTK treated tumour ECs, DC101 = DC101 treated ECs. A clear population of tumour ECs was revealed.

(C) Featureplot of Zeb1 expression across all cells showed increased density of Zeb1 expressing cells in tumour EC populations compared to non-tumour EC populations.

(D) Dotplot showing average expression and percent of cells expressing Zeb1 across EC phenotypes revealed increased proportions of tumour EC phenotype cells (proliferating, tip, neophalanx, immature and post capillary veins) to express Zeb1 compared to non-tumour ECs (capillaries type 1 and 2), albeit at a lower average expression.

(E) Volcano plot of ZEB1 DE analysis across EC phenotypes. Upregulated Zeb1 expression in phenotypes are shown in red and downregulated in blue. Non-significant in grey.

significantly differentially expressed between TEC, PTK and DC101 cells suggesting that ZEB1 expression is not directly regulated by perturbance in VEGF activity via anti-VEGF treatment. Zeb1 was also not differentially expressed between tip cells of TEC, PTK and DC101.

Since Zeb1 was notably expressed in the tip cell population, we applied scTenifoldKNK (Osorio *et al.*, 2022) to model an in-silico Zeb1 knockout specifically within TEC tip cells. Among the predicted significantly regulated (DR) genes, several angiogenesis-related and cell cycle-related genes (Jag1, Tgfbr2/3, Tek, Mcm2, Mcm3, Mcm4, Mcm5, Ccna2, Ccnb1, Cdca7, Cdca8) were highlighted, supporting a broad influence of Zeb1 on key endothelial programs (Fig 5.8A). Genes related to matrix remodelling and migration were also identified (Timp3, Col4a1/a2, Pxdn, Sparcl1, Ablim1, Ablim3 (Fig 5.6A). In addition, Vwf and Cdh5 were also predicted to be perturbed upon Zeb1 KO (Fig 5.6A), indicating Zeb1 to regulate key genes associated with endothelial identity. KEGG functional enrichment analysis of the DR genes identified MAPK signalling, adherens junction organisation and DNA replication pathways (Fig 5.8B), while GO terms pointed to processes such as leukocyte-EC adhesion , cell cycle progression, vascular development and epithelial to mesenchymal transition (Fig 5.8C). Multiple transcription factors exhibited predicted altered expression in the absence of Zeb1 including Klf and AP1 family TFs, suggesting Zeb1 can influence a network of TFs in tumour tip ECs that may be essential for tip cell behaviour (Fig 5.8D).

Finally, to determine whether Zeb1 levels vary throughout the cell cycle in tumour ECs, we interrogated the cell cycle data of the EndoDB associated with the mouse tumour EC scRNA-seq dataset. Zeb1 expression was enriched in G1 and G2M phases, with reduced expression at G1S and M stages. The dynamic expression of Zeb1 across phases of the cell cycle suggests a link between Zeb1 expression and proliferative or cell division processes in ECs (Fig 5.8E), indicating a role of Zeb1 in the proliferative behaviour of ECs in tumour vasculature.

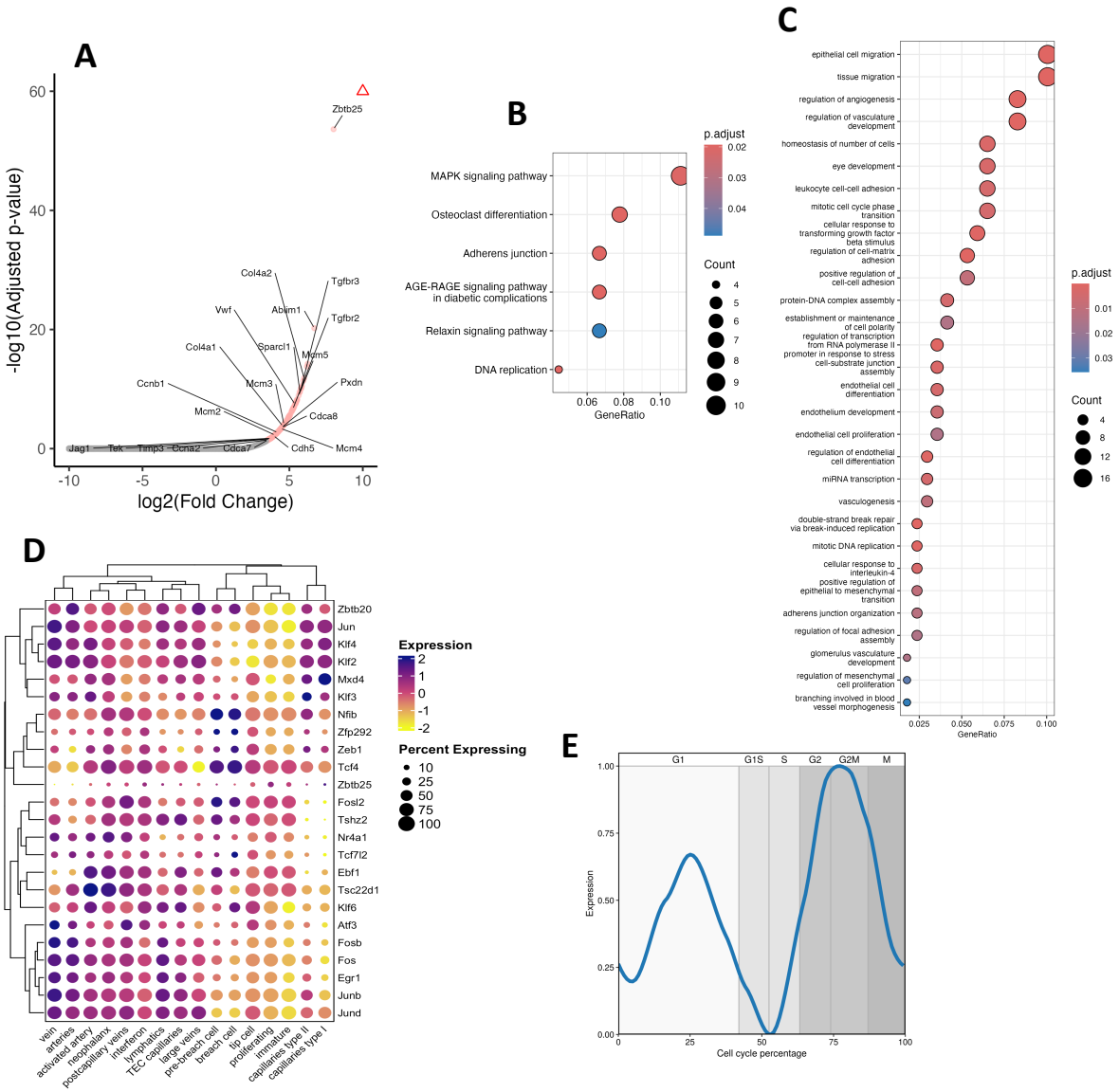


Figure 5.8. ***In-silico KO of Zeb1 in tumour tip ECs revealed differential regulation of genes related to angiogenesis, cell cycle, matrix remodelling and EC identity.***

(A) Differentially regulated (DR) genes predicted by *in-silico* Zeb1 KO in TEC tip ECs. Labelled DR genes related to cell cycle, angiogenesis, matrix remodelling and EC identity. Significant DR genes are in red, non-significant in grey. Zeb1 is represented as a red triangle.

(B) Dotplot of the KEGG pathways identified by functional enrichment analysis of the significant DR genes revealed regulation of MAPK signalling and adherens junctions.

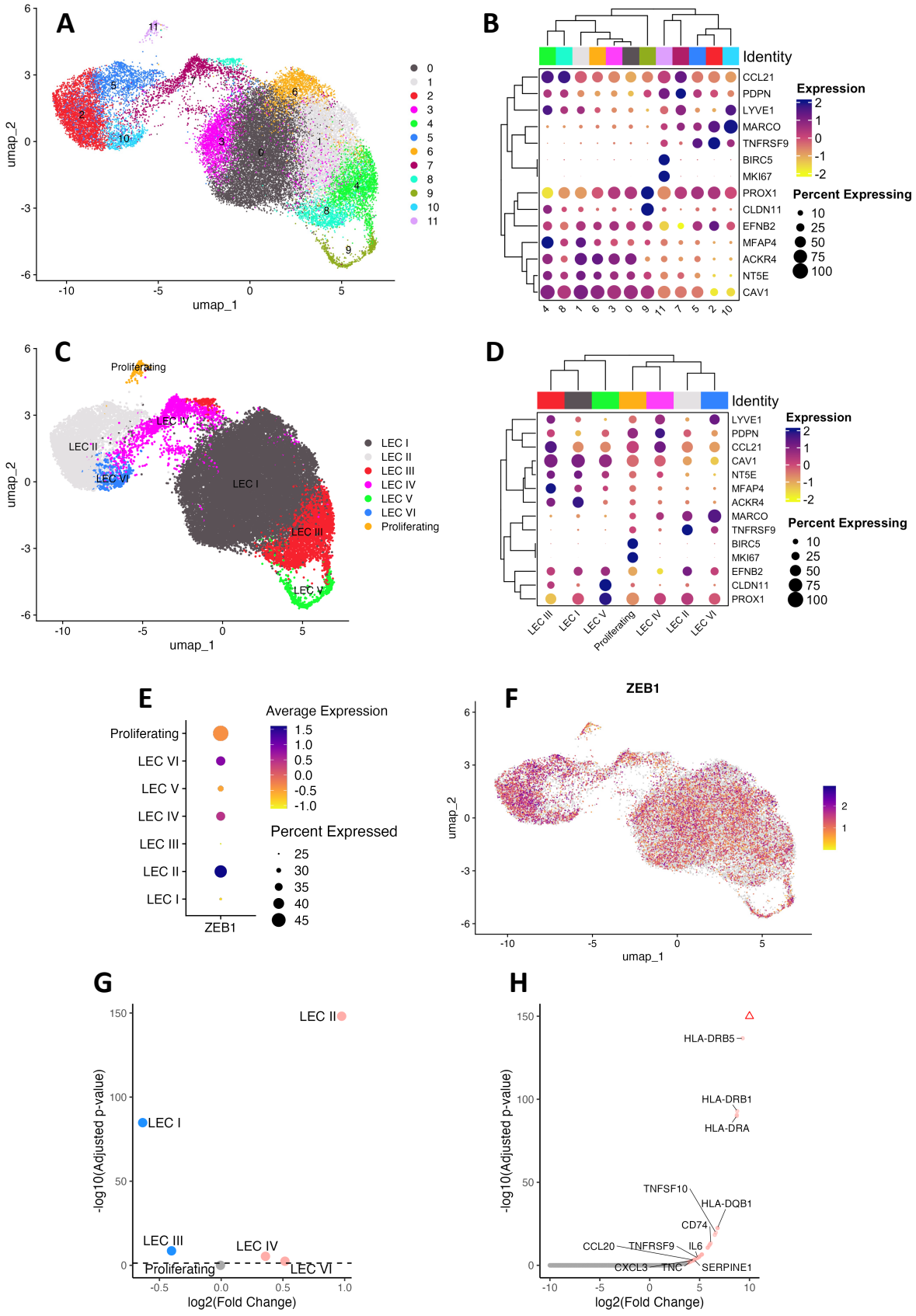
(C) Dotplot of Gene Ontology processes enriched from DR genes identified angiogenic and cell adhesion terms.

(D) Clustered dotplot of transcription factors identified in the *in-silico* KO of Zeb1 for all TEC ECs.

(E) The expression levels of Zeb1 shown as a line graph across phases of the cell cycle. The expression of Zeb1 peaks at G1 and G2/G2M stages, with the highest expression at G2/G2M, and is reduced in early G1, and G1S/S, and M, with the lowest expression at G1S/S, suggesting expression of Zeb1 is cell cycle regulated, or Zeb1 may play a role in cell cycle control at the G1 and G2 phases of the cell cycle in proliferating ECs. Data from scCycle tool (see methods).

5.3.5 ZEB1 is upregulated in subcapsular sinus floor lymphatic endothelial cells of the lymph node and is implicated in immune regulation

To further explore the expression of Zeb1 at a single cell level we analysed a publicly available dataset of lymphatic endothelial cells extracted from human lymph node (Takeda *et al.*, 2019). We identified 15 clusters across 35,856 cells. As per the original publication we removed clusters expressing heat shock proteins HSPA1A/B and inflammatory genes MX1-2 and IFIT1-3 due to evidence that expression of these genes are linked to dissociation, digestion and pipetting (van den Brink *et al.*, 2017). Non LEC clusters denoted by CCL19 (non-endothelial stromal cells) and JAM2 (blood endothelial cells) were also removed from the dataset, resulting in 12 LEC clusters (Fig 5.9A). To contextualise these clusters, we utilised markers discussed in the original publication to assign clusters to LEC I-VI subtypes (Fig 5.9B). We assigned clusters 0, 1, 3, and 6 to LEC I, 2 and 5 to LEC II, 4 and 8 to LEC III, 7 to LEC IV, 9 to LEC V and 10 to LEC VI (Fig 5.9C,D). Interestingly, we identified cluster 11 to be a proliferating LEC population which was not highlighted in the original publication (Fig 5.9C-D). The authors of the dataset (Takeda *et al.*, 2019) identified the LEC types to be associated with specific regions of lymph nodes, as follows. LEC I and III were found to correspond to the ceiling LECs of the subcapsular sinus (SCS) distinguished by ACKR4, NT5E and CAV1 expression. LEC II, which exhibits increased expression of TNFRSF9, corresponds to the floor LECs of the SCS. LEC IV matches the capillary LEC population, marked by PDPN, LYVE1 and CCL21, with reduced expression of EFNB2. LEC V localised to valve LECs, displaying increased CLDN11 signal. LEC VI includes medullary sinus (MS) and cortical sinus (CS) LECs, marked by MARCO and LYVE1. Proliferating LECs were annotated though unique expression of MKI67 and BIRC5. Notably, ZEB1 expression was highest in LEC II (SCS floor LECs) and lowest in LEC


A
umap_1
umap_2
B
Identity
CCL21
PDPN
LYVE1
MARCO
TNFRSF9
BIRC5
MKI67
PROX1
CLDN11
EFNB2
MFAP4
ACKR4
NT5E
CAV1
Expression
Percent Expressing
C
Proliferating
LEC I
LEC II
LEC III
LEC IV
LEC V
LEC VI
D
E
Average Expression
Percent Expressed
ZEB1
F
ZEB1
G
-log10(Adjusted p-value)
log2(Fold Change)
H
HLA-DRB5
HLA-DRB1
HLA-DRA
TNFSF10
HLA-DQB1
CD74
CCL20
TNFRSF9
IL6
CXCL3
TNC
SERPINE1

<u>Figure 5.9.</u> scRNA-seq analysis of a publicly available human lymph node LEC dataset identified ZEB1 expression to be enriched in the floor LECs of the subcapsular sinus.

(A) UMAP of 12 LEC clusters identified by scRNA-seq analysis.
(B) Expression of marker genes identified from the original publication (Takeda *et al.,* 2019) to assign phenotype to clusters in (A).
(C) UMAP of LECs labelled by inferred phenotype. LEC I & III correspond to ceiling LECs of the subcapsular sinus. LEC II corresponds to floor LECs of the subcapsular sinus. LEC IV corresponds to capillary LECs. LEC V corresponds to valve LECs. LEC VI corresponds to medullary sinus and cortical sinus LECs.
(D) Confirmation of phenotype assignment by marker expression.
(E) Dotplot of ZEB1 expression across lymph node LEC phenotypes revealed enrichment in LEC II, corresponding to floor LECs of the subcapsular sinus.
(F) Featureplot to visualise the ZEB1 expression across all cells of the dataset.
(G) Differential expression analysis of ZEB1 across lymph node LEC phenotypes. LEC II shows significant upregulation of ZEB1.
(H) *In-silico* KO analysis of ZEB1 in LEC II cells. Significantly differentially regulated genes are shown in red, non-significant in grey. Zeb1 is represented as a red triangle. Genes related to antigen presentation and extracellular matrix processes are labelled.

I and III (SCS ceiling LECs) (Fig 5.9E). Differential expression analysis of ZEB1 confirmed significant upregulation in LEC II compared to the other subtypes (Fig 5.9G), indicating that the floor LECs of the SCS harbour programmes associated with ZEB1, whereas LEC I and III showed downregulation. Proliferating LECs did not exhibit significant regulation of ZEB1 compared to all other subtypes (Fig 5.9G). Finally, to gain insight into the putative functions of ZEB1 within LEC II, we employed scTenifoldKNK (Osorio *et al.*, 2022) to generate an in-silico KO of ZEB1 within the LEC II subcluster. This analysis predicted perturbation of 40 genes related to antigen presentation and immune modulation (HLA genes, CD74, TNFSF10, TNFRSF9, IL6 CCL20 and CXCL3) and extracellular matrix (ECM) (TNC, SERPINE1) (Fig 5.9H). These findings raise the possibility that ZEB1 may regulate immune/inflammation and ECM related pathways within the SCS floor compartment of human lymph nodes.

5.4 Discussion

Interestingly, the original authors of the EndoDB cell atlas dataset showed the transcriptomic signatures of spleen and liver ECs to cluster together in a hierarchical clustering analysis (Kalucka *et al.*, 2020). These were the tissues with the top two proportion of ECs expressing Zeb1. Perhaps the transcriptomic consequence of Zeb1 in ECs within these tissues is required for healthy EC function in their environment and function. Kalucka *et al.,* (2020) also showed that the ECs of the liver and spleen highly expressed genes that were related to scavenging and immunoregulation, suggesting Zeb1 to be involved in these EC processes. Furthermore, Zeb1 may have a transcriptomic effect on the ECs in these tissue which lead the data for those tissues to cluster together. Transcription factor analysis performed by the original authors for each tissue EC group identified the upregulation of Gata4 in liver ECs compared to all other tissues and Gata6, Nfic and Nr5a1 to be expressed in spleen ECs. These TFs deserve further exploration to uncover a potential link with Zeb1. Furthermore, Kalucka *et al.,* (2020) identified unexpected ECs in their dataset including interferon-activated in the spleen and proliferating ECs in spleen and liver. The correlation between the presence of these phenotypes in healthy spleen and liver tissue ECs and the greatest proportion of Zeb1 expressing cells in the same tissue ECs warrants further investigation. The variability between expression of Zeb1 in healthy tissue ECs suggests that Zeb1 expression, and potentially behaviour, is context dependent at the organ level.

Analysis of Zeb1 expression in CNV point to a central role for Zeb1 in regulating EC phenotypes in the laser-induced CNV lesion. Zeb1 was broadly expressed across EC subtypes but exhibited notably higher expression in lesion-associated phenotypes, specifically tip and proliferating ECs. The *in-silico* KO analysis suggests that Zeb1 also shapes a broader transcriptional network, as virtual removal of Zeb1 was predicted to significantly impact

expression of AP-1 factors and several cell cycle-related genes. AP-1 components are known to regulate proliferation, stress responses and inflammatory pathways (Jia *et al.*, 2016; Hannemann *et al.*, 2017), processes relevant to neovascular lesions. In the context of CNV, which involves aberrant endothelial proliferation and pathological vascular remodelling, the regulation of AP-1 TFs alone upon Zeb1 KO might reflect the core pathways that are perturbed within lesion endothelial cells when Zeb1 function is lost. Functional enrichment analyses further support the idea that Zeb1 modulates angiogenic and cell survival pathways. GO terms and KEGG pathways revealed significant processes linked to endothelial activating, proliferation and angiogenesis, all of which are key features of the CNV lesion niche. Thus, Zeb1 may act as a regulatory hub, ensuring that angiogenic and proliferative signals are balanced. The decreased expression of Zeb1 around G1S transition is also consistent with a role in enabling ECs to initiate replication and may position Zeb1 as a checkpoint modulator of endothelial proliferation. Altogether, the CNV analysis data highlight Zeb1 as a potential regulator of angiogenic endothelial cell identity during CNV pathological conditions. Its elevated expression in lesion ECs, as well as its influence on AP1 and proliferative gene networks, is suggestive of the potential for Zeb1 to contribute directly to pathogenic neovascularisation. Future work is needed and could refine how Zeb1-driven networks intersect with other known angiogenic regulators and explore Zeb1 as a possible therapeutic target to modulate pathological choroidal neovascular growth.

We also leveraged a publicly available scRNA-seq data from a Lewis lung carcinoma model to elucidate the role of Zeb1 in EC subpopulations of the tumour-associated endothelium. This paper is a hallmark in terms of understanding the angiogenic endothelium and has formed the canon for angiogenic EC subtype annotation. A key observation was the elevated Zeb1 expression in tumour-associated clusters, particularly in tip cells, compared

with non-tumour endothelium. Zeb1 is known for its role in epithelial to mesenchymal transition (EMT), inducing a plastic phenotype. The higher expression of Zeb1 in tip cells potentially reflects the involvement of Zeb1 in regulating genes essential for migratory, invasive and proliferative behaviours.

Our *in-silico* KO analysis in TEC tip cells offered predicted mechanistic insights into how Zeb1 may shape tip cell gene networks. Genes implicated in extracellular matrix remodelling, cell junctions and MAPK signalling were differentially perturbed in the absence of Zeb1. These findings further suggest Zeb1's regulatory node within the angiogenic transcriptional program, influencing not only cell adhesion machinery but also growth and migration pathways critical to vascular sprouting. Furthermore, the predicted modulation of Vwf and Cdh5, genes linked to EC identity, is in line with the idea of EndoMT in which ECs lose their markers and gain mesenchymal related genes. The enrichment of cell cycle-associated transcripts among the Zeb1 KO targets and the dynamic expression of Zeb1 throughout the cell cycle suggested and interplay between Zeb1 and EC proliferation.

Taken together, the scRNA-seq analysis of a mouse lung tumour model predicted a multifaceted role of Zeb1 in tumour endothelial function. Results suggested a coordination of pro-angiogenic processes, such as cell junction integrity and proliferative signals. Future experiments investigating Zeb1 genetic ablation *in-vivo* could yield new strategies to disrupt pathological neovascularisation. Moreover, these data further emphasise the importance of detailed single-cell analyses to uncover the complexity of tumour-associated vascular phenotypes and the underlying regulatory circuits.

Our analysis of lymph node LEC scRNA-seq data highlights the diversity within the lymphatic vasculature and reveals ZEB1 as a key transcription factor enriched in the SCS floor, but not ceiling, compartment, suggesting a context-specific role for ZEB1 in regulating LEC

functions unique to the SCS floor such as antigen transport or immune cell trafficking (Takeda *et al.*, 2019). ZEB1 is well known for its role in mediating epithelial-to-mesenchymal transition (EMT) program as previously discussed. By analogy, in lymphatic endothelium, ZEB1 expression could modulate cytoskeletal dynamics or junctional integrity to support the barrier and transport properties of floor LECs. Interestingly, the in-silico ZEB1 KO analysis in LEC II suggests that ZEB1 may influence the expression of genes linked to antigen processing and immune regulation, including MHC class II family members. This finding raises the possibility that ZEB1 in floor LECs contributes to the mechanism in which lymph node LECs interface with immune cells. The potential regulation of these pathways by ZEB1 warrants further functional investigation, both to clarify how ZEB1 may shape LEC-specific immunological functions and to explore potential implications for immune tolerance within the lymph node. Going forward, targeted studies dissecting ZEB1's mechanistic role within LEC subtypes, particularly the SCS floor cells, could yield insights into the broader biology of lymph node function and lymphatic vessel specialization. Functional perturbation studies (e.g., CRISPR-mediated knockout of ZEB1 in vitro or in animal models) could help clarify whether ZEB1 directly modulates the expression of immune-related genes in LEC II and how this might affect antigen uptake, processing, or presentation to lymphocytes. Additionally, these findings could have clinical relevance, as dysregulation of ZEB1 may underlie or exacerbate pathological conditions involving lymphatic vasculature, such as chronic inflammation or tumour metastasis to lymph nodes. In summary, our results highlights a potentially subtype-specific role for ZEB1 in the human lymph node lymphatic endothelium, particularly within SCS floor LECs where it may orchestrate both structural and immunological functions. By expanding our understanding of the molecular programs that

define lymphatic endothelial heterogeneity, this work preludes further research into how ZEB1 enables the lymphatic system to operate as a component of the immune response.

Collectively, our single-cell transcriptomic analyses highlight that ZEB1/Zeb1 is not simply a background TF in ECs, but one with context-specific roles in regulating EC identity and function across developmental, homeostatic and pathological states. In the healthy spleen, Zeb1 was enriched particularly in venous-capillary and interferon-activated ECs, suggesting that Zeb1 may play a role in these ECs to adapt to a unique microenvironment that is specialised for immune-related processes. Indeed, the original publication indicated that spleen and liver ECs share transcriptomic features and both tissues displayed a comparatively high proportion of $Zeb1^{+}$ ECs. This could suggest that Zeb1 influences, or is influenced by, the immunoregulatory and metabolic requirements within specialised organs.

In the developing retina, Zeb1 expression was highest in tip cells, a phenotype essential for angiogenic sprouting, yet did not differ significantly between postnatal days 6 and 15. This observation contrasts with prior bulk qPCR studies, which suggested that Zeb1 might be more dynamically regulated during retina vascular quiescence entry. Nonetheless, *in-silico* KO of Zeb1 in all ECs in the dataset predicted Zeb1 to regulate the expression of cell cycle and DNA-repair related genes, emphasising that Zeb1 can govern fundamental processes involved in endothelial proliferation. Also, the gene predicted to show the greatest level of perturbance upon *in-silico* KO of Zeb1 was Cxcr4, a marker of tip cell identity, which is highly suggestive of Zeb1 regulating the induction of tip cell phenotype, or is involved in the function of tip cells as a key TF. The dual association of Zeb1 with both proliferative programs and tip cell identity emphasises the potentially multi-faceted implications of Zeb1 behaviour within ECs. Classical models of angiogenesis describe tip cells as non-proliferative, but migratory, while proliferating ECs are typically assigned to the stalk EC phenotype behind

the tip cells in the angiogenic sprout (Orozco-García *et al.*, 2023). The predicted regulation of proliferative and tip cell markers by *in-silico* Zeb1 KO in all ECs of the developing retina dataset can raise a couple of possibilities. First, Zeb1 is a key TF in EC behaviour in the developing retina, with potential implications in both proliferative ECs, and tip ECs as opposed to functioning specifically within a single phenotype. Second is the potential of Zeb1 to function as a transcriptional hub that integrates pro-migratory (tip) and proliferative pathways, enabling ECs to adopt a plastic phenotype with both tip-like and proliferative features. Transitional EC states during development may co-express migratory and proliferative signatures before adopting a strict phenotype, with Zeb1 potentially being key to this plasticity. The enrichment of Zeb1 in both tip and proliferating ECs in the developing retina may reflect its role in promoting EC adaptability rather than a contradiction of established angiogenic models.

Within pathological angiogenesis, we observed Zeb1 upregulation in choroidal neovascularisation (CNV) lesion ECs, particularly in tip and proliferating phenotypes. The *in-silico* KO further indicated that Zeb1 orchestrates a network of AP-1 transcription factors and cell cycle genes, suggesting a role in amplifying or maintaining the heightened proliferative and migratory demands of lesion-associated ECs. A comparable pattern emerged in the lewis lung carcinoma tumour endothelium, where Zeb1 was prominent in tip and other angiogenic EC phenotypes. The predicted perturbation of genes related to extracellular matrix remodelling, cell junctions and endothelial identity upon Zeb1 KO points to its role in guiding the active, plastic and invasive features of tumour-associated vasculature.

Finally, in the lymph node lymphatic EC dataset, ZEB1 was most highly expressed in subcapsular sinus (SCS) floor lymphatic ECs (LEC II), where it may support immune functions. *In-silico* KO analyses predicted dysregulation of genes involved in antigen presentation and

immunomodulatory signals. This finding extends the significance of ZEB1 to lymphatic compartments, implying it may be involved in how lymphatic vessels interface with migrating leukocytes or process antigens in the lymph node.

Taken together, these findings establish Zeb1/ZEB1 as a potential regulator of endothelial function across multiple organs and conditions. While the specific phenotypes in which Zeb1 is enriched vary (spleen venous-capillary ECs, choroidal lesion tip ECs, lung tumour tip ECs, developing retina tip ECs, lymph node floor LECs), the unifying theme is the implication of enriched Zeb1 expression in active or specialised subpopulations of the vasculature. Across models, the *in-silico* KO consistently linked Zeb1 to cell cycle progression, DNA replication, immune regulation and processes akin to epithelial to mesenchymal related programs in ECs, suggesting EndoMT. These analyses highlight Zeb1 as a potential transcriptional hub that can tune proliferation, migration and immunological functions in ECs. Future *in-vivo* experiments targeting Zeb1 may uncover how Zeb1 regulates vascular development and disease progression. Ultimately, these results underlie the need for a deeper understanding of Zeb1 biology to inform putative therapeutic strategies to target pathological angiogenesis.

Chapter 6: A combined scRNA-seq and text-mining approach elucidated putative functions of Zeb1 in partial EndoMT

6.1 Introduction

Endothelial-Mesenchymal Transition (EndoMT) describes the complex process in which endothelial cells lose endothelial characteristics and shift phenotype to adopt a mesenchymal-like state (Kovacic *et al.*, 2019; Piera-Velazquez and Jimenez, 2019). This is distinct from Epithelial to Mesenchymal Transition (EMT) but conceptual and signalling pathways overlap between the two processes. The process was first identified in 1975 through electron microscopy during a study of the endocardium and the formation of heart valves (Cui *et al.*, 2015; Choi *et al.*, 2020) and has since been implicated in several vascular-related pathologies including tumour-vasculature development, atherosclerosis, pulmonary fibrosis and Myocardial Infarction (MI) (Evrard *et al.*, 2016; Choi *et al.*, 2018, 2020; Bischoff, 2019; Gaikwad *et al.*, 2020; Jia *et al.*, 2021; Fan *et al.*, 2023). These pathological processes are often sustained by inflammation-related signalling pathways such as TGF-β, Notch and Wnt that drive the plastic nature of Endothelial Cells (ECs) and can initiate EndoMT (Cooley *et al.*, 2014; Lin *et al.*, 2018, 2023; Hultgren *et al.*, 2020; Ma *et al.*, 2020; Akil *et al.*, 2021). The transition through EndoMT is plastic, with an ability to reach a partial state as well as being reversible, displaying the adaptive characteristic of the process (Fang, Hultgren and Hughes, 2021; Yoshimatsu and Watabe, 2022; Slenders *et al.*, 2023). EndoMT is also necessary in heart development (Xiong *et al.*, 2018; Peng *et al.*, 2022; Hall *et al.*, 2024) and a partial state of EndoMT is proposed in normal angiogenesis, in which mesenchymal characteristics are required in order for vessels to sprout (Welch-Reardon, Wu and Hughes,

2015; Platel *et al.*, 2019; Akil *et al.*, 2021; Fang, Hultgren and Hughes, 2021; Yamashiro *et al.*, 2023; Fang *et al.*, 2024). During EndoMT a progressive reduction in the expression of endothelial markers such as CD31, VE Cadherin and vWF is observed with an increase in expression of mesenchymal markers including a-SMA, FSP-1, VIM, N-cadherin col type 1 and FN1 (Lu *et al.*, 2023). Along with a shift in specific marker expression, EndoMT is also characterised by the loss and gain of endothelial and mesenchymal cell characteristics including loss of cell-cell junctions and polarity and an increase in migratory and invasive properties (Piera-Velazquez and Jimenez, 2019). Furthermore, an increase in extracellular matrix invasion and reorganisation and a disruption in the endothelial monolayer is displayed (Bischoff, 2019; Lu *et al.*, 2023; Wiktorska, Sacewicz-Hofman and Niewiarowska, 2023). It is proposed that EndoMT is driven by certain transcription factors (TFs) that are known regulators of Epithelial to Mesenchymal Transition (EMT); SNAI1, SNAI2, ZEB1, ZEB2 and TWIST1 (Lu *et al.*, 2019). The complex interactions between these TFs is well understood in EMT, however while there are likely similarities between EndoMT and EMT the nature of the relationship between the drivers is not as well characterised in EndoMT (Fang, Hultgren and Hughes, 2021). Nevertheless, it is known that members of EndoMT inducing TGF-β, BMP, Notch, Wnt and signalling pathways, namely SMADs, β-catenin and NICD, can interact and form complexes with EMT/EndoMT TFs to modulate gene expression (Welch-Reardon, Wu and Hughes, 2015; Lu *et al.*, 2019).

Zeb1 is implicated in Epithelial to Mesenchymal Transition (EMT) and while it has been recorded in EndoMT-related studies, it is often described as a marker of EndoMT with the specific behaviour of Zeb1 in coordinating EndoMT remaining unclear and warranting further research (Lee, Jung and Heur, 2019; M. Zhang *et al.*, 2019; Choi *et al.*, 2020; Lee *et al.*, 2020; Shu, Butcher and Saint-Geniez, 2020; Fang, Hultgren and Hughes, 2021;

Yoshimatsu and Watabe, 2022; Lee *et al.*, 2023). However, a computational model of EndoMT predicted a loss of Zeb1 prevented mesenchymal differentiation, suggesting Zeb1 plays a key role in EndoMT (Weinstein, Mendoza and Álvarez-Buylla, 2020). Indeed, Zeb1 has been shown to regulate signalling pathways in ECs that are known signalling pathways that regulate EndoMT including BMP and Wnt signalling (Yu *et al.*, 2022; Lee *et al.*, 2023).

Recent advances in scRNA-seq technology has allowed the identification of EndoMT phenotypes in several conditions and pathologies because of the increased resolution now available to analyse EC heterogeneity (G. Zhao *et al.*, 2021; P. Zhao *et al.*, 2021; Ren *et al.*, 2023; Slenders *et al.*, 2023; Chen *et al.*, 2024; Lebas *et al.*, 2024). Importantly, a meta-analysis of scRNA-seq datasets identified EndoMT in COVD-19 infection, detecting an upregulation of EndoMT in COVID-19 patients (Zhang *et al.*, 2022). Here it was observed that early stages of EndoMT positively correlated with SARS-CoV-2 entry factors during lung infection whereas late stages did not, furthering the importance of understanding the dynamic nature of EndoMT and highlighting the impact of scRNA-seq analyses in elucidating signalling patterns (Zhang *et al.*, 2022). It is common in EC-focused scRNA-seq studies to enrich input material for CD31+ cells and deplete for CD45+ cells during sample preparation to obtain a pure EC population. However, there have been studies to suggest that ECs can also express CD45 (Nasim *et al.*, 2023). Additionally, it has been shown that mitral valve ECs can express CD45 after MI (Bischoff *et al.*, 2016) and recently that CD45 itself is sufficient to initiate EndoMT in human ECs (Nasim *et al.*, 2023). Furthermore, a recent preprint generated a tamoxifen-inducible EC-specific CD45 deficient mouse and through scRNA-seq discovered that loss of CD45 inhibited EndoMT marker expression in atherosclerotic mice (Peng *et al.*, 2024). Also, preliminary data in our lab hints towards a presence of a CD45+ lymphatic EC population. Therefore, excluding CD45+ cells from scRNA-seq analyses may remove potential

EndoMT cell populations, eliminating the ability to fully map the complex biological process. However, when retaining CD45+ cells *in-silico* analysis may prove difficult in discerning endothelial-marker-expressing-immune-cells from immune-marker-expressing-endothelial-cells. To counter this, careful validation of scRNA-seq cell markers through techniques such as IF are important and should be performed alongside scRNA-seq experiments, as seen in (Sokol *et al.*, 2023; AlZaim *et al.*, 2024).

Whilst the public availability of scRNA-seq data is a powerful tool in computationally screening ECs, a single dataset is usually focussed on a specific condition. Integrating several datasets together can provide a wider view of biological processes across experiments but can be time and computationally intensive, as well as requiring careful validation of batch effects. Text mining as a concept is a computational method of analysing large corpora of literature, which can provide a greater field of insight to a biological process as opposed to a targeted experimental approach. As such, it is a useful tool to generate hypotheses, as well as to complement experimental data. There are several applications of text mining, including identification of key terms, common themes in literature and sentiment analysis (Rebholz-Schuhmann, Oellrich and Hoehndorf, 2012). More specifically to biological research, text mining can be used to extract gene/protein names, identify pathways, link diseases to proteins, highlight drug-protein relationships and extract protein-protein interaction information in conjunction with bioinformatics tools to infer important biological relationships and putative therapeutic targets (Huang *et al.*, 2004; Natarajan *et al.*, 2006; Šarić *et al.*, 2006; Li *et al.*, 2010, 2015; Subramani *et al.*, 2015; Zhu *et al.*, 2015; Nezamuldeen and Jafri, 2023).

Here we computationally assess EndoMT in the response to MI through analysis of a publicly available scRNA-seq dataset that did not deplete for CD45 and coupled this with

text-mining based approaches to provide a targeted and global overview of EndoMT. Furthermore, we focussed the use of these methods with an aim to increase our understanding of the mediation of EndoMT by Zeb1. Since we apply a deeper analysis of this dataset and link it with a specific biological process we present these results as a separate chapter.

6.2 Hypothesis and aim

Hypothesis: *Zeb1* is dynamically regulated in EndoMT during post-MI tissue repair.

The hypothesis was tested through applying scRNA-seq analysis and text-mining techniques to address the following aim:

Aim: To investigate the involvement of *Zeb1* in EndoMT during cardiac injury by combining scRNA-seq, gene perturbation analyses and literature-derived interaction networks to uncover *Zeb1*-mediated regulatory signatures.

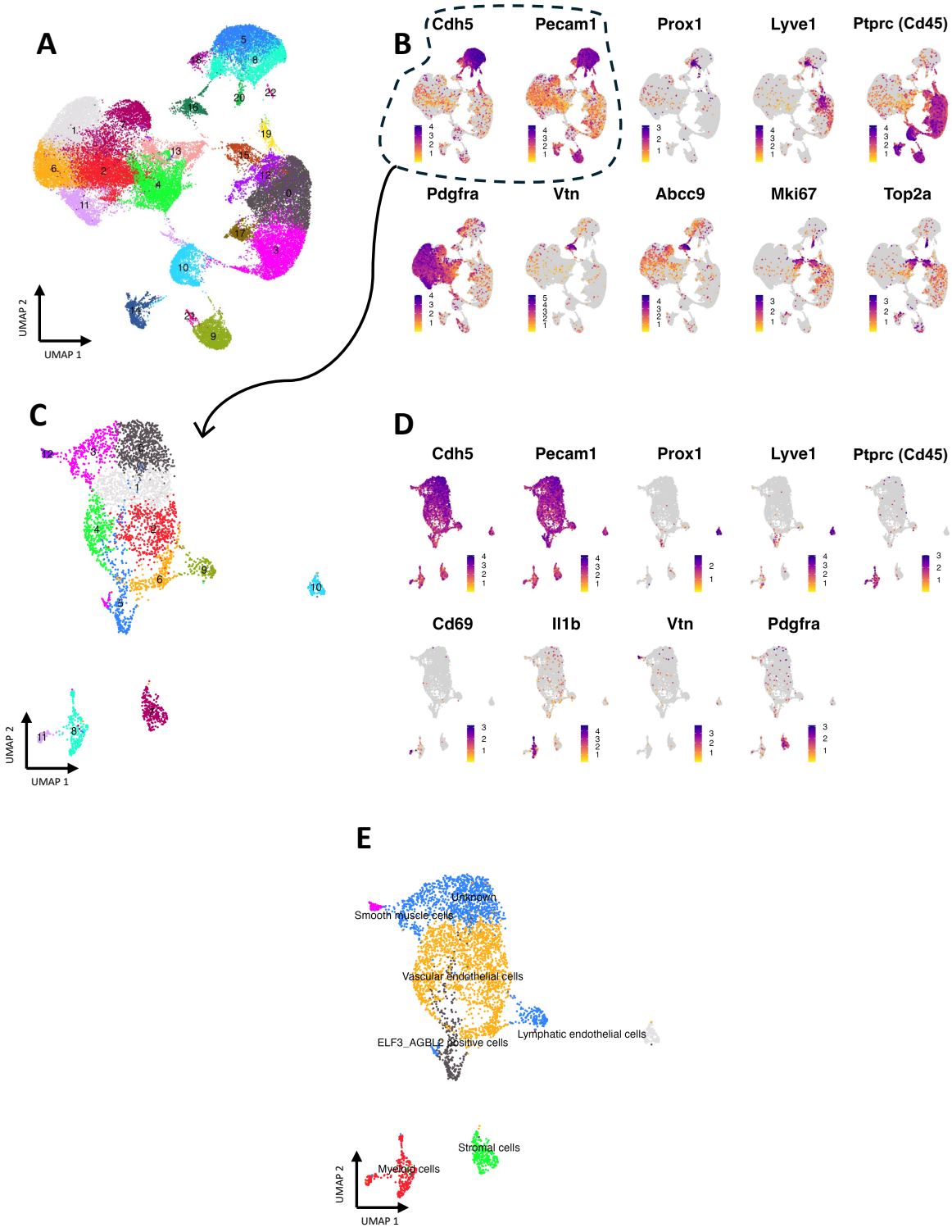
6.3 Results

6.3.1 In-silico isolation of Cdh5+/Pecam1+ cells identified sub-populations expressing pericyte, mesenchymal and immune related genes

To probe the role of Zeb1 within EndoMT, we utilised a publicly available scRNA-seq dataset of non-cardiomyocyte fractions of murine hearts subjected to MI that had previously been used to study EndoMT in a pathological response (Forte *et al.*, 2020; Tombor *et al.*, 2021) Sequencing was performed at days 0 (homeostasis), 1, 3, 5, 7, 14 and 28 post injury

(Forte *et al.*, 2020). Reanalysis of the data identified 51,512 cells passing QC across 23 cell clusters (Fig 6.1A). Cells were assigned phenotypes based on the expression of canonical markers into ECs (*Cdh5+/Pecam1+*) (Fig 6.1B), LECs (*Cdh5+/Pecam1+/Lyve1+/Prox1+*), Proliferating cells (*Mki67+/Top2a+*), Monocytes/Macrophages (*Ptprc+/Cd14+*), Mesenchymal (*Pdgfra+/Serpine1+*) and Pericytes (*Vtn+/Abcc9+*) (Fig. 6.1B). Subsetting and reclustering of *Cdh5+/Pecam1+* populations resulted in 4239 cells and 13 clusters (Fig 6.1C). Several clusters expressed markers associated with other non-EC cell types; cluster 11 B-cells (*Ptprc+/Cd69+*), cluster 8 immune-related cells (*Ptprc+/Il1b+*), cluster 12 pericyte-like (*Vtn+*) and cluster 7 mesenchymal-like (*Pdgfra+*) (Fig 6.1D). Along with assignment of cell phenotype based on known canonical markers, we applied an automated cell-type annotation tool (*ScType* (Ianevski, Giri and Aittokallio, 2022)) to approach this task in an unbiased manner and to potentially validate any doubts of EC phenotype. The results assigned clusters 8 and 11 to Myeloid cells, cluster 7 to Stromal cells and cluster 12 to Smooth muscle cells (Fig 6.1E), in line with manual annotation. Interestingly, some of the clusters that were manually deemed to be ECs are assigned an “Unknown” phenotype by automated analysis (Fig 6.1E). This is likely due to the limitation of the tool, which uses an in-built cell marker database for the annotation and may not include the marker genes required to assign phenotype to the “Unknown” clusters. It may however indicate a difference in phenotype of the ECs that are automatically labelled “Unknown” compared to those labelled Vascular endothelial cells.

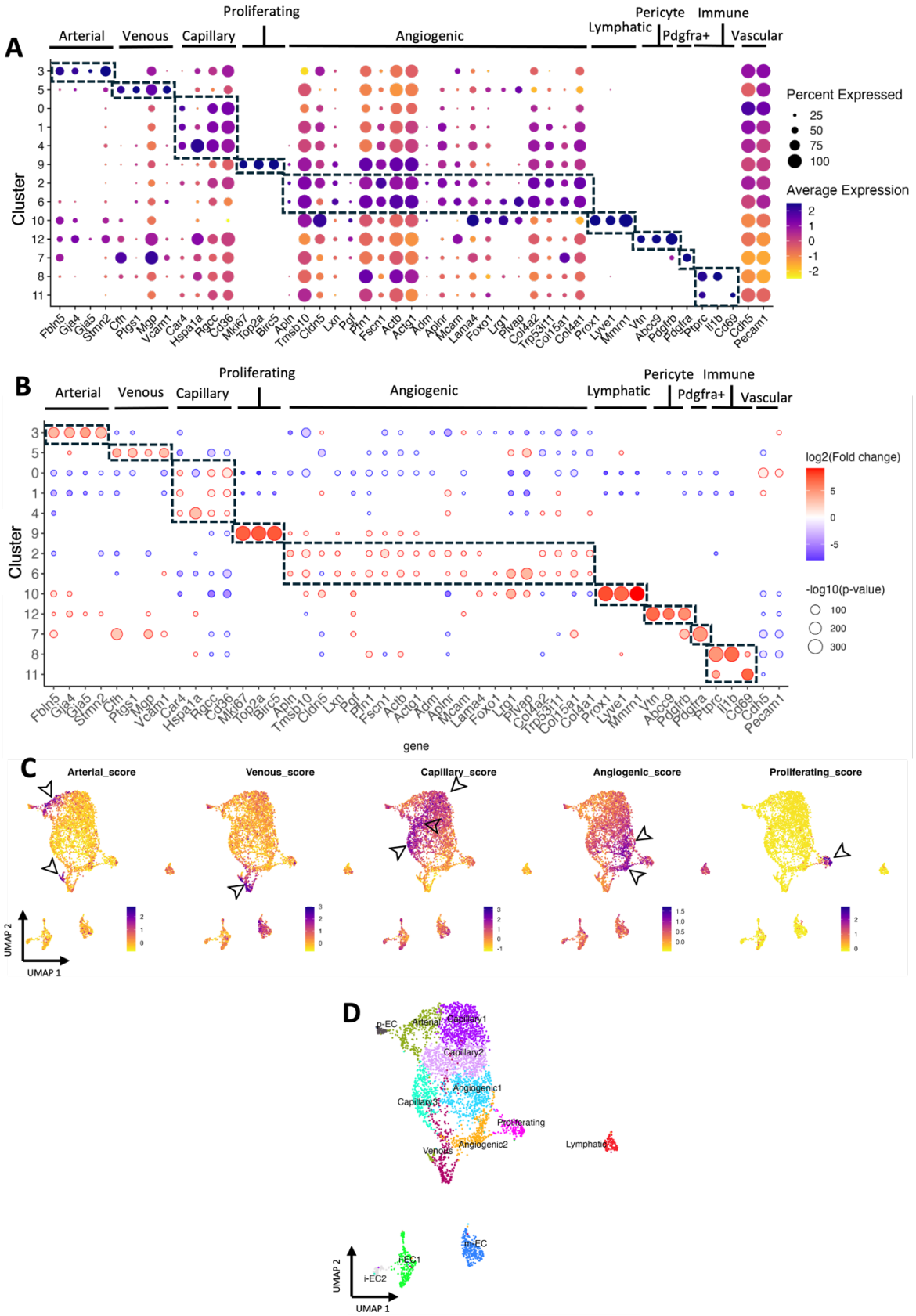
Our initial approach was to remove myeloid-like clusters but retain the pericyte and mesenchymal-like clusters due to our focus on EndoMT. However, a recent EC single-nucleus RNA-sequencing preprint (AlZaim *et al.*, 2024) prompted us to review our approach. In the manuscript, AlZaim *et al.* identified adipose endothelial cells (AdECs) from adipose tissue



<u>Figure 6.1.</u> Reanalysis of a publicly available murine myocardial infarction scRNA-seq dataset identified 13 clusters of Cdh5+/Pecam1+ cells.

(A) UMAP plot representing all cells within the reanalysed dataset identified 23 clusters.
(B) Featureplot of canonical cell type markers. *Cdh5+/Pecam1+* cells are circled.
(C) Subset and reclustered *Cdh5+/Pecam1+* cells revealed 13 clusters.
(D) Featureplot confirming *Cdh5+/Pecam1+* expression in the subset. Other cell markers are also plot to highlight potential non-ECs.
(E) scType automated classification of clusters to compare with manual cluster assignment.

through CDH5, PECAM1 and ERG expression. Importantly, CD45 was not depleted. Within the AdECs, the authors identified populations they termed sub-endothelial AdECs (sub-AdECs) which displayed a decreased expression of CDH5 and PECAM1 and increased expression of markers genes that are commonly assigned to fibroblasts and leukocyte cell types (LAMA2, NEGR1, PDGFRA, PTPRC, and MRC1). Furthermore, the authors then confirmed sub-AdECs that express NEGR1, PDGFRA and CD45 as well as EC markers through IHC and flow cytometry (AlZaim *et al.*, 2024). We lack this validation due to our use of a publicly available dataset. However since cardiac ECs expressing CD45 have previously been identified (Bischoff *et al.*, 2016) and CD45 has been shown to drive EndoMT (Nasim *et al.*, 2023), we decided to follow the approach of (AlZaim *et al.*, 2024) and retain all *Cdh5+/Pecam1+* cells. Vascular EC clusters were assigned phenotypes based on canonical marker signatures identified from literature (see methods section 2.4.5) (Fig 6.2A-C) and in line with (AlZaim *et al.*, 2024) we also saw a reduction of endothelial markers and an increase in non-endothelial markers in clusters 7, 8, 11 and 12 (Fig 6.2A,B). We dubbed clusters 8 and 11 as immune-ECs (i-EC1 and i-EC2 respectively), 12 as pericyte-ECs (p-ECs) and 7 as mesenchymal-ECs (m-ECs) (Fig 6.2D). We annotated cluster 5 to venous ECs (Fig 6.2D) which was classed as ELF3_AGBL2 positive cells by automated cell type annotation (Fig 6.1E). Interestingly, ELF3 (E74 Like ETS Transcription Factor 3) has been implicated as a negative regulator of EMT in bladder carcinoma (Gondkar *et al.*, 2019; Subbalakshmi *et al.*, 2023) while in ECs, ELF3 mediates an increased secretion of IGF1 and VEGF, thus promoting EC proliferation, migration and angiogenesis in epithelial ovarian cancer (Seo *et al.*, 2022).

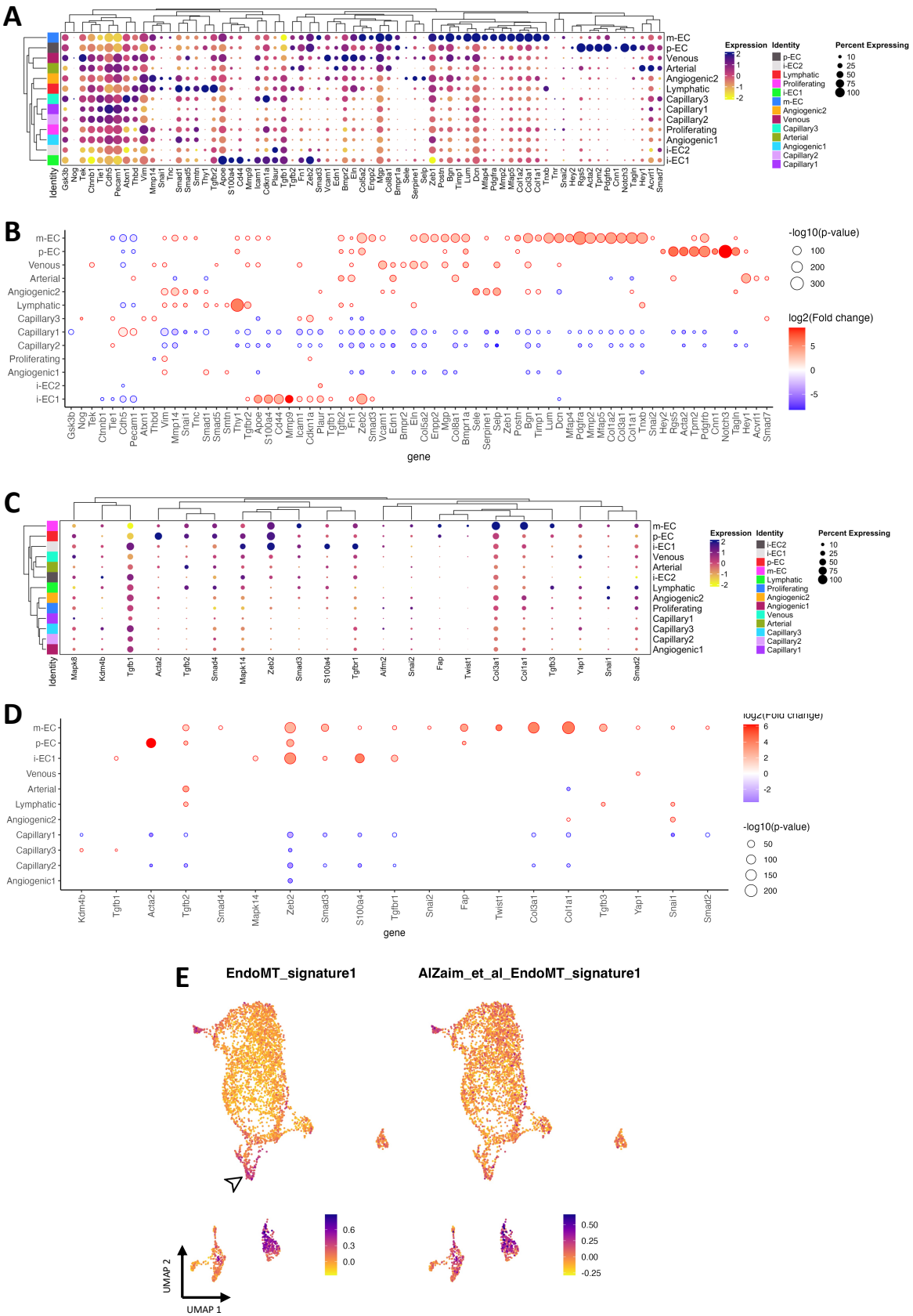

A
Arterial
Venous
Capillary
Proliferating
Angiogenic
Lymphatic
Pericyte
Pdgfra+
Immune
Vascular
Cluster
Percent Expressed
25
50
75
100
Average Expression
2
1
0
-1
-2
Fbln5 Gja4 Gja5 Stmn2 Cfh Ptgs1 Mgp Vcam1 Car4 Hspa1a Rgcc Cd36 Mki67 Top2a Birc5 Apln Tmsb10 Cldn5 Lxn Pgf Ptn1 Fscn1 Actb Actg1 Adm Aplnr Mcam Lama4 Foxo1 Lrg1 Plvap Col4a2 Trp53i11 Col15a1 Col4a1 Prox1 Lyve1 Mmrn1 Vtn Abcc9 Pdgfrb Pdgfra Ptprc Il1b Cd69 Cdh5 Pecam1
B
log2(Fold change)
-log10(p-value)
100
200
300
gene
C
Arterial_score
Venous_score
Capillary_score
Angiogenic_score
Proliferating_score
UMAP 2
UMAP 1
D
p-EC
Arterial
Capillary1
Capillary2
Angiogenic1
Capillary3
Proliferating
Venous
Angiogenic2
Lymphatic
p-EC
l-EC1
l-EC2
UMAP 2
UMAP 1

<u>Figure 6.2.</u> Annotation of Cdh5+/Pecam1+ cell clusters to EC phenotypes based on canonical marker genes.

(A) Dotplot displaying the average expression and percent of cells expressing canonical EC phenotype markers across clusters. Markers are boxed corresponding to the EC phenotype labelled.
(B) Differential expression of canonical markers of EC phenotype across clusters. Compared to (A) which shows expression levels, the differential regulation supports EC phenotype assignment.
(C) Featureplot of module scores (compiled gene signatures) of canonical EC phenotype markers. Cell clusters with increased module scores are highlighted with arrows. This is used to visualise the expression analysis of markers in (A) and (B). Module scores are calculated with the expression of the canonical markers assigned to a phenotype in (A, B).
(D) UMAP of *Cdh5+/Pecam1+* cells with cluster annotated to EC phenotypes based on results from (A), (B) and (C).

6.3.2 Expression analysis of EndoMT-related genes derived from literature identified EndoMT-like cell clusters

To analyse which cell populations may represent an EndoMT-like phenotype, EndoMT markers were collated from literature with which to probe the current dataset. m-EC, p-EC, venous, arterial, angiogenic2, lymphatic and i-EC1 displayed the most EndoMT-like phenotype based on expression and upregulation of EndoMT-related genes and a downregulation of endothelial markers (Fig 6.3A,B). Capillary1 and Capillary2 clusters displayed a downregulation of EndoMT related genes (Fig 6.3B). Furthermore, Capillary1 showed an upregulation of Cdh5 and Pecam1, indicating the most endothelial-like cluster (Fig 6.3B). Interestingly, m-EC and p-EC populations had an upregulation of different EndoMT-related genes (Fig 6.3B), indicating a varied EndoMT response between the pericyte and mesenchymal like cells. We compared the literature-based EndoMT signature with the one used by AlZaim *et al.* and found that we identified the venous population to show an increased EndoMT score compared to the AlZaim *et al*. signature (Fig 6.3C-E).


A
m-EC
p-EC
Venous
Arterial
Angiogenic2
Lymphatic
Capillary3
Capillary1
Capillary2
Proliferating
Angiogenic1
i-EC2
i-EC1
Expression
Identity
Percent Expressing
B
-log10(p-value)
log2(Fold change)
gene
C
D
-log10(p-value)
gene
E
EndoMT_signature1
AlZaim_et_al_EndoMT_signature1
UMAP 2
UMAP 1

<u>Figure 6.3.</u> Identification of EndoMT-like clusters based on an EndoMT signature derived from literature and comparison with a published EndoMT signature identified increased EndoMT-like expression in venous ECs.

(A-B) Clustered dotplot of expression of EndoMT-related genes across clusters (A) and differential expression analysis of EndoMT-related genes (B) for the EndoMT signature used in this thesis. Populations with increased expression and upregulation of genes in the EndoMT signature are deemed to be EndoMT-like.
(C-D) Same as (A-B) but with the EndoMT signature used by AlZaim *et al.,* (2024).
(E) Featureplots comparing EndoMT modules scores used in this thesis and AlZaim *et al.,* (2024). An increased EndoMT module score of the signature used in this thesis was observed in the venous EC cluster and is highlighted with an arrow.

6.3.3 Generation of endothelial, mesenchymal and EndoMT scores identified venous ECs to be associated with an increased mesenchymal signature

Inspired by AlZaim *et al.*, we generated endothelial and mesenchymal scores based on gene signatures (see methods) where positive and negative values represent an increased or decreased endothelial/mesenchymal score (Fig 6.4A,B). We categorised the *Cdh5+/Pecam1+* cells into 4 categories, EC-/MES-, EC-/MES+, EC+/MES- and EC+/MES+ (Fig 6.4A,B) and found Capillary1 to form the majority of cell type within the EC+/MES- group as well as the greatest proportion of Capillary1 cells to be EC+/MES-, corroborating this cluster to be the most EC like. Interestingly, we found venous ECs to be the largest proportion of cell type in EC+/MES+ cells suggesting venous cells to display both endothelial and mesenchymal signatures, perhaps in a partial EndoMT state (Fig 6.4C). Furthermore, 53% of all venous ECs were annotated to the EC+/MES+ group (Fig 6.4D). Lymphatic, m-EC, p-EC and i-EC1 phenotypes were largely assigned to EC-/MES+, validating these to be the least endothelial and most mesenchymal phenotypes (Fig 6.4D). Projecting the endothelial and mesenchymal score categories onto the UMAP of EC cell clusters validated the venous population to display a more mesenchymal-like phenotype compared to Capillary1 and Capillary2 populations (Fig

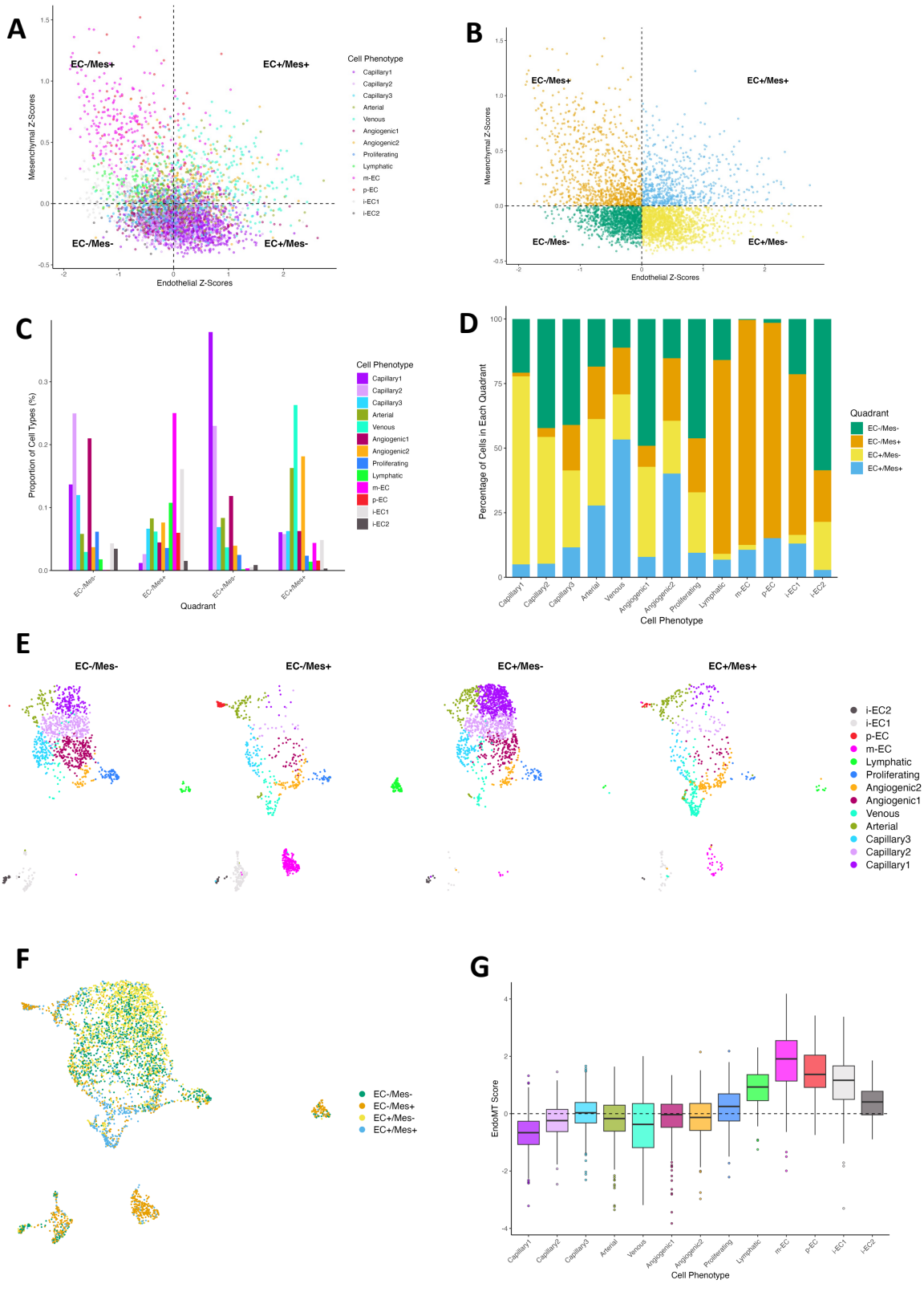

A
EC-/Mes+
EC+/Mes+
EC-/Mes-
EC+/Mes-
Mesenchymal Z-Scores
Endothelial Z-Scores
Cell Phenotype
Capillary1
Capillary2
Capillary3
Arterial
Venous
Angiogenic1
Angiogenic2
Proliferating
Lymphatic
m-EC
p-EC
i-EC1
i-EC2
B
EC-/Mes+
EC+/Mes+
EC-/Mes-
EC+/Mes-
Mesenchymal Z-Scores
Endothelial Z-Scores
C
Proportion of Cell Types (%)
EC-/Mes-
EC-/Mes+
EC+/Mes-
EC+/Mes+
Quadrant
Cell Phenotype
D
Percentage of Cells in Each Quadrant
Quadrant
EC-/Mes-
EC-/Mes+
EC+/Mes-
EC+/Mes+
Capillary1
Capillary2
Capillary3
Arterial
Venous
Angiogenic1
Angiogenic2
Proliferating
Lymphatic
m-EC
p-EC
i-EC1
i-EC2
Cell Phenotype
E
EC-/Mes-
EC-/Mes+
EC+/Mes-
EC+/Mes+
i-EC2
i-EC1
p-EC
m-EC
Lymphatic
Proliferating
Angiogenic2
Angiogenic1
Venous
Arterial
Capillary3
Capillary2
Capillary1
F
EC-/Mes-
EC-/Mes+
EC+/Mes-
EC+/Mes+
G
EndoMT Score
Capillary1
Capillary2
Capillary3
Arterial
Venous
Angiogenic1
Angiogenic2
Proliferating
Lymphatic
m-EC
p-EC
i-EC1
i-EC2
Cell Phenotype

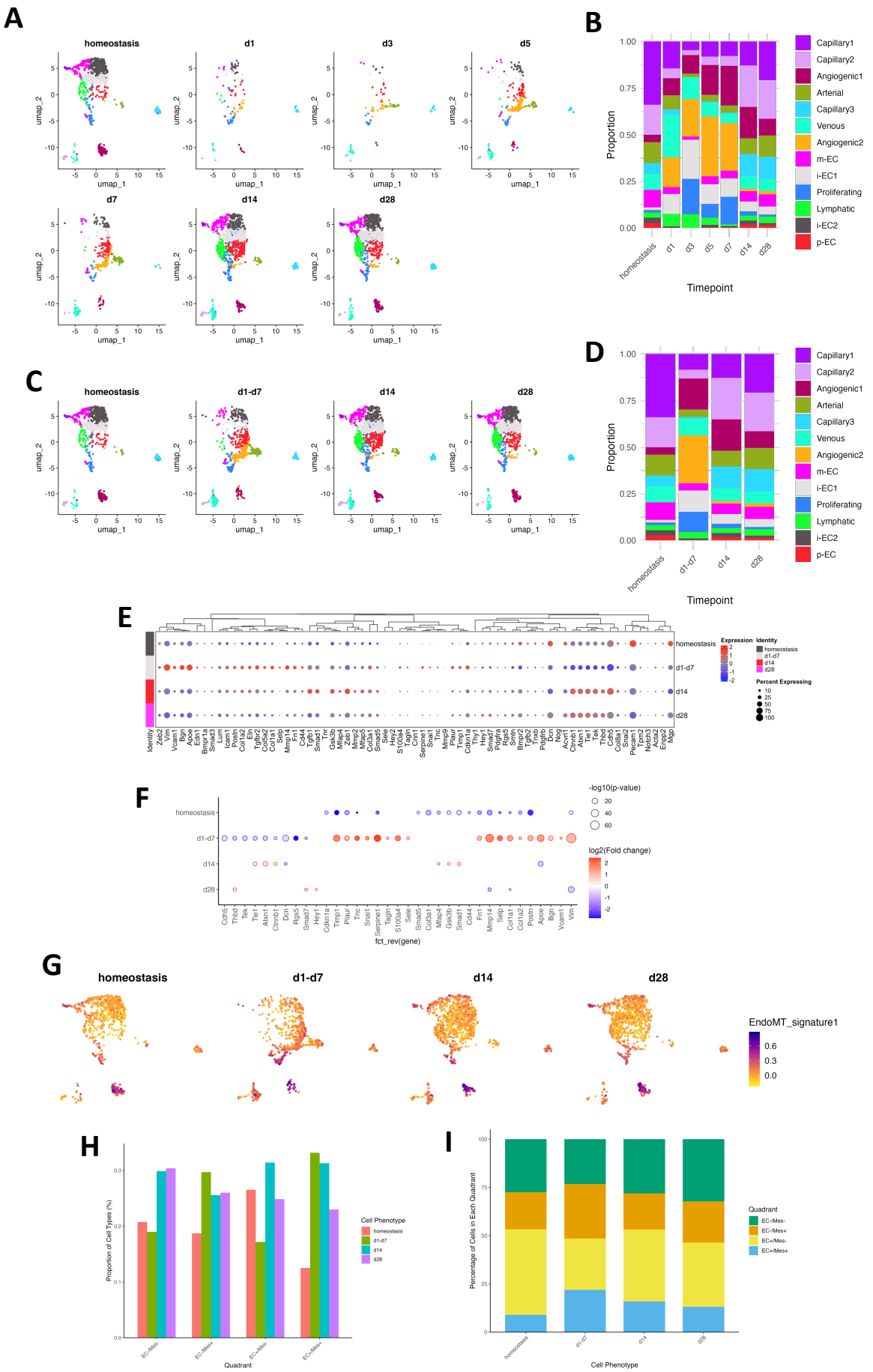
Figure 6.4. ***Venous endothelial cells display endothelial and mesenchymal positive scores.***

(A) Scatterplot of endothelial and mesenchymal scores for cells of each phenotype. The plot is sectioned into EC-/MES+, EC+/MES+, EC-/MEC- and EC+/MES- annotations based on endothelial and mesenchymal scores. Venous ECs were found to be EC+/MES+, suggesting a partial EndoMT state.
(B) Same as (A) but coloured by endothelial and mesenchymal score annotation.
(C) Bar plot showing the proportion of cell clusters in each EC/MES annotation. Venous ECs were the majority of EC+/MES+ cells.
(D) Stacked bar plot showing the proportion of EC/MES annotations in each cell cluster. ~50% of venous ECs were EC+/MES+, indicating half the venous ECs to be in a partial EndoMT state.
(E) UMAP plot of ECs split by EC/MES annotation.
(F) UMAP of all ECs coloured by EC/MES annotation.
(G) Box plot of EndoMT scores for each cell cluster showed an increase in EndoMT score in the m-EC and p-EC cell phenotypes.

6.4E,F). We replicated these analyses using the EndoMT signature from AlZaim *et al.* and found that the proportion of venous ECs annotated to EC+/MES+ was reduced to 33% as well as the proportion of EC+/MES+ cells being venous was reduced and no longer the majority (Appendix 4.3). We calculated an EndoMT score based on the endothelial and mesenchymal scores as detailed by AlZaim *et al.,* (see methods) and applied this to the EC populations. We identified Proliferating, Lymphatic, m-EC, p-EC, i-EC1 and i-EC2 to display a positive EndoMT score and venous ECs to show an increase in EndoMT score compared to Capillary1 (Fig 6.4G).

6.3.4 Expression analysis of EndoMT-related genes across days post myocardial infarction found days 1-7 to upregulate EndoMT markers

The original dataset provided data for individual timepoints of d1, d3, d5 and d7. However, due to the low number of cells in each of these timepoints we opted to merge them together into d1-d7 to make the data more comparable with homeostasis, d14 and d28 timepoints (Fig 6.5A,C). At days 1-7 post MI the proportion of capillary cells decreased compared to homeostasis and returned at days 14 and 28 (Fig 6.5C,D). The proportion of


A
homeostasis
d1
d3
d5
d7
d14
d28
umap_1
umap_2
B
Proportion
Timepoint
Capillary1
Capillary2
Angiogenic1
Arterial
Capillary3
Venous
Angiogenic2
m-EC
i-EC1
Proliferating
Lymphatic
i-EC2
p-EC
C
homeostasis
d1-d7
d14
d28
D
E
Identity
Expression
Percent Expressing
F
-log10(p-value)
log2(Fold change)
fct_rev(gene)
G
EndoMT_signature1
H
Proportion of Cell Types (%)
Cell Phenotype
Quadrant
I
Percentage of Cells in Each Quadrant
EC-/Mes-
EC-/Mes+
EC+/Mes-
EC+/Mes+

<u>Figure 6.5.</u> Days 1-7 post myocardial infarction (MI) exhibit increased expression of EndoMT-related genes.

(A) UMAP plot split by days post MI. Days 1-7 had fewer cells compared to homeostasis and days 14 and 28 timepoints.
(B) Stacked bar plot showing the proportions of cell clusters in days post MI.
(C) UMAP plot split by days post MI with merged days 1-7 to handle the low cell number for days 1-7.
(D) Same as (B) but for (C). There was an increased proportion of Angiogenic1, Angiogenic2 and Proliferating phenotypes at days 1-7. Reduced Capillary1 and Capillary2 phenotype proportions was also observed at days 1-7, but began to return at days 14-28.
(E) Clustered dotplot of EndoMT-related genes across days post MI. EC markers had reduced expression at days 1-7 while EndoMT-related gene expression was increased.
(F) Differential expression analysis of EndoMT-related genes across days post MI. EC markers were downregulated at days 1-7 while EndoMT-related genes were upregulated.
(G) Featureplot of EndoMT-related genes module score used in this thesis (detailed in Fig 6.3E) split by days post MI. Venous ECs displayed in increased EndoMT signature at days 1-7.
(H) Barplot showing the proportion of EC/MES annotations consisting of days post MI. Days 1-7 post MI formed the greatest proportion of cells in EC-/MS+ and EC+/MES+ states.
(I) Stacked barplot showing the proportion of days post MI consisting of EC/MES annotations. Days 1-7 have the greatest proportion of EC+/MES+ cells compared to other timepoints.

Angiogenic1, Angiogenic2 and Proliferating ECs increased, suggestive of an active state before reducing at days 14 and 28 (Fig 6.5C,D). Interestingly, Angiogenic2 ECs were mostly only present at days 1-7 post MI (Fig 6.5C,D). Venous ECs did not appear to change in proportion across the timepoints (Fig 6.5C,D). Expression analysis of EndoMT-related genes found days 1-7 to downregulate EC markers and upregulate EndoMT-related genes compared to other timepoints, suggesting ECs at days 1-7 to be the most EndoMT-like (Fig 6.5E,F). Applying the previously generated EndoMT signature module score onto the UMAP plot of days post MI revealed the venous ECs and days 1-7 had an increased EndoMT signature expression compared to venous ECs at other timepoints, indicative of an EndoMT-like response in venous EC to MI. (Fig 6.5G) . Days 1-7 also formed the greatest proportion of cells in EC-/MES+ and EC+/MES+ and the lowest proportion of cells in EC-/MES- and EC+/MES- suggesting ECs at days 1-7 have a more mesenchymal-like phenotype compared to other timepoints (Fig 6.5H). Days 1-7 also had the greatest percentage of cells in EC+/MES+

compared to other timepoints, with the proportion reducing at days 14 and 28 (Fig 6.5I), suggesting there may be an increase in ECs expressing a mesenchymal-like phenotype in response to MI, with a return to homeostasis levels over time.

6.3.5 Transcription factor analysis identified Zeb1 TF activity to be increased in EC+/MES+ cells and at days 1-7 post MI

With an aim to understand the transcriptional mechanism behind the observed results, we performed TF activity analysis to identify TFs whose target signatures are perturbed, rather than simply focussing on the expression levels of the TFs themselves. Across all ECs, we identified the top 100 TFs that display the most variable behaviour across cell clusters (Fig 6.6A). We observed i-EC1, p-EC, m-EC and Capillary3 ECs to display an increase in the behaviour of a shared group of TFs, suggesting Capillary3 displays a TF signature similar to the mesenchymal-like ECs. Furthermore, it was noted that several TFs of the AP-1 family are enriched in these ECs suggesting AP-1 factors to play a role in the mesenchymal-like phenotype. Hif1a is also enriched, indicating the hypoxia signalling pathway to be involved in the more mesenchymal ECs. We then assessed the top 10 TFs with the highest activity score for each EC cluster (Fig 6.6B). The top TFs of Capillary1 and Capillary2 showed very little activity in the more mesenchymal-like ECs. The top 10 TFs of Capillary3 and Angiogenic2 cell clusters were also increased in m-EC, p-EC and i-EC1, suggesting Capillary3 and Angiogenic2 to express mesenchymal-like TF activity. Interestingly, the TF with the second highest activity in venous ECs was ZEB2, a known driver of EndoMT, suggesting venous ECs to display and EndoMT-like state. We applied the TF analysis to the EC/MES groups of cells to identify which TFs are potentially active in these categories. The top variable TFs across groups were largely separated by MES+/MES- status (Fig 6.6C).

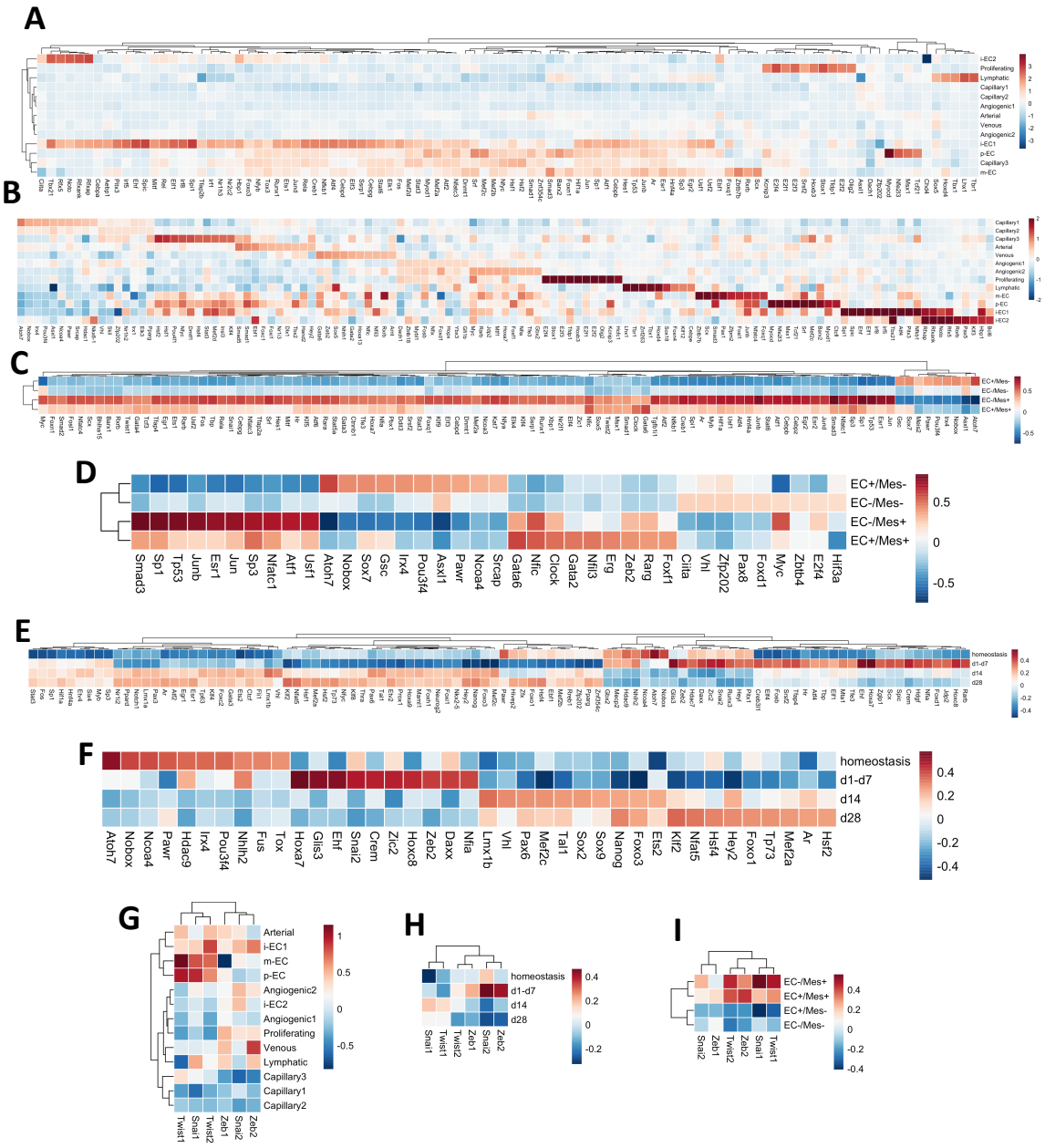


Figure 6.6. Zeb1 transcriptional activity is increased in venous ECs, proliferating ECs, EC+/MES+ ECs and at days 1-7 post myocardial infarction (MI).

The inferred mean transcription factor (TF) activity across all cells in a given category (e.g., phenotype, days post MI etc) is represented as a scale with an increased activity represented by a positive score (red) and decreased activity with a negative score (blue) and plot as a heatmap.

(A) Top 100 most variable TF activity across EC phenotypes. I-EC1, p-EC, m-EC and Capillary3 phenotypes had a shared increased TF activity.

(B) Top 10 TFs with the highest activity for each EC phenotype. Increased ZEB2 activity was observed in venous ECs.

(C) Top 100 most variable TF activity across EC/MES annotations. TF activities were largely separated by MES+/- status.

(D) Top 10 TFs with the highest activity across EC/MES annotations. Zeb2 and Erg had increased activity in EC+/MES+.

(E) Top 100 most variable TF activity across days post MI. Zeb2 activity was increased at days 1-7 post MI.

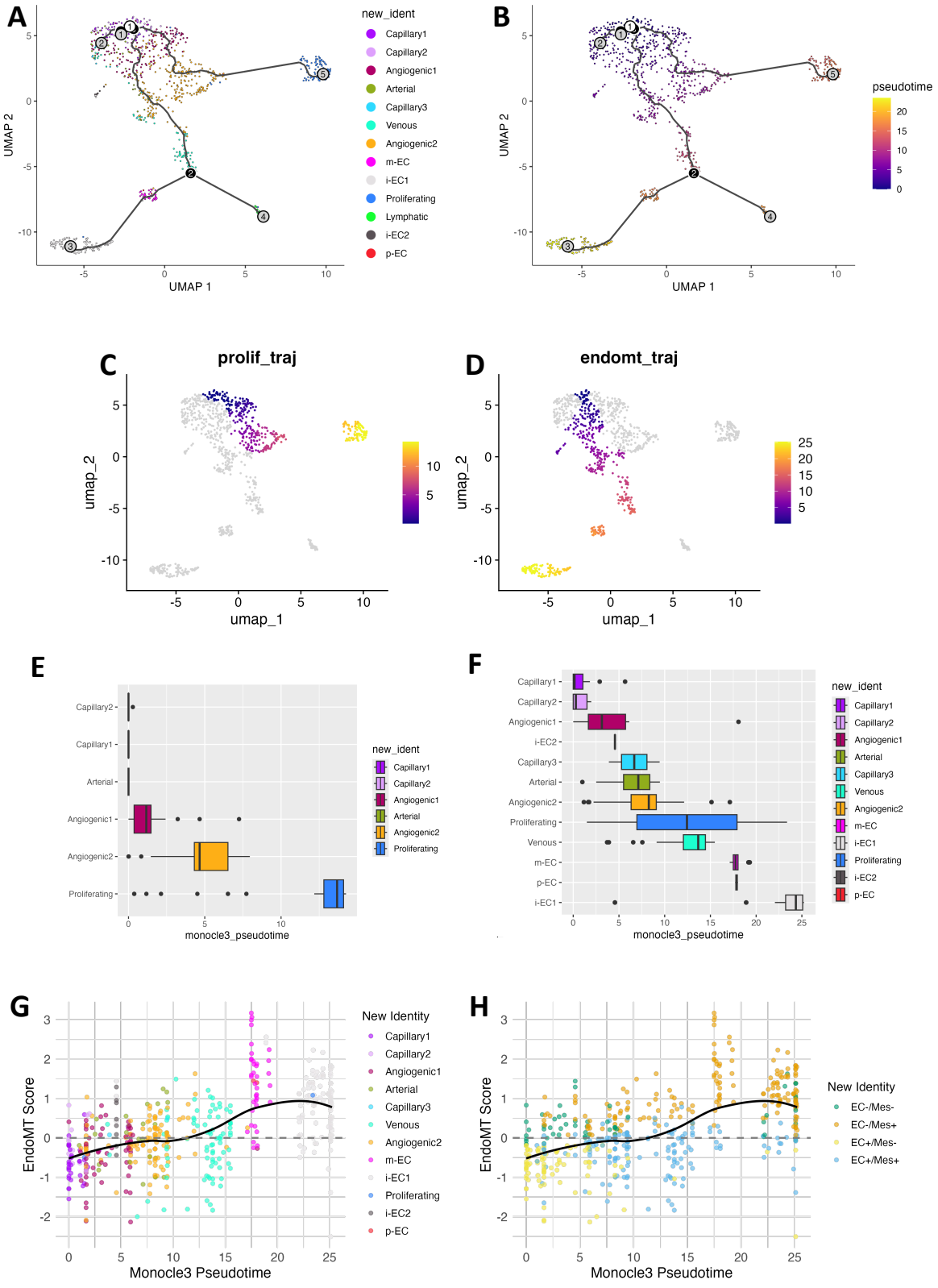
(F) Top 10 TFs with the highest activity for days post MI. Zeb2 had one of the highest TF activities at days 1-7 post MI.
(G-I) TF activity of main EndoMT driving TFs across EC phenotypes (G), days post MI (H) and EC/MES annotation (I). Zeb1 had increased activity in Proliferating and Venous phenotypes, days 1-7 post MI and in EC+/MES+ cells.

However, 17 TFs were identified to have increased activity in EC-/MES+, the group dominated by m-EC, p-EC and i-EC1 cells, including Klf4, a TF we previously showed to be directly regulated by ZEB1 in HUVECs (Chapter 4). Furthermore, we identified Twist1 and Twist2 EndoMT drivers to have increased activity in EC-/MES+ and EC+/MES+ cells. Plotting the TFs with the top activity for each group identified Zeb2 activity to be increased in the MES+ cell groups, whilst being one of the TFs with the highest activity in EC+/MES+ cells (Fig 6.6D). Interestingly, Erg, Nfil3, Gata2 and Foxf1 showed increased activity in EC+/MES+ only, suggesting these TFs to be potential drivers of this transient phenotype. We next applied the TF analysis to days post MI to identify the most variable TF activities across timepoints (Fig 6.6E). We observed a TF signature that increased in activity at days 1-7. Zeb2 activity was increased at days 1-7 while Snai2, another driver of EndoMT, showed activity at homeostasis as well as an increase at days 1-7 post MI. Interestingly, Foxo1 showed increased activity at homeostasis and day 28 and showed a decrease at days 1-7, suggesting decreased Foxo1 activity to be associated with a potential EndoMT response to MI. Furthering this analysis we found Zeb2 and Snai1 to be amongst the TFs with the highest activity in days 1-7 post MI, with Foxo1 one of the highest at day 28 (Fig 6.6F). To focus our attention on EndoMT we calculated activity scores for the main drivers; Zeb1, Zeb2, Twist1, Twist2, Snai1 and Snai2 for each EC phenotype (Fig 6.6G), days post MI (Fig 6.6H) and EC/MES groups (Fig 6.6I). We found Zeb1 to show reduced activity in Capillary1, Capillary2 and Capillary3 ECs and its highest activity in Proliferating, Venous and Lymphatic EC with a slight increase in activity in Angiogenic2 ECs (Fig 6.6G). Interestingly, Zeb1 showed its lowest activity in m-EC ECs, which

displayed high activity for Twist1, Twist2 and Snai1 (Fig 6.6G). Twist1, Twist2 and Snai1 did not show increased activity in Angiogenic2 or Venous ECs (Fig 6.6G). Snai2 showed increased expression in Angiogenic2 ECs but not Venous (Fig 6.6G). Zeb2 showed a slight increase in activity in Angiogenic2 ECs, with the highest score in Venous ECs (Fig 6.6G). Snai2 was the only EndoMT driver to show an increase in activity at homeostasis (Fig 6.6H). Zeb1, Zeb2 and Snai2 showed an increase in activity at days 1-7 post MI, with Zeb1 and Zeb2 only showing activity at this timepoint (Fig 6.6H). Twist1 and Snai1 did not show activity at homeostasis or days 1-7, but did increase in activity at day 14 (Fig 6.6H). The TF activity pattern of EndoMT drivers across days post MI suggests a transition starting with Snai2 followed by Zeb1/Zeb2/Snai2 and ending with Twist1/Snai1 which may represent the regulation of the EndoMT process in response to MI. All bar Zeb1 of the EndoMT drivers showed decreased TF activity in EC+/MES- and EC-/MES- groups (Fig 6.6I), suggesting these TFs to be associated with a MES+ phenotype. Zeb1 did show an increase in activity in EC-/MES-, albeit very little (Fig 6.6I). Zeb1 was the only EndoMT driver to show increased activity in EC+/MES+ and not EC-/MES+ (Fig 6.6I), indicating Zeb1 to be a potential regulator of the EC+/MES+ cell group which consisted mostly of Venous ECs and may be a partial EndoMT state.

6.3.6 Trajectory analysis suggests venous ECs to be a partial state along the EndoMT axis and did not identify Zeb1 expression to significantly change through EndoMT

To infer how the more mesenchymal-like ECs may obtain their phenotype and whether EndoMT plays a role we carried out trajectory analysis on days 1-7 post MI ECs to plot a predicted transition between cell phenotypes across pseudotime (Fig 6.7A). Since EndoMT is the transition into a mesenchymal-like state from an endothelial origin, we


A
UMAP 2
UMAP 1
new_ident
Capillary1
Capillary2
Angiogenic1
Arterial
Capillary3
Venous
Angiogenic2
m-EC
i-EC1
Proliferating
Lymphatic
i-EC2
p-EC
B
pseudotime
C
prolif_traj
umap_2
umap_1
D
endomt_traj
E
monocle3_pseudotime
F
monocle3_pseudotime
G
EndoMT Score
Monocle3 Pseudotime
New Identity
H
EndoMT Score
Monocle3 Pseudotime
New Identity
EC-/Mes-
EC-/Mes+
EC+/Mes-
EC+/Mes+

<u>Figure 6.7.</u> Trajectory analysis suggests venous ECs to be a partial state along the EndoMT axis at days 1-7 post myocardial infarction (MI).

(A) UMAP of subset and reclustered ECs at days 1-7 post MI with a with trajectory originating from the most EC-like cells (Capillary1) based on EC marker expression.
(B) The same as (A) coloured by pseudotime.
(C) Trajectory towards proliferating ECs.
(D) Trajectory towards mesenchymal ECs.
(E) Boxplot of EC phenotypes ordered along proliferation trajectory pseudotime. Pseudotime shows cells to transition through an angiogenic phenotype before proliferating.
(F) Boxplot of EC phenotypes ordered along EndoMT trajectory pseudotime. Pseudotime shows cells to transition into a venous phenotype before becoming more mesenchymal.
(G) Scatter plot of EndoMT score for EC phenotypes ordered along EndoMT pseudotime. Venous ECs show an increase in EndoMT score.
(H) Scatter plot of EndoMT score for EC/MES annotations along EndoMT pseudotime. EC+/MES+ states are induced in the middle of the trajectory before becoming EC-/MES+

specified the pseudotime origin to be Capillary1 ECs which we previously showed to be the most EC-like based on canonical EC marker expression. We observed 2 trajectories originating from a branch in the Capillary1 ECs (Fig 6.7A). The first terminated in Proliferating ECs via Angiogenic1 and Angiogenic2 ECs with an increase in EndoMT score across pseudotime, suggesting EndoMT to play a role in the derivation of angiogenic and proliferative ECs from capillaries (Fig 6.7A,B,C,E). The second trajectory branched in venous ECs to terminate in Lymphatic and i-EC1 ECs (Fig 6.7A,B,D). We focused on the trajectory between Capillary1 and i-EC1 and found the trajectory to go through Angiogenic2 and Venous ECs (Fig 6.7A,B,D,F,G), suggesting a pro-angiogenic phenotype is induced before a venous phenotype, eventually leading to an increased mesenchymal phenotype (Fig 6.7D,F). Moreover, there was an increase in EndoMT score along the trajectory (Fig 6.7G), suggesting angiogenic and venous ECs to display a transient state in the EndoMT process. In agreement, we observed the EC+/MES+ state to be induced in the middle of the trajectory (Fig 6.7H), indicating a partial EndoMT-like state. Indeed, we saw a decrease in endothelial marker gene expression (including Cdh5 and Pecam1) and an increase in EndoMT related gene expression

(including Zeb2, Fn1 and Tagln) across the pseudotime (Appendix 4.2). Interestingly, ZEB1 expression was not significantly changed across the trajectory.

6.3.7 Expression analysis of Zeb1 revealed angiogenic, proliferative and mesenchymal-like EC phenotypes show an increased proportion of cells to express Zeb1 compared to the most EC-like phenotype without a change in expression levels

While Zeb1 expression did not significantly change along the trajectory between EC and mesenchymal ECs at d1-d7, the increase in predicted Zeb1 TF activity at d1-d7, the most EndoMT-like timepoint, EC+/MES+ scoring ECs and venous ECs (Fig 6.6G-I) prompted us to further investigate the mechanism of Zeb1 behaviour. We found that while expression of Zeb1 did not change across days post MI, the percentage of cells expressing Zeb1 at days 1-7, 14 and 28 was increased compared to homeostasis (Fig 6.8A). Furthermore, the percent of cells expressing Zeb1 was highest in EC-/MES+ and EC+/MES+ cells, without an increase in average Zeb1 expression (Fig 6.8B). Across all timepoints, Zeb1 expression was highest in m-ECs (Fig 6.8C). The lowest percent of cells expressing Zeb1 was observed in Capillary1, Capillary2 and Arterial ECs which were deemed the most EC-like (Fig 6.8C). The highest percent expressing of Zeb1 was in m-ECs, with all other EC phenotypes showing an increase in the percentage of cells expressing Zeb1 compared to Capillary1 and Capillary2, the most endothelial-like phenotypes (Fig 6.8C). Focusing on the EC phenotypes at days 1-7 post MI did not identify significant differential expression of Zeb1, however Capillary1 and Capillary2 continued to display the lowest percent of cells expressing Zeb1 with m-EC, Angiogenic2 and Proliferating to show the greatest percent of cells expressing Zeb1 (Fig 6.8D). These results indicate the induction of Zeb1 expression in cells to be associated with angiogenic, proliferative and EndoMT-like states without a significant change in the level of expression

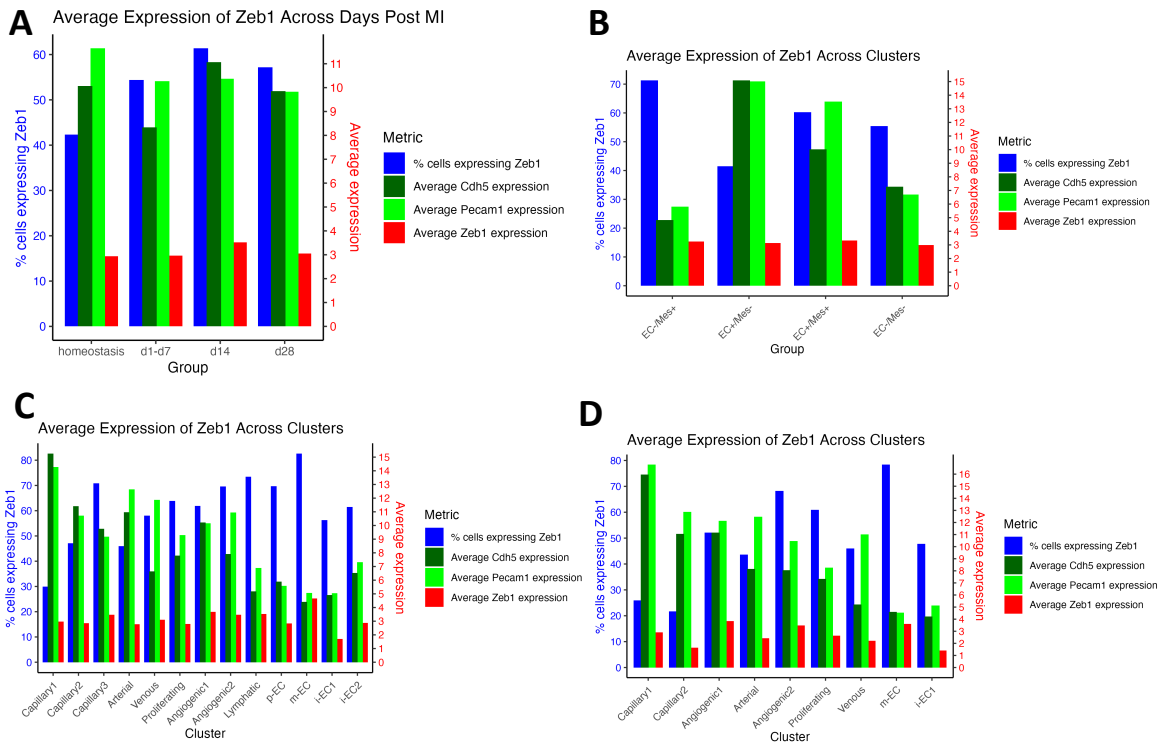


Figure 6.8. ***The percent of cells expressing Zeb1 is increased in EC+/MES+ cells and in angiogenic ECs.***

(A) Barchart of percent of cells expressing Zeb1 (blue) and average expression of Zeb1 (red), Cdh5 (dark green) and Pecam1 (light green) across days post MI. The percentage of cells expressing Zeb1 was increased at days 1-7, 14 and 28 post MI compared to homeostasis

(B) Same as (A) but for EC/MES state. The percent of cells expressing Zeb1 was lowest in EC+/MES- cells.

(C) Same as (A) but for EC phenotypes. The percent of cells expressing Zeb1 was lowest in Capillary1 ECs, those deemed most EC-like.

(D) Same as (C) but for days 1-7 post MI. i-EC2, Capillary3 and p-EC phenotypes were removed due to low cell number. Percent of cells expressing Zeb1 was lowest in Capillary1 and Capillary2 phenotypes and highest in m-EC, Angiogenic2 and Proliferating.

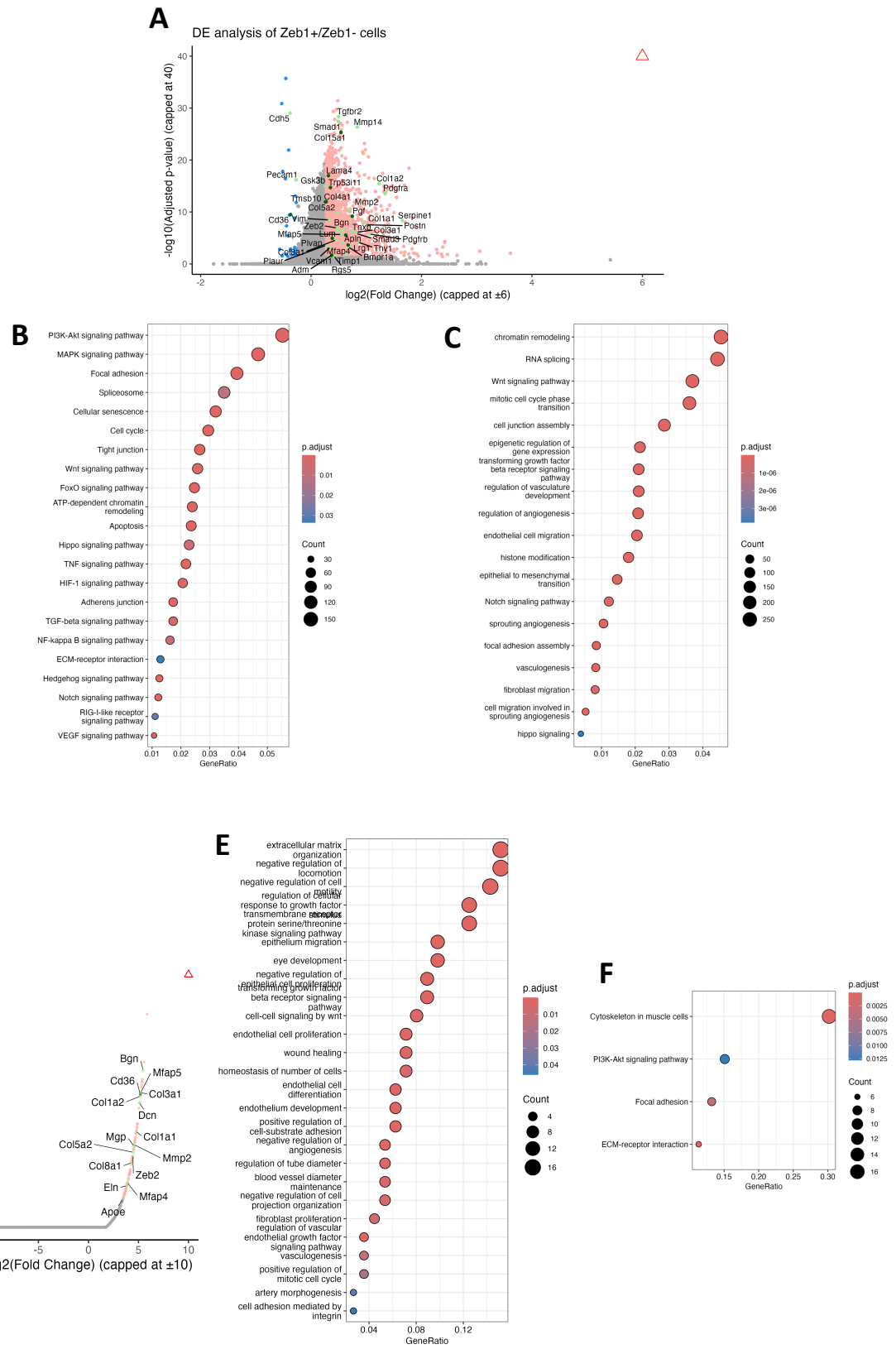
levels themselves.

To further investigate the mechanism of Zeb1 behaviour we performed differential expression of Zeb1+ and Zeb1- cells across all time points. Differential expression analysis identified 4550 upregulated and 1417 downregulated DEGs (Fig 6.9A). The upregulated genes included EndoMT and angiogenic related genes including Zeb2, a main driver of EndoMT (Fig 6.9A), suggesting cells expressing Zeb1 display an upregulation of Zeb2 but does not necessarily mean Zeb1 regulates Zeb2. Furthermore, the most upregulated EndoMT-

related gene was Serpine1 (Fig 6.9A), a mesenchymal marker. Downregulated genes in Zeb1+ ECs included EC markers Cdh5, Pecam1 as well as Cd36, which is known to perform an anti-angiogenic function in ECs (Simantov and Silverstein, 2003; Cho, 2012). The upregulation of EndoMT and pro-angiogenic related genes and downregulation of EC genes and anti-angiogenic Cd36 suggests Zeb1+ cells are in a more active-like state and have a reduced EC-like phenotype. These results align with the increased percent of cells expressing Zeb1 to be associated with Angiogenic2, Proliferative and m-EC phenotypes. Functional enrichment analysis of DEGs between Zeb1+ and Zeb1- ECs identified significant GO terms and KEGG pathways related to EMT, TGFB, EC migration, EC development, vascular associated smooth muscle cell proliferation, angiogenesis and vasculature development, Wnt signalling, Notch signalling, Hippo signalling, regulation of cell adhesion, focal adhesion regulation of cell migration, ECM organisation, epigenetic regulation of gene expression, mRNA splicing and cell cycle (Fig 6.9B,C). These results suggests genes to be differentially expressed in Zeb1+ cells are involved in several aspects of EC activation and EndoMT.

6.3.8 In-silico KO of Zeb1 revealed perturbation of EndoMT-related genes and processes

To gain further insight into the regulatory of role of Zeb1 we employed an *in-silico* KO technique scTenifoldKNK (Osorio *et al.*, 2022) that has recently been applied to EC research (Guduric-Fuchs *et al.*, 2024) to predict perturbations in gene expression upon Zeb1 KO. Across all timepoints we identified 113 perturbed genes (Fig 6.9D). Celf2 displayed the greatest level of regulation by Zeb1 KO. Interestingly, this gene has been implicated in mRNA splicing and is essential in the transition of ECs to T1 pre-Hematopoietic stem cells (HSCs), suggesting a role in cellular homeostasis (T. Guo *et al.*, 2024) The predicted perturbation of


A
DE analysis of Zeb1+/Zeb1- cells
-log10(Adjusted p-value) (capped at 40)
log2(Fold Change) (capped at ±6)
Cdh5
Tgfbr2
Mmp14
Smad1
Col15a1
Pecam1
Gsk3b
Trp53i11
Lama4
Col1a2
Pdgfra
Tmsb10
Col4a1
Col5a2
Mmp2
Pgf
Cd36
Vim
Zeb2
Bgn
Col1a1
Serpine1
Mfap5
Lum
Tnxb
Col3a1
Postn
Plvap
Apln
Smad3
Pdgfrb
Cdh5
Trap4
Lrg1
Thy1
Plaur
Vcam1
Vimp1
Bmpr1a
Adm
Rgs5
B
PI3K-Akt signaling pathway
MAPK signaling pathway
Focal adhesion
Spliceosome
Cellular senescence
Cell cycle
Tight junction
Wnt signaling pathway
FoxO signaling pathway
ATP-dependent chromatin remodeling
Apoptosis
Hippo signaling pathway
TNF signaling pathway
HIF-1 signaling pathway
Adherens junction
TGF-beta signaling pathway
NF-kappa B signaling pathway
ECM-receptor interaction
Hedgehog signaling pathway
Notch signaling pathway
RIG-I-like receptor signaling pathway
VEGF signaling pathway
GeneRatio
p.adjust
Count
C
chromatin remodeling
RNA splicing
Wnt signaling pathway
mitotic cell cycle phase transition
cell junction assembly
epigenetic regulation of gene expression
transforming growth factor beta receptor signaling pathway
regulation of vasculature development
regulation of angiogenesis
endothelial cell migration
histone modification
epithelial to mesenchymal transition
Notch signaling pathway
sprouting angiogenesis
focal adhesion assembly
vasculogenesis
fibroblast migration
cell migration involved in sprouting angiogenesis
hippo signaling
GeneRatio
p.adjust
Count
D
-log10(Adjusted p-value) (capped at 12)
log2(Fold Change) (capped at ±10)
Bgn
Mfap5
Cd36
Col3a1
Col1a2
Dcn
Mgp
Col1a1
Col5a2
Mmp2
Col8a1
Zeb2
Eln
Mfap4
Apoe
E
extracellular matrix organization
negative regulation of locomotion
negative regulation of cell motility
regulation of cellular response to growth factor
transmembrane receptor protein serine/threonine kinase signaling pathway
epithelium migration
eye development
negative regulation of epithelial cell proliferation
transforming growth factor beta receptor signaling pathway
cell-cell signaling by wnt
endothelial cell proliferation
wound healing
homeostasis of number of cells
endothelial cell differentiation
endothelium development
positive regulation of cell-substrate adhesion
negative regulation of angiogenesis
regulation of tube diameter
blood vessel diameter maintenance
negative regulation of cell projection organization
fibroblast proliferation
regulation of vascular endothelial growth factor signaling pathway
vasculogenesis
positive regulation of mitotic cell cycle
artery morphogenesis
cell adhesion mediated by integrin
GeneRatio
p.adjust
Count
F
Cytoskeleton in muscle cells
PI3K-Akt signaling pathway
Focal adhesion
ECM-receptor interaction
GeneRatio
p.adjust
Count

<u>Figure 6.9.</u> EndoMT-related genes were predicted to be perturbed in response to in-silico KO of Zeb1.

(A) Differential expression analysis of Zeb1+ and Zeb1- cells for all ECs shown as a volcano plot with upregulated genes in red and downregulated genes in blue. EndoMT-related genes are shown in green and angiogenic-related genes in dark green. Zeb1 is represented as a red triangle.
(B) Dotplot of functional enrichment analysis of Zeb1+/Zeb1- differential expressed genes (DEGs) against the KEGG database.
(C) Gene Ontology functional enrichment analysis of DEGs identified pro-angiogenic processes.
(D) Differentially regulated (DR) genes predicted by *in-silico* Zeb1 KO in ECs across all days post MI. Labelled and coloured in green are significantly DR EndoMT-related genes. Other significant DR genes are in red, non-significant in grey. Zeb1 is represented as a red triangle.
(E) Gene ontology functional enrichment analysis of DR genes predicted by *in-silico* Zeb1 KO represented as a dotplot. Processes related to ECM organisation, EC proliferation and adhesion were enriched.
(F) KEGG pathway functional enrichment analysis of DR genes predicted by *in-silico* Zeb1 KO represented as a dotplot. Focal adhesion and ECM-receptor interaction pathways were enriched.

Celf2 expression by Zeb1 indicated Zeb1 may play a role in splicing and EC homeostasis. We identified 15 EndoMT-related genes to be perturbed by *in-silico* Zeb1 KO including Zeb2, along with collagens Col1a2, Col3a1, Col1a1, Col5a2 and Col8a1 (Fig 6.9D) suggesting Zeb1 may regulate Zeb2 and collagens involved in EndoMT. Functional enrichment analysis of the perturbed genes led to significant GO terms associated with ECM organisation, cell motility, TGF-B and Wnt signaling and regulation of endothelial proliferation and adhesion (Fig 6.9E,F). These findings indicate that Zeb1 is involved in orchestrating ECM remodeling, growth factor signaling pathways and the balance between EC quiescence and motility.

6.3.9 Text-mining and network analysis of 421 abstracts identified 623 genes/proteins related to EndoMT and 22 core network hubs

The analysis of this chapter has focussed on EndoMT in a single dataset and pathology. To expand the analysis and encompass an overview of the EndoMT process we employed a text-mining approach to extract information from relevant publications. We

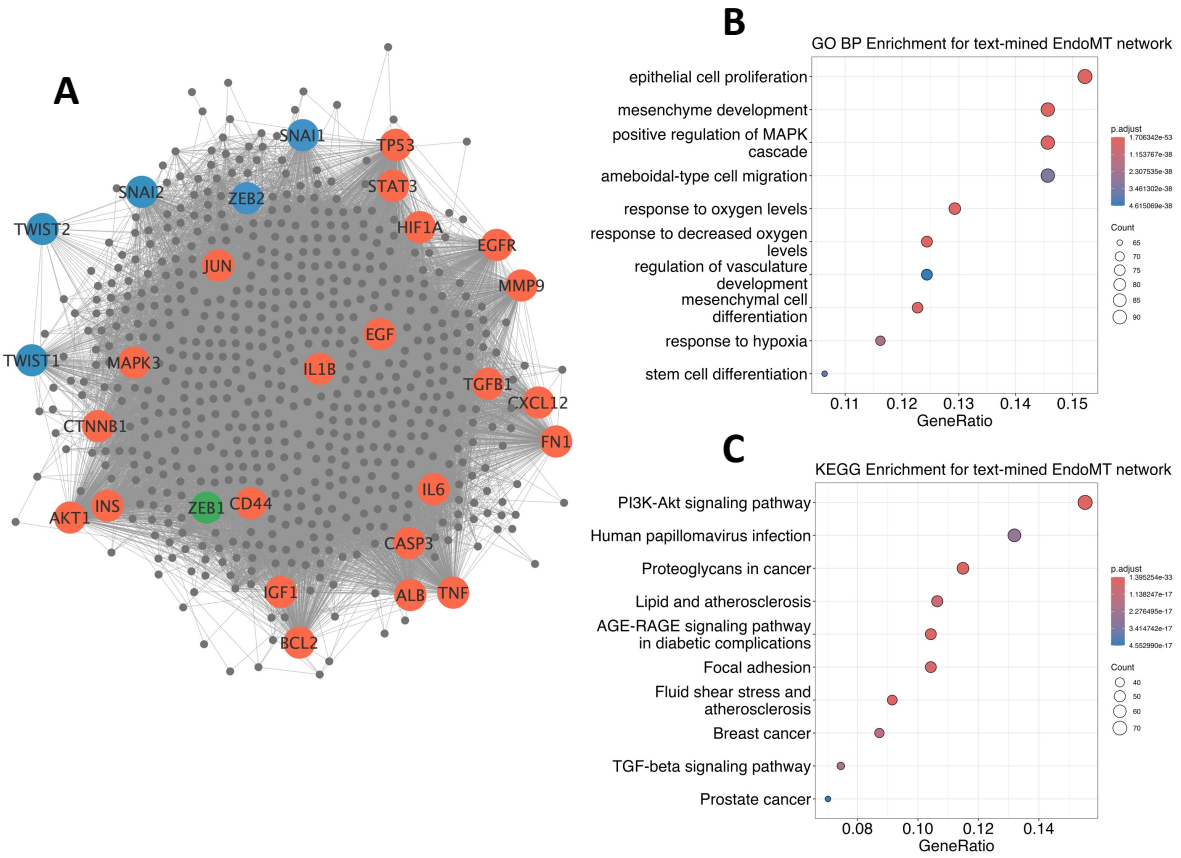


Figure 6.10. ***Network analysis of genes/proteins identified from text-mining of EndoMT-related abstracts retrieved from PubMed Central identified highly interconnected hub nodes that may modulate core EndoMT mechanisms.***

(A) STRING PPI network generation of 623 EndoMT-related genes extracted from text-mining. Hub genes, those with the greatest connectivity, are shown in red, ZEB1 in green and other key drivers of EndoMT in blue.

(B) Gene Ontology functional enrichment analysis of the 623 text-mined EndoMT genes identified vasculature development, epithelial cell proliferation and mesenchyme development processes.

(C) KEGG pathway functional enrichment analysis of the 623 text-mined EndoMT genes revealed specific signalling pathways including PI3K-Akt, AGE-RAGE and TGF-beta, as well as focal adhesion.

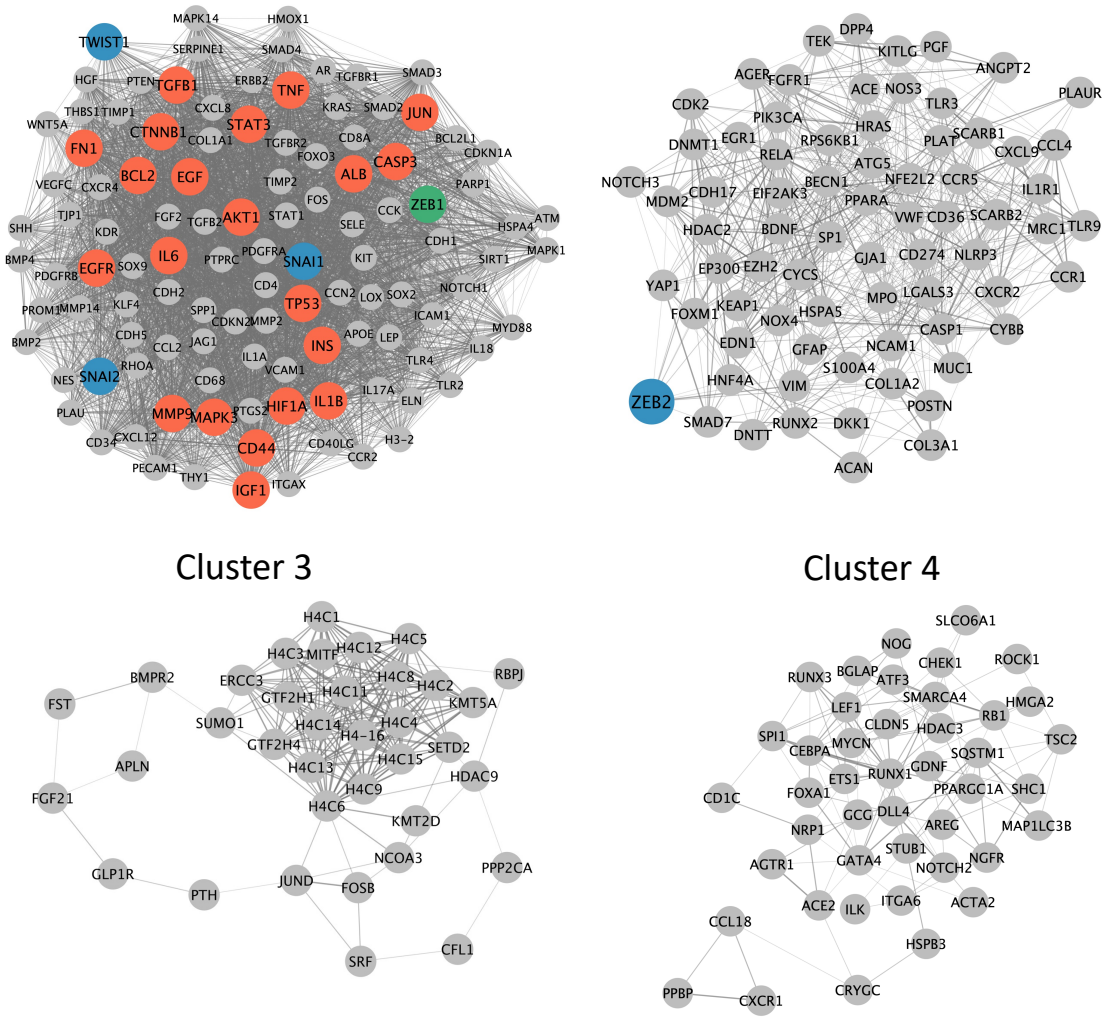
identified 421 relevant abstracts from PubMedCentral related to EndoMT. Named entity recognition (NER) through the Tagger tool returned 623 unique gene/protein IDs from the 421 abstracts, which are deemed to be EndoMT-related proteins and were subsequently subjected to protein-protein interaction network analysis, resulting in a highly connected network (Fig 6.10A). We applied 5 algorithms to identify hub proteins - those deemed to be integral to and putative regulators of the PPI network. The consensus of the algorithms

identified 22 hub proteins which may form a core EndoMT regulatory signature and included AKT1, ALB, BCL2, CASP3, CD44, CTNNB1, CXCL12, EGF, EGFR, FN1, HIF1A, IGF1, IL1B, IL6, INS, JUN, MAPK3, MMP9, STAT3, TGFB1, TNF, TP53 (Fig 6.10A). It is proposed that these hub proteins lie at the core of the text-mined network and are putative key regulators of EndoMT. HIF1A, JUN, STAT3 and TP53 are transcription factors whose transcription profiles could allude to a greater understanding of the EndoMT process. We also identified ZEB2, SNAI1, SNAI2, TWIST1 and TWIST2, known drivers of EndoMT, and ZEB1 within the network (Fig 6.10A). Functional enrichment analysis of the network identified epithelial cell proliferation, mesenchyme development, response to oxygen levels and regulation of vasculature development to be amongst the significant GO terms (Fig 6.10B). KEGG pathway analysis identified PI3K-Akt signalling, AGE-RAGE signalling, TGF-beta signalling and focal adhesion (Fig 6.10C).

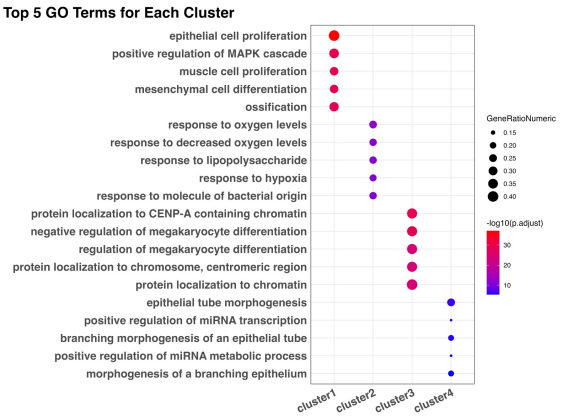
6.3.10 Network analysis of 623 text-mined proteins revealed four highly connected clusters providing insight into protein network linked to specific processes

To gain insight into the processes involved within the proposed EndoMT network, we applied the clustering algorithm MCODE to identify modules within the network. Four highly connected subnetworks (clusters) were derived from the main network (Fig 6.11A). These clusters may serve as functional sub-modules of highly connected proteins, further shedding light on EndoMT processes. Cluster 1 had an MCODE score of 81.0 and consisted of 111 proteins, where MCODE score represents the connectivity of the cluster. Interestingly, all 22hub proteins were found within this cluster (Fig 6.11A). MCODE clusters 2, 3 and 4 had MCODE scores of 17.1, 11.2 and 5.5 respectively,. Functional enrichment analysis shed light on the processes related to each subcluster (Fig 6.11B,C). Cluster 1 contains proteins

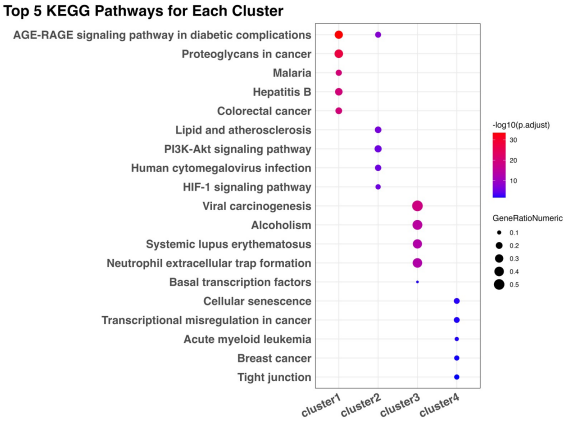
A


Cluster 1
Cluster 2
Cluster 3
Cluster 4

B


Top 5 GO Terms for Each Cluster
epithelial cell proliferation
positive regulation of MAPK cascade
muscle cell proliferation
mesenchymal cell differentiation
ossification
response to oxygen levels
response to decreased oxygen levels
response to lipopolysaccharide
response to hypoxia
response to molecule of bacterial origin
protein localization to CENP-A containing chromatin
negative regulation of megakaryocyte differentiation
regulation of megakaryocyte differentiation
protein localization to chromosome, centromeric region
protein localization to chromatin
epithelial tube morphogenesis
positive regulation of miRNA transcription
branching morphogenesis of an epithelial tube
positive regulation of miRNA metabolic process
morphogenesis of a branching epithelium
cluster1
cluster2
cluster3
cluster4
GeneRatioNumeric
-log10(p.adjust)

C


Top 5 KEGG Pathways for Each Cluster
AGE-RAGE signaling pathway in diabetic complications
Proteoglycans in cancer
Malaria
Hepatitis B
Colorectal cancer
Lipid and atherosclerosis
PI3K-Akt signaling pathway
Human cytomegalovirus infection
HIF-1 signaling pathway
Viral carcinogenesis
Alcoholism
Systemic lupus erythematosus
Neutrophil extracellular trap formation
Basal transcription factors
Cellular senescence
Transcriptional misregulation in cancer
Acute myeloid leukemia
Breast cancer
Tight junction
cluster1
cluster2
cluster3
cluster4
-log10(p.adjust)
GeneRatioNumeric

<u>Figure 6.11.</u> MCODE analysis of the text-mined network identified 4 sub-clusters corresponding to specific processes.

(A) MCODE sub-clusters representing highly interconnected modules within the text-mined network in Fig 6.10A. Colouring of nodes the same as Fig 6.10A.
(B) Dotplot of the top 5 enriched GO terms for each cluster.
(C) Dotplot of the top 5 enriched KEGG pathways for each cluster.
MCODE cluster 1 shows enrichment for cell proliferation and MAPK pathways. MCODE cluster 2 shows processes related to oxygen levels and HIF-1 signalling. MCODE cluster 3 was enriched for chromatin and protein localisation to the chromosome processes. MCODE cluster 4 contained genes related to branching and morphogenesis of the epithelium.

implicated in cell proliferation and the MAPK pathway as well as the AGE-RAGE signalling pathway. Response to oxygen levels and HIF-1 signalling were enriched in cluster 2, indicating that the proteins likely are involved in the hypoxic response in EndoMT. Interestingly, cluster 3 contained proteins associated with chromatin and protein localisation to the chromosome, perhaps alluding to the proteins responsible for regulating the transcriptional changes driving EndoMT. Cluster 4 related to branching and morphogenesis of the epithelium and miRNA transcription and would warrant further research into these proteins potentially being involved in endothelial morphogenesis during EndoMT (Fig 6.11B,C). Interestingly, the cellular senescence pathway was enriched along with tight junctions in cluster 4, suggesting these genes to be involved with the altering of junctions during EndoMT.

6.3.11 Text-mined network identified a predicted core Zeb1 interactome of EndoMT-related genes that contains 21 of 22 network hub proteins.

To focus on the role ZEB1 may play in the EndoMT network, we selected all nodes that are predicted to form a direct interaction with ZEB1 and produced a subnetwork that indicates a core predicted ZEB1-EndoMT interactome of 113 proteins (Fig 6.12A). Interestingly, 21 of the 22 hubs were present in the network (Fig 6.12A), suggesting ZEB1 can

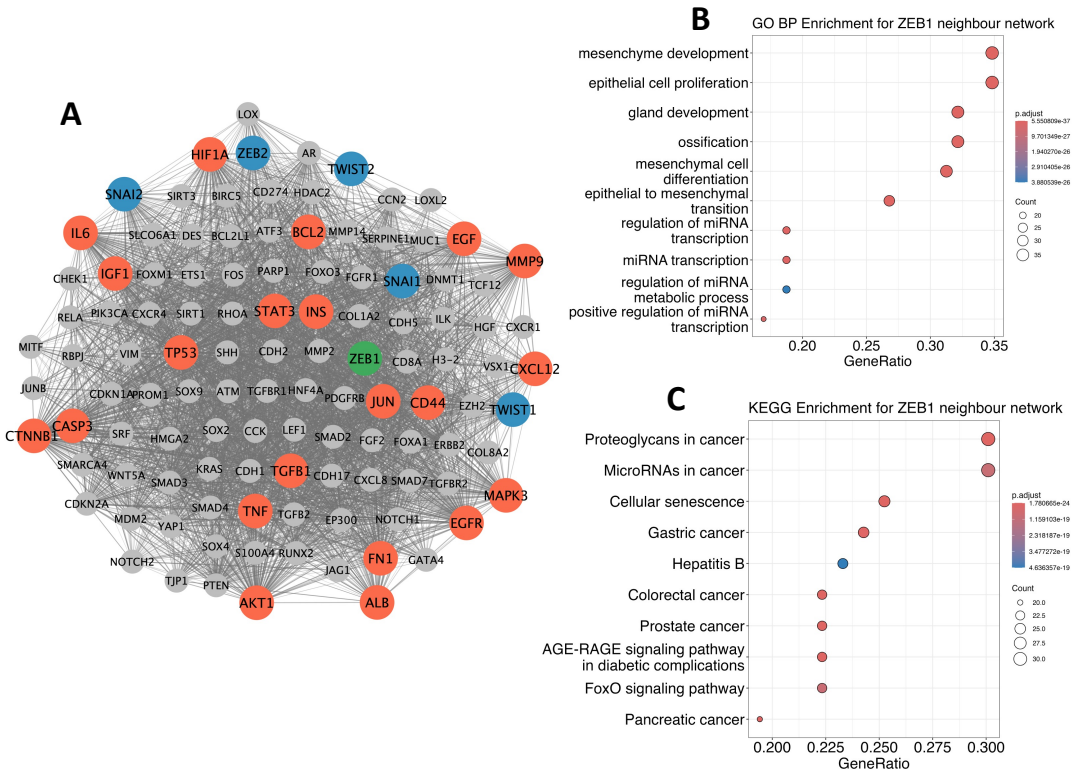


Figure 6.12. ***Network of direct Zeb1 interactors involved 21 of 22 hub genes.***

(A) Network of first neighbour nodes of Zeb1, forming direct predicted interactions with Zeb1. Coloured the same as Fig 6.10A.

(B) Enriched Gene Ontology terms for the Zeb1 direct network.

(C) Enriched KEGG pathways for the Zeb1 direct network.

Epithelial to mesenchymal transition, miRNA transcription and cellular senescence pathways were associated with ZEB1 interactors.

directly interact with the majority of the core EndoMT gene signature. However, hub protein IL1B was not present in the ZEB1 interactome. The ZEB1 interactome also included EndoMT drivers SNAI1, SNAI2, TWIST1, TWIST2 and ZEB2 (Fig 6.12A). Functional enrichment analysis revealed epithelial to mesenchymal transition to be associated with the ZEB1 interactome along with miRNA transcription and cellular senescence (Fig 6.12B,C).

6.3.12 Cross-referencing text-mining with a publicly available bulk RNA-seq EndoMT dataset in different EC models revealed a central EndoMT core signature.

Comparison our text-mined list of genes/proteins involved in EndoMT against a publicly available dataset of DEGs identified in human umbilical vein endothelial cells

(HUVECs), human pulmonary microvascular endothelial cells (HPMVECs) and human aortic endothelial cells (HAECs) undergoing EndoMT stimulated by TGF-B1 and IL1B treatment (Bronson, Lyu and Xiong, 2023) revealed overlaps between the datasets, with 108 genes/proteins being common amongst all (Fig 6.13A). The 108 overlapping genes may provide the core basis of the EndoMT process that is required to drive the transition regardless of biological context. Interestingly, none of the publicly available DEGs identified ZEB1 to be differentially expressed upon stimulation of EndoMT. Furthermore, we found that HAEC DEGs included ZEB2, SNAI1 and SNAI2, HPMVEC differentially expressed ZEB2 and SNAI1 but not SNAI2 and HUVECs SNAI1 and SNAI2 but not ZEB2, indicating that different EC populations utilise different drivers upon stimulation of EndoMT, with SNAI1 being a common factor. Within the overlapping genes we identified 7 hubs of the text-mined network; BCL2, CD44, CXCL12, FN1, IL1B, IL6 and TNF (Fig 6.13B), further indicating these genes to have a key role in EndoMT. Aside from SNAI1, the overlapping genes included other TFs; ATF3, BACH1, ETS1, FOXM1, HES1, JUNB, MSX1, MYCN, NR3C2, RUNX1 and SOX17 which are potential candidates for regulating EndoMT and would warrant further research.

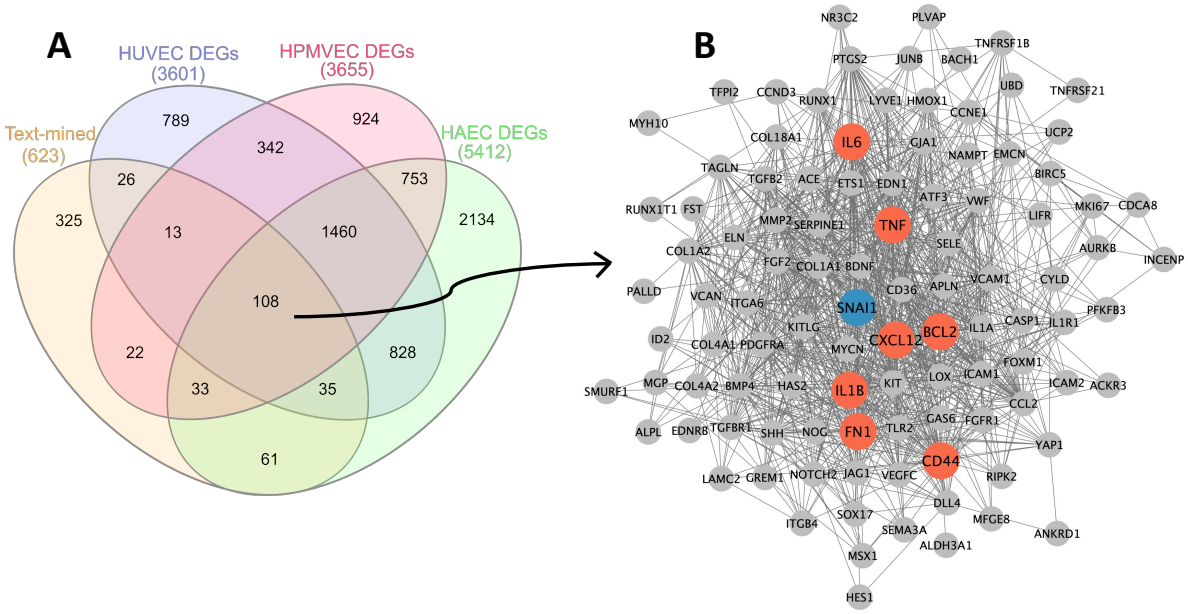


***Figure 6.13.* 108 genes overlap between text-mined EndoMT-related genes and DEGs identified from an EndoMT RNA-seq public dataset of 3 in-vitro EC models.**

(A) Venn diagram showing the overlap of text-mined EndoMT-related genes and DEGs identified from EndoMT stimulation in HUVECs, HPMVECs and HAEC DEGs. A core signature of 108 genes was identified.

(B) Network of the 108 overlapping genes identified in (A) that included EndoMT driver SNAI1 and hub genes CD44, IL6, TNF, BCL2, CXCL12, IL1B and FN1 identified in Fig 6.10A.

6.3.13 Comparison of text-mining extracted EndoMT related genes with HUVEC ZEB1 KD DEGs and ZEB1 HUVEC ChIP-seq peaks revealed a shared set of 16 genes

Combining several approaches within this thesis, we examined the overlap between genes identified in EndoMT-related text mining, DEGs identified from ZEB1 KD in HUVECs (Chapter 3) and genes annotated to ZEB1 ChIP-seq peaks in HUVECs (Chapter 4) (Fig 6.14A). We identified a shared, central core of 16 genes regulated by ZEB1 (Fig 6.14A,B). Interestingly, none of the hub genes identified from the text-mining network analysis were included. This overlap contained 4 TFs; ATF3, BACH1, ETS1 and KLF4 which are putative candidates for a central regulation of EndoMT by ZEB1 (Fig 6.14B). We also observed CXCR4

(a tip cell marker) and ICAM1 (an adhesion marker) to be present (Fig 6.14B), indicating a potential regulation of EndoMT by ZEB1 during sprouting angiogenesis (Welch-Reardon, Wu and Hughes, 2015; Fang, Hultgren and Hughes, 2021).

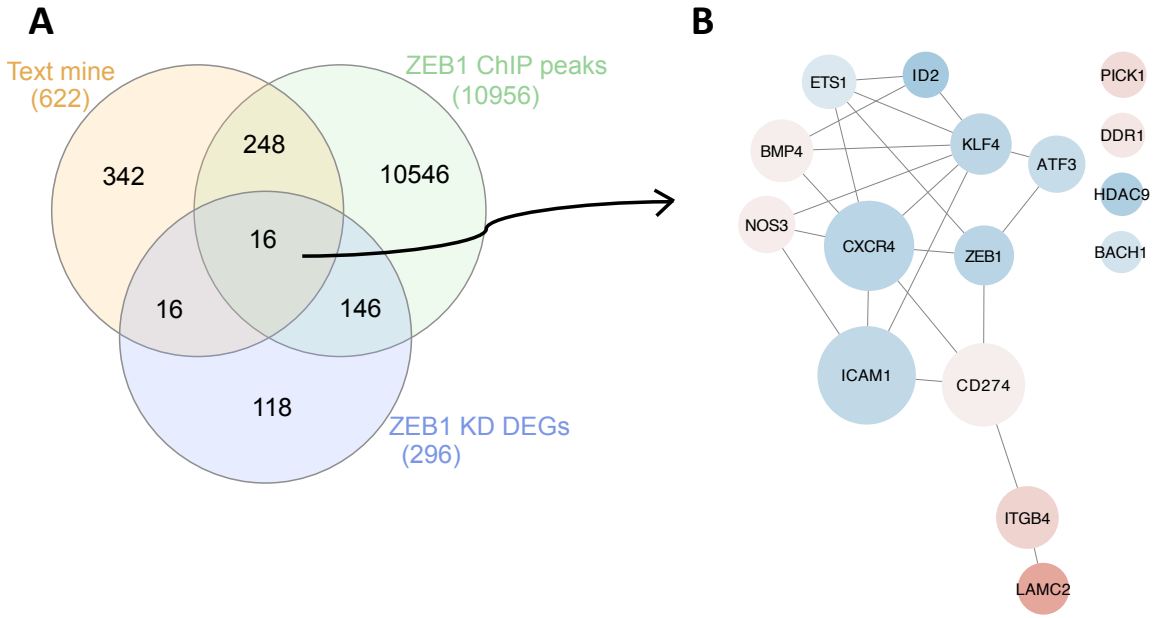


Figure 6.14. ***16 genes overlap between text-mined EndoMT related genes, DEGs identified by ZEB1 KD RNA-seq analyses in chapter 3 and enriched peaks in ZEB1 HUVEC ChIP-seq in chapter 4.***

(A) Venn diagram showing the overlap between genes identified by text-mining, DEGs from RNA-seq analysis of ZEB1 KD in HUVECs (chapter 3) and enriched ZEB1 HUVEC ChIP-seq peaks (chapter 4). Combined analysis identified 16 genes to be directly regulated by ZEB1 and present in the EndoMT text mining analysis.

(B) Network of the 16 overlapping genes identified in (A). Network was derived from the total network of ZEB1 KD HUVEC DEGs in Fig 3.3A. 5 TFs were included in the overlap: ATF3, BACH1, ETS1, KLF4 and ZEB1. The tip cell marker CXCR4 and adhesion marker ICAM1 were also identified.

6.3.14 A publication related to EndoMT released after the text-mining analysis included results predicted by text-mining

We searched for research papers related to EndoMT that were published after we ran our text-mining analysis, and so could not have been included in our study, to identify whether our approach correctly predicted any novel findings. Indeed, a paper identified mitochondrial calcium signalling as a 'previously unknown regulator of End(o)MT' (Lebas *et*

al., 2024). The functional enrichment analysis results of the text-mined network revealed several terms related to calcium signalling, indicating a correct predictive link between EndoMT and calcium signalling. Interestingly, BCL2, CTNNB1, CXCL12, EGF, IGF1 and TNF hub proteins are members of the calcium signalling GO terms, indicating the potential role of these hub proteins within the EndoMT-calcium relationship. Indeed, BCL2 has been implicated in EndoMT associated with an upregulation of anti-apoptotic factors (Yoshimatsu and Watabe, 2022) and also in mitochondrial calcium signalling (Morris *et al.*, 2021). While this result suggests our text-mining to be a valid approach to generating hypotheses, due to time constraints we have not yet been able to search for other publications to validate the results.

6.4 Discussion

In this study, we leveraged a publicly available scRNA-seq dataset of murine hearts subjected to MI alongside a large-scale text-mining approach to explore the transcriptional landscape underlying EndoMT and, in particular, the role of ZEB1. Our reanalysis of non-cardiomyocyte fractions (Cdh5+/Pecam1+) identified a diversity of endothelial clusters, some of which exhibit mesenchymal, immune and pericyte-like features. By combining curated EndoMT-related gene signatures with TF activity profiling, we found evidence of EndoMT-like processes in several subpopulations, most prominently at early post-injury timepoints (days 1-7) and within venous, pericyte-like, mesenchymal-like and angiogenic endothelial clusters.

A central finding was the multifaceted behaviour of ZEB1 in these populations. While the overall average expression level of ZEB1 did not markedly change during MI, the proportion of cells expressing ZEB1 was increased in more mesenchymal or activated states, particularly at days 1-7 post MIU. Furthermore, cells expressing ZEB1 tended to

downregulate core endothelial genes (Cdh5 and Pecam1) and the anti-angiogenic genes CD36 while upregulating pro-angiogenic and EndoMT-related genes including ZEB2. These observations argue that ZEB1 does not necessarily need to undergo an induction at the transcript level, instead its role may involve enabling specific subsets of endothelial cells to adopt or maintain a more activated phenotype that can support both mesenchymal transition and neovascularisation. Consistent with this, *in-silico* KO analysis predicted that removal of ZEB1 would perturb key ECM and TGF-B signalling genes, implicating ZEB1 in ECM remodelling, cell motility and mesenchymal differentiation which are hallmarks of EndoMT.

Notably, the TF-activity analyses revealed a contrasting pattern of EndoMT drivers. While SNAI1, SNAI2, TWIST1, TWIST2 and ZEB2 activity was associated with fully mesenchymal or immune-like endothelial states, ZEB1 activity showed a unique association with hybrid endothelial and mesenchymal phenotypes. This suggests that ZEB1 may preferentially help sustain a partial EndoMT program rather than driving cells fully into a mesenchymal fate, as is predicted to occur within tip cells (Welch-Reardon, Wu and Hughes, 2015; Fang, Hultgren and Hughes, 2021). Such partial EndoMT states could be critical for processes like sprouting angiogenesis, ECM remodelling and immune cell interactions, each of which is integral to the post-infarction repair process. However, the TF analysis needs to be carefully considered as ZEB1 activity is calculated based on expression change of 62 ZEB1 targets. We have previously shown in this thesis that ZEB1 can target and regulate more than 62 genes.

Out text-mining approach further corroborated the potential importance of ZEB1 in EndoMT. Across 421 abstracts relating to EndoMT we identified 623 unique genes/proteins forming a highly interconnect protein-protein interaction network that contained well-known EMT drivers (SNAI1, TWIST1/2, ZEB1/2) and 22 core “hub” proteins involved in

proliferation, survival and inflammatory signalling. Within this expansive network, ZEB1 was predicted to have direct interactions with 21 of the 22 hubs. These network analyses therefore place ZEB1 at the center of multiple EndoMT-related pathways, linking it to key regulatory proteins and TFs necessary for endothelial plasticity.

Taken together, our results position ZEB1 as a nuanced modulator rather than a simple on/off switch in EndoMT. Instead of undergoing transcriptional induction, ZEB1 appears to be expressed by a subset of ECs that respond to MI by shifting toward more mesenchymal or angiogenic phenotypes. This model is consistent with current EndoMT literature which point to hybrid or partial transition states as critical for angiogenesis and tissue remodelling. In the context of MI, such partial EndoMT might allow endothelial cells to proliferate or migrate while retaining aspects of an endothelial identity, thereby facilitating neovascularisation and ECM reorganisation during the healing process.

Despite these insights, limitations remain. First, our analysis was restricted to transcript-level data from a single publicly available scRNA-seq dataset. Direct experimental validation such as lineage tracing or protein-level assays would be needed to confirm that cells expressing ZEB1 do indeed undergo partial EndoMT *in-vivo*. Second, while text mining provided a broad predictive network of potential ZEB1 interactions, such approaches cannot confirm functional relevance without further mechanistic evidence. Further work could address these limitations by integrating multi-omic datasets (e.g., ATAC-seq, proteomics and spatial transcriptomics and by developing *in-vivo* models for conditional ZEB1 depletion in ECs. The latter would be especially informative for pinpointing how ZEB1-driven partial EndoMT might shape the remodelling process, angiogenesis and ultimately functional recovery of the heart post-MI. As both scRNA-seq reanalysis and network-based text mining indicate, ZEB1 interfaces with many of the pathways known to drive or modulate EndoMT,

making it an intriguing candidate for targeted studies aimed at mitigating maladaptive cardiac remodelling or promoting reparative angiogenesis.

In summary, our reanalysis of scRNA-seq data and large-scale text mining highlight the predictive role of Zeb1 in modulating partial EndoMT states and emphasise the complexity of EndoMT regulation in the injured heart. These findings open avenues for deeper mechanistic studies and potential therapeutic interventions that exploit the plasticity of ECs.

Chapter 7: Adult inducible knockout of Zeb1 does not alter mouse retinal vascular area or endothelial cell number

7.1 Introduction

The mammalian retina is a highly intricated tissue that converts visual information into neural signals. Its stratified architecture includes neuronal, glial and vascular components intricately arranges to support photoreceptor function and achieve visual acuity (Wässle, 2004). In mice, the retinal vasculature is arranged in a trilaminar network, superficial, intermediate and deep plexuses, that develop and mature postnatally. Proper maintenance of these vascular layers is critical for retinal health. Disruptions in vascular homeostasis can results in pathologies such a retinopathy, ischemia or neovascularisation (Saint-Geniez and D'Amore, 2004; Fruttiger, 2007) due to dysregulated angiogenic remodelling. Angiogenesis in the retina is carefully orchestrated through interactions among various cell types including astrocytes, glia and endothelial cells and tightly regulated molecular signals. Key pro-angiogenic factors like vascular endothelial growth factor (VEGF) guide vessel outgrowth which transcription factors modulate endothelial cell identity and stability (Gerhardt and Betsholtz, 2003). Because of this balance, examining the function of a single transcription factor within the retinal microenvironment can yield significant insights into both physiological and pathological processes.

Zinc finger E-box binding homeobox 1 (ZEB1) is a transcription factor best known for its role in epithelial-mesenchymal transition (EMT), a process essential during embryogenesis and, when aberrantly regulated, implicated in metastasis and fibrosis (Thiery and Sleeman, 2006). Beyond EMT, ZEB1 participates in multiple regulatory circuits,

influencing cell proliferation, differentiation and survival (Peinado, Olmeda and Cano, 2007). Recently, ZEB1 endothelial cell knockout (ECKO) in mouse retina led to hyper-proliferation of ECs and vessel abnormalities, indicating ZEB1 to be required for EC quiescence entry in the developing retina vasculature (Yu *et al.*, 2022). Conversely, it has also been shown that deletion or knockdown of ZEB1 reduced mouse retinal microvascular endothelial cell proliferation and angiogenesis (Jin *et al.*, 2020), highlighting the nuanced behaviour of ZEB1. Questions remain about whether, and to what extent, ZEB1 directly affects adult retinal vasculature.

The Cre/loxP recombination system is a well-established genetic tool for spatiotemporal control of gene expression in mice (Sauer and Henderson, 1988). Cre recombinase recognises loxP sites engineered around a gene of interest, enabling targeted excision or knockout or that gene in specific tissues or at particular developmental stages. This offers a powerful approach to study gene function in organs such as the retina, where timing and location of a gene disruption are critical. An inducible Cre system adds a further layer of control by requiring an external stimulus, commonly tamoxifen administration, to activate Cre recombinase (Feil, Valtcheva and Feil, 2009). This inducible model allows researchers to bypass embryonic or early postnatal lethality that might arise from a conventional knockout, enabling the study of gene function in adult tissues. In the context of ZEB1 an inducible Cre system facilitates the acute deletion of this transcription factor in adult retinal cells, ensuring that any observed phenotypic changes can be attributed specifically to ZEB1 loss in fully developed tissue.

Recent unpublished work carried out within the lab group identified Zeb1 inducible endothelial cell knockout ($Zeb1^{iECKO}$) in adult mice to result in increased vessel leakage within choroid lesions induced by choroidal neovascularisation (CNV), a model of age-related

macular degeneration, indicating reduced endothelial integrity resulting in increased permeability and an exacerbated pathological effect. Furthermore, $Zeb1^{iECKO}$ led to an increase in $Cd31^{+}$ neovascular lesion size, suggesting loss of Zeb1 induces aberrant, pathological angiogenesis. During development, $Zeb1^{iECKO}$ in p5 mice was shown to negatively impact vascular extension and EC number at the angiogenic front in the retina, revealing loss of Zeb1 reduces developmental angiogenesis. These results highlight the intricate behaviour of Zeb1 within different contexts.

Taken together, the intricate regulation of retinal vasculature by transcription factors and the established importance of ZEB1 in vascular and epithelial contexts highlight the necessity of studying the function of ZEB1 in adult retina. By combining the power of inducible genetic tools with *in-vivo* analyses of retinal vasculature, this work aims to shed new light on how ZEB1 shapes adult retinal homeostasis. In addition, we intend to use the results gathered in this work as a backdrop of observed phenotype to complement future scRNA-seq studies of mouse retina ECs.

7.2 Hypothesis and aim

Hypothesis: Adult induced endothelial *Zeb1* KO ($Zeb1^{iECKO}$) will perturb the vascular phenotype of the mouse retina.

The hypothesis was tested through immunofluorescence (IF) imaging and analysis techniques to address the following aim:

Aim: To evaluate the vascular consequences of endothelial *Zeb1* loss *in-vivo*, focusing on vessel morphology and EC distribution in the adult retina.

7.3 Results

7.3.1 Adult induced Zeb1 KO via the iECKO model resulted in significant reduction of Zeb1 mRNA expression in murine lung Cd31⁺ cells specifically – results obtained by Kathryn Green

In order to ensure that the inducible endothelial cell knockout (iECKO) model was efficient, we confirmed Zeb1 KO at the RNA level in adult mouse lung $Cd31^+$ cells (Fig 7.1A-D). First, the extraction of Cd31+ cells validated through determining Cd31 expression levels across the input (all cells), $Cd31^-$ and $Cd31^+$ fractions normalised against GAPDH expression. We observed significant enrichment of Cd31 expression in the $Cd31^+$ fraction compared to input and $Cd31^-$ fractions, indicating a successful enrichment of $Cd31^+$ cells. This was seen in both control and $ZEB1^{iECKO}$ mice (Fig 7.1A).

Zeb1 mRNA levels were next quantified in each cell fraction from control mice using GAPDH as a reference (Fig 7.1B). This analysis showed a marked enrichment of Zeb1 mRNA in the $Cd31^+$ population compared to the $Cd31^-$ population, indicating that ZEB1 expression in the mouse lung is predominantly derived from $Cd31^+$ cells. Zeb1 mRNA levels were then evaluated in the $Cd31^-$ fractions of control and $Zeb1^{iECKO}$ mouse lungs and revealed no significant difference (Fig 7.1C). Analysis of Zeb1 mRNA expression in $Cd31^+$ cell fractions across control and $Zeb1^{iECKO}$ samples revealed a significant reduction in Zeb1 mRNA abundance in the $Zeb1^{iECKO}$ group (Fig 7.1D), confirming the inducible transgenic knockout in adult mice reduces Zeb1 expression specifically in $Cd31^+$ cells with no detectable impact on Zeb1 levels in $Cd31^-$ cell populations.

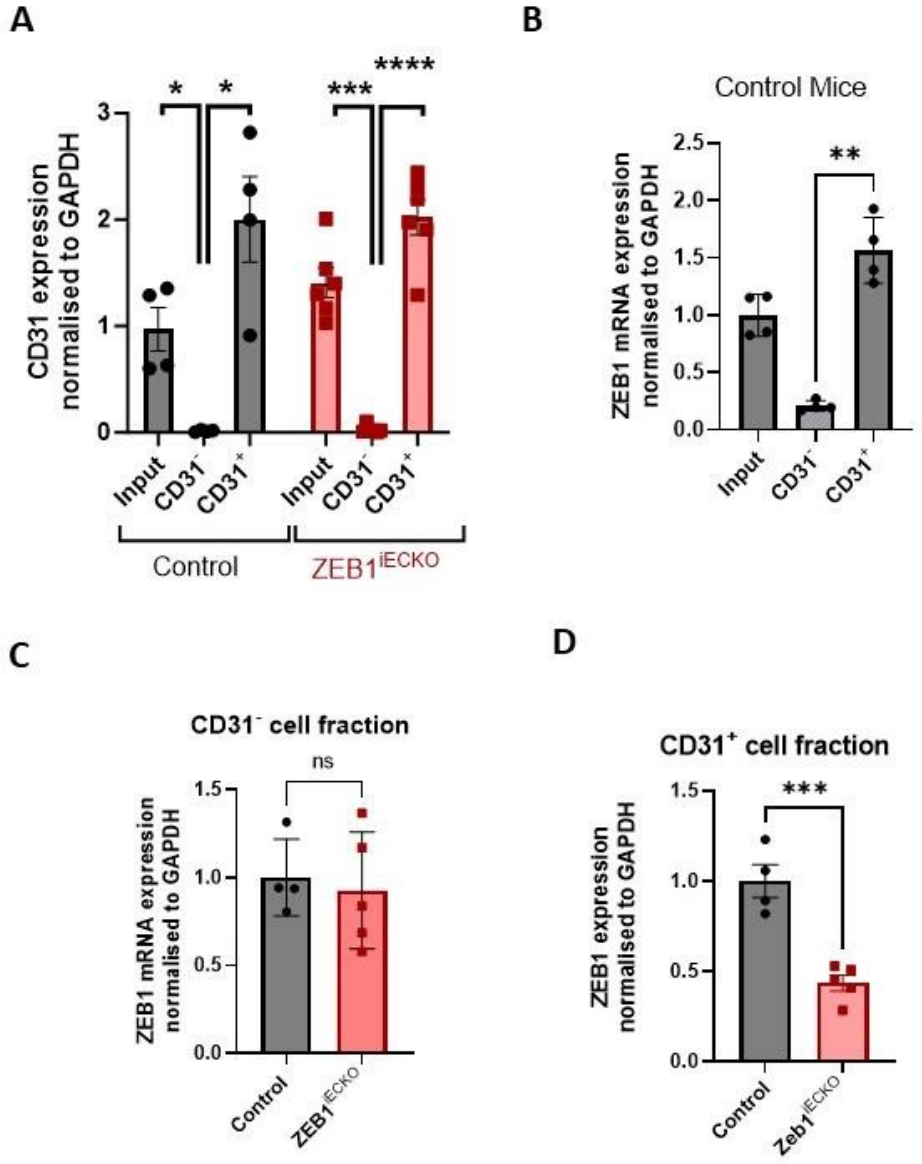


Figure 7.1. ***Significant reduction of ZEB1 mRNA expression in CD31⁺ ZEB1^{iECKO} cells. Data was analysed and figure created by Kathryn Green.***

(A) CD31 expression normalised to GAPDH across cell fractions, demonstrating enrichment of cell expressing CD31 in the CD31⁺ fraction. Input vs. CD31⁻ and CD31⁻ vs. CD31⁺ were compared using a paired t-test, revealing significant results.

(B) ZEB1 expression normalised to GAPDH across all fractions in control only, expressed relative to the input fraction.

(C) ZEB1 mRNA expression in CD31⁻ cells between control and ZEB1^{iECKO}, expressed relative to control.

(D) ZEB1 mRNA expression in CD31⁺ cells between control and ZEB1^{iECKO}, expressed relative to control.

All data are presented as mean + SEM. (A) and (B) were analysed with a paired t-test. (C) and (D) were analysed with an unpaired t-test. * $p < 0.05$, ** $p < 0.005$, *** $p < 0.0005$. Data was analysed and figure created by Kathryn Green.

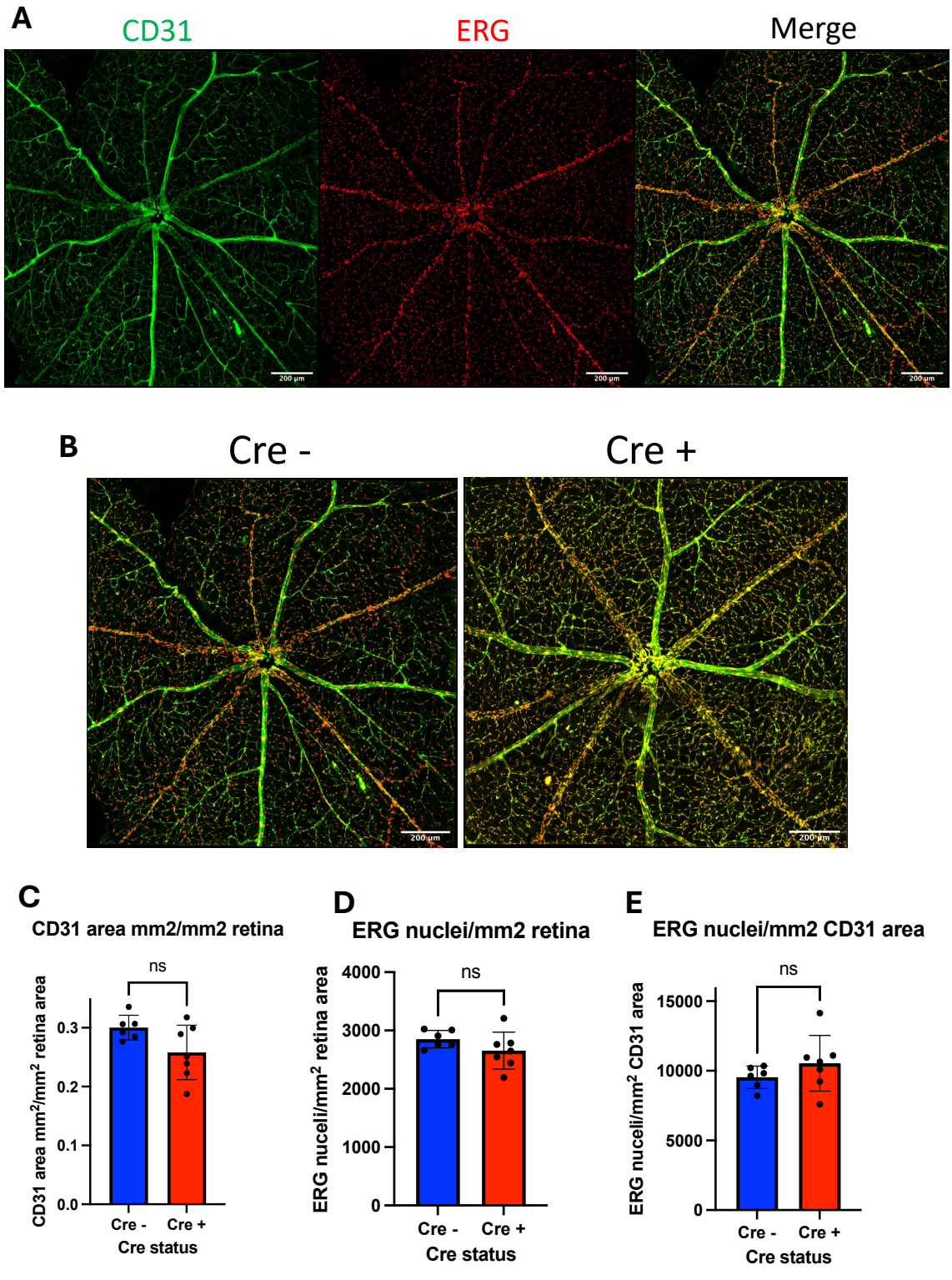
t-test. * $p < 0.05$, ** $p < 0.005$, *** $p < 0.0005$. Data was analysed and figure created by Kathryn Green.

Although these results were obtained by Kathryn Green, optimisation of $Cd31^+$ cell extraction from adult mouse lungs was performed by me, with confirmation of the $Cd31^+$ cell enrichment and Zeb1 KO in the iECKO model being used by the lab group. It was deemed important to include these results to provide completeness to the chapter, but the work to confirm $Cd31^+$ enrichment and Zeb1 KO was not solely mine.

7.3.2 Adult induced Zeb1 KO did not significantly impact the vascular area or number of endothelial cell nuclei in adult mouse retina

In order to determine the phenotypic effect of $Zeb1^{iECKO}$ in adult mouse retina vasculature, immunofluorescent staining of flat-mounted retinas was performed. The images reflected a well organised vascular network with Cd31 (Liu and Shi, 2012) while EC nuclei marked with Erg (Haber *et al.*, 2015) were apparent within the same endothelial network (Fig 7.2A). The overlay of both markers demonstrated that Erg^+ nuclei were clearly localised to $Cd31^+$ vasculature, confirming the endothelial identity of these cells (Fig 7.2A,B). Comparison of $Cd31^+$ area normalised to the total retina tissue area between $ZEB1^{fl/fl}$ Cdh5 Cre-$ERT2^{+/-}$ (Cre+) and $ZEB1^{fl/fl}$ Cdh5 Cre-$ERT2^{-/-}$ (Cre-) retina (n = 7 and 6 respectively) revealed no significant difference (Fig 7.2C), suggesting $Zeb1^{iECKO}$ in adult mouse retina did not perturb vascular area. We then quantified Erg^+ nuclei normalised to retina area between Cre+ and Cre- mice to investigate whether $Zeb1^{iECKO}$ resulted in an increase or decrease of ECs. We found no significant difference between Cre- and Cre+ retina, identifying $Zeb1^{iECKO}$ in adult mouse retina does not impact the number of ECs (Fig 7.2D). In addition, we quantified the number of ECs normalised to $Cd31^+$ area and found no significant difference between Cre- and Cre+ mice (Fig 7.2E). Since the adult mouse retina exists as three distinct vascular layers; superficial, intermediate and deep vascular plexuses, we focussed our

analysis to determine whether Zeb1^{iECKO} in adult mouse retina impacts the vascular area of individual layers (Fig 7.3A-D). As before, we did not observe a significant difference between Cre- and Cre+ retina for vessel area or EC number (Fig 7.3B-D), suggesting Zeb1^{iECKO} in adult mouse retina does not alter vascular area or EC count at the plexus level.



<u>Figure 7.2.</u> CD31⁺ area, ERG nuclei counts and ERG nuclei per mm² of CD31⁺ area of the adult mouse retina vasculature were not significantly altered between Cre- and Cre+ mice.

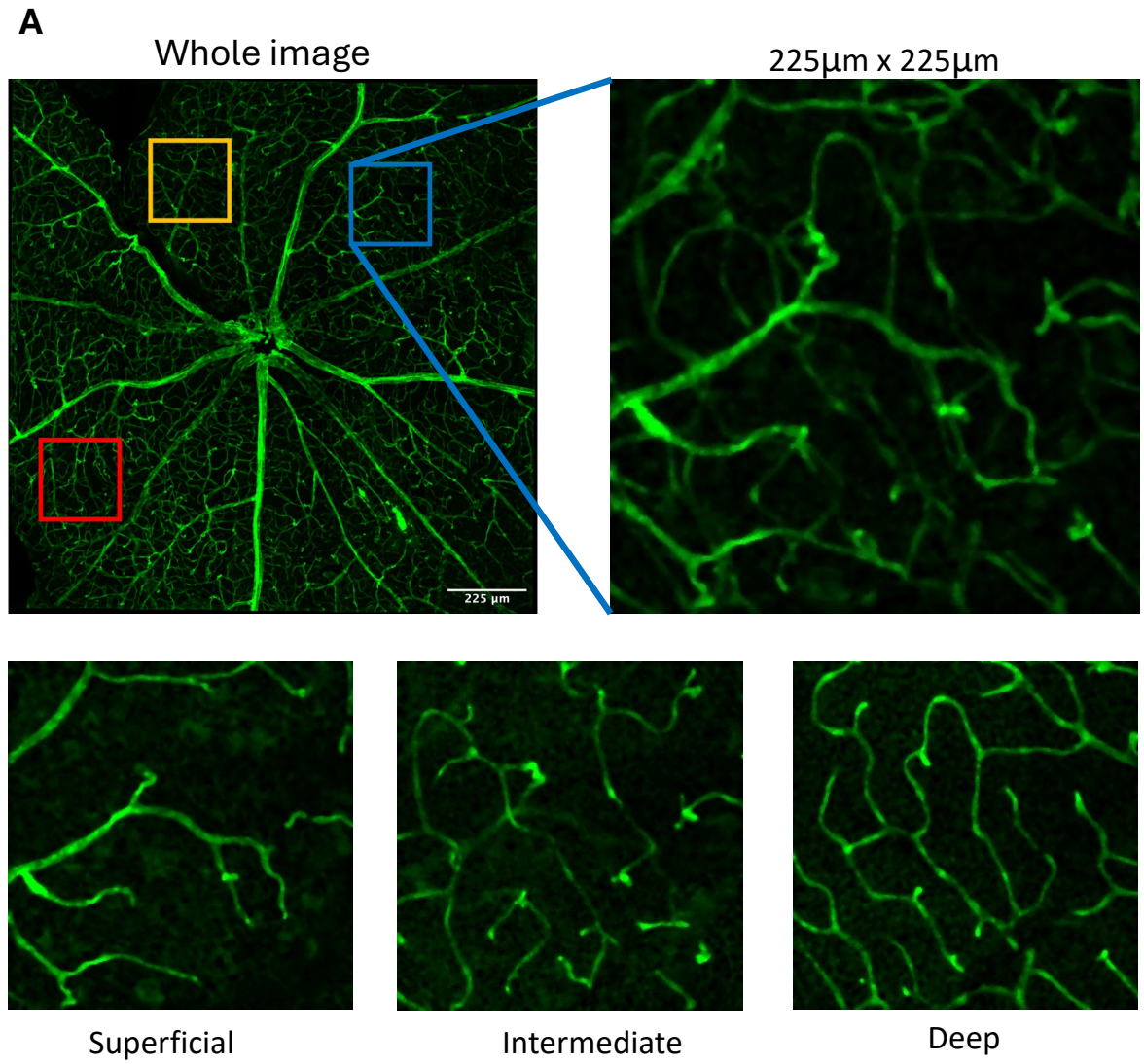
(A) Example image of retina vasculature centred on the optic nerve for $CD31^+$ (green), ERG^+ (red) and a merged image. Images were taken at 20x magnification as a 5x5 tile scan. The images are maximum projection Z-stacks, with background removed by rolling ball radius of 50 pixels and the CD31 channel has a median filter applied at 2.0 pixels. The scale bar represents 200μm.

(B) Merged image examples for Cre- and Cre+ retina.

(C – E) Data analysis of the Cre- (n=6) and Cre+ (n=6) mouse retina. The data are represented as columns and plot as a scatter plot with bar, displaying the value for each sample and the mean with standard deviation (SD). Statistical analyses to determine the significance were performed using two-tailed unpaired t-test with a significance threshold of $p < 0.05$. ns = not significant. (C) $CD31^+$ area in mm^2 normalised to area of the retina in mm^2. (B) Number of ERG^+ nuclei normalised to the area of the retina in mm^2. (C) Number of ERG^+ nuclei normalised to $CD31^+$ are in mm^2.

7.4 Discussion

The primary objective of this study was to determine whether adult endothelial-specific knockout of Zeb1 ($Zeb1^{iECKO}$) alters the vascular phenotype within adult mouse retina. Previous work in the lab revealed Zeb1 to reduce angiogenesis in the developing mouse retina. However, in the adult retinal vasculature examined here, loss of Zeb1 did not significantly alter vessel area of the number of ECs at either the whole retina level or within individual plexuses. These findings suggest that in fully developed, non-pathological conditions, the retinal vasculature may exhibit enough homeostatic stability or compensatory mechanisms to mask or mitigate the Zeb1 loss under normal physiological conditions. Alternatively, the combination of the results in this work with previous lab findings may suggest that Zeb1 does not induce angiogenesis or regression in a homeostatic, quiescent environment, but that it does play a role under angiogenic or pathological conditions when an external stimuli has already induced the shift away from quiescence. Another possible explanation for the lack of an overt phenotype lies in the potential context-dependence of Zeb1 function. While previous lab results report Zeb1 deletion to enhance pathological angiogenesis in CNV and disrupt developmental angiogenesis, the quiescent


A
Whole image
225µm x 225µm
225 µm
Superficial
Intermediate
Deep
B
Superficial Plexus CD31 Vascular Area Fraction
ns
Vessel area fraction
0.15
0.10
0.05
0.00
Cre -
Cre +
Cre Status
C
Intermediate Plexus CD31 Vascular Area Fraction
ns
Vessel area fraction
0.20
0.15
0.10
0.05
0.00
Cre -
Cre +
Cre Status
D
Deep Plexus CD31 Vascular Area Fraction
ns
Vessel area fraction
0.25
0.20
0.15
0.10
0.05
0.00
Cre -
Cre +
Cre status

<u>Figure 7.3.</u> CD31⁺ area of the superficial, intermediate and deep plexuses of the adult mouse retina vasculature were not significantly altered between Cre- and Cre+ mice.

(A) Example of extracting regions of interest to analyse the superficial, intermediate and deep plexuses.

(B-D) Data analysis of the Cre- (n=5) and Cre+ (n=6) mouse retina. The data are represented as columns and plot as a scatter plot with bar, displaying the value for each sample and the mean with standard deviation (SD). Statistical analyses to determine the significance were performed using two-tailed unpaired t-test with a significance threshold of $p < 0.05$. ns = not significant. $CD31^+$ area in mm^2 normalised to area of the retina in mm^2 for the superficial (B), intermediate (C) and deep (D) plexuses.

adult retina may be less sensitive to loss of Zeb1 unless challenged by stressors (e.g. injury). Indeed, in neonatal settings, ECs are highly proliferative and more reliant on factors regulating angiogenic growth, whereas adult ECs exist in a largely stable, non-proliferative state that may require stronger perturbations, such as pathological stimuli, to unveil a Zeb1-dependent effect. These points raise the importance of combining transcriptomics with immunofluorescence-based assays to understand if Zeb1 has a significant transcriptional effect on adult retinal ECs without displaying an obvious vascular phenotype. Furthermore, in a previous chapter of this thesis we explored the DNA-binding behaviour of Zeb1 via ChIP-seq analysis of HUVECs *in-vitro*. Performing Zeb1 ChIP-seq of *ex-vivo* ECs obtained from adult mouse retina in combination with ATAC-seq would provide a valuable comparison of accessible chromatin regions bound by Zeb1 and how that differs from cultured ECs, shedding light on mechanisms behind the lack of observed phenotype in adult mouse retina vasculature.

There are several limitations to this study that must be observed. First, we confirmed Zeb1 KO at the transcript level only. To validate this, confirmation at the protein level via western blot will need to be performed. Furthermore, we also began optimising the immunofluorescent staining of Zeb1, Erg and DAPI in adult mouse vasculature in an attempt to visualise the loss of Zeb1 in retinal ECs. Demonstrating protein-level changes in the retina would exclude the possibility that any remaining ZEB1 protein persists or that local

compensatory mechanisms upregulate an alternative isoform in vascular endothelium. Another limitation was our decision to image the retina as a Z-stack with 2.5µm intervals. We initially used this approach as we intended to measure the retina as a whole and this was deemed the optimal parameter to balance required resolution with time taken to image. Upon deciding to analyse individual plexuses after our initial whole image analysis, we noticed we did not have the resolution to easily and clearly obtain a distinct intermediate plexus image and so the results for the intermediate vascular layer should be considered with this in mind. Indeed, another study that focuses on analysis individual plexuses used 1µm Z-slices for their Z-stack to more precisely distinguish the boundaries of each plexus (Rust *et al.*, 2019). This does not come without difficulty, as it would increase the time taken to image the tissue and we would need to focus on regions of interest at the microscope instead of computationally post-imaging. We were able to obtain images for the superficial and deep plexuses using the Z-stack of 2.5µm slices, but an increased resolution in imaging parameter would be required for more sensitive measurements (e.g. intermediate plexus analysis and 3D volumetric analysis of vessels). A further consideration is the potential for Cre-mediated toxicity. As highlighted by (Brash *et al.*, 2020; Rashbrook, Brash and Ruhrberg, 2022), certain endothelial-specific Cre-ERT2 strains can exhibit off-target or Cre-driven toxicity, particularly at higher tamoxifen doses in neonatal mice. Although the current work examined adult mice and used standard tamoxifen dosage protocols, subclinical effects of Cre activation cannot be fully discounted. Moreover, the fact that we did observe robust Zeb1 knockdown in lung $Cd31^{+}$ cells after Cre induction confirms that recombination was successful, yet any subtle Cre toxicity or baseline tamoxifen effect could potentially mask an underlying phenotype, especially one that might be subtle in the adult retina. To negate this, appropriate controls

would be employed in future as a recent study suggests (Rashbrook, Brash and Ruhrberg, 2022).

It is important to note that the non-significant result observed here does not necessarily invalidate the physiological significance of Zeb1 in adult retinal vasculature. Instead, it highlights the importance of context in revealing specific functions. Indeed, previous data from the lab showed that Zeb1 plays a more pronounced role under pathological or developmental conditions. Thus, a logical extension of this work would be to evaluate $Zeb1^{iECKO}$ mice under further pathological models and conditions, or to explore the potential impact of $Zeb1^{iECKO}$ in different tissues.

In conclusion, our findings show that adult Zeb1 knockout in retinal endothelial cells does not significantly alter vascular area or endothelial cell number within quiescent adult retina. In addition, the results in this study highlights the importance of considering other validation methods (further immunofluorescent staining, knockout validation at gene and protein levels, combination with omics experiments) in interpreting non-significant results. Future experiments will include further omics-based experiments including bulk RNA-seq, scRNA-seq, proteomics, ChIP-seq and ATAC-seq approaches to explore the transcriptional and protein level changes that accompany the lack of observed phenotype in the adult mouse retina vasculature.

Chapter 8: Discussion

The role of ZEB1 in endothelial cells (ECs) has remained relatively unexplored compared to its extensively studied function in epithelial-to-mesenchymal transition (EMT), where it acts as a master regulator of cellular plasticity and migration (Drápela *et al.*, 2020; Schwab *et al.*, 2024). The work presented across this thesis collectively show that ZEB1 is a versatile transcriptional regulator whose effects on endothelial phenotype, angiogenesis and EndoMT can vary depending on the biological context. Multiple lines of evidence spanning siRNA KD and RNA-seq, genome-wide binding assays, single-cell transcriptomic analyses and an inducible KO mouse model demonstrate that ZEB1 exerts control over numerous endothelial processes. These include cell adhesion, inflammatory signalling, pro-angiogenic states and transitions towards mesenchymal-like states. This multifaceted regulation aligns with the understanding of endothelial TFs as context-dependent modulators rather than simple on/off switches (De Val and Black, 2009; Potente, Gerhardt and Carmeliet, 2011). At the same time, the data reveal that the impact of ZEB1 on vascular homeostasis can be subtle or negligible under quiescent conditions but becomes pronounced in an active EC state by developmental or pathological stimuli, paralleling observations with other TFs in ECs such as KLF2, which showed differential activity depending on shear stress state (Doddaballapur *et al.*, 2015). These results expand on the established role of ZEB1 as a master regulator of EMT (Nieto *et al.*, 2016).

The siRNA-mediated KD of ZEB1 in HUVECs provides an incisive view of the regulatory scope of ZEB1. Bulk RNA-seq identified 296 DEGs, including canonical endothelial and mesenchymal markers, tip cell regulators and inflammatory mediators. The prominent upregulation of key pro-angiogenic genes (e.g. GRB7) and mesenchymal markers (e.g. TALGN, COL1A1/2) upon ZEB1 KD revealed that ZEB1 can restrain certain pro-angiogenic and

mesenchymal programs in ECs. Such processes have been identified as paradigms to describe how angiogenic ECs may acquire migratory phenotypes via expression of mesenchymal genes during tip cell formation (Welch-Reardon *et al.*, 2014; Welch-Reardon, Wu and Hughes, 2015; Hultgren *et al.*, 2020; Fang, Hultgren and Hughes, 2021). GRB7 upregulation following ZEB1 KD was particularly notable, as GRB7 has been shown to be a promoter of angiogenesis via VEGFA secretion in ovarian cancer cells (Xu *et al.*, 2021) and has been suggested as an antiangiogenic target (García-Palmero *et al.*, 2013), suggesting repression by ZEB1 may act as brake on angiogenic responses. We have not found this regulatory relationship to be previously described and may represent a novel mechanism by which ZEB1 could modulate angiogenesis. Downregulation of inflammatory and adhesion-related genes (e.g. ICAM1, VCAM1) after ZEB1 KD implied that ZEB1 sustains or modulates immune-EC interactions. These findings resonate with studies demonstrating the promotion of immune-modulatory functions of ZEB1 in breast cancer cells (Katsura *et al.*, 2017) and with evidence of ZEB1 maintaining cell-cell adhesion and polarity in pancreatic and breast cancer cells (Aghdassi *et al.*, 2012; Maturi *et al.*, 2018; Drápela *et al.*, 2020). Additionally, ICAM1 and VCAM1 are known to be closely associated with angiogenesis and EC migration (Kong *et al.*, 2018; Bui, Wiesolek and Sumagin, 2020; Kaur *et al.*, 2023), with ZEB1-mediated expression of these adhesion genes suggesting a roles in EC adhesion during angiogenesis. Furthermore, the downregulation of canonical tip EC markers (CXCR4 and UNC5B) is highly suggestive of ZEB1 expression being required to induce a pro-angiogenic like EC phenotype. The activation of tip cell markers by ZEB1 directly links ZEB1 to EC heterogeneity and angiogenesis, with the expression of CXCR4 upregulated by the DLL4-NOTCH signalling pathway during the distinction of EC phenotypes within the sprouting angiogenesis process (Y. Guo *et al.*, 2024). UNC5B also plays crucial roles in tip cell migration and vessel patterning, having been shown

to be regulated by notch signalling to suppress EC proliferation, migration, junction activity and retinal plexus branching (Raza *et al.*, 2024). Furthermore, in a scRNA-seq experiment of P6 and P10 mouse retinas UNC5B demonstrated increased expression in tip ECs in the superficial plexus at P6, and also showed high expression in diving tip cells that invade the neuroretina at P10 (Furtado *et al.*, 2023). The downregulation of both CXCR4 and UNC5B upon ZEB1 KD suggests that ZEB1 may be required for tip cell specification or maintenance, positioning it within the tip cell signalling network that includes DLL4/NOTCH. These findings emphasise that ZEB1 does not functional as purely pro or anti-angiogenic, but rather can direct a balance of pathways, some of which promote endothelial quiescence and barrier function, while others facilitate migratory or inflammatory phenotypes. This was reinforced in the scRNA-seq analysis chapters 6 and 7. This behaviour of a balanced regulatory approach is reminiscent of master EC TFs such as ERG, which can both promote and restrain different aspects of EC function (Dryden *et al.*, 2012; Birdsey *et al.*, 2015; Shah, Birdsey and Randi, 2016; Kalna *et al.*, 2019). Network and regulon analysis of the ZEB1 KD HUVEC DEGs further showed that ZEB1 influences genes involved in splicing, inflammation and EC phenotype identity factors (ESRP2, IRF1, CXCR4), corroborating reports of ZEB1 regulating epithelial splicing machinery (Maturi *et al.*, 2018; Y. Zhang *et al.*, 2019; Perez-Oquendo and Gibbons, 2022). The wide-reaching transcriptional consequences of ZEB1 align with established models of ZEB1 in epithelial systems, where it serves as a broad regulator of migration, polarity and cytoskeletal organisation during EMT (Nieto *et al.*, 2016). The data here suggest that much of this regulatory breadth carries over into endothelial contexts, but that the overall phenotypic observation induced by ZEB1 may depend on local cues and EC phenotype-specific modulators during angiogenic remodelling.

Exploration of the DNA-binding landscape of ZEB1 in HUVECs via ChIP-seq revealed 77.70% of ZEB1 peaks to localise within promoter regions of transcripts, underlining a strong promoter-centric mode of gene regulation. This promoter bias was higher than our analysis of an ERG HUVEC ChIP-seq dataset (Kalna *et al.*, 2019) which showed 41.47% ERG binding sites in transcript promoter regions, suggesting ZEB1 to function primarily as a direct transcriptional regulator rather than through long-range enhancer interactions. Moreover, integrating ChIP-seq with RNA-seq and publicly available datasets of histone marks, ERG HUVEC ChIP-seq and ZEB1 TNBC ChIP-seq revealed several factors of ZEB1 binding behaviour. We identified a significant fraction of ZEB1-bound loci to overlap with ERG binding, with ERG being a master regulator of endothelial identity (Birdsey *et al.*, 2015). Motif analysis showed an enrichment of ERG, FLI1 and AP-1 motifs, implying that ZEB1 often collaborates or co-binds with these TFs in ECs. In HUVECs, nearly half of ZEB1 peaks overlapped with ERG peaks, suggesting that ZEB1 can either enhance or modulate ERG-driven transcriptional programs, possibly linking endothelial identity signals to the DNA-binding profile of ZEB1. Indeed, combined knockdown of ERG and FLI1 in HUVECs has been shown to trigger EndoMT (Nagai *et al.*, 2018), along with ERG promoting vascular stability and growth through Wnt/B-Catenin signalling (Birdsey *et al.*, 2015), displaying similar behaviours between ERG and ZEB1 and when combined with the overlap in ChIP-seq data reinforces the idea that ZEB1 and ERG may act together in ECs. This putative integrative function of ZEB1 and ERG aligns with studies that describe EC fate decisions, such as arteriovenous specification, in which a network of transcription factors is observed as opposed to an individual factor in controlling EC behaviour (Aranguren *et al.*, 2013; Fish and Wythe, 2015). We also found ZEB1 binding to coincide with H3K27ac and H3K4me3 marked regions, implying a regulatory role in open and actively transcribed chromatin. Importantly, direct ChIP-seq evidence of ZEB1 at the

promoters of both key EC and mesenchymal markers (e.g., PECAM1, CDH5, ACTA2, CDH2) supports a mechanistic basis for ZEB1 involvement in processes like EndoMT, tip cell specification and cell-cell junction dynamics. The fact that genes related to these processes were present in the ZEB1 KD transcriptome in HUVECs highlights a coherent link between ZEB1 and EC phenotype management.

The analysis of scRNA-seq data from diverse tissues and conditions collectively showed that ZEB1 is not uniformly expressed by all ECs but can be enriched in specific subsets. Subsequent experiments at the protein level will be essential to reveal if this is also true of the gene product. We identified ZEB1 to show the greatest expression in spleen venous-capillary ECs compared to other organ ECs, potentially linking ZEB1 to the immunoregulatory and scavenging roles of the spleen (Mebius and Kraal, 2005; Lewis, Williams and Eisenbarth, 2019). Furthermore, ZEB1 expression was enriched in tip cell-like or proliferative EC phenotypes within developing retina, CNV and lung tumour vasculature, implicating ZEB1 in driving or supporting angiogenesis and EC plasticity. The association with proliferative ECs aligns with known roles of ZEB1 within mitosis and the cell cycle in ECs of the cornea (Jin *et al.*, 2020) and other contexts including several cancer cell lines (Fouani *et al.*, 2020; B.-W. Liu *et al.*, 2023; Genetta *et al.*, 2023). ZEB1 expression analysis was also extended towards the endothelial cells of the lymph node, identifying notably increased expression in subcapsular sinus floor LECs, pointing to a possible role in immune-LEC crosstalk and an indication of ZEB1 being localised to specific LEC phenotypes within the human lymph node. Lymphatic ECs of the lymph node are specialised for antigen capture and presentation to immune cells, suggesting ZEB1 expression may be linked to these immunoregulatory functions (Malhotra *et al.*, 2012; Jalkanen and Salmi, 2020). A recurrent theme from these data is that ZEB1 expression might not be discernible under stable,

quiescent conditions but is stimulated when ECs adopt a more dynamic, plastic phenotype in tip and proliferating ECs. Moreover, *In-silico* KO analyses predicted that loss of ZEB1 would disrupt cell cycle, ECM, TGF-B/Wnt signalling pathways, pro-angiogenic, migratory and EndoMT programs, reflecting the multipronged programs that ZEB1 coordinates. Indeed, ZEB1 has previously been shown to activate Wnt signalling in endothelial progenitors (Yu *et al.*, 2022), which, albeit a different cell type, adds credibility to the *in-silico* KO and suggests ZEB1 can influence the same signalling pathways across different cell types.

Through use of bulk RNA-seq, ChIP-seq and scRNA-seq we accentuate ZEB1 involvement in EndoMT, a counterpart to EMT in which endothelial cells acquire mesenchymal features. Collectively, the omics-based analyses suggests that ZEB1 binds and regulates mesenchymal markers (e.g., ACTA2, VIM, TAGLN) and EndoMT drivers such as ZEB2. In addition, we also unveiled a potential interplay between the drivers of EndoMT through TF activity analysis, with ZEB1 showing an association with partial/early EndoMT rather than full transition. The concept of partial EndoMT is being investigated as a distinct cellular state that may be required for sprouting angiogenesis (Welch-Reardon, Wu and Hughes, 2015; Platel *et al.*, 2019), suggesting ZEB1 may be involved in the plasticity of ECs during this process. Evidence was also provided that suggests ZEB1 may bridge endothelial and mesenchymal signals by co-binding with ETS factors and AP-1, enabling dynamic shifts toward more migratory or activated EC phenotypes without necessarily undergoing complete EC identity loss. Additionally, the text mining approach expanded the putative ZEB1 interactome to encompass a wide network of core EndoMT proteins and inflammatory/angiogenic mediators (IL6, FN1, MMP9, TGFB1). Such global analysis suggests that ZEB1 has the capacity to interface with major EndoMT regulatory axes (TGF-B, Wnt/B-catenin, MAPK), thereby acting as a central hub for interplay among these pathways.

In contrast to the transcriptional disruptions observed *in-vitro* and in actively remodelling or pathological tissues, the inducible KO of Zeb1 in adult mouse ECs had no observable morphology phenotype in quiescent retinal vasculature in the analyses we performed. Neither total vascular area nor EC number changed upon Zeb1 loss, including at the level of separate plexuses. These findings reinforce an overarching theme that ZEB1 functional necessity may be conditional, as is observed with other major EC TFs that regulate angiogenesis (Payne, Neal and De Val, 2024). While it is predicted to modulate plasticity, EndoMT and angiogenesis under stress or developmental contexts, a stable microenvironment such as adult healthy retina appears to circumvent ZEB1 deficiency, reflecting endothelial cell states of low turnover, stable barrier function and minimal ongoing angiogenesis that may not require the regulatory functions of ZEB1 (Kur, Newman and Chan-Ling, 2012; Selvam, Kumar and Fruttiger, 2018; Rust *et al.*, 2019). Indeed, prior observations from the lab show ZEB1 critically influences pathological or developmental retinal angiogenesis, supporting this context dependent model. Consequently, the normal adult retina where ECs are largely quiescent and rarely undergoing large-scale sprouting provides fewer triggers that require ZEB1. This contextual model not only aligns with the results provided throughout this thesis but highlights that negative or null phenotypes can be highly informative. Absent of a perturbation (e.g., ischemic injury or exogenous pro-angiogenic cues), Zeb1 KO may not induce a phenotype and instead functions in response to stimuli and is recruited during vascular remodelling. Further efforts might combine omics-based approaches with adult induced Zeb1 KO of various tissues and models of vascular pathology, such as ischemia-reperfusion injury, laser-induced CNV or hyperglycaemic retinopathy, to reveal whether Zeb1 loss unmasks a defective or exaggerative angiogenic response at a phenotypic and transcriptomic/proteomic level.

A cardinal insight from this thesis is that ZEB1 impact on EC biology is situational. In normal, quiescent adult vasculature, ZEB1 loss may cause minimal to no significant phenotypic changes. Under developmental or disease-driven angiogenesis, or in orchestrating EndoMT, ZEB1 emerges as a potentially critical modulator. This context dependence implies that designing therapeutic strategies targeting ZEB1 must account for the tissue state, whether it is actively remodelling, inflamed or stable. In addition, the contextuality of ZEB1 function may make it an ideal candidate for pathological angiogenesis as altered ZEB1 function via drug targeting may impact the pro-angiogenic nature of vascular diseases without affecting vasculature under homeostatic conditions. This selective targeting potential would be a step towards addressing limitations of current anti-angiogenic therapies which can compromise normal vascular function (Carmeliet and Jain, 2011; Eelen *et al.*, 2020; Lopes-Coelho *et al.*, 2021; Qian *et al.*, 2023). Further experimentation would be required to fully make this claim, with analyses of models that measure vessel leakage in adult quiescent vasculature for example. The capacity of ZEB1 to repress certain pro-angiogenic genes (e.g., GRB7) while simultaneously coordinating classical invasive programs (e.g., ECM remodelling, mesenchymal marker expression) may explain the ability of ZEB1 to coordinate EC behaviour depending on the contextual requirements of a given EC. Future *in-vivo* models that combine lineage tracing of ZEB1-expressing ECs with tissue-level readouts of vessel remodelling could illuminate how ZEB1 transitions from a gatekeeper to enabler of angiogenesis. This thesis also demonstrated how combining multi-omics techniques offers a more nuanced view of ZEB1 function. Scaling up these approaches to include spatial transcriptomics and proteomics would further clarify how ZEB1 distribution in tissues correlates with local microenvironment cues and epigenetic modifications. The publicly available scRNA-seq datasets used in this work emphasised the role of ZEB1 in pathological

vessel growth. Potentially, partial inhibition of ZEB1 could limit disease-related vascular abnormalities or dampen EndoMT-driven fibrosis without harming quiescent vasculature. Indeed, prior breast cancer studies have linked ZEB1 to tumour angiogenesis and metastasis (Liu *et al.*, 2016; Zhang *et al.*, 2018). Future clinical or translational work might explore whether small-molecule modulators of ZEB1 pathways can selectively disrupt pathological neovascular networks. The interplay between ZEB1 and other EndoMT drivers is briefly alluded to within this thesis, with indication that ZEB1 may be associated with a partial or hybrid EndoMT state in which ECs have increased mesenchymal marker expression but have not lost their EC identity. This potential partial plasticity driven by ZEB1 can be beneficial, or even required, for vessel sprouting (Welch-Reardon, Wu and Hughes, 2015; Fang, Hultgren and Hughes, 2021) yet detrimental when it promotes pathological remodelling or barrier breakdown. Dissecting how ZEB1 differs from the other EndoMT drivers in their genomic binding and co-factor usage in ECs would help shed light on overlapping and distinct EndoMT pathways. Analysis such as dual KO models could indicate whether a combination of EndoMT drivers is required to fully drive the EndoMT transition and if ZEB1 alone can act to induce a partial state. Motif enrichment and peak overlap in ChIP-seq strongly suggested that ZEB1 co-binds with ETS (ERG) and AP-1 TF family TFs. Additional biochemical validation (e.g., co-immunoprecipitation, sequential ChIP) would clarify how stable such complexes are and whether ERG or AP-1 is strictly required for the majority of ZEB1 occupancy of DNA in ECs. Similarly, exploring the functional synergy against antagonism between ZEB1 and these other factors can guide future research in precisely defining which gene programs rely on direct ZEB1 contact versus indirect complexes.

Collectively, the data presented in this thesis shift our perspective of ZEB1 in endothelial biology from a narrow association with EndoMT toward a broader view of ZEB1

as a powerful, conditionally active transcriptional regulator of EC phenotype. This expanded view positions ZEB1 within the current understanding of EC TFs as context-dependent modulators of vascular function (Payne, Neal and De Val, 2024). By bridging the gap between quiescent and activated states, normal and disease settings and promoter versus enhancer targeting, ZEB1 confers an adaptive plasticity upon endothelium, helping shape processes as diverse as immune cell recruitment, angiogenesis and partial mesenchymal transition. Yet, as the adult inducible ZEB1 KO retina experiments suggested, ZEB1 is not universally essential under stable physiological conditions. Future work will refine this understanding further, leveraging *in-vivo* models, multi-omics analyses and targeted manipulations of ZEB1 regulatory complexes. Along that path, ZEB1 may prove a promising target for conditions where aberrant vascular plasticity underpins pathology, from tumour progression to chronic inflammatory diseases. The interplay between ZEB1 pro and anti-angiogenic capacities, its putative partial EndoMT induction and its co-factor dependent binding provide a solid basis for generating hypothesis to uncover novel complexities in ZEB1 function. Overall, this thesis consolidates a unifying principle: ZEB1 is a context-dependent modulator in ECs, orchestrating dynamic endothelial programs that can influence vascular homeostasis and disease.

Appendix

The methods in Appendix 1 were performed by Dr. Amy P Lynch and the methods in Appendix 2 and 3 performed by Kathryn Green.

Appendix 1. Supplementary methods to chapter 3 - ZEB1 knockdown via siRNA in HUVECs revealed a modulation of adhesion, angiogenesis and inflammation related processes and uncovered a predicted ZEB1 regulatory network

Appendix 1.1 Cell culture

Human Umbilical Vein Endothelial Cells (HUVECs) derived from pooled donors were acquired from Promocell. The cells were maintained in Endothelial Cell Growth Medium (ECGM) (Promocell) supplemented with 2% Endothelial Growth Supplements (Promocell) at 37°C in an atmosphere of 5% CO_2. Once cultures reached 80–90% confluency, they were passaged. This involved washing the cells with sterile PBS and then detaching them using a Trypsin/EDTA solution at concentrations of 0.04% and 0.03%, respectively. Following detachment, cells were pelleted by centrifugation at 100×G, resuspended in complete media, and then seeded into new flasks. To ensure optimal growth, cells were never split at a ratio exceeding 1:5 so that confluency did not drop below 40%. Regular examinations confirmed that the cells retained their characteristic cobblestone morphology, and only cells from passages 2 to 7 were used in subsequent experiments.

Appendix 1.2 siRNA knockdown of ZEB1

HUVECs were grown as above and plated at 2.5 x 10^5 cells per 6 well in ECGM. After 24h the media was replaced with 800µl OptiMEM (Gibco). Transfection of cells was performed with 200nM of a smartpool siRNA against ZEB1 (siRNA ID s229972, Thermo Fischer) or a non-silencing control (Dharmacon Reagents) diluted in OptiMEM (Gibco) and PromoFectin-HUVEC (Promocell). Cells were incubated for 4h with oligonucleotides before changing media for ECGM. RNA samples were extracted at 48h post transduction or 72h for protein extraction before confirmation of successful knockdown by Western blot.

Appendix 1.3 RNA extraction and sequencing

RNA extraction was performed using RNeasy Mini Kit (Cat No. 74104, QIAGEN) as per the standard protocol provided with the kit. RNA purity was examined by NanoDrop with 280/260 values > 1.75. Further quality control (Nanodrop, agarose gel electrophoresis, and Agilent 200) to ensure sufficient RNA concentration and integrity followed by library preparation was carried out by Novogene Inc (Hong Kong, China) with subsequent sequencing by Illumina HiSeq platforms in a paired-end manner to a depth of 20M reads. Triplicates were generated for each condition.

Appendix 2. Supplementary methods to chapter 4 - Comprehensive and unbiased analysis of ZEB1 binding patterns in HUVECs via ChIP-seq

Appendix 2.1 Cell culture

Same as section 2.1.1.

Appendix 2.2 ChIP (Chromatin-immunoprecipitation)-seq

Chromatin immunoprecipitation was conducted using the Active Motif ChIP-IT High Sensitivity kit. Unless stated otherwise, all buffers used were those provided in the kit, with their compositions detailed in Table 2. HUVECs from passages 2 to 7 were plated in 150 mm dishes containing 20 mL of complete media and grown until they reached full confluency before processing for ChIP. Fixation was initiated by directly adding 2 mL of Complete Cell Fixation Solution to the culture medium in each dish, followed by gentle rocking at room temperature for 15 minutes. Fixation was halted by adding 1.1 mL of Stop Solution to each dish and rocking for an additional 5 minutes at room temperature. Cells were then detached using a rubber policeman and pelleted by centrifugation at 1,250×G for 3 minutes at 4°C. After discarding the supernatant, the pellet was resuspended in 10 mL of ice-cold PBS Wash Buffer and centrifuged at 1,250×G at 4°C twice. The final cell pellet was kept on ice. Subsequently, the pellet was resuspended in 5 mL of Chromatin Prep Buffer supplemented with 5 µL of Protease Inhibition Cocktail and 5 µL of 100 mM PMSF, then incubated on ice for 10 minutes. Cell lysis was achieved by transferring the suspension to a chilled dounce homogenizer and performing 30 strokes. The homogenate was then centrifuged at 1,250×G for 3 minutes at 4°C. The pellet was resuspended in 500 µL of ChIP buffer with an additional 5 µL of Protease inhibitor cocktail and 5 µL of 100 mM PMSF, followed by a 10-minute incubation on ice before proceeding with chromatin shearing. Shearing was performed using the Bioruptor® Cooled Sonicator (Diagenode) at 4°C for 35 cycles, each cycle consisting of 30 seconds on and 30 seconds off. Following sonication, the sample was centrifuged at 16,000×G for 2 minutes at 4°C to pellet cellular debris. A 25 µL aliquot of the supernatant was taken for assessing chromatin quality and shearing efficiency, while the remaining

chromatin was stored at −80°C. For chromatin quality analysis, 175 µL of TE buffer (pH 8.0) and 1 µL of RNAse A were added to the 25 µL aliquot, and the mixture was incubated in a thermocycler at 37°C for 1 hour. Next, 2 µL of Proteinase K was added and incubated at 37°C for 2 hours. The mixture was then transferred to a new Eppendorf tube along with 83 µL of Precipitation Buffer, 2 µL of Carrier, and 750 µL of absolute ethanol, and stored at −80°C overnight for DNA precipitation. The following day, the sample was centrifuged at 16,000×G for 15 minutes at 4°C to pellet the DNA. After discarding the supernatant, the DNA pellet was air-dried for 10–15 minutes and then resuspended in 25 µL of DNA purification elution buffer. The resuspension was aided by a 10-minute room temperature incubation and vortexing to ensure complete dissolution. DNA concentration was determined by measuring absorbance at 260 nm using a Nanodrop. For quality assessment, 500 ng of input DNA was mixed with 1 µL of 500 mM NaCl and adjusted to a final volume of 10 µL with sterile water, then subjected to thermocycler incubation at 100°C for 20 minutes, followed by 50°C for 5 minutes. Samples were mixed with gel loading buffer and loaded onto a 2% agarose gel containing ethidium bromide (Sigma), electrophoresed at 120 V for 5–10 minutes, and imaged using a Licor gel imager. Each immunoprecipitation reaction was prepared by combining 4 µg of ZEB1 primary antibody (Proteintech) or 4 µg of rabbit IgG control, 5 µL of protease inhibitor cocktail, 5 µL of Blocker Mix, approximately 10 µg of sheared chromatin, and bringing the volume to 200 µL with ChIP buffer. These reactions were rotated end-to-end overnight at 4°C. Protein G agarose beads were pre-washed by mixing equal volumes of TE buffer (pH 8.0) with the beads and centrifuging at 1,250×G to pellet the beads, discarding the supernatant; this wash step was repeated twice. Then, 30 µL of Protein G beads were added to each immunoprecipitation reaction, which was subsequently rotated end-to-end for 3 hours at 4°C. After adding 600 µL of ChIP buffer to the reaction, the entire mixture was transferred to

a ChIP filtration column. Flow-through was allowed to drain by gravity and discarded. The columns were then washed five times with 900 µL of Wash Buffer AM1, followed by centrifugation at 1,250×G for 3 minutes to remove residual buffer. Elution was performed by adding 50 µL of pre-warmed (37°C) Elution Buffer AM4 to the column, incubating at room temperature for 5 minutes, and then centrifuging at 1,250×G for 3 minutes. The eluted DNA was then processed for purification by adding 2 µL of Proteinase K, and incubating in a thermocycler for 30 minutes at 55°C followed by 2 hours at 80°C. To verify correct pH, 500 µL of DNA purification buffer and 5 µL of 3 M Sodium Acetate were added, with a bright yellow colour indicating the appropriate pH. Each sample was subsequently passed through a DNA purification column, centrifuged at 14,000 rpm for 1 minute with the flow-through discarded, and washed with 750 µL of DNA Purification Wash Buffer (80% ethanol). After a brief centrifugation (1 minute, then an additional 2 minutes to dry the membrane), the purified DNA was eluted by adding 36 µL of pre-warmed (37°C) DNA Purification Elution Buffer directly to the column and centrifuging at 1,250×G for 1 minute. The final purified ChIP DNA was then sent to Novogene for Illumina sequencing.

Appendix 3. Supplementary methods to chapter 7 - Adult inducible knockout of Zeb1 does not alter mouse retinal vascular area or endothelial cell number

Appendix 3.1 Inducible endothelial cell knockout (iECKO) mouse model

C57BL/6 ZEB1$^{fl/fl}$ Cdh5 Cre-ERT2 mice were bred internally at the University of Nottingham's Biological Support Unit. The ZEB1$^{fl/fl}$ line was originally provided by Thomas Brabletz (Brabletz *et al.*, 2017) and the Cdh5 Cre-ERT2 line was provided by Ralf Adams

(Sörensen, Adams and Gossler, 2009). All animal work adhered to the requirements of the Animal Scientific Procedures Act (ASPA) of 1986 under Home Office authority. The experiments described in this work were conducted under UK Home Office Licence PPL PE6932817F or PPL P3E735452, both held by Professor David O. Bates. Experimental work was performed using male and female mice, with all genotyping carried out by Transnetyx Inc. Breeding of ZEB1$^{fl/fl}$ Cdh5 Cre-ERT2$^{+/-}$ and ZEB1$^{fl/fl}$ Cdh5 Cre-ERT2$^{-/-}$ was conducted to generate mixed litters containing both genotypes for comparative studies. Animal health and welfare decision were made under the guidance of Named Animal Care and Welfare Officers (NACWO) and the Named Veterinary Surgeon (NVS).

Appendix 3.2 Tamoxifen-induced endothelial ZEB1 knockout (iECKO) in adult mice

Tamoxifen stock was prepared by dissolving 100mg of Tamoxifen (Sigma) in 1mL of 100% ethanol (Thermo) at 37°C followed by the addition of 9 mL of sterile sunflower oil under a class II safety cabinet. Adult ZEB1$^{fl/fl}$ Cdh5 Cre-ERT2$^{+/-}$ and ZEB1$^{fl/fl}$ Cdh5 Cre-ERT2$^{-/-}$ mice aged 8-12 weeks were administered a daily intraperitoneal (IP) dose of tamoxifen at 1mg per 25g body weight for five consecutive days. This regimen induces the endothelial cell-specific knockout of ZEB1 in ZEB1$^{fl/fl}$ Cdh5 Cre-ERT2$^{+/-}$ while ZEB1$^{fl/fl}$ Cdh5 Cre-ERT2$^{-/-}$ mice serve as controls lacking Cre recombinase. Animals were monitored and weighed in the days leading up to tamoxifen administration to confirm good health. On dosing days, mice were weighed and checked for welfare each morning, then observed for at least one hour following dosing and again approximately five hours later. If no issues were detected, daily checks ceased 24 hours after the final dose and were reduced to twice per week. Any mice exhibiting signs of pain, adverse effects or poor health were monitored more closely with

input from the NACWO or NVS. Animals losing more than 20% of their initial body weight or displaying continued ill health were euthanised via schedule I cervical dislocation.

Appendix 3.3 DNAse treatment

DNase treatment was carried out using the Promega RQ1 RNase-Free DNase kit. Unless stated otherwise, 2µg of RNA was combined with 2µL of DNase buffer and 2µL of DNase in a final volume of 18µL (adjusted with RNase-free water). The mixture was incubated in a thermocycler at 37°C for 30 minutes, followed by the addition of 2µL of DNase stop solution. The reaction was then incubated at 65°C for 10 minutes to inactivate the DNase.

Appendix 3.4 cDNA synthesis

For reverse transcription, µg of DNase-treated RNA (in a total volume of 20µL) was used with the Takara PrimeScript RT Master Mix kit. Unless otherwise indicated, the recommended volume of master mix was added to the RNA, and the mixture was incubated in a thermocycler at 37°C for 15 minutes, followed by 85°C for 5 seconds. The resulting cDNA was stored at −20°C for future use.

Appendix 3.5 Digital droplet PCR (ddPCR)

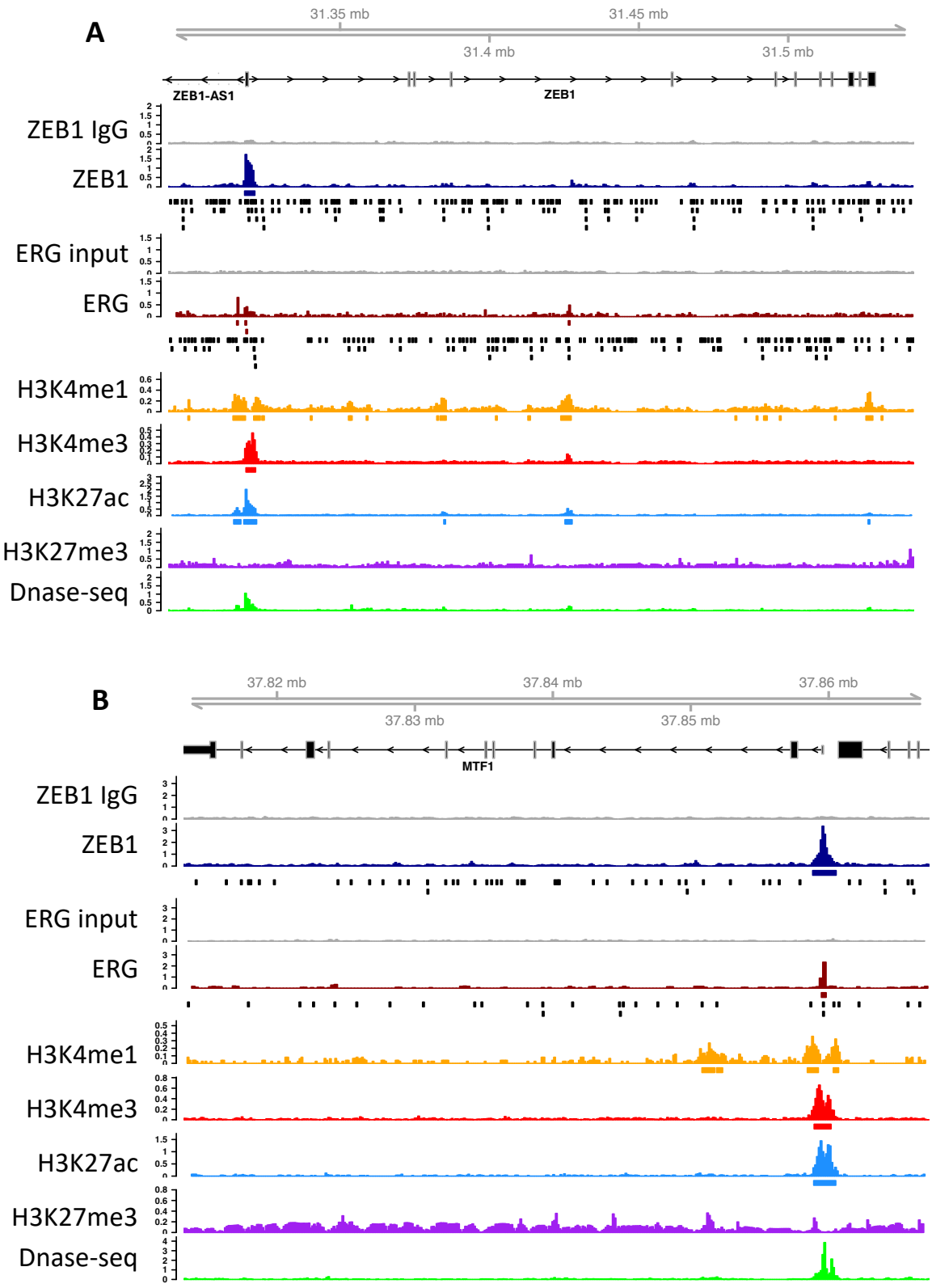
An amount of cDNA ranging from 50ng to 320ng was used for ddPCR. Reactions were prepared using either 2× or 4× digital droplet master mix (BioRad), plus a murine 10× TaqMan probe for Zeb1 (Thermo Fisher), Cd31 (Thermo Fisher) or GAPDH (Thermo Fisher), and brought to a final volume of 25µL with water. Droplet generation was performed on a BioRad

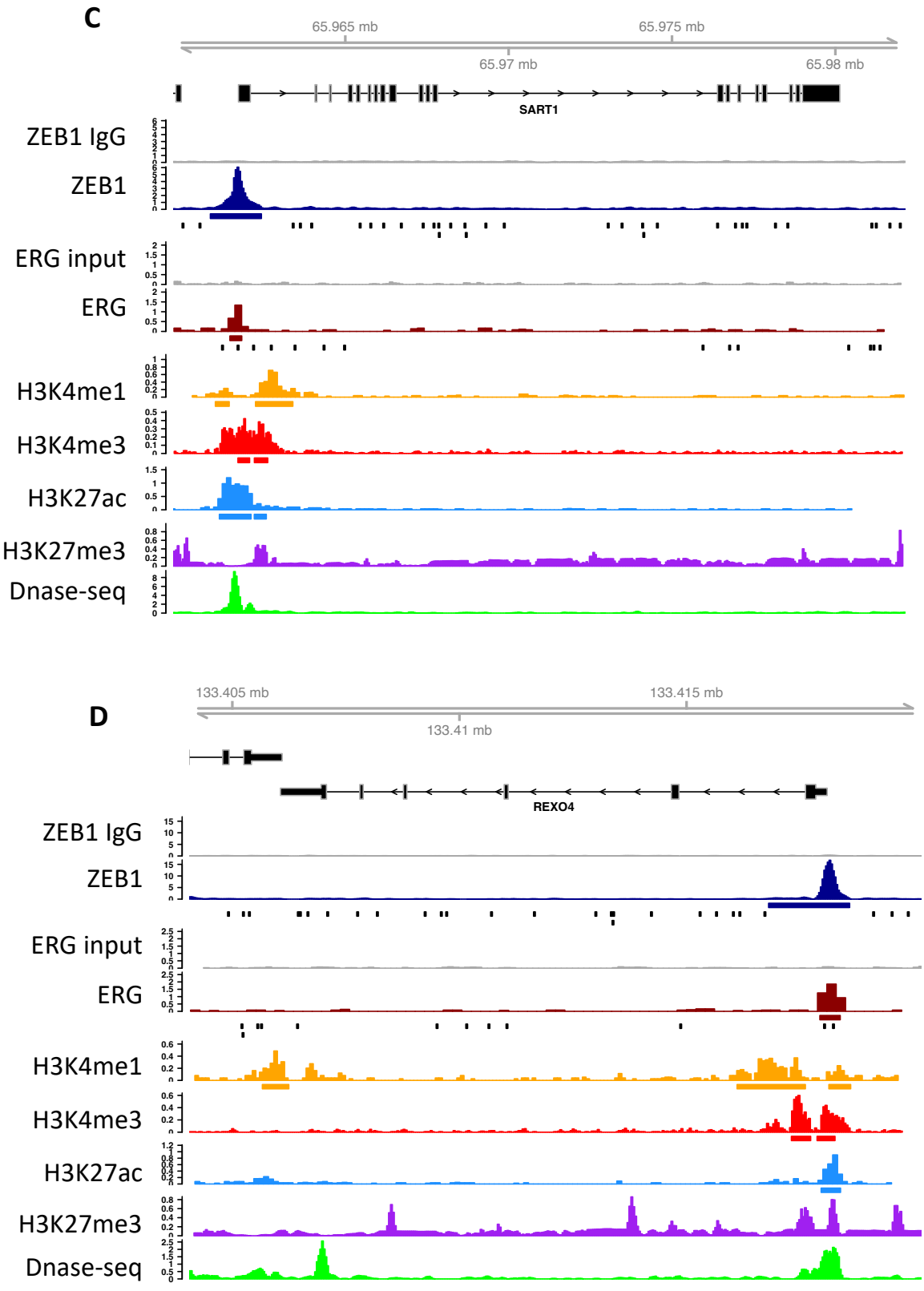
droplet generator using 70µL of droplet generator oil (BioRad). The prepared droplets were then subjected to a thermocycling protocol consisting of an initial 95°C incubation for 10 minutes, followed by 40 cycles of 95°C for 30 seconds and 60°C for 1 minute, concluding with a 10 minute final step at 9 °C. Afterward, droplets were analysed using the QX100 Droplet Reader (BioRad).

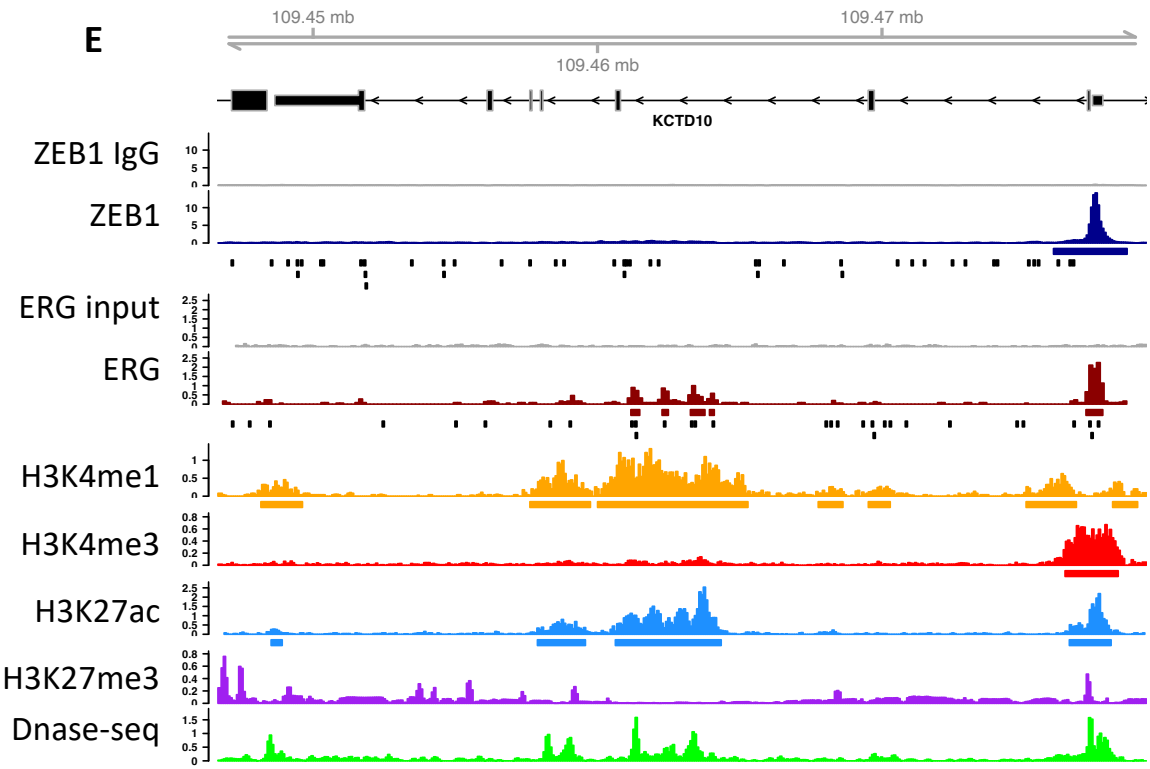
Appendix 3.6 Digital droplet PCR (ddPCR) data analysis

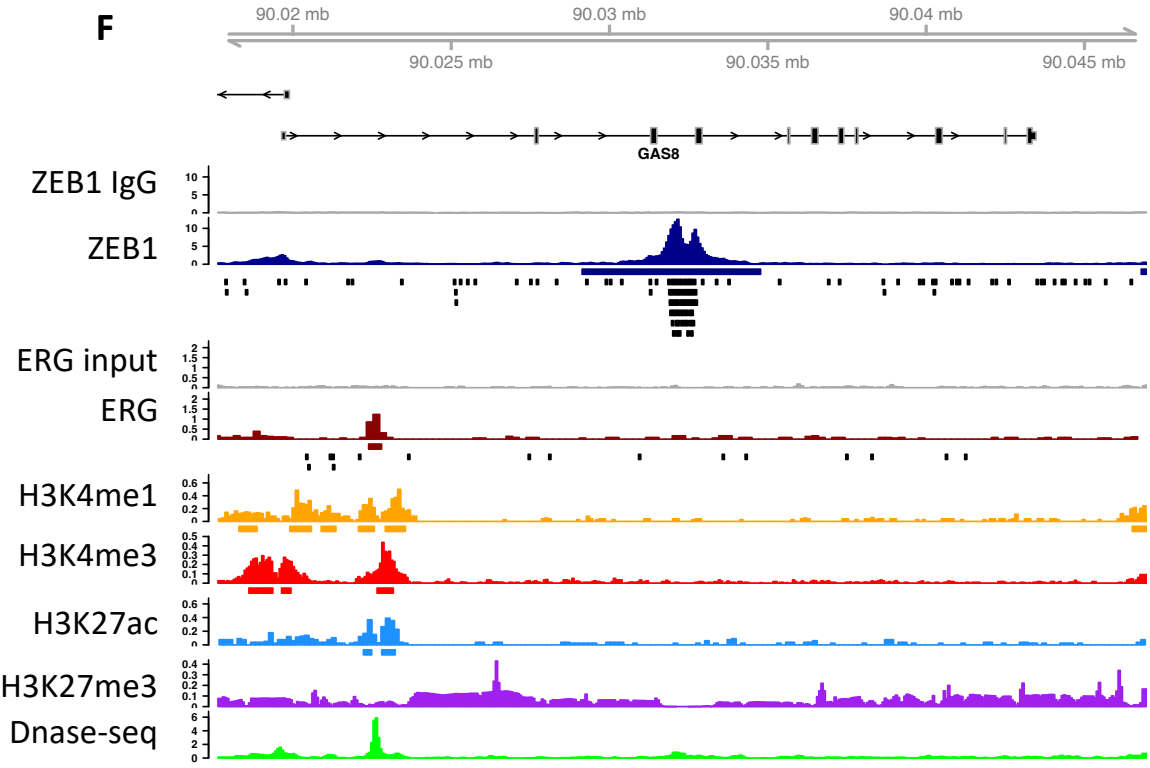
The data collected from ddPCR analysis was analysed under GraphPad Prism v9.2.0 (https://www.graphpad.com/). Statistical analyses to determine significance were performed using paired or unpaired t-test where appropriate (specified in text) with a significance threshold of $P < 0.05$.

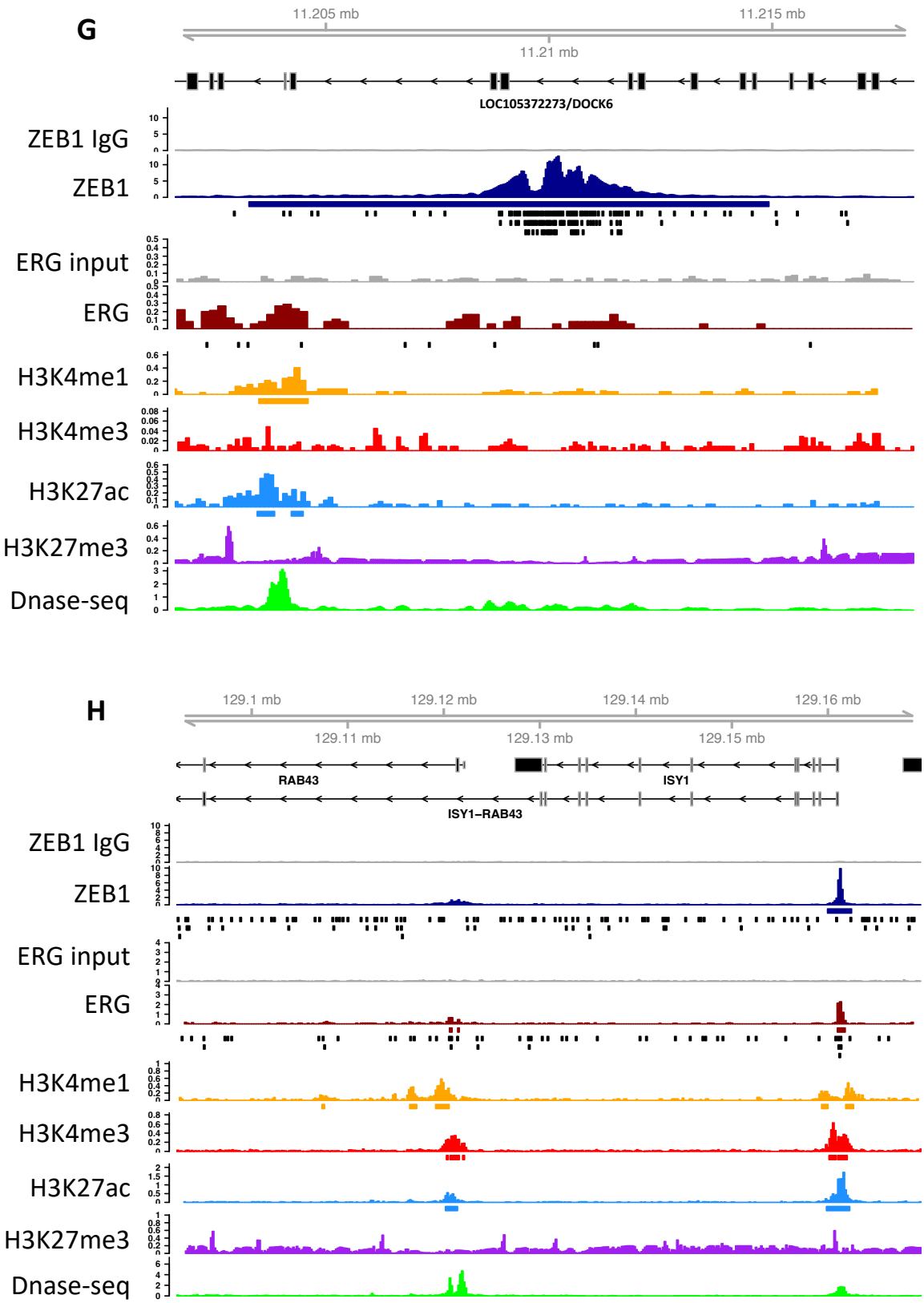
Appendix 4. Supplementary figures

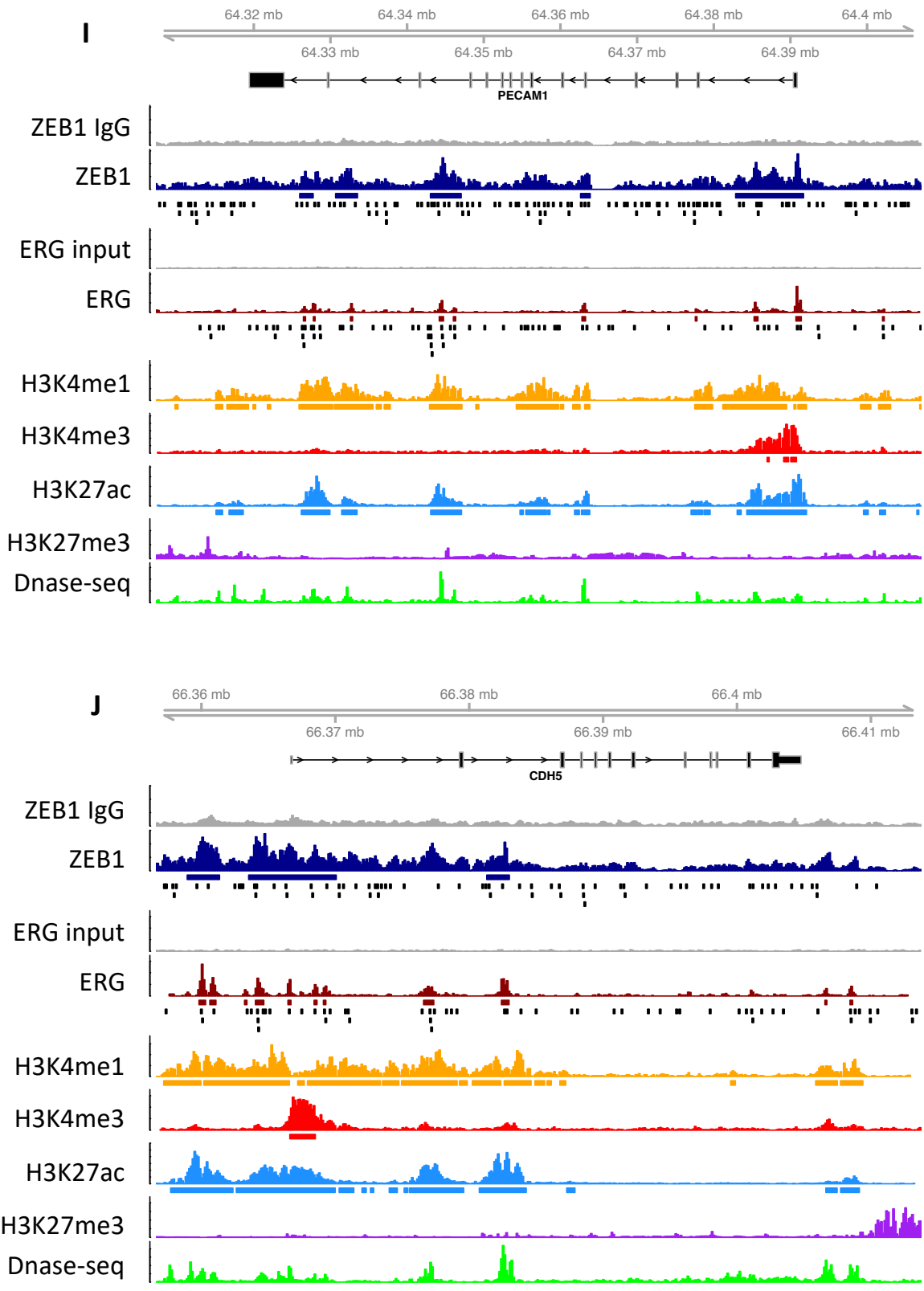

A
31.35 mb
31.45 mb
31.4 mb
31.5 mb
ZEB1-AS1
ZEB1
ZEB1 IgG
ZEB1
ERG input
ERG
H3K4me1
H3K4me3
H3K27ac
H3K27me3
Dnase-seq
B
37.82 mb
37.84 mb
37.86 mb
37.83 mb
37.85 mb
MTF1
ZEB1 IgG
ZEB1
ERG input
ERG
H3K4me1
H3K4me3
H3K27ac
H3K27me3
Dnase-seq

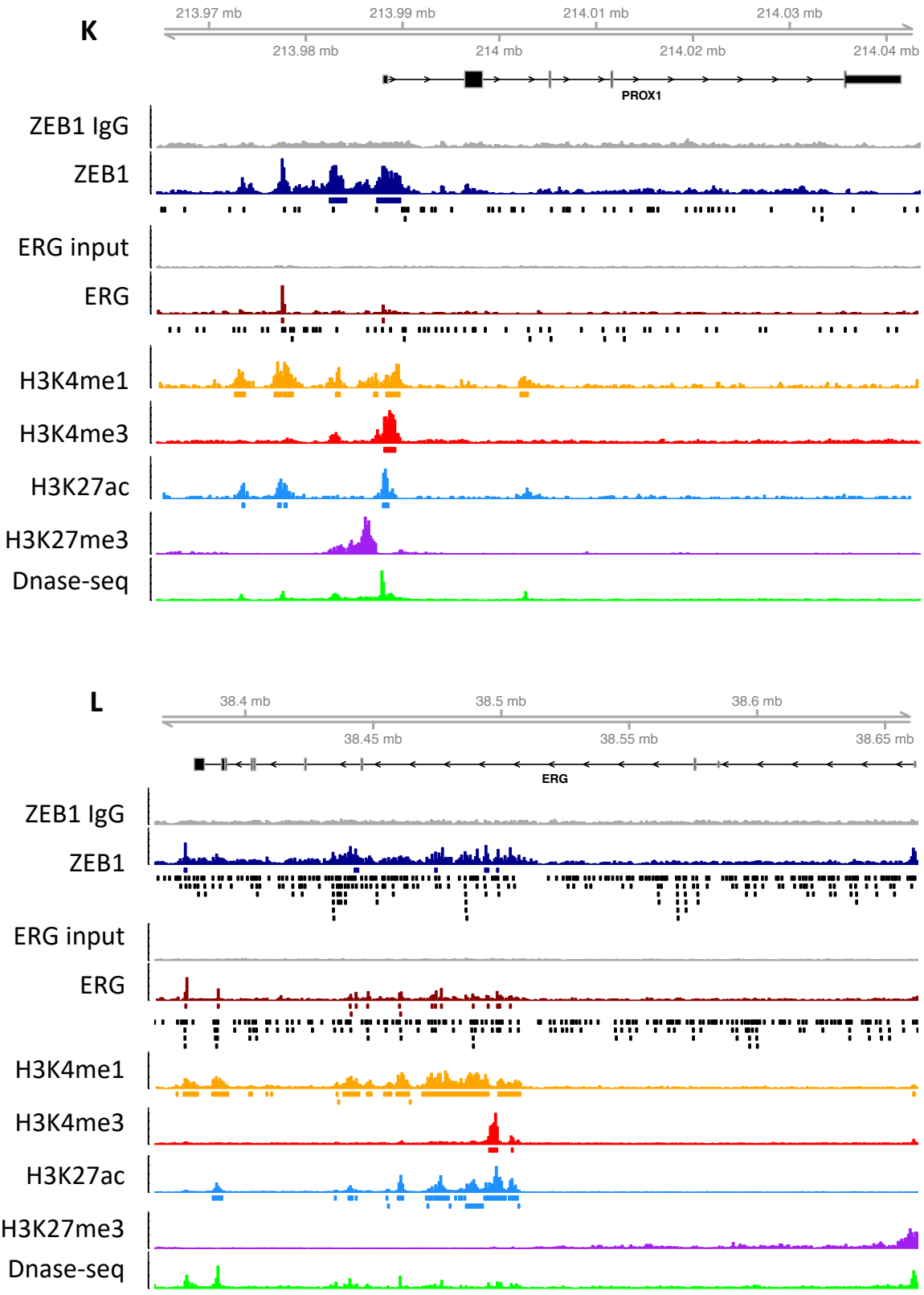

C
65.965 mb
65.975 mb
65.97 mb
65.98 mb
SART1
ZEB1 IgG
ZEB1
ERG input
ERG
H3K4me1
H3K4me3
H3K27ac
H3K27me3
Dnase-seq
D
133.405 mb
133.415 mb
133.41 mb
REXO4
ZEB1 IgG
ZEB1
ERG input
ERG
H3K4me1
H3K4me3
H3K27ac
H3K27me3
Dnase-seq

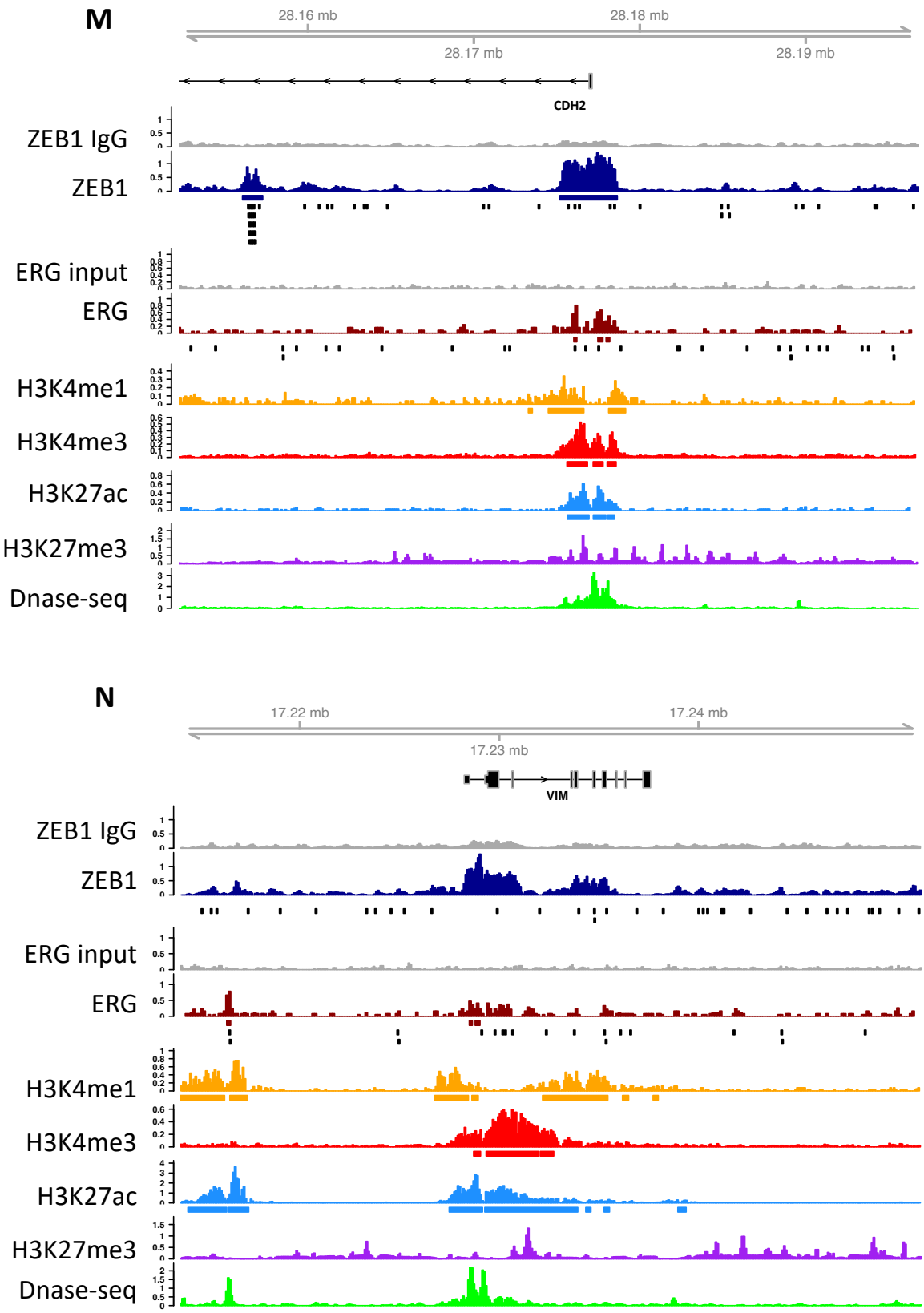

E
109.45 mb
109.47 mb
109.46 mb
KCTD10
ZEB1 IgG
ZEB1
ERG input
ERG
H3K4me1
H3K4me3
H3K27ac
H3K27me3
Dnase-seq

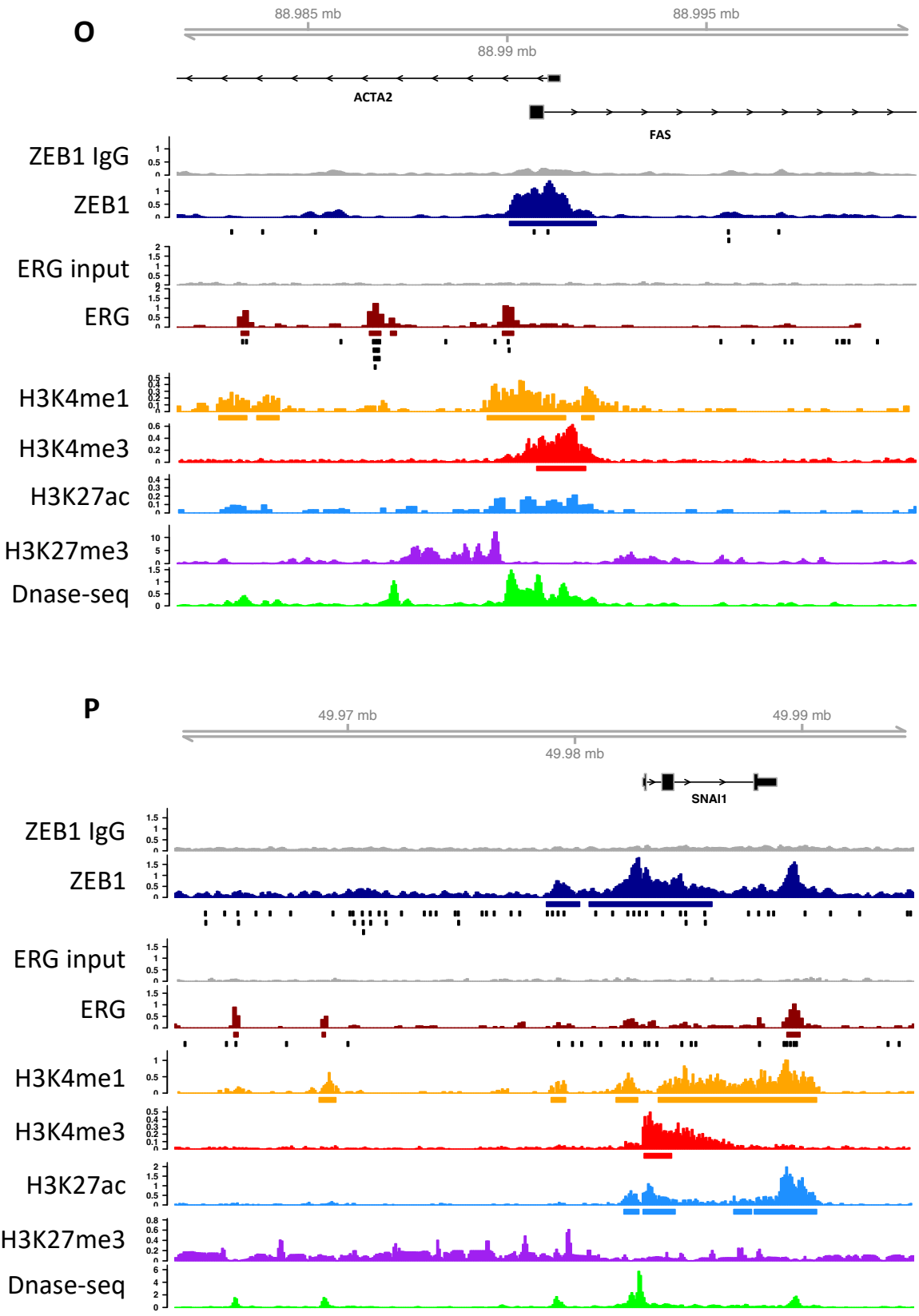

F
90.02 mb
90.03 mb
90.04 mb
90.025 mb
90.035 mb
90.045 mb
GAS8
ZEB1 IgG
ZEB1
ERG input
ERG
H3K4me1
H3K4me3
H3K27ac
H3K27me3
Dnase-seq

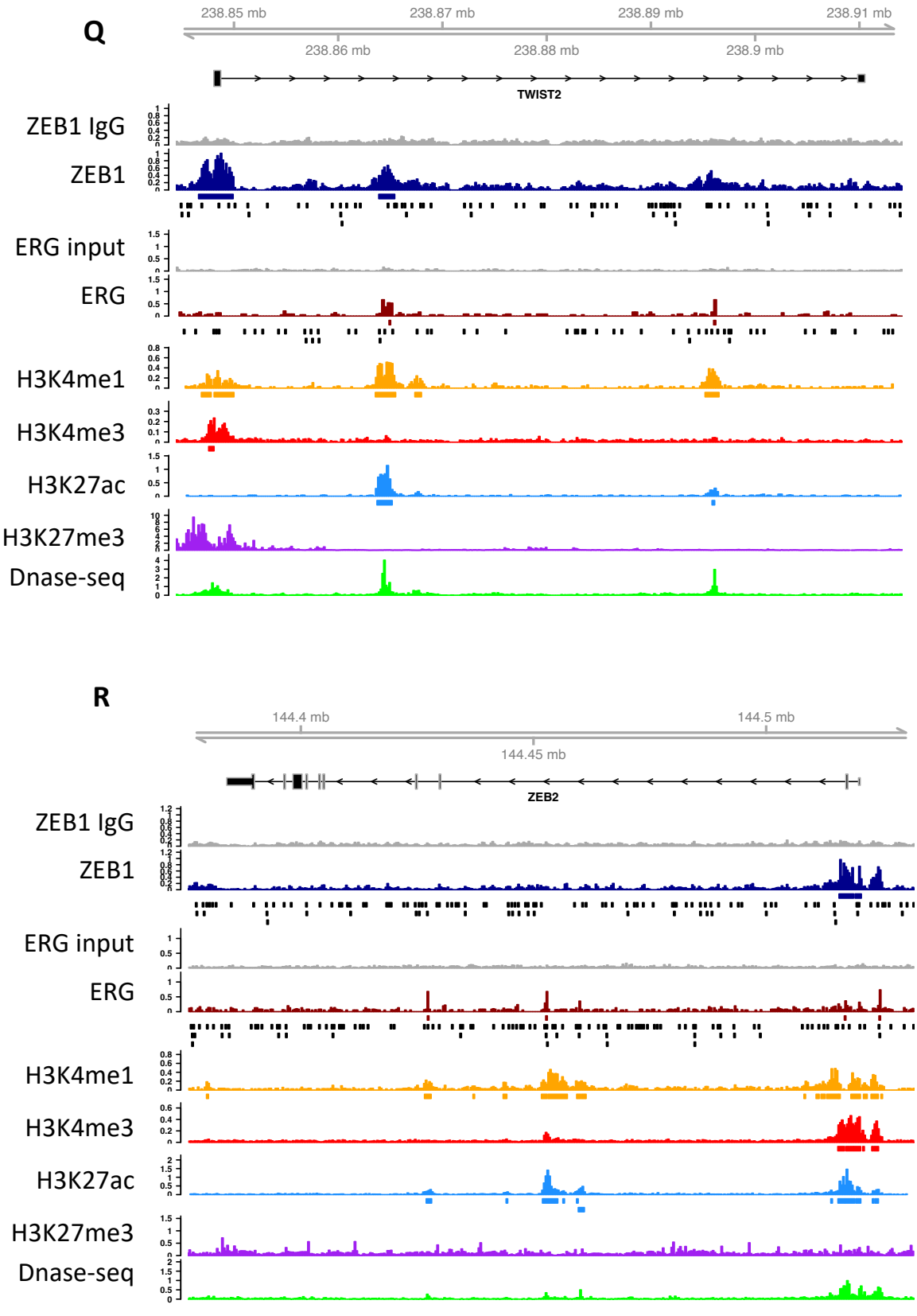

G
11.205 mb
11.215 mb
11.21 mb
LOC105372273/DOCK6
ZEB1 IgG
ZEB1
ERG input
ERG
H3K4me1
H3K4me3
H3K27ac
H3K27me3
Dnase-seq
H
129.1 mb
129.12 mb
129.14 mb
129.16 mb
129.11 mb
129.13 mb
129.15 mb
RAB43
ISY1
ISY1–RAB43
ZEB1 IgG
ZEB1
ERG input
ERG
H3K4me1
H3K4me3
H3K27ac
H3K27me3
Dnase-seq

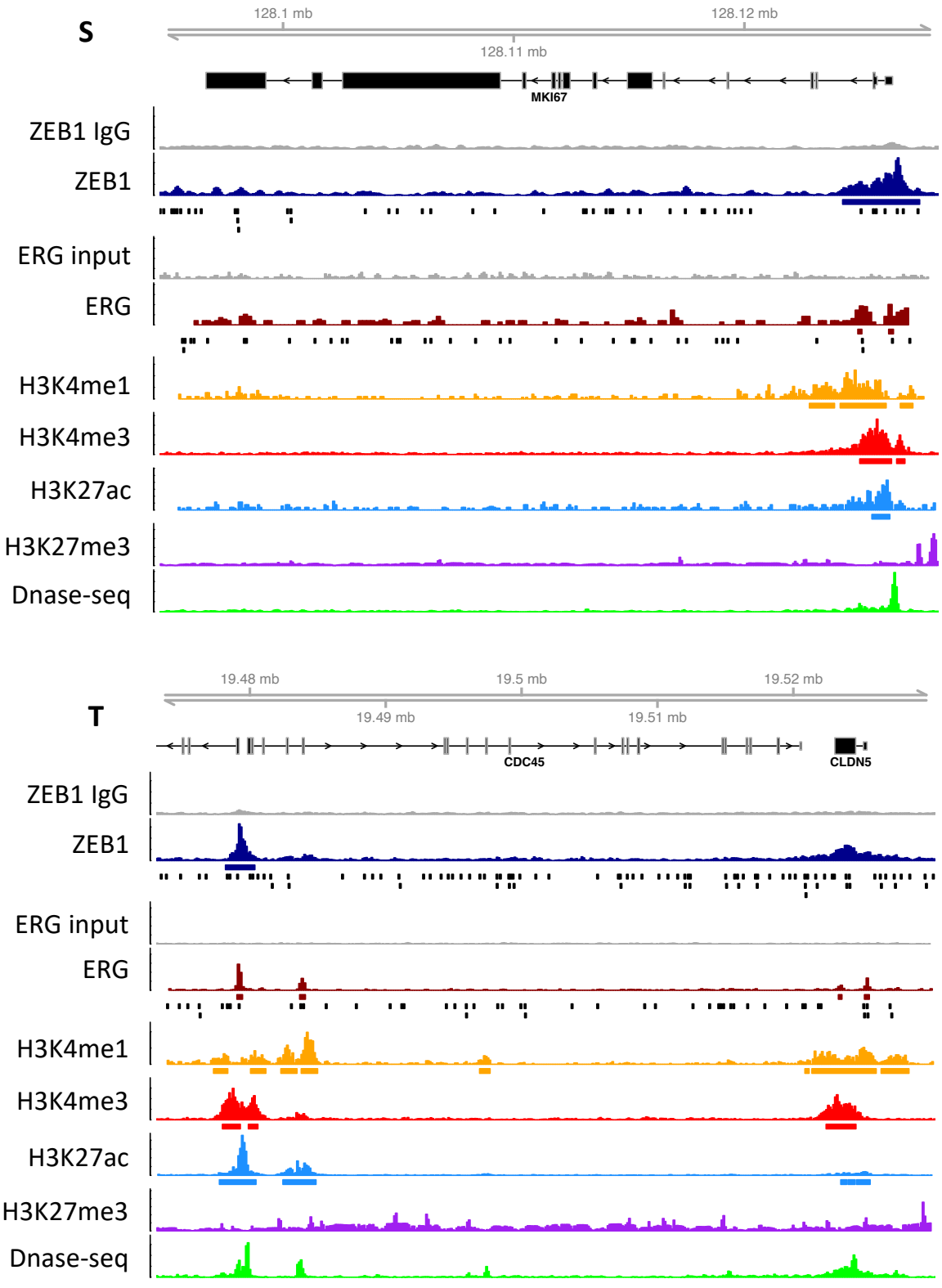

I
64.32 mb
64.34 mb
64.36 mb
64.38 mb
64.4 mb
64.33 mb
64.35 mb
64.37 mb
64.39 mb
PECAM1
ZEB1 IgG
ZEB1
ERG input
ERG
H3K4me1
H3K4me3
H3K27ac
H3K27me3
Dnase-seq
J
66.36 mb
66.38 mb
66.4 mb
66.37 mb
66.39 mb
66.41 mb
CDH5
ZEB1 IgG
ZEB1
ERG input
ERG
H3K4me1
H3K4me3
H3K27ac
H3K27me3
Dnase-seq

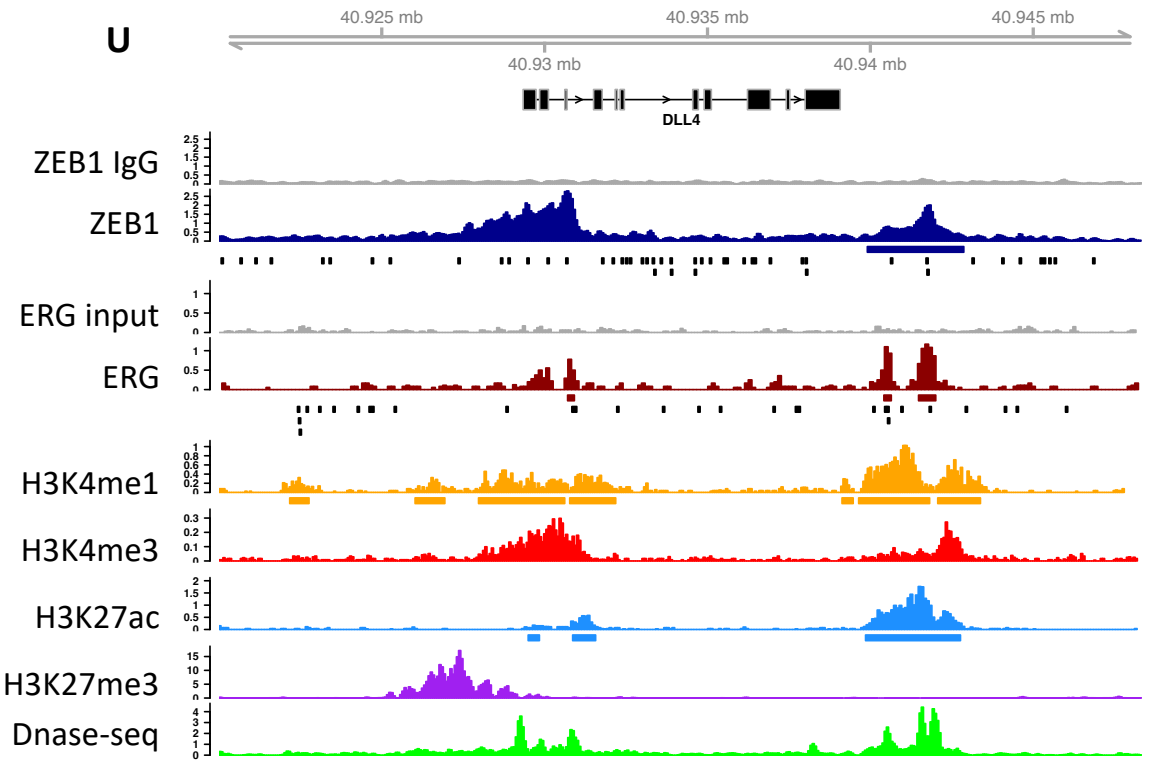

K
213.97 mb
213.99 mb
214.01 mb
214.03 mb
213.98 mb
214 mb
214.02 mb
214.04 mb
PROX1
ZEB1 IgG
ZEB1
ERG input
ERG
H3K4me1
H3K4me3
H3K27ac
H3K27me3
Dnase-seq
L
38.4 mb
38.5 mb
38.6 mb
38.45 mb
38.55 mb
38.65 mb
ERG
ZEB1 IgG
ZEB1
ERG input
ERG
H3K4me1
H3K4me3
H3K27ac
H3K27me3
Dnase-seq

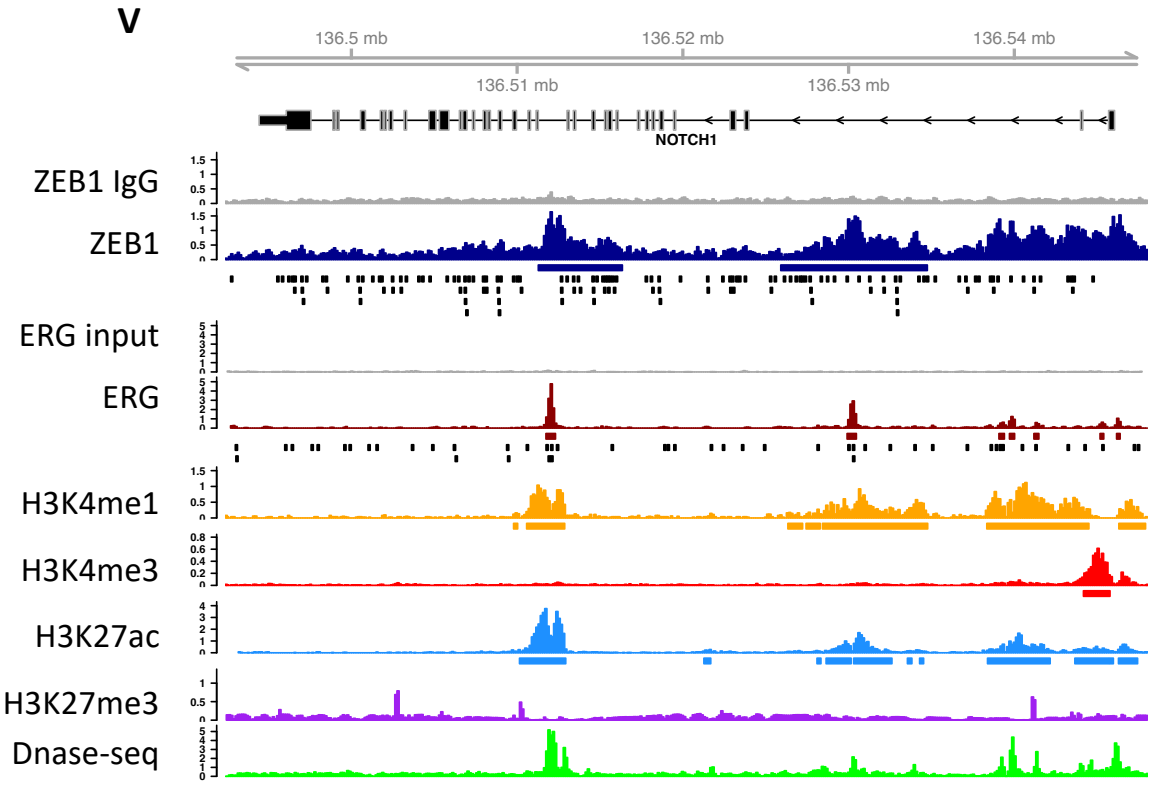

M
28.16 mb
28.18 mb
28.17 mb
28.19 mb
CDH2
ZEB1 IgG
ZEB1
ERG input
ERG
H3K4me1
H3K4me3
H3K27ac
H3K27me3
Dnase-seq
N
17.22 mb
17.24 mb
17.23 mb
VIM
ZEB1 IgG
ZEB1
ERG input
ERG
H3K4me1
H3K4me3
H3K27ac
H3K27me3
Dnase-seq

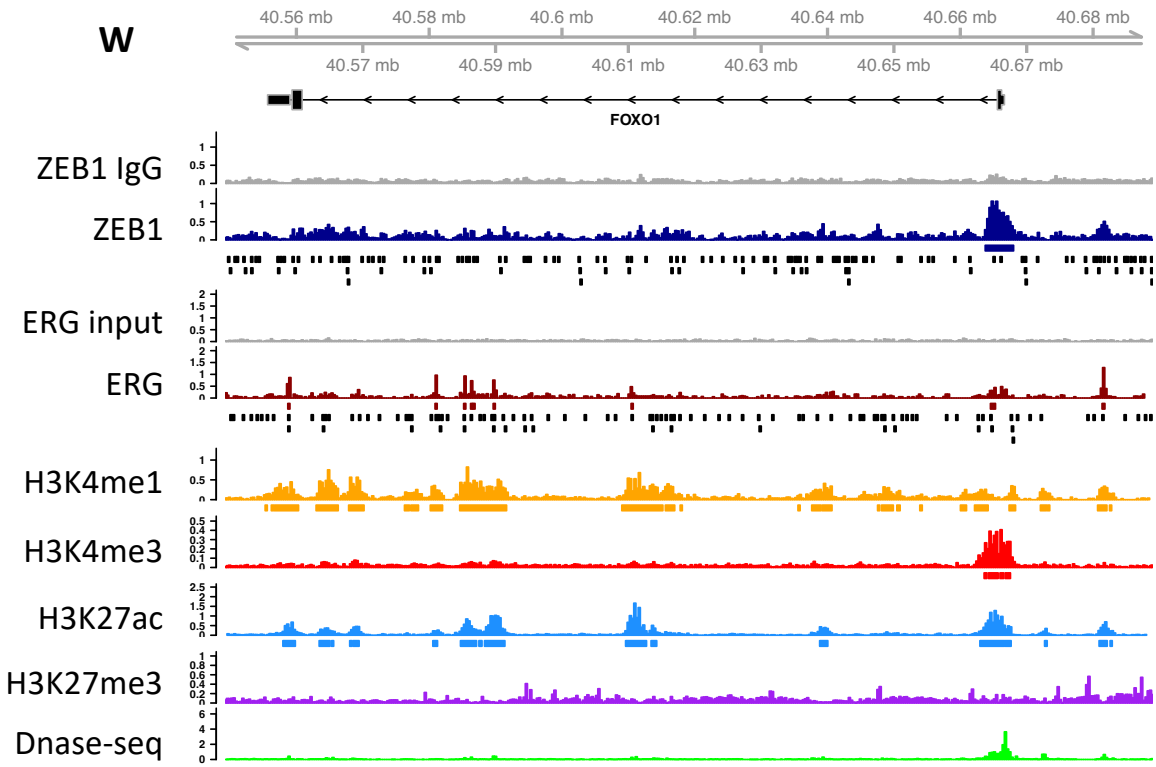

O
88.985 mb
88.995 mb
88.99 mb
ACTA2
FAS
ZEB1 IgG
ZEB1
ERG input
ERG
H3K4me1
H3K4me3
H3K27ac
H3K27me3
Dnase-seq
P
49.97 mb
49.99 mb
49.98 mb
SNAI1
ZEB1 IgG
ZEB1
ERG input
ERG
H3K4me1
H3K4me3
H3K27ac
H3K27me3
Dnase-seq


Q
238.85 mb
238.87 mb
238.89 mb
238.91 mb
238.86 mb
238.88 mb
238.9 mb
TWIST2
ZEB1 IgG
ZEB1
ERG input
ERG
H3K4me1
H3K4me3
H3K27ac
H3K27me3
Dnase-seq
R
144.4 mb
144.5 mb
144.45 mb
ZEB2
ZEB1 IgG
ZEB1
ERG input
ERG
H3K4me1
H3K4me3
H3K27ac
H3K27me3
Dnase-seq


S
128.1 mb
128.12 mb
128.11 mb
MKI67
ZEB1 IgG
ZEB1
ERG input
ERG
H3K4me1
H3K4me3
H3K27ac
H3K27me3
Dnase-seq
T
19.48 mb
19.5 mb
19.52 mb
19.49 mb
19.51 mb
CDC45
CLDN5
ZEB1 IgG
ZEB1
ERG input
ERG
H3K4me1
H3K4me3
H3K27ac
H3K27me3
Dnase-seq

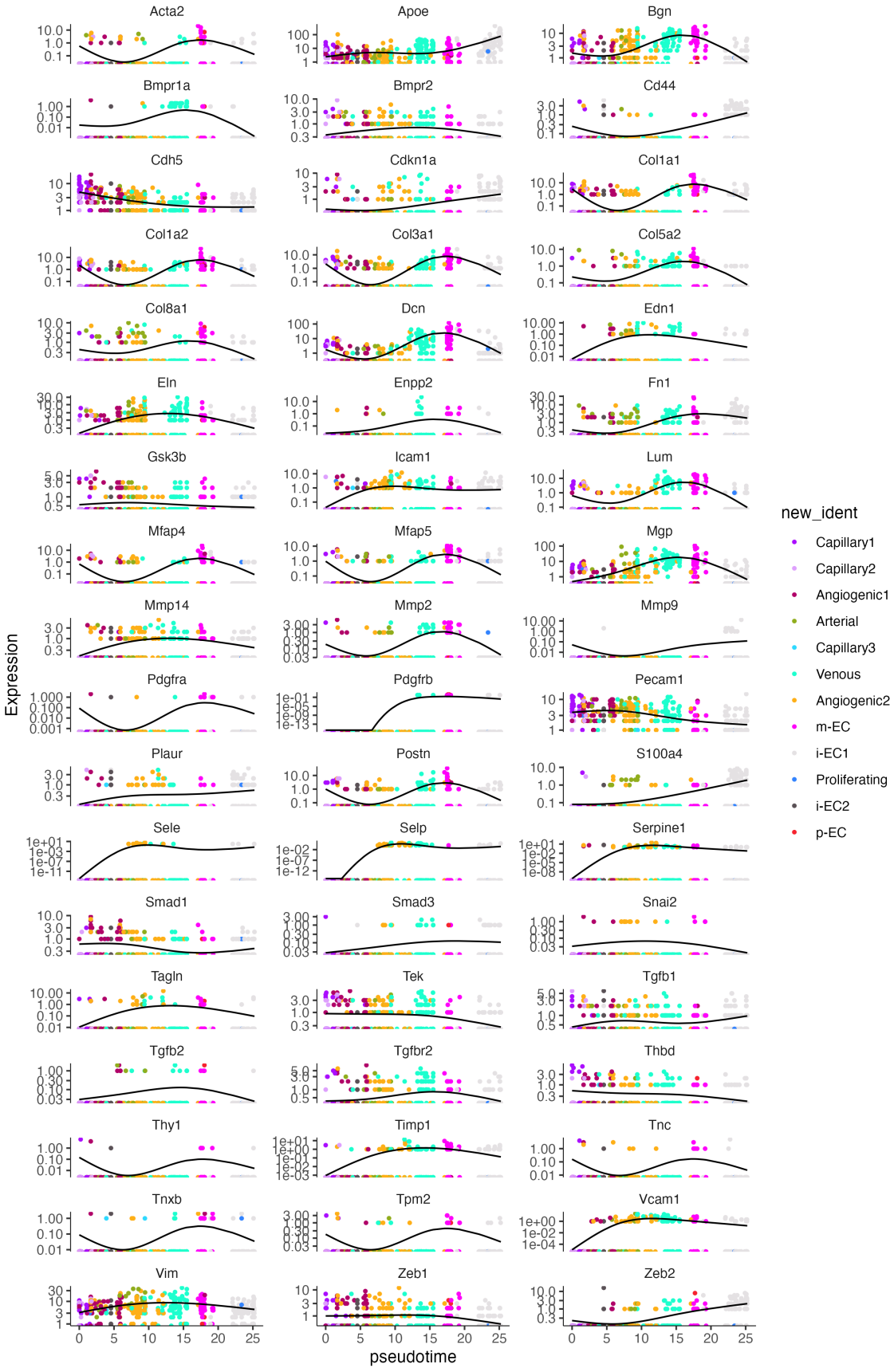

U
40.925 mb
40.935 mb
40.945 mb
40.93 mb
40.94 mb
DLL4
ZEB1 IgG
ZEB1
ERG input
ERG
H3K4me1
H3K4me3
H3K27ac
H3K27me3
Dnase-seq


V
136.5 mb
136.52 mb
136.54 mb
136.51 mb
136.53 mb
NOTCH1
ZEB1 IgG
ZEB1
ERG input
ERG
H3K4me1
H3K4me3
H3K27ac
H3K27me3
Dnase-seq

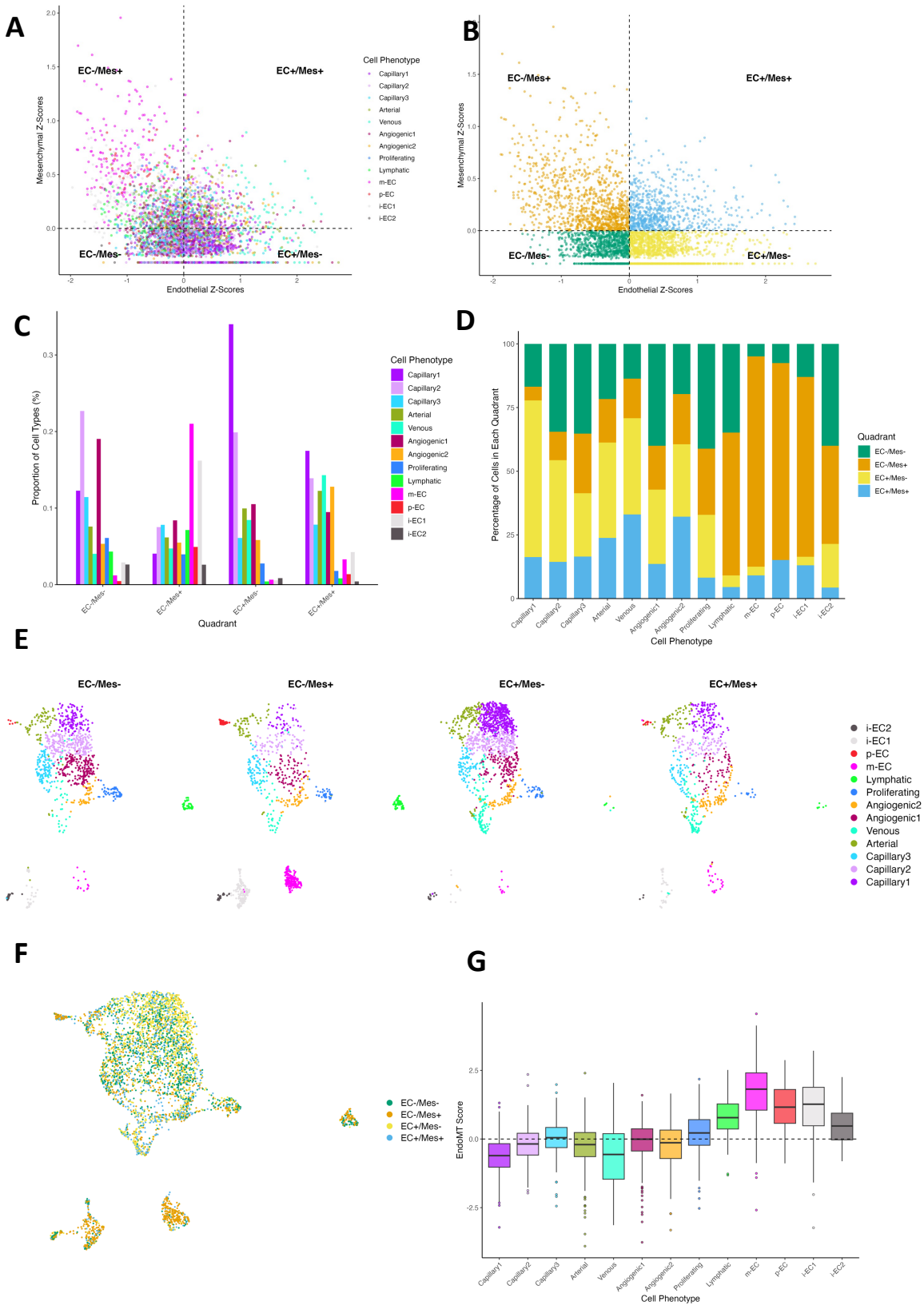


Appendix 4.1. **Signalling tracks of genes of interest in HUVECs for ZEB1, ERG, H3K4me1, H3K4me3, H3K27ac, H3K27me3 and DNase-seq.**

Signalling tracks for HUVEC ChIP-seq data are labelled by their respective transcription factor or histone mark. ZEB1 ChIP-seq signal is shown in blue against the IgG control in grey. Reproducible ZEB1 peaks identified by IDR analysis are shown as a blue bar beneath the ZEB1 signal track. The predicted presence of ZEB1 motif is denoted by black bars below to ZEB1 peak track. Reanalysis of a publicly available ERG ChIP-seq is shown in brown against the input control in grey. ERG peaks detected by MACS2 are shown as brown bars with predicted ERG motif locations as black boxes below the ERG peak track. H3K4me1 is shown as yellow with peaks identified by MACS2 as a yellow bar. H3K4me3 id displayed in red, with peaks identified by MACS2 as a red bar. H3K27ac is shown in light blue with peaks detected by MACS2 as a light blue bar. The Y axis represents bins per million (BPM) normalisation as calculated by the *bamCoverage* command of deepTools. BigWig tracks of H3K27me3 is shown in purple and DNase-seq in green. Genes displayed; (A) ZEB1/ZEB1-AS1 (B) MTF1 (C) SART1 (D) REXO4 (E) KCTD10 (F) GAS8 (G) LOC105372273/DOCK6 (H) ISY1-RAB43 (I) PECAM1 (J) CDH5 (K) PROX1 (L) ERG (M) CDH2 (N) VIM (O) ACTA2 (P) SNAI1 (Q) TWIST2 (R) ZEB1 (S) MKI67 (T) CDC45 (U) DLL4 (V) NOTCH1 (W) FOXO1.



Appendix 4.2. **Gene expression of EndoMT-related genes across the predicted EndoMT pseudotime.**



Appendix 4.3. **Alzaim *et al.*, (2024) EndoMT signature analyses.**

These analyses mirror Figure 6.4 but utilise the EndoMT signature employed by AlZaim *et al.*, as a comparison.

Other works and Team Science

Other relevant work carried out throughout the PhD are recorded here. Several other training courses and personal projects were also carried out but are not detailed.

Other projects:

RNA-seq

- RNA-seq analysis of ZEB1 knockdown in human dermal lymphatic endothelial cells (HDLECs) to assess the transcriptional consequences of ZEB1 in lymphatic endothelial cells.
- HUVEC vs HDLEC RNA-seq analysis as a basic example of differing transcriptomes of EC subtypes.
- RNA-seq analysis of primary isolated HUVECs vs commercially available HUVECs to highlight the transcriptomic impact of different models of the same cell type.
- Various 3' bulk RNA-seq analyses. This required substantial optimisation to correctly handle UMIs and matching of data through FASTQ tags.
    - Confluent vs subconfluent LECs
    - Interphase vs synchronous LECs
    - Confluent vs subconfluent HUVECs
    - Interphase vs synchronous HELAs
    - ZEB1 knockdown in HELAs
- Clustering gene expression profiles across samples to identifying co-expression between genes.

ChIP-seq

- ZEB1 HDLEC ChIP-seq. After rigorous quality control it was deemed the experiment had poor enrichment. To extract some level of information all signal across replicates was combined. This experiment is being repeated.

scRNA-seq

- Analyses of multiple other EC scRNA-seq dataset. Both from raw data and pre-aligned data.

Miscellaneous bioinformatics – some examples

- Comparing tools e.g. edgeR vs DESeq2
- Python vs R for scRNA-seq analysis
- Comparing source code of commonly used R heatmap packages to understand differences in clustering results
- Comparing older with newer versions of packages for reproducing published results (e.g., Monocle 2 vs Monocle 3 for trajectory analysis).

Machine learning to categorise research papers based on abstract

- A tool was developed to categorise research papers based on abstracts through machine learning and language processing. This was also extended to retrieve author information to generate collaboration networks between researchers, institutes and countries.

Text-mining

- Development of a custom program to extract gene/protein names from abstracts in line with relevant copyright rules.

- Extraction and inference of protein-protein interactions from sentence analysis through grammatical patters.
- The aim was to generate a command line programme to automate text mining.

Optimising in house scRNA-seq of mouse retinal endothelial cells and other wet lab techniques

- Animal licence PIL A + B certification obtained.
- Shadowing other lab members in training animal husbandry and handling.
- Tissue dissociation and maintaining viability of isolated ECs.
- MACS and FACS technique comparisons to enrich CD31+ cell populations to extract ECs from mouse tissue.
- RNA extraction and quantification.
- Techniques to confirm knockout including western blot.
- Basic cell culture techniques.

Team science:

- Miscellaneous bioinformatics for other groups including troubleshooting processes and validating the results.
- Extracting RNA from pig mitochondria, sequencing and analysing the RNA-seq data.
- Several rounds of various murine tissue dissection including retina and lung for other groups.
- Undergraduate and masters student project allocation through applying an algorithm based on dissatisfaction score.
- Working closely with undergraduate and masters students to teach and aid in driving bioinformatics projects.

- Two months work experience as a python software developer on the COVID-Curated and Open aNalysis aNd rEsearCh platform (CO-CONNECT) project.

COVID-19 (and other) impact statements

COVID-19 impact statement

This PhD began in October 2020, coinciding with the COVID-19 lockdown. This resulted in a significant delay to training, induction and data generation. Even after returning to laboratories, the mandated working conditions and limited hours made research difficult. This resulted in a significant stall in the training and qualifications required to carry out the proposed PhD project. To attempt to counteract this, we turned largely to bioinformatics approaches. As with all PhD students, COVID greatly impacted this PhD.

Animal unit closure impact statement

Unfortunately, in 2024 the BSU animal unit at the University of Nottingham was shut down. This resulted in us not be able to complete a scRNA-seq study on ZEB1^{IECKO} adult retinal endothelial cells which would have complimented chapter 7 of this thesis. We had spent a lot of time optimising the extraction of viable endothelial cells to carry out this study.

Personal difficulties impact statement

My first child was born in March 2024, during the final year of this PhD. Unfortunately, both mother and baby had complications during birth, which led to 2 weeks in the neo-natal unit and long-term physical and mental consequences for my partner. I have also struggled mentally, having been present in the operating theatre when difficulties were realised. This has put significant pressure on my studies and has significantly impacted the output of the project and the completion of the thesis.

References

'10XGenomics/cellranger' (2024). 10x Genomics. Available at: https://github.com/10XGenomics/cellranger (Accessed: 11 December 2024).

Abbott, N.J., Rönnbäck, L. and Hansson, E. (2006) 'Astrocyte–endothelial interactions at the blood–brain barrier', *Nature Reviews Neuroscience*, 7(1), pp. 41–53. Available at: https://doi.org/10.1038/nrn1824.

Abhinand, C.S. *et al.* (2016) 'VEGF-A/VEGFR2 signaling network in endothelial cells relevant to angiogenesis', *Journal of Cell Communication and Signaling*, 10(4), pp. 347–354. Available at: https://doi.org/10.1007/s12079-016-0352-8.

Abraham, S. *et al.* (2008) 'Integrin β1 Subunit Controls Mural Cell Adhesion, Spreading, and Blood Vessel Wall Stability', *Circulation Research*, 102(5), pp. 562–570. Available at: https://doi.org/10.1161/CIRCRESAHA.107.167908.

Abraham, S. *et al.* (2015) 'A Rac/Cdc42 exchange factor complex promotes formation of lateral filopodia and blood vessel lumen morphogenesis', *Nature Communications*, 6(1), p. 7286. Available at: https://doi.org/10.1038/ncomms8286.

Adams, R.H. and Alitalo, K. (2007) 'Molecular regulation of angiogenesis and lymphangiogenesis', *Nature Reviews Molecular Cell Biology*, 8(6), pp. 464–478. Available at: https://doi.org/10.1038/nrm2183.

Adams, R.H. and Eichmann, A. (2010) 'Axon Guidance Molecules in Vascular Patterning', *Cold Spring Harbor Perspectives in Biology*, 2(5), p. a001875. Available at: https://doi.org/10.1101/cshperspect.a001875.

Aghdassi, A. *et al.* (2012) 'Recruitment of histone deacetylases HDAC1 and HDAC2 by the transcriptional repressor ZEB1 downregulates E-cadherin expression in pancreatic cancer', *Gut*, 61(3), pp. 439–448. Available at: https://doi.org/10.1136/gutjnl-2011-300060.

Aird, W.C. (2007) 'Phenotypic Heterogeneity of the Endothelium', *Circulation Research*, 100(2), pp. 174–190. Available at: https://doi.org/10.1161/01.RES.0000255690.03436.ae.

Aird, W.C. (2012) 'Endothelial cell heterogeneity', *Cold Spring Harbor Perspectives in Medicine*, 2(1), p. a006429. Available at: https://doi.org/10.1101/cshperspect.a006429.

Akil, A. *et al.* (2021) 'Notch Signaling in Vascular Endothelial Cells, Angiogenesis, and Tumor Progression: An Update and Prospective', *Frontiers in Cell and Developmental Biology*, 9. Available at: https://doi.org/10.3389/fcell.2021.642352.

Alvandi, Z. and Bischoff, J. (2021) 'Endothelial-Mesenchymal Transition in Cardiovascular Disease', *Arteriosclerosis, Thrombosis, and Vascular Biology*, 41(9), pp. 2357–2369. Available at: https://doi.org/10.1161/ATVBAHA.121.313788.

AlZaim, I. *et al.* (2024) 'Defining the Vascular Niche of Human Adipose Tissue Across Metabolic Conditions'. bioRxiv, p. 2024.09.22.610444. Available at: https://doi.org/10.1101/2024.09.22.610444.

Amersfoort, J., Eelen, G. and Carmeliet, P. (2022) 'Immunomodulation by endothelial cells — partnering up with the immune system?', *Nature Reviews Immunology*, 22(9), pp. 576–588. Available at: https://doi.org/10.1038/s41577-022-00694-4.

Andrade, J. *et al.* (2021) 'Control of endothelial quiescence by FOXO-regulated metabolites', *Nature Cell Biology*, 23(4), pp. 413–423. Available at: https://doi.org/10.1038/s41556-021-00637-6.

Andrews, S. (2010) 'FastQC: A Quality Control Tool for High Throughput Sequence Data [Online]. Available online at: http://www.bioinformatics.babraham.ac.uk/projects/fastqc/'.

Angrisani, A. *et al.* (2021) 'The emerging role of the KCTD proteins in cancer', *Cell Communication and Signaling*, 19(1), p. 56. Available at: https://doi.org/10.1186/s12964-021-00737-8.

Aranguren, X.L. *et al.* (2013) 'Unraveling a novel transcription factor code determining the human arterial-specific endothelial cell signature', *Blood*, 122(24), pp. 3982–3992. Available at: https://doi.org/10.1182/blood-2013-02-483255.

Armstrong, E.J. and Bischoff, J. (2004) 'Heart Valve Development', *Circulation Research*, 95(5), pp. 459–470. Available at: https://doi.org/10.1161/01.RES.0000141146.95728.da.

Armulik, A., Genové, G. and Betsholtz, C. (2011) 'Pericytes: Developmental, Physiological, and Pathological Perspectives, Problems, and Promises', *Developmental Cell*, 21(2), pp. 193–215. Available at: https://doi.org/10.1016/j.devcel.2011.07.001.

Arnaoutova, I. and Kleinman, H.K. (2010) 'In vitro angiogenesis: endothelial cell tube formation on gelled basement membrane extract', *Nature Protocols*, 5(4), pp. 628–635. Available at: https://doi.org/10.1038/nprot.2010.6.

Asahara, T. *et al.* (1997) 'Isolation of Putative Progenitor Endothelial Cells for Angiogenesis', *Science*, 275(5302), pp. 964–966. Available at: https://doi.org/10.1126/science.275.5302.964.

Ashburner, M. *et al.* (2000) 'Gene Ontology: tool for the unification of biology', *Nature Genetics*, 25(1), pp. 25–29. Available at: https://doi.org/10.1038/75556.

Augustin, H.G. and Koh, G.Y. (2024) 'A systems view of the vascular endothelium in health and disease', *Cell*, 187(18), pp. 4833–4858. Available at: https://doi.org/10.1016/j.cell.2024.07.012.

Bader, G.D. and Hogue, C.W. (2003) 'An automated method for finding molecular complexes in large protein interaction networks', *BMC Bioinformatics*, 4(1), p. 2. Available at: https://doi.org/10.1186/1471-2105-4-2.

Badia-i-Mompel, P. *et al.* (2022) 'decoupleR: ensemble of computational methods to infer biological activities from omics data', *Bioinformatics Advances*, 2(1), p. vbac016. Available at: https://doi.org/10.1093/bioadv/vbac016.

Barber, C.L. and Iruela-Arispe, M.L. (2006) 'The Ever-Elusive Endothelial Progenitor Cell: Identities, Functions and Clinical Implications', *Pediatric Research*, 59(4), pp. 26–32. Available at: https://doi.org/10.1203/01.pdr.0000203553.46471.18.

Barski, A. *et al.* (2007) 'High-Resolution Profiling of Histone Methylations in the Human Genome', *Cell*, 129(4), pp. 823–837. Available at: https://doi.org/10.1016/j.cell.2007.05.009.

Benson, C.E. and Southgate, L. (2021) 'The DOCK protein family in vascular development and disease', *Angiogenesis*, 24(3), pp. 417–433. Available at: https://doi.org/10.1007/s10456-021-09768-8.

Bergers, G. and Benjamin, L.E. (2003) 'Tumorigenesis and the angiogenic switch', *Nature Reviews Cancer*, 3(6), pp. 401–410. Available at: https://doi.org/10.1038/nrc1093.

Bergers, G. and Hanahan, D. (2008) 'Modes of resistance to anti-angiogenic therapy', *Nature Reviews Cancer*, 8(8), pp. 592–603. Available at: https://doi.org/10.1038/nrc2442.

Bergers, G. and Song, S. (2005) 'The role of pericytes in blood-vessel formation and maintenance', *Neuro-Oncology*, 7(4), pp. 452–464. Available at: https://doi.org/10.1215/S1152851705000232.

Bharadwaj, A.S. *et al.* (2013) 'Role of the Retinal Vascular Endothelial Cell in Ocular Disease', *Progress in retinal and eye research*, 32, pp. 102–180. Available at: https://doi.org/10.1016/j.preteyeres.2012.08.004.

Birdsey, G.M. *et al.* (2015) 'The Endothelial Transcription Factor ERG Promotes Vascular Stability and Growth through Wnt/β-Catenin Signaling', *Developmental Cell*, 32(1), pp. 82–96. Available at: https://doi.org/10.1016/j.devcel.2014.11.016.

Bischoff, J. *et al.* (2016) 'CD45 Expression in Mitral Valve Endothelial Cells After Myocardial Infarction', *Circulation research*, 119(11), pp. 1215–1225. Available at: https://doi.org/10.1161/CIRCRESAHA.116.309598.

Bischoff, J. (2019) 'Endothelial-to-Mesenchymal Transition', *Circulation Research*, 124(8), pp. 1163–1165. Available at: https://doi.org/10.1161/CIRCRESAHA.119.314813.

Blandinières, A. *et al.* (2023) 'Results of an international survey about methods used to isolate human endothelial colony-forming cells: guidance from the SSC on Vascular Biology of the ISTH', *Journal of Thrombosis and Haemostasis*, 21(9), pp. 2611–2619. Available at: https://doi.org/10.1016/j.jtha.2023.06.014.

Blighe, K. and Lun, A. (2024) 'PCAtools: PCAtools: Everything Principal Components Analysis.', *R package version 2.18.0* [Preprint]. Available at: https://github.com/kevinblighe/PCAtools.

Böhm, F. and Pernow, J. (2007) 'The importance of endothelin-1 for vascular dysfunction in cardiovascular disease', *Cardiovascular Research*, 76(1), pp. 8–18. Available at: https://doi.org/10.1016/j.cardiores.2007.06.004.

Brabletz, S. *et al.* (2011) 'The ZEB1/miR-200 feedback loop controls Notch signalling in cancer cells', *The EMBO Journal*, 30(4), pp. 770–782. Available at: https://doi.org/10.1038/emboj.2010.349.

Brabletz, S. *et al.* (2017) 'Generation and characterization of mice for conditional inactivation of Zeb1', *Genesis (New York, N.Y.: 2000)*, 55(4). Available at: https://doi.org/10.1002/dvg.23024.

Brabletz, S. and Brabletz, T. (2010) 'The ZEB/miR-200 feedback loop—a motor of cellular plasticity in development and cancer?', *EMBO reports*, 11(9), pp. 670–677. Available at: https://doi.org/10.1038/embor.2010.117.

Brash, J.T. *et al.* (2020) 'Tamoxifen-Activated CreERT Impairs Retinal Angiogenesis Independently of Gene Deletion', *Circulation Research*, 127(6), pp. 849–850. Available at: https://doi.org/10.1161/CIRCRESAHA.120.317025.

van den Brink, S.C. *et al.* (2017) 'Single-cell sequencing reveals dissociation-induced gene expression in tissue subpopulations', *Nature Methods*, 14(10), pp. 935–936. Available at: https://doi.org/10.1038/nmeth.4437.

Bronson, R., Lyu, J. and Xiong, J. (2023) 'Transcriptome analysis reveals molecular signature and cell-type difference of Homo sapiens endothelial-to-mesenchymal transition', *G3 Genes|Genomes|Genetics*, 13(12), p. jkad243. Available at: https://doi.org/10.1093/g3journal/jkad243.

Brutsaert, D.L. (2003) 'Cardiac Endothelial-Myocardial Signaling: Its Role in Cardiac Growth, Contractile Performance, and Rhythmicity', *Physiological Reviews*, 83(1), pp. 59–115. Available at: https://doi.org/10.1152/physrev.00017.2002.

Buenrostro, J.D. *et al.* (2013) 'Transposition of native chromatin for fast and sensitive epigenomic profiling of open chromatin, DNA-binding proteins and nucleosome position', *Nature Methods*, 10(12), pp. 1213–1218. Available at: https://doi.org/10.1038/nmeth.2688.

Bui, T.M., Wiesolek, H.L. and Sumagin, R. (2020) 'ICAM-1: A master regulator of cellular responses in inflammation, injury resolution, and tumorigenesis', *Journal of leukocyte biology*, 108(3), pp. 787–799. Available at: https://doi.org/10.1002/JLB.2MR0220-549R.

Bulger, M. and Groudine, M. (2011) 'Functional and Mechanistic Diversity of Distal Transcription Enhancers', *Cell*, 144(3), pp. 327–339. Available at: https://doi.org/10.1016/j.cell.2011.01.024.

Cahill, P.A. and Redmond, E.M. (2016) 'Vascular endothelium – Gatekeeper of vessel health', *Atherosclerosis*, 248, pp. 97–109. Available at: https://doi.org/10.1016/j.atherosclerosis.2016.03.007.

Cano, E. *et al.* (2024) 'Intramyocardial Sprouting Tip Cells Specify Coronary Arterialization', *Circulation Research*, 135(6), pp. 671–684. Available at: https://doi.org/10.1161/CIRCRESAHA.124.324868.

Cao, J. *et al.* (2019) 'The single-cell transcriptional landscape of mammalian organogenesis', *Nature*, 566(7745), pp. 496–502. Available at: https://doi.org/10.1038/s41586-019-0969-x.

Cao, Y. (2007) 'Angiogenesis modulates adipogenesis and obesity', *The Journal of Clinical Investigation*, 117(9), pp. 2362–2368. Available at: https://doi.org/10.1172/JCI32239.

Caramel, J., Ligier, M. and Puisieux, A. (2018) 'Pleiotropic Roles for ZEB1 in Cancer', *Cancer Research*, 78(1), pp. 30–35. Available at: https://doi.org/10.1158/0008-5472.CAN-17-2476.

Carmeliet, P. (2000) 'Mechanisms of angiogenesis and arteriogenesis', *Nature Medicine*, 6(4), pp. 389–395. Available at: https://doi.org/10.1038/74651.

Carmeliet, P. (2003) 'Angiogenesis in health and disease', *Nature Medicine*, 9(6), pp. 653–660. Available at: https://doi.org/10.1038/nm0603-653.

Carmeliet, P. and Jain, R.K. (2000) 'Angiogenesis in cancer and other diseases', *Nature*, 407(6801), pp. 249–257. Available at: https://doi.org/10.1038/35025220.

Carmeliet, P. and Jain, R.K. (2011) 'Molecular mechanisms and clinical applications of angiogenesis', *Nature*, 473(7347), pp. 298–307. Available at: https://doi.org/10.1038/nature10144.

Carroll, T.S. *et al.* (2014) 'Impact of artifact removal on ChIP quality metrics in ChIP-seq and ChIP-exo data', *Frontiers in Genetics*, 5, p. 75. Available at: https://doi.org/10.3389/fgene.2014.00075.

Castellon, X. and Bogdanova, V. (2016) 'Chronic Inflammatory Diseases and Endothelial Dysfunction', *Aging and Disease*, 7(1), pp. 81–89. Available at: https://doi.org/10.14336/AD.2015.0803.

Chalise, U., Becirovic-Agic, M. and Lindsey, M.L. (2023) 'The cardiac wound healing response to myocardial infarction', *WIREs Mechanisms of Disease*, 15(1), p. e1584. Available at: https://doi.org/10.1002/wsbm.1584.

Chambers, S.E.J. *et al.* (2025) 'Human endothelial colony forming cells (ECFCs) require endothelial protein C receptor (EPCR) for cell cycle progression and angiogenic activity', *Angiogenesis*, 28(3), p. 30. Available at: https://doi.org/10.1007/s10456-025-09982-8.

Chari, T. and Pachter, L. (2023) 'The specious art of single-cell genomics', *PLOS Computational Biology*, 19(8), p. e1011288. Available at: https://doi.org/10.1371/journal.pcbi.1011288.

Chavkin, N.W. *et al.* (2022) 'Endothelial cell cycle state determines propensity for arterial-venous fate', *Nature Communications*, 13(1), p. 5891. Available at: https://doi.org/10.1038/s41467-022-33324-7.

Chen, B. *et al.* (2019) 'Prognostic value of ZEB-1 in solid tumors: a meta-analysis', *BMC Cancer*, 19(1), p. 635. Available at: https://doi.org/10.1186/s12885-019-5830-y.

Chen, D. *et al.* (2025) 'VEGF counteracts shear stress-determined arterial fate specification during capillary remodeling'. bioRxiv, p. 2024.01.23.576920. Available at: https://doi.org/10.1101/2024.01.23.576920.

Chen, L.-J. *et al.* (2024) 'Single-cell RNA sequencing unveils unique transcriptomic signatures of endothelial cells and role of ENO1 in response to disturbed flow', *Proceedings of the National Academy of Sciences*, 121(5), p. e2318904121. Available at: https://doi.org/10.1073/pnas.2318904121.

Chen, Q. *et al.* (2016) 'Endothelial cells are progenitors of cardiac pericytes and vascular smooth muscle cells', *Nature Communications*, 7(1), p. 12422. Available at: https://doi.org/10.1038/ncomms12422.

Chen, W. *et al.* (2019) 'The endothelial tip-stalk cell selection and shuffling during angiogenesis', *Journal of Cell Communication and Signaling*, 13(3), pp. 291–301. Available at: https://doi.org/10.1007/s12079-019-00511-z.

Chen, W. *et al.* (2021) 'The expression and prognostic value of REXO4 in hepatocellular carcinoma', *Journal of Gastrointestinal Oncology*, 12(4), pp. 1704–1717. Available at: https://doi.org/10.21037/jgo-21-98.

Chen, X. *et al.* (2023) 'Interferon regulatory factor 1 (IRF1) inhibits lung endothelial regeneration following inflammation-induced acute lung injury', *Clinical Science (London, England : 1979)*, 137(5), pp. 367–383. Available at: https://doi.org/10.1042/CS20220876.

Cheng, J. *et al.* (2024) 'KCTD10 regulates brain development by destabilizing brain disorder–associated protein KCTD13', *Proceedings of the National Academy of Sciences*, 121(12), p. e2315707121. Available at: https://doi.org/10.1073/pnas.2315707121.

Cheung, N., Mitchell, P. and Wong, T.Y. (2010) 'Diabetic retinopathy', *The Lancet*, 376(9735), pp. 124–136. Available at: https://doi.org/10.1016/S0140-6736(09)62124-3.

Chin, C.-H. *et al.* (2014) 'cytoHubba: identifying hub objects and sub-networks from complex interactome', *BMC Systems Biology*, 8(4), p. S11. Available at: https://doi.org/10.1186/1752-0509-8-S4-S11.

Cho, J.G. *et al.* (2018) 'Endothelial to Mesenchymal Transition Represents a Key Link in the Interaction between Inflammation and Endothelial Dysfunction', *Frontiers in Immunology*, 9, p. 294. Available at: https://doi.org/10.3389/fimmu.2018.00294.

Cho, J.S. *et al.* (2024) 'NRP1-expressing monocyte/macrophages promote arteriogenesis in the ischemic limb'. bioRxiv, p. 2024.02.11.579823. Available at: https://doi.org/10.1101/2024.02.11.579823.

Cho, S. (2012) 'CD36 as a therapeutic target for endothelial dysfunction in stroke', *Current pharmaceutical design*, 18(25), pp. 3721–3730.

Choi, C.K. and Chen, C.S. (2014) 'Jostling for position in angiogenic sprouts: continuous rearrangement of cells explained by differential adhesion dynamics', *The EMBO Journal*, 33(10), pp. 1089–1090. Available at: https://doi.org/10.1002/embj.201488452.

Choi, K. *et al.* (1998) 'A common precursor for hematopoietic and endothelial cells', *Development*, 125(4), pp. 725–732. Available at: https://doi.org/10.1242/dev.125.4.725.

Choi, K.J. *et al.* (2020) 'Endothelial-to-mesenchymal transition in anticancer therapy and normal tissue damage', *Experimental & Molecular Medicine*, 52(5), pp. 781–792. Available at: https://doi.org/10.1038/s12276-020-0439-4.

Choi, S.-H. *et al.* (2018) 'Tumour-vasculature development via endothelial-to-mesenchymal transition after radiotherapy controls CD44v6+ cancer cell and macrophage polarization', *Nature Communications*, 9(1), p. 5108. Available at: https://doi.org/10.1038/s41467-018-07470-w.

Chu, L.-H. *et al.* (2016) 'A multiscale computational model predicts distribution of anti-angiogenic isoform VEGF165b in peripheral arterial disease in human and mouse', *Scientific Reports*, 6(1), p. 37030. Available at: https://doi.org/10.1038/srep37030.

Ciszewski, W.M. *et al.* (2021) 'Cytoskeleton Reorganization in EndMT—The Role in Cancer and Fibrotic Diseases', *International Journal of Molecular Sciences*, 22(21), p. 11607. Available at: https://doi.org/10.3390/ijms222111607.

Claesson-Welsh, L. (2015) 'Vascular permeability—the essentials', *Upsala Journal of Medical Sciences*, 120(3), pp. 135–143. Available at: https://doi.org/10.3109/03009734.2015.1064501.

Claesson-Welsh, L., Dejana, E. and McDonald, D.M. (2021) 'Permeability of the endothelial barrier: identifying and reconciling controversies', *Trends in molecular medicine*, 27(4), pp. 314–331. Available at: https://doi.org/10.1016/j.molmed.2020.11.006.

Clere, N., Renault, S. and Corre, I. (2020) 'Endothelial-to-Mesenchymal Transition in Cancer', *Frontiers in Cell and Developmental Biology*, 8. Available at: https://doi.org/10.3389/fcell.2020.00747.

Comijn, J. *et al.* (2001) 'The Two-Handed E Box Binding Zinc Finger Protein SIP1 Downregulates E-Cadherin and Induces Invasion', *Molecular Cell*, 7(6), pp. 1267–1278. Available at: https://doi.org/10.1016/S1097-2765(01)00260-X.

Cooke, J.P. and Losordo, D.W. (2015) 'Modulating the Vascular Response to Limb Ischemia', *Circulation Research*, 116(9), pp. 1561–1578. Available at: https://doi.org/10.1161/CIRCRESAHA.115.303565.

Cooley, B.C. *et al.* (2014) 'TGF-β signaling mediates endothelial-to-mesenchymal transition (EndMT) during vein graft remodeling', *Science Translational Medicine*, 6(227), p. 227ra34. Available at: https://doi.org/10.1126/scitranslmed.3006927.

Corada, M., Morini, M.F. and Dejana, E. (2014) 'Signaling Pathways in the Specification of Arteries and Veins', *Arteriosclerosis, Thrombosis, and Vascular Biology*, 34(11), pp. 2372–2377. Available at: https://doi.org/10.1161/ATVBAHA.114.303218.

Coultas, L., Chawengsaksophak, K. and Rossant, J. (2005) 'Endothelial cells and VEGF in vascular development', *Nature*, 438(7070), pp. 937–945. Available at: https://doi.org/10.1038/nature04479.

Crawford, T.N. *et al.* (2009) 'Diabetic retinopathy and angiogenesis', *Current Diabetes Reviews*, 5(1), pp. 8–13. Available at: https://doi.org/10.2174/157339909787314149.

Cui, X. *et al.* (2015) 'Venous Endothelial Marker COUP-TFII Regulates the Distinct Pathologic Potentials of Adult Arteries and Veins', *Scientific Reports*, 5, p. 16193. Available at: https://doi.org/10.1038/srep16193.

Danecek, P. *et al.* (2021) 'Twelve years of SAMtools and BCFtools', *GigaScience*, 10(2), p. giab008. Available at: https://doi.org/10.1093/gigascience/giab008.

Davidson, D. *et al.* (2005) 'Fibroblast Growth Factor (FGF) 18 Signals through FGF Receptor 3 to Promote Chondrogenesis*', *Journal of Biological Chemistry*, 280(21), pp. 20509–20515. Available at: https://doi.org/10.1074/jbc.M410148200.

De Bock, K., Cauwenberghs, S. and Carmeliet, P. (2011) 'Vessel abnormalization: another hallmark of cancer?: Molecular mechanisms and therapeutic implications', *Current Opinion in Genetics & Development*, 21(1), pp. 73–79. Available at: https://doi.org/10.1016/j.gde.2010.10.008.

De Smet, F. *et al.* (2009) 'Mechanisms of Vessel Branching', *Arteriosclerosis, Thrombosis, and Vascular Biology*, 29(5), pp. 639–649. Available at: https://doi.org/10.1161/ATVBAHA.109.185165.

De Val, S. and Black, B.L. (2009) 'Transcriptional control of endothelial cell development', *Developmental Cell*, 16(2), pp. 180–195. Available at: https://doi.org/10.1016/j.devcel.2009.01.014.

Deanfield, J.E., Halcox, J.P. and Rabelink, T.J. (2007) 'Endothelial Function and Dysfunction', *Circulation*, 115(10), pp. 1285–1295. Available at: https://doi.org/10.1161/CIRCULATIONAHA.106.652859.

De Bock, K. *et al.* (2013) 'Role of PFKFB3-Driven Glycolysis in Vessel Sprouting', *Cell*, 154(3), pp. 651–663. Available at: https://doi.org/10.1016/j.cell.2013.06.037.

von Degenfeld, G. *et al.* (2006) 'Microenvironmental VEGF distribution is critical for stable and functional vessel growth in ischemia', *FASEB journal: official publication of the Federation of American Societies for Experimental Biology*, 20(14), pp. 2657–2659. Available at: https://doi.org/10.1096/fj.06-6568fje.

Dejana, E., Hirschi, K.K. and Simons, M. (2017) 'The molecular basis of endothelial cell plasticity', *Nature Communications*, 8, p. 14361. Available at: https://doi.org/10.1038/ncomms14361.

Dejana, E., Tournier-Lasserve, E. and Weinstein, B.M. (2009) 'The Control of Vascular Integrity by Endothelial Cell Junctions: Molecular Basis and Pathological Implications', *Developmental Cell*, 16(2), pp. 209–221. Available at: https://doi.org/10.1016/j.devcel.2009.01.004.

Demir, R., Seval, Y. and Huppertz, B. (2007) 'Vasculogenesis and angiogenesis in the early human placenta', *Acta Histochemica*, 109(4), pp. 257–265. Available at: https://doi.org/10.1016/j.acthis.2007.02.008.

Demir, R., Yaba, A. and Huppertz, B. (2010) 'Vasculogenesis and angiogenesis in the endometrium during menstrual cycle and implantation', *Acta Histochemica*, 112(3), pp. 203–214. Available at: https://doi.org/10.1016/j.acthis.2009.04.004.

DiPietro, L.A. (2016) 'Angiogenesis and wound repair: when enough is enough', *Journal of Leukocyte Biology*, 100(5), pp. 979–984. Available at: https://doi.org/10.1189/jlb.4MR0316-102R.

Dobin, A. *et al.* (2013) 'STAR: ultrafast universal RNA-seq aligner', *Bioinformatics*, 29(1), pp. 15–21. Available at: https://doi.org/10.1093/bioinformatics/bts635.

Doddaballapur, A. *et al.* (2015) 'Laminar shear stress inhibits endothelial cell metabolism via KLF2-mediated repression of PFKFB3', *Arteriosclerosis, Thrombosis, and Vascular Biology*, 35(1), pp. 137–145. Available at: https://doi.org/10.1161/ATVBAHA.114.304277.

Donato, A.J. *et al.* (2015) 'Cellular and molecular biology of aging endothelial cells', *Journal of Molecular and Cellular Cardiology*, 89, pp. 122–135. Available at: https://doi.org/10.1016/j.yjmcc.2015.01.021.

Doncheva, N.T. *et al.* (2019) 'Cytoscape StringApp: Network Analysis and Visualization of Proteomics Data', *Journal of Proteome Research*, 18(2), pp. 623–632. Available at: https://doi.org/10.1021/acs.jproteome.8b00702.

Drápela, S. *et al.* (2020) 'ZEB1: A Critical Regulator of Cell Plasticity, DNA Damage Response, and Therapy Resistance', *Frontiers in Molecular Biosciences*, 7. Available at: https://doi.org/10.3389/fmolb.2020.00036.

Dryden, N.H. *et al.* (2012) 'The Transcription Factor Erg Controls Endothelial Cell Quiescence by Repressing Activity of Nuclear Factor (NF)-κB p65', *The Journal of Biological Chemistry*, 287(15), pp. 12331–12342. Available at: https://doi.org/10.1074/jbc.M112.346791.

Dudley, A.C. and Griffioen, A.W. (2023) 'Pathological angiogenesis: mechanisms and therapeutic strategies', *Angiogenesis*, 26(3), pp. 313–347. Available at: https://doi.org/10.1007/s10456-023-09876-7.

Durand, S. *et al.* (2024) 'ZEB1 controls a lineage-specific transcriptional program essential for melanoma cell state transitions', *Oncogene*, 43(20), pp. 1489–1505. Available at: https://doi.org/10.1038/s41388-024-03010-7.

Durinck, S. *et al.* (2009) 'Mapping identifiers for the integration of genomic datasets with the R/Bioconductor package biomaRt', *Nature Protocols*, 4(8), pp. 1184–1191. Available at: https://doi.org/10.1038/nprot.2009.97.

Eelen, G. *et al.* (2020) 'Basic and Therapeutic Aspects of Angiogenesis Updated', *Circulation Research*, 127(2), pp. 310–329. Available at: https://doi.org/10.1161/CIRCRESAHA.120.316851.

Egeblad, M. and Werb, Z. (2002) 'New functions for the matrix metalloproteinases in cancer progression', *Nature Reviews Cancer*, 2(3), pp. 161–174. Available at: https://doi.org/10.1038/nrc745.

Egginton, S. (2009) 'Invited review: activity-induced angiogenesis', *Pflügers Archiv - European Journal of Physiology*, 457(5), pp. 963–977. Available at: https://doi.org/10.1007/s00424-008-0563-9.

Eisenberg, L.M. and Markwald, R.R. (1995) 'Molecular regulation of atrioventricular valvuloseptal morphogenesis', *Circulation Research*, 77(1), pp. 1–6. Available at: https://doi.org/10.1161/01.res.77.1.1.

Ernst, J. and Kellis, M. (2012) 'ChromHMM: automating chromatin-state discovery and characterization', *Nature Methods*, 9(3), pp. 215–216. Available at: https://doi.org/10.1038/nmeth.1906.

Esquiva, G., Grayston, A. and Rosell, A. (2018) 'Revascularization and endothelial progenitor cells in stroke', *American Journal of Physiology-Cell Physiology*, 315(5), pp. C664–C674. Available at: https://doi.org/10.1152/ajpcell.00200.2018.

Evans, C.E., Iruela-Arispe, M.L. and Zhao, Y.-Y. (2021) 'Mechanisms of Endothelial Regeneration and Vascular Repair and Their Application to Regenerative Medicine', *The American Journal of Pathology*, 191(1), pp. 52–65. Available at: https://doi.org/10.1016/j.ajpath.2020.10.001.

Evrard, S.M. *et al.* (2016) 'Endothelial to mesenchymal transition is common in atherosclerotic lesions and is associated with plaque instability', *Nature Communications*, 7(1), p. 11853. Available at: https://doi.org/10.1038/ncomms11853.

Fadini, G.P. *et al.* (2020) 'Impaired Regeneration Contributes to Poor Outcomes in Diabetic Peripheral Artery Disease', *Arteriosclerosis, Thrombosis, and Vascular Biology*, 40(1), pp. 34–44. Available at: https://doi.org/10.1161/ATVBAHA.119.312863.

Fan, M. *et al.* (2023) 'Lactate promotes endothelial-to-mesenchymal transition via Snail1 lactylation after myocardial infarction', *Science Advances*, 9(5), p. eadc9465. Available at: https://doi.org/10.1126/sciadv.adc9465.

Fan, Z. *et al.* (2021) 'Exercise-induced angiogenesis is dependent on metabolically primed ATF3/4+ endothelial cells', *Cell Metabolism*, 33(9), pp. 1793-1807.e9. Available at: https://doi.org/10.1016/j.cmet.2021.07.015.

Fang, J., Wang, Z. and Miao, C. (2023) 'Angiogenesis after ischemic stroke', *Acta Pharmacologica Sinica*, 44(7), pp. 1305–1321. Available at: https://doi.org/10.1038/s41401-023-01061-2.

Fang, J.S. and Hirschi, K.K. (2019) 'Molecular regulation of arteriovenous endothelial cell specification', *F1000Research*, 8, p. F1000 Faculty Rev-1208. Available at: https://doi.org/10.12688/f1000research.16701.1.

Fang, J.S., Hultgren, N.W. and Hughes, C.C.W. (2021) 'Regulation of Partial and Reversible Endothelial-to-Mesenchymal Transition in Angiogenesis', *Frontiers in Cell and Developmental Biology*, 9. Available at: https://doi.org/10.3389/fcell.2021.702021.

Fang, Z. *et al.* (2024) 'GTF2H4 regulates partial EndMT via NF-κB activation through NCOA3 phosphorylation in ischemic diseases', *The Innovation*, 5(2), p. 100565. Available at: https://doi.org/10.1016/j.xinn.2024.100565.

Farfán, N. *et al.* (2018) 'The transcriptional factor ZEB1 represses Syndecan 1 expression in prostate cancer', *Scientific Reports*, 8(1), p. 11467. Available at: https://doi.org/10.1038/s41598-018-29829-1.

Feil, S., Valtcheva, N. and Feil, R. (2009) 'Inducible Cre mice', *Methods in Molecular Biology (Clifton, N.J.)*, 530, pp. 343–363. Available at: https://doi.org/10.1007/978-1-59745-471-1_18.

Feldker, N. *et al.* (2020) 'Genome-wide cooperation of EMT transcription factor ZEB1 with YAP and AP-1 in breast cancer', *The EMBO Journal*, 39(17), p. e103209. Available at: https://doi.org/10.15252/embj.2019103209.

Félétou, M. and Vanhoutte, P.M. (2006) 'Endothelial dysfunction: a multifaceted disorder (The Wiggers Award Lecture)', *American Journal of Physiology-Heart and Circulatory Physiology*, 291(3), pp. H985–H1002. Available at: https://doi.org/10.1152/ajpheart.00292.2006.

Feng, Y., Wang, C. and Wang, G. (2022) 'Inhibition of KCTD10 Affects Diabetic Retinopathy Progression by Reducing VEGF and Affecting Angiogenesis', *Genetics Research*, 2022, p. 4112307. Available at: https://doi.org/10.1155/2022/4112307.

Ferdous, A. *et al.* (2009) 'Nkx2–5 transactivates the Ets-related protein 71 gene and specifies an endothelial/endocardial fate in the developing embryo', *Proceedings of the National Academy of Sciences*, 106(3), pp. 814–819. Available at: https://doi.org/10.1073/pnas.0807583106.

Ferrara, N. (2004) 'Vascular endothelial growth factor: basic science and clinical progress', *Endocrine Reviews*, 25(4), pp. 581–611. Available at: https://doi.org/10.1210/er.2003-0027.

Ferrara, N. and Adamis, A.P. (2016) 'Ten years of anti-vascular endothelial growth factor therapy', *Nature Reviews Drug Discovery*, 15(6), pp. 385–403. Available at: https://doi.org/10.1038/nrd.2015.17.

Fish, J.E. and Wythe, J.D. (2015) 'The molecular regulation of arteriovenous specification and maintenance', *Developmental Dynamics*, 244(3), pp. 391–409. Available at: https://doi.org/10.1002/dvdy.24252.

Flamme, I., Frölich, T. and Risau, W. (1997) 'Molecular mechanisms of vasculogenesis and embryonic angiogenesis', *Journal of Cellular Physiology*, 173(2), pp. 206–210. Available at: https://doi.org/10.1002/(SICI)1097-4652(199711)173:2<206::AID-JCP22>3.0.CO;2-C.

Förstermann, U. and Sessa, W.C. (2012) 'Nitric oxide synthases: regulation and function', *European Heart Journal*, 33(7), pp. 829–837. Available at: https://doi.org/10.1093/eurheartj/ehr304.

Forte, E. *et al.* (2020) 'Dynamic Interstitial Cell Response during Myocardial Infarction Predicts Resilience to Rupture in Genetically Diverse Mice', *Cell Reports*, 30(9), pp. 3149-3163.e6. Available at: https://doi.org/10.1016/j.celrep.2020.02.008.

Fouani, L. *et al.* (2020) 'During mitosis ZEB1 "switches" from being a chromatin-bound epithelial gene repressor, to become a microtubule-associated protein', *Biochimica et Biophysica Acta (BBA) - Molecular Cell Research*, 1867(7), p. 118673. Available at: https://doi.org/10.1016/j.bbamcr.2020.118673.

Franco, C.A. *et al.* (2015) 'Dynamic Endothelial Cell Rearrangements Drive Developmental Vessel Regression', *PLOS Biology*, 13(4), p. e1002125. Available at: https://doi.org/10.1371/journal.pbio.1002125.

Fraser, H.M. and Duncan, W.C. (2005) 'Vascular morphogenesis in the primate ovary', *Angiogenesis*, 8(2), pp. 101–116. Available at: https://doi.org/10.1007/s10456-005-9004-y.

Frausto, R.F. *et al.* (2019) 'ZEB1 insufficiency causes corneal endothelial cell state transition and altered cellular processing', *PLOS ONE*, 14(6), p. e0218279. Available at: https://doi.org/10.1371/journal.pone.0218279.

Fruttiger, M. (2007) 'Development of the retinal vasculature', *Angiogenesis*, 10(2), pp. 77–88. Available at: https://doi.org/10.1007/s10456-007-9065-1.

Fu, R., Lv, W.-C., *et al.* (2020) 'Endothelial ZEB1 promotes angiogenesis-dependent bone formation and reverses osteoporosis', *Nature Communications*, 11(1), p. 460. Available at: https://doi.org/10.1038/s41467-019-14076-3.

Fu, R., Li, Y., *et al.* (2020) 'Inactivation of endothelial ZEB1 impedes tumor progression and sensitizes tumors to conventional therapies', *The Journal of Clinical Investigation*, 130(3), pp. 1252–1270. Available at: https://doi.org/10.1172/JCI131507.

Fung, S.S.M. *et al.* (2021) 'Endothelial cell density in children with posterior polymorphous corneal dystrophy: a longitudinal case-control study', *Eye*, 35(12), pp. 3397–3403. Available at: https://doi.org/10.1038/s41433-021-01451-y.

Furey, T.S. (2012) 'ChIP–seq and beyond: new and improved methodologies to detect and characterize protein–DNA interactions', *Nature Reviews Genetics*, 13(12), pp. 840–852. Available at: https://doi.org/10.1038/nrg3306.

Furtado, J. *et al.* (2023) 'Netrin-1 binding to Unc5B regulates Blood-Retina Barrier integrity'. bioRxiv, p. 2023.01.21.525006. Available at: https://doi.org/10.1101/2023.01.21.525006.

Gaikwad, A.V. *et al.* (2020) 'Endothelial to mesenchymal transition (EndMT) and vascular remodeling in pulmonary hypertension and idiopathic pulmonary fibrosis', *Expert Review of Respiratory Medicine*, 14(10), pp. 1027–1043. Available at: https://doi.org/10.1080/17476348.2020.1795832.

García-Palmero, I. *et al.* (2013) 'Nuclear magnetic resonance imaging of tumour growth and neovasculature performance in vivo reveals Grb7 as a novel antiangiogenic target', *NMR in biomedicine*, 26(9), pp. 1059–1069. Available at: https://doi.org/10.1002/nbm.2918.

Gardner, T.W. *et al.* (2000) 'Review Paper: New Insights into the Pathophysiology of Diabetic Retinopathy: Potential Cell-Specific Therapeutic Targets', *Diabetes Technology & Therapeutics*, 2(4), pp. 601–608. Available at: https://doi.org/10.1089/15209150050502023.

Gariano, R.F. and Gardner, T.W. (2005) 'Retinal angiogenesis in development and disease', *Nature*, 438(7070), pp. 960–966. Available at: https://doi.org/10.1038/nature04482.

Genetta, T.L. *et al.* (2023) 'ZEB1 promotes non-homologous end joining double-strand break repair', *Nucleic Acids Research*, 51(18), pp. 9863–9879. Available at: https://doi.org/10.1093/nar/gkad723.

Gerhardt, H. *et al.* (2003) 'VEGF guides angiogenic sprouting utilizing endothelial tip cell filopodia', *The Journal of Cell Biology*, 161(6), pp. 1163–1177. Available at: https://doi.org/10.1083/jcb.200302047.

Gerhardt, H. (2008) 'VEGF and endothelial guidance in angiogenic sprouting', *Organogenesis*, 4(4), pp. 241–246.

Gerhardt, H. and Betsholtz, C. (2003) 'Endothelial-pericyte interactions in angiogenesis', *Cell and Tissue Research*, 314(1), pp. 15–23. Available at: https://doi.org/10.1007/s00441-003-0745-x.

Geudens, I. and Gerhardt, H. (2011) 'Coordinating cell behaviour during blood vessel formation', *Development*, 138(21), pp. 4569–4583. Available at: https://doi.org/10.1242/dev.062323.

Ghafouri-Fard, S. *et al.* (2023) 'A review on the role of ZEB1-AS1 in human disorders', *Pathology - Research and Practice*, 245, p. 154486. Available at: https://doi.org/10.1016/j.prp.2023.154486.

Girling, J.E. and Rogers, P.A.W. (2009) 'Regulation of endometrial vascular remodelling: role of the vascular endothelial growth factor family and the angiopoietin–TIE signalling system', *Reproduction*, 138(6), pp. 883–893. Available at: https://doi.org/10.1530/REP-09-0147.

Glass, C.A., Harper, S.J. and Bates, D.O. (2006) 'The anti-angiogenic VEGF isoform VEGF165b transiently increases hydraulic conductivity, probably through VEGF receptor 1 in vivo', *The Journal of Physiology*, 572(1), pp. 243–257. Available at: https://doi.org/10.1113/jphysiol.2005.103127.

Gondkar, K. *et al.* (2019) 'E74 like ETS transcription factor 3 (ELF3) is a negative regulator of epithelial- mesenchymal transition in bladder carcinoma', *Cancer Biomarkers: Section A of Disease Markers*, 25(2), pp. 223–232. Available at: https://doi.org/10.3233/CBM-190013.

Gong, H. *et al.* (2017) 'Endothelial to mesenchymal transition in the cardiovascular system', *Life Sciences*, 184, pp. 95–102. Available at: https://doi.org/10.1016/j.lfs.2017.07.014.

Goumans, M.-J., van Zonneveld, A.J. and ten Dijke, P. (2008) 'Transforming Growth Factor *β*–Induced Endothelial-to-Mesenchymal Transition: A Switch to Cardiac Fibrosis?', *Trends in*

Cardiovascular Medicine, 18(8), pp. 293–298. Available at: https://doi.org/10.1016/j.tcm.2009.01.001.

Goveia, J. *et al.* (2020) 'An Integrated Gene Expression Landscape Profiling Approach to Identify Lung Tumor Endothelial Cell Heterogeneity and Angiogenic Candidates', *Cancer Cell*, 37(1), pp. 21-36.e13. Available at: https://doi.org/10.1016/j.ccell.2019.12.001.

Gresham, R.C.H., Bahney, C.S. and Leach, J.K. (2021) 'Growth factor delivery using extracellular matrix-mimicking substrates for musculoskeletal tissue engineering and repair', *Bioactive Materials*, 6(7), pp. 1945–1956. Available at: https://doi.org/10.1016/j.bioactmat.2020.12.012.

Gu, Z. (2022) 'Complex heatmap visualization', *iMeta*, 1(3), p. e43. Available at: https://doi.org/10.1002/imt2.43.

Guduric-Fuchs, J. *et al.* (2024) 'A new gene signature for endothelial senescence identifies self-RNA sensing by retinoic acid-inducible gene I as a molecular facilitator of vascular aging', *Aging Cell*, 23(9), p. e14240. Available at: https://doi.org/10.1111/acel.14240.

Guier, C.P. *et al.* (2025) 'Posterior Polymorphous Corneal Dystrophy', in *StatPearls*. Treasure Island (FL): StatPearls Publishing. Available at: http://www.ncbi.nlm.nih.gov/books/NBK430880/ (Accessed: 28 March 2025).

Guo, J. *et al.* (2022) 'Aging and aging-related diseases: from molecular mechanisms to interventions and treatments', *Signal Transduction and Targeted Therapy*, 7(1), pp. 1–40. Available at: https://doi.org/10.1038/s41392-022-01251-0.

Guo, T. *et al.* (2024) 'Loss of RNA-binding protein CELF2 promotes acute leukemia development via FAT10-mTORC1', *Oncogene*, 43(19), pp. 1476–1487. Available at: https://doi.org/10.1038/s41388-024-03006-3.

Guo, Y. *et al.* (2024) 'Role of cell rearrangement and related signaling pathways in the dynamic process of tip cell selection', *Cell Communication and Signaling*, 22(1), p. 24. Available at: https://doi.org/10.1186/s12964-023-01364-1.

Gustafsson, T. and Kraus, W.E. (2001) 'Exercise-induced angiogenesis-related growth and transcription factors in skeletal muscle, and their modification in muscle pathology', *Frontiers in Bioscience-Landmark*, 6(3), pp. 75–89. Available at: https://doi.org/10.2741/gustafss.

Haber, M.A. *et al.* (2015) 'ERG is a novel and reliable marker for endothelial cells in central nervous system tumors', *Clinical Neuropathology*, 34(3), pp. 117–127. Available at: https://doi.org/10.5414/NP300817.

Hahne, F. and Ivanek, R. (2016) 'Visualizing Genomic Data Using Gviz and Bioconductor', *Methods in Molecular Biology (Clifton, N.J.)*, 1418, pp. 335–351. Available at: https://doi.org/10.1007/978-1-4939-3578-9_16.

Hall, I.F. *et al.* (2024) 'Endothelial to mesenchymal transition: at the axis of cardiovascular health and disease', *Cardiovascular Research*, 120(3), pp. 223–236. Available at: https://doi.org/10.1093/cvr/cvae021.

Hanahan, D. and Folkman, J. (1996) 'Patterns and Emerging Mechanisms of the Angiogenic Switch during Tumorigenesis', *Cell*, 86(3), pp. 353–364. Available at: https://doi.org/10.1016/S0092-8674(00)80108-7.

Hanahan, D. and Weinberg, R.A. (2011) 'Hallmarks of Cancer: The Next Generation', *Cell*, 144(5), pp. 646–674. Available at: https://doi.org/10.1016/j.cell.2011.02.013.

Hannemann, N. *et al.* (2017) 'The AP-1 Transcription Factor c-Jun Promotes Arthritis by Regulating Cyclooxygenase-2 and Arginase-1 Expression in Macrophages', *The Journal of Immunology*, 198(9), pp. 3605–3614. Available at: https://doi.org/10.4049/jimmunol.1601330.

Hansen, K.D. *et al.* (2011) 'Sequencing technology does not eliminate biological variability', *Nature biotechnology*, 29(7), pp. 572–573. Available at: https://doi.org/10.1038/nbt.1910.

Hao, Y. *et al.* (2024) 'Dictionary learning for integrative, multimodal and scalable single-cell analysis', *Nature Biotechnology*, 42(2), pp. 293–304. Available at: https://doi.org/10.1038/s41587-023-01767-y.

Harel, S. *et al.* (2021) 'ETS1, ELK1, and ETV4 Transcription Factors Regulate Angiopoietin-1 Signaling and the Angiogenic Response in Endothelial Cells', *Frontiers in Physiology*, 12. Available at: https://doi.org/10.3389/fphys.2021.683651.

He, Q. *et al.* (2021) 'Biological Functions and Regulatory Mechanisms of Hypoxia-Inducible Factor-1α in Ischemic Stroke', *Frontiers in Immunology*, 12. Available at: https://doi.org/10.3389/fimmu.2021.801985.

Heberle, H. *et al.* (2015) 'InteractiVenn: a web-based tool for the analysis of sets through Venn diagrams', *BMC Bioinformatics*, 16(1), p. 169. Available at: https://doi.org/10.1186/s12859-015-0611-3.

Heinz, S. *et al.* (2010) 'Simple Combinations of Lineage-Determining Transcription Factors Prime cis-Regulatory Elements Required for Macrophage and B Cell Identities', *Molecular Cell*, 38(4), pp. 576–589. Available at: https://doi.org/10.1016/j.molcel.2010.05.004.

Hellström, M. *et al.* (2007) 'Dll4 signalling through Notch1 regulates formation of tip cells during angiogenesis', *Nature*, 445(7129), pp. 776–780. Available at: https://doi.org/10.1038/nature05571.

Heloterä, H. and Kaarniranta, K. (2022) 'A Linkage between Angiogenesis and Inflammation in Neovascular Age-Related Macular Degeneration', *Cells*, 11(21), p. 3453. Available at: https://doi.org/10.3390/cells11213453.

Herbert, S.P. and Stainier, D.Y.R. (2011a) 'Molecular control of endothelial cell behaviour during blood vessel morphogenesis', *Nature Reviews Molecular Cell Biology*, 12(9), pp. 551–564. Available at: https://doi.org/10.1038/nrm3176.

Herbert, S.P. and Stainier, D.Y.R. (2011b) 'Molecular control of endothelial cell behaviour during blood vessel morphogenesis', *Nature Reviews Molecular Cell Biology*, 12(9), pp. 551–564. Available at: https://doi.org/10.1038/nrm3176.

Hervé Pagès *et al.* (2023) 'AnnotationDbi: Manipulation of SQLite-based annotations in Bioconductor'. Available at: https://bioconductor.org/packages/AnnotationDbi.

Hillen, F. and Griffioen, A.W. (2007) 'Tumour vascularization: sprouting angiogenesis and beyond', *Cancer Metastasis Reviews*, 26(3–4), pp. 489–502. Available at: https://doi.org/10.1007/s10555-007-9094-7.

Ho, V.C. *et al.* (2012) 'Elevated Vascular Endothelial Growth Factor Receptor-2 Abundance Contributes to Increased Angiogenesis in Vascular Endothelial Growth Factor Receptor-1–Deficient Mice', *Circulation*, 126(6), pp. 741–752. Available at: https://doi.org/10.1161/CIRCULATIONAHA.112.091603.

Hodges, N.A., Suarez-Martinez, A.D. and Murfee, W.L. (2018) 'Understanding angiogenesis during aging: opportunities for discoveries and new models', *Journal of Applied Physiology*, 125(6), pp. 1843–1850. Available at: https://doi.org/10.1152/japplphysiol.00112.2018.

Höllbacher, B. *et al.* (2020) 'Seq-ing answers: Current data integration approaches to uncover mechanisms of transcriptional regulation', *Computational and Structural Biotechnology Journal*, 18, pp. 1330–1341. Available at: https://doi.org/10.1016/j.csbj.2020.05.018.

Hong, L. *et al.* (2020) 'Semaphorin 7A promotes endothelial to mesenchymal transition through ATF3 mediated TGF-β2/Smad signaling', *Cell Death & Disease*, 11(8), p. 695. Available at: https://doi.org/10.1038/s41419-020-02818-x.

Hong, X. *et al.* (2016) 'Reprogramming towards endothelial cells for vascular regeneration', *Genes & Diseases*, 3(3), pp. 186–197. Available at: https://doi.org/10.1016/j.gendis.2016.02.003.

Horiguchi, K. *et al.* (2012) 'TGF-β drives epithelial-mesenchymal transition through δEF1-mediated downregulation of ESRP', *Oncogene*, 31(26), pp. 3190–3201. Available at: https://doi.org/10.1038/onc.2011.493.

Hu, X. *et al.* (2014) 'KCTD10 is critical for heart and blood vessel development of zebrafish', *Acta Biochimica et Biophysica Sinica*, 46(5), pp. 377–386. Available at: https://doi.org/10.1093/abbs/gmu017.

Huang, K. *et al.* (2025) 'Angiogenesis during diabetic wound repair: from mechanism to therapy opportunity', *Burns & Trauma*, 13, p. tkae052. Available at: https://doi.org/10.1093/burnst/tkae052.

Huang, M. *et al.* (2004) 'Discovering patterns to extract protein-protein interactions from full biomedical texts', in *Proceedings of the International Joint Workshop on Natural Language Processing in Biomedicine and its Applications - JNLPBA '04*. *the International Joint Workshop*, Geneva, Switzerland: Association for Computational Linguistics, p. 22. Available at: https://doi.org/10.3115/1567594.1567599.

Hultgren, N.W. *et al.* (2020) 'Slug regulates the Dll4-Notch-VEGFR2 axis to control endothelial cell activation and angiogenesis', *Nature Communications*, 11(1), p. 5400. Available at: https://doi.org/10.1038/s41467-020-18633-z.

Ianevski, A., Giri, A.K. and Aittokallio, T. (2022) 'Fully-automated and ultra-fast cell-type identification using specific marker combinations from single-cell transcriptomic data', *Nature Communications*, 13(1), p. 1246. Available at: https://doi.org/10.1038/s41467-022-28803-w.

Inampudi, C. *et al.* (2018) 'Angiogenesis in peripheral arterial disease', *Current Opinion in Pharmacology*, 39, pp. 60–67. Available at: https://doi.org/10.1016/j.coph.2018.02.011.

J Larsson (2024) 'eulerr: Area-Proportional Euler and Venn Diagrams with Ellipses'. Available at: https://CRAN.R-project.org/package=eulerr.

Jain, R.K. (2003) 'Molecular regulation of vessel maturation', *Nature Medicine*, 9(6), pp. 685–693. Available at: https://doi.org/10.1038/nm0603-685.

Jain, R.K. (2005) 'Normalization of Tumor Vasculature: An Emerging Concept in Antiangiogenic Therapy', *Science*, 307(5706), pp. 58–62. Available at: https://doi.org/10.1126/science.1104819.

Jalkanen, S. and Salmi, M. (2020) 'Lymphatic endothelial cells of the lymph node', *Nature Reviews Immunology*, 20(9), pp. 566–578. Available at: https://doi.org/10.1038/s41577-020-0281-x.

Janky, R. *et al.* (2014) 'iRegulon: From a Gene List to a Gene Regulatory Network Using Large Motif and Track Collections', *PLoS Computational Biology*, 10(7), p. e1003731. Available at: https://doi.org/10.1371/journal.pcbi.1003731.

Jensen, L.J. (2016) 'One tagger, many uses: Illustrating the power of ontologies in dictionary-based named entity recognition', *CEUR Workshop Proceedings*, 1747.

Jensen, L.J. (2024) 'larsjuhljensen/tagger'. Available at: https://github.com/larsjuhljensen/tagger (Accessed: 11 December 2024).

Ji, H. *et al.* (2023) 'CXCL8 Promotes Endothelial-to-Mesenchymal Transition of Endothelial Cells and Protects Cells from Erastin-Induced Ferroptosis via CXCR2-Mediated Activation of the NF-κB Signaling Pathway', *Pharmaceuticals*, 16(9), p. 1210. Available at: https://doi.org/10.3390/ph16091210.

Ji, L. *et al.* (2021) 'Neurovascular regulation in diabetic retinopathy and emerging therapies', *Cellular and Molecular Life Sciences: CMLS*, 78(16), pp. 5977–5985. Available at: https://doi.org/10.1007/s00018-021-03893-9.

Jia, J. *et al.* (2016) 'AP-1 transcription factor mediates VEGF-induced endothelial cell migration and proliferation', *Microvascular research*, 105, pp. 103–108. Available at: https://doi.org/10.1016/j.mvr.2016.02.004.

Jia, M. *et al.* (2022) 'Deletion of BACH1 Attenuates Atherosclerosis by Reducing Endothelial Inflammation', *Circulation Research*, 130(7), pp. 1038–1055. Available at: https://doi.org/10.1161/CIRCRESAHA.121.319540.

Jia, W. *et al.* (2021) 'Trajectory modeling of endothelial-to-mesenchymal transition reveals galectin-3 as a mediator in pulmonary fibrosis', *Cell Death & Disease*, 12(4), pp. 1–14. Available at: https://doi.org/10.1038/s41419-021-03603-0.

Jiang, L. *et al.* (2020) 'Bach1-induced suppression of angiogenesis is dependent on the BTB domain', *eBioMedicine*, 51. Available at: https://doi.org/10.1016/j.ebiom.2019.102617.

Jiang, S. and Mortazavi, A. (2018) 'Integrating ChIP-seq with other functional genomics data', *Briefings in Functional Genomics*, 17(2), pp. 104–115. Available at: https://doi.org/10.1093/bfgp/ely002.

Jin, L. *et al.* (2020) 'Zeb1 promotes corneal neovascularization by regulation of vascular endothelial cell proliferation', *Communications Biology*, 3(1), pp. 1–10. Available at: https://doi.org/10.1038/s42003-020-1069-z.

Jordanovski, D. *et al.* (2013) 'The Hypoxia-Inducible Transcription Factor ZNF395 Is Controlled by IκB Kinase-Signaling and Activates Genes Involved in the Innate Immune Response and Cancer', *PLOS ONE*, 8(9), p. e74911. Available at: https://doi.org/10.1371/journal.pone.0074911.

Jourde-Chiche, N. *et al.* (2019) 'Endothelium structure and function in kidney health and disease', *Nature Reviews Nephrology*, 15(2), pp. 87–108. Available at: https://doi.org/10.1038/s41581-018-0098-z.

Kadl, A. and Leitinger, N. (2005) 'The role of endothelial cells in the resolution of acute inflammation', *Antioxidants & Redox Signaling*, 7(11–12), pp. 1744–1754. Available at: https://doi.org/10.1089/ars.2005.7.1744.

Kalna, V. *et al.* (2019) 'The Transcription Factor ERG Regulates Super-Enhancers Associated With an Endothelial-Specific Gene Expression Program', *Circulation Research*, 124(9), pp. 1337–1349. Available at: https://doi.org/10.1161/CIRCRESAHA.118.313788.

Kalucka, J. *et al.* (2018) 'Quiescent Endothelial Cells Upregulate Fatty Acid β-Oxidation for Vasculoprotection via Redox Homeostasis', *Cell Metabolism*, 28(6), pp. 881-894.e13. Available at: https://doi.org/10.1016/j.cmet.2018.07.016.

Kalucka, J. *et al.* (2020) 'Single-Cell Transcriptome Atlas of Murine Endothelial Cells', *Cell*, 180(4), pp. 764-779.e20. Available at: https://doi.org/10.1016/j.cell.2020.01.015.

Kaluza, D. *et al.* (2013) 'Histone Deacetylase 9 Promotes Angiogenesis by Targeting the Antiangiogenic MicroRNA-17–92 Cluster in Endothelial Cells', *Arteriosclerosis, Thrombosis, and Vascular Biology*, 33(3), pp. 533–543. Available at: https://doi.org/10.1161/ATVBAHA.112.300415.

Kanehisa, M. (2019) 'Toward understanding the origin and evolution of cellular organisms', *Protein Science*, 28(11), pp. 1947–1951. Available at: https://doi.org/10.1002/pro.3715.

Kanehisa, M. *et al.* (2023) 'KEGG for taxonomy-based analysis of pathways and genomes', *Nucleic Acids Research*, 51(D1), pp. D587–D592. Available at: https://doi.org/10.1093/nar/gkac963.

Kanehisa, M. and Goto, S. (2000) 'KEGG: Kyoto Encyclopedia of Genes and Genomes', *Nucleic Acids Research*, 28(1), pp. 27–30. Available at: https://doi.org/10.1093/nar/28.1.27.

Kans, J. (2024) 'Entrez Direct: E-utilities on the Unix Command Line', in *Entrez Programming Utilities Help [Internet]*. National Center for Biotechnology Information (US). Available at: https://www.ncbi.nlm.nih.gov/books/NBK179288/ (Accessed: 11 December 2024).

Katsura, A. *et al.* (2017) 'ZEB1-regulated inflammatory phenotype in breast cancer cells', *Molecular Oncology*, 11(9), pp. 1241–1262. Available at: https://doi.org/10.1002/1878-0261.12098.

Kaur, G. *et al.* (2023) 'Vascular cell-adhesion molecule 1 (VCAM-1) regulates JunB-mediated IL-8/CXCL1 expression and pathological neovascularization', *Communications Biology*, 6(1), p. 516. Available at: https://doi.org/10.1038/s42003-023-04905-z.

Kaya-Okur, H.S. *et al.* (2019) 'CUT&Tag for efficient epigenomic profiling of small samples and single cells', *Nature Communications*, 10(1), p. 1930. Available at: https://doi.org/10.1038/s41467-019-09982-5.

Kharchenko, P.V. (2021) 'The triumphs and limitations of computational methods for scRNA-seq', *Nature Methods*, 18(7), pp. 723–732. Available at: https://doi.org/10.1038/s41592-021-01171-x.

Kim, T.H. and Dekker, J. (2018) 'ChIP–Quantitative Polymerase Chain Reaction (ChIP-qPCR)', *Cold Spring Harbor Protocols*, 2018(5), p. pdb.prot082628. Available at: https://doi.org/10.1101/pdb.prot082628.

Kissane, R.W. and Egginton, S. (2019) 'Exercise-mediated angiogenesis', *Current Opinion in Physiology*, 10, pp. 193–201. Available at: https://doi.org/10.1016/j.cophys.2019.06.005.

Koenig, A.L. *et al.* (2022) 'Single-cell transcriptomics reveals cell-type-specific diversification in human heart failure', *Nature Cardiovascular Research*, 1(3), pp. 263–280. Available at: https://doi.org/10.1038/s44161-022-00028-6.

Kong, D.-H. *et al.* (2018) 'Emerging Roles of Vascular Cell Adhesion Molecule-1 (VCAM-1) in Immunological Disorders and Cancer', *International Journal of Molecular Sciences*, 19(4), p. 1057. Available at: https://doi.org/10.3390/ijms19041057.

Korn, C. and Augustin, H.G. (2015) 'Mechanisms of Vessel Pruning and Regression', *Developmental Cell*, 34(1), pp. 5–17. Available at: https://doi.org/10.1016/j.devcel.2015.06.004.

Kovacic, J.C. *et al.* (2012) 'Epithelial-to-Mesenchymal and Endothelial-to-Mesenchymal Transition', *Circulation*, 125(14), pp. 1795–1808. Available at: https://doi.org/10.1161/CIRCULATIONAHA.111.040352.

Kovacic, J.C. *et al.* (2019) 'Endothelial to Mesenchymal Transition in Cardiovascular Disease', *Journal of the American College of Cardiology*, 73(2), pp. 190–209. Available at: https://doi.org/10.1016/j.jacc.2018.09.089.

Krebs, A.M. *et al.* (2017) 'The EMT-activator Zeb1 is a key factor for cell plasticity and promotes metastasis in pancreatic cancer', *Nature Cell Biology*, 19(5), pp. 518–529. Available at: https://doi.org/10.1038/ncb3513.

Krishnamoorthi, M.K. *et al.* (2022) 'An In Vitro Platform to Study Reversible Endothelial-to-Mesenchymal Transition', *Frontiers in Pharmacology*, 13. Available at: https://doi.org/10.3389/fphar.2022.912660.

Krueger, J. *et al.* (2011) 'Flt1 acts as a negative regulator of tip cell formation and branching morphogenesis in the zebrafish embryo', *Development*, 138(10), pp. 2111–2120. Available at: https://doi.org/10.1242/dev.063933.

Kur, J., Newman, E.A. and Chan-Ling, T. (2012) 'Cellular and physiological mechanisms underlying blood flow regulation in the retina and choroid in health and disease', *Progress in Retinal and Eye Research*, 31(5), pp. 377–406. Available at: https://doi.org/10.1016/j.preteyeres.2012.04.004.

Laan, S.N.J. *et al.* (2024) 'Endothelial colony-forming cells in the spotlight: insights into the pathophysiology of von Willebrand disease and rare bleeding disorders', *Journal of Thrombosis and Haemostasis*, 22(12), pp. 3355–3365. Available at: https://doi.org/10.1016/j.jtha.2024.08.011.

Lähteenvuo, J. and Rosenzweig, A. (2012) 'Effects of Aging on Angiogenesis', *Circulation Research*, 110(9), pp. 1252–1264. Available at: https://doi.org/10.1161/CIRCRESAHA.111.246116.

Lamalice, L., Le Boeuf, F. and Huot, J. (2007) 'Endothelial Cell Migration During Angiogenesis', *Circulation Research*, 100(6), pp. 782–794. Available at: https://doi.org/10.1161/01.RES.0000259593.07661.1e.

Lambert, S.A. *et al.* (2018) 'The Human Transcription Factors', *Cell*, 172(4), pp. 650–665. Available at: https://doi.org/10.1016/j.cell.2018.01.029.

Lan, H. *et al.* (2022) 'Pro-angiogenic role of ZEB1 in skin wound healing by upregulating VEGFA via microRNA-206 suppression', *Experimental Dermatology*, 31(9), pp. 1392–1401. Available at: https://doi.org/10.1111/exd.14607.

Landt, S.G. *et al.* (2012) 'ChIP-seq guidelines and practices of the ENCODE and modENCODE consortia', *Genome Research*, 22(9), pp. 1813–1831. Available at: https://doi.org/10.1101/gr.136184.111.

Langmead, B. and Salzberg, S.L. (2012) 'Fast gapped-read alignment with Bowtie 2', *Nature methods*, 9(4), pp. 357–359. Available at: https://doi.org/10.1038/nmeth.1923.

Larsen, J.E. *et al.* (2016) 'ZEB1 drives epithelial-to-mesenchymal transition in lung cancer', *The Journal of Clinical Investigation*, 126(9), pp. 3219–3235. Available at: https://doi.org/10.1172/JCI76725.

Laschke, M.W., Gu, Y. and Menger, M.D. (2022) 'Replacement in angiogenesis research: Studying mechanisms of blood vessel development by animal-free in vitro, in vivo and in

silico approaches', *Frontiers in Physiology*, 13. Available at: https://doi.org/10.3389/fphys.2022.981161.

Lebas, M. *et al.* (2024) 'Integrated single-cell RNA-seq analysis reveals mitochondrial calcium signaling as a modulator of endothelial-to-mesenchymal transition', *Science Advances*, 10(32), p. eadp6182. Available at: https://doi.org/10.1126/sciadv.adp6182.

Lecce, L. *et al.* (2021) 'Histone deacetylase 9 promotes endothelial-mesenchymal transition and an unfavorable atherosclerotic plaque phenotype', *The Journal of Clinical Investigation*, 131(15), p. e131178. Available at: https://doi.org/10.1172/JCI131178.

Leclech, C., Natale, C.F. and Barakat, A.I. (2020) 'The basement membrane as a structured surface – role in vascular health and disease', *Journal of Cell Science*, 133(18), p. jcs239889. Available at: https://doi.org/10.1242/jcs.239889.

Lee, H.-W. *et al.* (2023) 'BMPR1A promotes ID2-ZEB1 interaction to suppress excessive endothelial to mesenchymal transition', *Cardiovascular Research*, 119(3), pp. 813–825. Available at: https://doi.org/10.1093/cvr/cvac159.

Lee, J. *et al.* (2020) 'ZEB1 Mediates Fibrosis in Corneal Endothelial Mesenchymal Transition Through SP1 and SP3', *Investigative Ophthalmology & Visual Science*, 61(8), p. 41. Available at: https://doi.org/10.1167/iovs.61.8.41.

Lee, J., Jung, E. and Heur, M. (2019) *Injury induces endothelial to mesenchymal transition in the mouse corneal endothelium in vivo via FGF2*. Molecular Vision. Available at: http://www.molvis.org/molvis/v25/22/ (Accessed: 17 December 2024).

Lee, J.H. *et al.* (2008) 'Interferon regulatory factor-1 (IRF-1) regulates VEGF-induced angiogenesis in HUVECs', *Biochimica et Biophysica Acta (BBA) - Molecular Cell Research*, 1783(9), pp. 1654–1662. Available at: https://doi.org/10.1016/j.bbamcr.2008.04.006.

Lei, X. *et al.* (2020) 'Identification of a novel tumor angiogenesis inhibitor targeting Shh/Gli1 signaling pathway in Non-small cell lung cancer', *Cell Death & Disease*, 11(4), pp. 1–13. Available at: https://doi.org/10.1038/s41419-020-2425-0.

Levitsky, V.G. *et al.* (2014) 'Application of experimentally verified transcription factor binding sites models for computational analysis of ChIP-Seq data', *BMC Genomics*, 15(1), p. 80. Available at: https://doi.org/10.1186/1471-2164-15-80.

Lewis, S.M., Williams, A. and Eisenbarth, S.C. (2019) 'Structure-function of the immune system in the spleen', *Science immunology*, 4(33), p. eaau6085. Available at: https://doi.org/10.1126/sciimmunol.aau6085.

Li, L. *et al.* (2019) 'HN1L-mediated transcriptional axis AP-2γ/METTL13/TCF3-ZEB1 drives tumor growth and metastasis in hepatocellular carcinoma', *Cell Death & Differentiation*, 26(11), pp. 2268–2283. Available at: https://doi.org/10.1038/s41418-019-0301-1.

Li, M. *et al.* (2015) 'A Novel Approach for Protein-Named Entity Recognition and Protein-Protein Interaction Extraction', *Mathematical Problems in Engineering*, 2015, p. e942435. Available at: https://doi.org/10.1155/2015/942435.

Li, Q. *et al.* (2011) 'Measuring reproducibility of high-throughput experiments', *The Annals of Applied Statistics*, 5(3), pp. 1752–1779. Available at: https://doi.org/10.1214/11-AOAS466.

Li, W. *et al.* (2021) 'Alterations in the spatiotemporal expression of the chemokine receptor CXCR4 in endothelial cells cause failure of hierarchical vascular branching', *Developmental Biology*, 477, pp. 70–84. Available at: https://doi.org/10.1016/j.ydbio.2021.05.008.

Li, X. *et al.* (2010) 'A mouse protein interactome through combined literature mining with multiple sources of interaction evidence', *Amino Acids*, 38(4), pp. 1237–1252. Available at: https://doi.org/10.1007/s00726-009-0335-7.

Li, X. *et al.* (2022) 'The SETD8/ELK1/bach1 complex regulates hyperglycaemia-mediated EndMT in diabetic nephropathy', *Journal of Translational Medicine*, 20(1), p. 147. Available at: https://doi.org/10.1186/s12967-022-03352-4.

Li, X., Sun, X. and Carmeliet, P. (2019) 'Hallmarks of Endothelial Cell Metabolism in Health and Disease', *Cell Metabolism*, 30(3), pp. 414–433. Available at: https://doi.org/10.1016/j.cmet.2019.08.011.

Li, Y. *et al.* (2019) 'Dual Roles of the AMP-Activated Protein Kinase Pathway in Angiogenesis', *Cells*, 8(7), p. 752. Available at: https://doi.org/10.3390/cells8070752.

Li, Z. *et al.* (2019) 'Single-cell transcriptome analyses reveal novel targets modulating cardiac neovascularization by resident endothelial cells following myocardial infarction', *European Heart Journal*, 40(30), pp. 2507–2520. Available at: https://doi.org/10.1093/eurheartj/ehz305.

Li, Z.-D. *et al.* (2005) 'VEGF induces proliferation, migration, and TGF-β1 expression in mouse glomerular endothelial cells via mitogen-activated protein kinase and phosphatidylinositol 3-kinase', *Biochemical and Biophysical Research Communications*, 334(4), pp. 1049–1060. Available at: https://doi.org/10.1016/j.bbrc.2005.07.005.

Liao, Y., Smyth, G.K. and Shi, W. (2014) 'featureCounts: an efficient general purpose program for assigning sequence reads to genomic features', *Bioinformatics*, 30(7), pp. 923–930. Available at: https://doi.org/10.1093/bioinformatics/btt656.

Lin, K.-C. *et al.* (2023) 'Jagged/Notch proteins promote endothelial-mesenchymal transition-mediated pulmonary arterial hypertension via upregulation of the expression of GATAs', *Journal of Cellular and Molecular Medicine*, 27(8), pp. 1110–1130. Available at: https://doi.org/10.1111/jcmm.17723.

Lin, Q.-Q. *et al.* (2018) 'Roles of notch signaling pathway and endothelial-mesenchymal transition in vascular endothelial dysfunction and atherosclerosis', *European Review for Medical and Pharmacological Sciences*, 22(19), pp. 6485–6491. Available at: https://doi.org/10.26355/eurrev_201810_16062.

Lindholm, M.E. *et al.* (2014) 'The human skeletal muscle transcriptome: sex differences, alternative splicing, and tissue homogeneity assessed with RNA sequencing', *The FASEB Journal*, 28(10), pp. 4571–4581. Available at: https://doi.org/10.1096/fj.14-255000.

Lindner, P. *et al.* (2020) 'EMT transcription factor ZEB1 alters the epigenetic landscape of colorectal cancer cells', *Cell Death & Disease*, 11(2), pp. 1–13. Available at: https://doi.org/10.1038/s41419-020-2340-4.

Liu, B.-W. *et al.* (2023) 'The p53/ZEB1-PLD3 feedback loop regulates cell proliferation in breast cancer', *Cell Death & Disease*, 14(11), p. 751. Available at: https://doi.org/10.1038/s41419-023-06271-4.

Liu, L. *et al.* (2016) 'ZEB1 Upregulates VEGF Expression and Stimulates Angiogenesis in Breast Cancer', *PLoS ONE*, 11(2), p. e0148774. Available at: https://doi.org/10.1371/journal.pone.0148774.

Liu, L. and Shi, G.-P. (2012) 'CD31: beyond a marker for endothelial cells', *Cardiovascular Research*, 94(1), pp. 3–5. Available at: https://doi.org/10.1093/cvr/cvs108.

Liu, Y. *et al.* (2024) 'Recent advances in endothelial colony-forming cells: from the transcriptomic perspective', *Journal of Translational Medicine*, 22(1), p. 313. Available at: https://doi.org/10.1186/s12967-024-05108-8.

Liu, Z. *et al.* (2023) 'Insights gained from single-cell RNA analysis of murine endothelial cells in aging hearts', *Heliyon*, 9(8), p. e18324. Available at: https://doi.org/10.1016/j.heliyon.2023.e18324.

Lobov, I. and Mikhailova, N. (2018) 'The Role of Dll4/Notch Signaling in Normal and Pathological Ocular Angiogenesis: Dll4 Controls Blood Vessel Sprouting and Vessel Remodeling in Normal and Pathological Conditions', *Journal of Ophthalmology*, 2018(1), p. 3565292. Available at: https://doi.org/10.1155/2018/3565292.

Long, H. *et al.* (2023) 'Endothelial cells adopt a pro-reparative immune responsive signature during cardiac injury', *Life Science Alliance*, 7(2), p. e202201870. Available at: https://doi.org/10.26508/lsa.202201870.

Lopes-Coelho, F. *et al.* (2021) 'Anti-Angiogenic Therapy: Current Challenges and Future Perspectives', *International Journal of Molecular Sciences*, 22(7), p. 3765. Available at: https://doi.org/10.3390/ijms22073765.

Love, M.I., Huber, W. and Anders, S. (2014) 'Moderated estimation of fold change and dispersion for RNA-seq data with DESeq2', *Genome Biology*, 15(12), p. 550. Available at: https://doi.org/10.1186/s13059-014-0550-8.

Lu, C. *et al.* (2007) 'Gene Alterations Identified by Expression Profiling in Tumor-Associated Endothelial Cells from Invasive Ovarian Carcinoma', *Cancer Research*, 67(4), pp. 1757–1768. Available at: https://doi.org/10.1158/0008-5472.CAN-06-3700.

Lu, D. *et al.* (2023) 'Endothelial-to-mesenchymal transition: New insights into vascular calcification', *Biochemical Pharmacology*, 213, p. 115579. Available at: https://doi.org/10.1016/j.bcp.2023.115579.

Lu, J. *et al.* (2022) 'ZEB1: Catalyst of immune escape during tumor metastasis', *Biomedicine & Pharmacotherapy*, 153, p. 113490. Available at: https://doi.org/10.1016/j.biopha.2022.113490.

Lu, X. *et al.* (2019) 'Endothelial-to-mesenchymal transition: pathogenesis and therapeutic targets for chronic pulmonary and vascular diseases', *Biochemical pharmacology*, 168, pp. 100–107. Available at: https://doi.org/10.1016/j.bcp.2019.06.021.

Luk, C. *et al.* (2022) 'Paracrine Role of the Endothelium in Metabolic Homeostasis in Health and Nutrient Excess', *Frontiers in Cardiovascular Medicine*, 9. Available at: https://doi.org/10.3389/fcvm.2022.882923.

Ma, J. *et al.* (2020) 'TGF-β-Induced Endothelial to Mesenchymal Transition in Disease and Tissue Engineering', *Frontiers in Cell and Developmental Biology*, 8, p. 260. Available at: https://doi.org/10.3389/fcell.2020.00260.

Machanick, P. and Bailey, T.L. (2011) 'MEME-ChIP: motif analysis of large DNA datasets', *Bioinformatics*, 27(12), pp. 1696–1697. Available at: https://doi.org/10.1093/bioinformatics/btr189.

Mack, J.J. and Iruela-Arispe, M.L. (2018) 'NOTCH regulation of the endothelial cell phenotype', *Current Opinion in Hematology*, 25(3), pp. 212–218. Available at: https://doi.org/10.1097/MOH.0000000000000425.

Madoiwa, S. (2015) 'Recent advances in disseminated intravascular coagulation: endothelial cells and fibrinolysis in sepsis-induced DIC', *Journal of Intensive Care*, 3, p. 8. Available at: https://doi.org/10.1186/s40560-015-0075-6.

MAEDA, H. (2012) 'Vascular permeability in cancer and infection as related to macromolecular drug delivery, with emphasis on the EPR effect for tumor-selective drug targeting', *Proceedings of the Japan Academy. Series B, Physical and Biological Sciences*, 88(3), pp. 53–71. Available at: https://doi.org/10.2183/pjab.88.53.

Malagoli Tagliazucchi, G. *et al.* (2023) 'Genomic and microenvironmental heterogeneity shaping epithelial-to-mesenchymal trajectories in cancer', *Nature Communications*, 14(1), p. 789. Available at: https://doi.org/10.1038/s41467-023-36439-7.

Malhotra, D. *et al.* (2012) 'Transcriptional profiling of stroma from inflamed and resting lymph nodes defines immunological hallmarks', *Nature immunology*, 13(5), pp. 499–510. Available at: https://doi.org/10.1038/ni.2262.

Markwald, R.R., Fitzharris, T.P. and Smith, W.N.A. (1975) 'Structural analysis of endocardial cytodifferentiation', *Developmental Biology*, 42(1), pp. 160–180. Available at: https://doi.org/10.1016/0012-1606(75)90321-8.

Marques-Coelho, D. *et al.* (2021) 'Differential transcript usage unravels gene expression alterations in Alzheimer's disease human brains', *npj Aging and Mechanisms of Disease*, 7(1), pp. 1–15. Available at: https://doi.org/10.1038/s41514-020-00052-5.

Marsh, S. (2021) 'scCustomize: Custom Visualizations & Functions for Streamlined Analyses of Single Cell Sequencing.' Available at: https://doi.org/RRID:SCR_024675.

Martin, M. (2011) 'Cutadapt removes adapter sequences from high-throughput sequencing reads', *EMBnet.journal*, 17(1), pp. 10–12. Available at: https://doi.org/10.14806/ej.17.1.200.

Martín-Bórnez, M. *et al.* (2023) 'New Insights into the Reparative Angiogenesis after Myocardial Infarction', *International Journal of Molecular Sciences*, 24(15), p. 12298. Available at: https://doi.org/10.3390/ijms241512298.

Matsuda, K. *et al.* (2017) 'ChIP-seq analysis of genomic binding regions of five major transcription factors highlights a central role for ZIC2 in the mouse epiblast stem cell gene regulatory network', *Development (Cambridge, England)*, 144(11), pp. 1948–1958. Available at: https://doi.org/10.1242/dev.143479.

Maturi, V. *et al.* (2018) 'Genome–wide binding of transcription factor ZEB1 in triple-negative breast cancer cells', *Journal of Cellular Physiology*, 233(10), pp. 7113–7127. Available at: https://doi.org/10.1002/jcp.26634.

McCracken, I.R. *et al.* (2022) 'Mapping the developing human cardiac endothelium at single-cell resolution identifies MECOM as a regulator of arteriovenous gene expression', *Cardiovascular Research*, 118(14), pp. 2960–2972. Available at: https://doi.org/10.1093/cvr/cvac023.

McDonald, A.I. *et al.* (2018) 'Endothelial Regeneration of Large Vessels Is a Biphasic Process Driven by Local Cells with Distinct Proliferative Capacities', *Cell Stem Cell*, 23(2), pp. 210-225.e6. Available at: https://doi.org/10.1016/j.stem.2018.07.011.

Mebius, R.E. and Kraal, G. (2005) 'Structure and function of the spleen', *Nature Reviews Immunology*, 5(8), pp. 606–616. Available at: https://doi.org/10.1038/nri1669.

Medici, D., Potenta, S. and Kalluri, R. (2011) 'Transforming growth factor-β2 promotes Snail-mediated endothelial–mesenchymal transition through convergence of Smad-dependent and Smad-independent signalling', *Biochemical Journal*, 437(3), pp. 515–520. Available at: https://doi.org/10.1042/BJ20101500.

Medina, R.J. *et al.* (2010) 'Molecular analysis of endothelial progenitor cell (EPC) subtypes reveals two distinct cell populations with different identities', *BMC Medical Genomics*, 3, p. 18. Available at: https://doi.org/10.1186/1755-8794-3-18.

Medina, R.J. *et al.* (2017) 'Endothelial Progenitors: A Consensus Statement on Nomenclature', *Stem Cells Translational Medicine*, 6(5), pp. 1316–1320. Available at: https://doi.org/10.1002/sctm.16-0360.

van Meeteren, L.A. and ten Dijke, P. (2012) 'Regulation of endothelial cell plasticity by TGF-β', *Cell and Tissue Research*, 347(1), pp. 177–186. Available at: https://doi.org/10.1007/s00441-011-1222-6.

Meng, Z. *et al.* (2023) 'Bach1 modulates AKT3 transcription to participate in hyperglycaemia-mediated EndMT in vascular endothelial cells', *Clinical and Experimental Pharmacology and Physiology*, 50(6), pp. 443–452. Available at: https://doi.org/10.1111/1440-1681.13759.

Meyer, C.A. and Liu, X.S. (2014) 'Identifying and mitigating bias in next-generation sequencing methods for chromatin biology', *Nature Reviews Genetics*, 15(11), pp. 709–721. Available at: https://doi.org/10.1038/nrg3788.

Mintet, E. *et al.* (2015) 'Identification of Endothelial-to-Mesenchymal Transition as a Potential Participant in Radiation Proctitis', *The American Journal of Pathology*, 185(9), pp. 2550–2562. Available at: https://doi.org/10.1016/j.ajpath.2015.04.028.

Mirotsou, M. *et al.* (2011) 'Paracrine mechanisms of stem cell reparative and regenerative actions in the heart', *Journal of molecular and cellular cardiology*, 50(2), pp. 280–289. Available at: https://doi.org/10.1016/j.yjmcc.2010.08.005.

Miyamura, Y. *et al.* (2024) 'FOXO1 stimulates tip cell-enriched gene expression in endothelial cells', *iScience*, 27(3), p. 109161. Available at: https://doi.org/10.1016/j.isci.2024.109161.

Moonen, J.-R. *et al.* (2022) 'KLF4 recruits SWI/SNF to increase chromatin accessibility and reprogram the endothelial enhancer landscape under laminar shear stress', *Nature Communications*, 13(1), p. 4941. Available at: https://doi.org/10.1038/s41467-022-32566-9.

Moradi, S.Z. *et al.* (2022) 'Regenerative Medicine and Angiogenesis; Focused on Cardiovascular Disease', *Advanced Pharmaceutical Bulletin*, 12(4), pp. 686–699. Available at: https://doi.org/10.34172/apb.2022.072.

Moriya, J. and Minamino, T. (2017) 'Angiogenesis, Cancer, and Vascular Aging', *Frontiers in Cardiovascular Medicine*, 4, p. 65. Available at: https://doi.org/10.3389/fcvm.2017.00065.

Morris, J.L. *et al.* (2021) 'Bcl-2 Family of Proteins in the Control of Mitochondrial Calcium Signalling: An Old Chap with New Roles', *International Journal of Molecular Sciences*, 22(7), p. 3730. Available at: https://doi.org/10.3390/ijms22073730.

Moya, I.M. *et al.* (2012) 'Stalk Cell Phenotype Depends on Integration of Notch and Smad1/5 Signaling Cascades', *Developmental Cell*, 22(3), pp. 501–514. Available at: https://doi.org/10.1016/j.devcel.2012.01.007.

Muhammad, I.I. *et al.* (2019) 'RNA-seq and ChIP-seq as Complementary Approaches for Comprehension of Plant Transcriptional Regulatory Mechanism', *International Journal of Molecular Sciences*, 21(1), p. 167. Available at: https://doi.org/10.3390/ijms21010167.

Mujagic, E. *et al.* (2013) 'Induction of aberrant vascular growth, but not of normal angiogenesis, by cell-based expression of different doses of human and mouse VEGF is species-dependent', *Human Gene Therapy Methods*, 24(1), pp. 28–37. Available at: https://doi.org/10.1089/hgtb.2012.197.

Muller, W.A. (2011) 'Mechanisms of leukocyte transendothelial migration', *Annual Review of Pathology*, 6, pp. 323–344. Available at: https://doi.org/10.1146/annurev-pathol-011110-130224.

Müller-Dott, S. *et al.* (2023) 'Expanding the coverage of regulons from high-confidence prior knowledge for accurate estimation of transcription factor activities', *Nucleic Acids Research*, 51(20), pp. 10934–10949. Available at: https://doi.org/10.1093/nar/gkad841.

Nagai, N. *et al.* (2018) 'Downregulation of ERG and FLI1 expression in endothelial cells triggers endothelial-to-mesenchymal transition', *PLOS Genetics*, 14(11), p. e1007826. Available at: https://doi.org/10.1371/journal.pgen.1007826.

Nasim, S. *et al.* (2023) 'CD45 Is Sufficient to Initiate Endothelial-to-Mesenchymal Transition in Human Endothelial Cells—Brief Report', *Arteriosclerosis, Thrombosis, and Vascular Biology*, 43(5), pp. e124–e131. Available at: https://doi.org/10.1161/ATVBAHA.122.318172.

Natarajan, J. *et al.* (2006) 'Text mining of full-text journal articles combined with gene expression analysis reveals a relationship between sphingosine-1-phosphate and invasiveness of a glioblastoma cell line', *BMC Bioinformatics*, 7(1), p. 373. Available at: https://doi.org/10.1186/1471-2105-7-373.

Nawaz, I.M. *et al.* (2019) 'Human vitreous in proliferative diabetic retinopathy: Characterization and translational implications', *Progress in Retinal and Eye Research*, 72, p. 100756. Available at: https://doi.org/10.1016/j.preteyeres.2019.03.002.

Neumann, P. *et al.* (2018) 'The lncRNA GATA6-AS epigenetically regulates endothelial gene expression via interaction with LOXL2', *Nature Communications*, 9(1), p. 237. Available at: https://doi.org/10.1038/s41467-017-02431-1.

Nezamuldeen, L. and Jafri, M.S. (2023) 'Protein–Protein Interaction Network Extraction Using Text Mining Methods Adds Insight into Autism Spectrum Disorder', *Biology*, 12(10), p. 1344. Available at: https://doi.org/10.3390/biology12101344.

Ngo, D.T.M. *et al.* (2014) 'Antiangiogenic Actions of Vascular Endothelial Growth Factor-A165b, an Inhibitory Isoform of Vascular Endothelial Growth Factor-A, in Human Obesity', *Circulation*, 130(13), pp. 1072–1080. Available at: https://doi.org/10.1161/CIRCULATIONAHA.113.008171.

Niethamer, T.K. *et al.* (2023) 'Atf3 defines a population of pulmonary endothelial cells essential for lung regeneration', *eLife*, 12, p. e83835. Available at: https://doi.org/10.7554/eLife.83835.

Nieto, M.A. *et al.* (2016) 'EMT: 2016', *Cell*, 166(1), pp. 21–45. Available at: https://doi.org/10.1016/j.cell.2016.06.028.

Nils Gehlenborg (2019) 'UpSetR: A More Scalable Alternative to Venn and Euler Diagrams for Visualizing Intersecting Sets'. Available at: https://CRAN.R-project.org/package=UpSetR.

Noels, H. *et al.* (2014) 'Deficiency of Endothelial Cxcr4 Reduces Reendothelialization and Enhances Neointimal Hyperplasia After Vascular Injury in Atherosclerosis-Prone Mice', *Arteriosclerosis, Thrombosis, and Vascular Biology*, 34(6), pp. 1209–1220. Available at: https://doi.org/10.1161/ATVBAHA.113.302878.

Okonechnikov, K., Conesa, A. and García-Alcalde, F. (2016) 'Qualimap 2: advanced multi-sample quality control for high-throughput sequencing data', *Bioinformatics*, 32(2), pp. 292–294. Available at: https://doi.org/10.1093/bioinformatics/btv566.

Okumura, N. *et al.* (2015) 'Involvement of ZEB1 and Snail1 in excessive production of extracellular matrix in Fuchs endothelial corneal dystrophy', *Laboratory Investigation*, 95(11), pp. 1291–1304. Available at: https://doi.org/10.1038/labinvest.2015.111.

O'Neill, C.L. *et al.* (2018) 'The Vasoreparative Potential of Endothelial Colony Forming Cells: A Journey Through Pre-clinical Studies', *Frontiers in Medicine*, 5. Available at: https://doi.org/10.3389/fmed.2018.00273.

Orozco-García, E. *et al.* (2023) 'Endothelial plasticity across PTEN and Hippo pathways: A complex hormetic rheostat modulated by extracellular vesicles', *Translational Oncology*, 31, p. 101633. Available at: https://doi.org/10.1016/j.tranon.2023.101633.

Osorio, D. *et al.* (2020) 'scTenifoldNet: A Machine Learning Workflow for Constructing and Comparing Transcriptome-wide Gene Regulatory Networks from Single-Cell Data', *Patterns*, 1(9), p. 100139. Available at: https://doi.org/10.1016/j.patter.2020.100139.

Osorio, D. *et al.* (2022) 'scTenifoldKnk: An efficient virtual knockout tool for gene function predictions via single-cell gene regulatory network perturbation', *Patterns*, 3(3), p. 100434. Available at: https://doi.org/10.1016/j.patter.2022.100434.

Ouarné, M., Pena, A. and Franco, C.A. (2021) 'From remodeling to quiescence: The transformation of the vascular network', *Cells & Development*, 168, p. 203735. Available at: https://doi.org/10.1016/j.cdev.2021.203735.

Ozawa, C.R. *et al.* (2004) 'Microenvironmental VEGF concentration, not total dose, determines a threshold between normal and aberrant angiogenesis', *The Journal of Clinical Investigation*, 113(4), pp. 516–527. Available at: https://doi.org/10.1172/JCI18420.

Paik, D.T. *et al.* (2020) 'Single-cell RNA-seq Unveils Unique Transcriptomic Signatures of Organ-Specific Endothelial Cells', *Circulation*, 142(19), pp. 1848–1862. Available at: https://doi.org/10.1161/CIRCULATIONAHA.119.041433.

Palasubramaniam, J., Wang, X. and Peter, K. (2019) 'Myocardial Infarction—From Atherosclerosis to Thrombosis', *Arteriosclerosis, Thrombosis, and Vascular Biology*, 39(8), pp. e176–e185. Available at: https://doi.org/10.1161/ATVBAHA.119.312578.

Pardali, E. *et al.* (2017) 'TGF-?-Induced Endothelial-Mesenchymal Transition in Fibrotic Diseases', *International Journal of Molecular Sciences*, 18(10), p. 2157. Available at: https://doi.org/10.3390/ijms18102157.

Park, P.J. (2009) 'ChIP–seq: advantages and challenges of a maturing technology', *Nature Reviews Genetics*, 10(10), pp. 669–680. Available at: https://doi.org/10.1038/nrg2641.

Parker, B.S. *et al.* (2004) 'Alterations in Vascular Gene Expression in Invasive Breast Carcinoma', *Cancer Research*, 64(21), pp. 7857–7866. Available at: https://doi.org/10.1158/0008-5472.CAN-04-1976.

Patan, S. (2004) 'Vasculogenesis and angiogenesis', *Cancer Treatment and Research*, 117, pp. 3–32. Available at: https://doi.org/10.1007/978-1-4419-8871-3_1.

Payne, S., Neal, A. and De Val, S. (2024) 'Transcription factors regulating vasculogenesis and angiogenesis', *Developmental Dynamics*, 253(1), pp. 28–58. Available at: https://doi.org/10.1002/dvdy.575.

Peinado, H., Olmeda, D. and Cano, A. (2007) 'Snail, Zeb and bHLH factors in tumour progression: an alliance against the epithelial phenotype?', *Nature Reviews Cancer*, 7(6), pp. 415–428. Available at: https://doi.org/10.1038/nrc2131.

Pekowska, A. *et al.* (2011) 'H3K4 tri-methylation provides an epigenetic signature of active enhancers', *The EMBO Journal*, 30(20), pp. 4198–4210. Available at: https://doi.org/10.1038/emboj.2011.295.

Pelechano, V. and Steinmetz, L.M. (2013) 'Gene regulation by antisense transcription', *Nature Reviews Genetics*, 14(12), pp. 880–893. Available at: https://doi.org/10.1038/nrg3594.

Peng, Q. *et al.* (2022) 'The Role of Endothelial-to-Mesenchymal Transition in Cardiovascular Disease', *Cells*, 11(11), p. 1834. Available at: https://doi.org/10.3390/cells11111834.

Peng, Q. *et al.* (2024) 'Novel Role of Endothelial CD45 in Regulating Endothelial-to-Mesenchymal Transition in Atherosclerosis'. bioRxiv, p. 2024.09.03.610974. Available at: https://doi.org/10.1101/2024.09.03.610974.

Perez-Oquendo, M. and Gibbons, D.L. (2022) 'Regulation of ZEB1 Function and Molecular Associations in Tumor Progression and Metastasis', *Cancers*, 14(8), p. 1864. Available at: https://doi.org/10.3390/cancers14081864.

Person, A.D., Klewer, S.E. and Runyan, R.B. (2005) 'Cell Biology of Cardiac Cushion Development', in *International Review of Cytology*. Academic Press, pp. 287–335. Available at: https://doi.org/10.1016/S0074-7696(05)43005-3.

Phng, L.-K. and Gerhardt, H. (2009) 'Angiogenesis: A Team Effort Coordinated by Notch', *Developmental Cell*, 16(2), pp. 196–208. Available at: https://doi.org/10.1016/j.devcel.2009.01.015.

Piera-Velazquez, S. and Jimenez, S.A. (2019) 'Endothelial to Mesenchymal Transition: Role in Physiology and in the Pathogenesis of Human Diseases', *Physiological Reviews*, 99(2), pp. 1281–1324. Available at: https://doi.org/10.1152/physrev.00021.2018.

Pinel, G.D. *et al.* (2022) 'Endothelial Cell RNA-Seq Data: Differential Expression and Functional Enrichment Analyses to Study Phenotypic Switching', in *Angiogenesis*. Humana, New York, NY, pp. 369–426. Available at: https://doi.org/10.1007/978-1-0716-2059-5_29.

Pitulescu, M.E. *et al.* (2017) 'Dll4 and Notch signalling couples sprouting angiogenesis and artery formation', *Nature Cell Biology*, 19(8), pp. 915–927. Available at: https://doi.org/10.1038/ncb3555.

Platel, V. *et al.* (2019) 'Endothelial-to-Mesenchymal Transition (EndoMT): Roles in Tumorigenesis, Metastatic Extravasation and Therapy Resistance', *Journal of Oncology*, 2019(1), p. 8361945. Available at: https://doi.org/10.1155/2019/8361945.

Pober, J.S. and Sessa, W.C. (2007) 'Evolving functions of endothelial cells in inflammation', *Nature Reviews Immunology*, 7(10), pp. 803–815. Available at: https://doi.org/10.1038/nri2171.

Poole, D.C. *et al.* (2013) 'Skeletal muscle capillary function: contemporary observations and novel hypotheses', *Experimental Physiology*, 98(12), pp. 1645–1658. Available at: https://doi.org/10.1113/expphysiol.2013.073874.

Postigo, A.A. *et al.* (2003) 'Regulation of Smad signaling through a differential recruitment of coactivators and corepressors by ZEB proteins', *The EMBO Journal*, 22(10), pp. 2453–2462. Available at: https://doi.org/10.1093/emboj/cdg226.

Potenta, S., Zeisberg, E. and Kalluri, R. (2008) 'The role of endothelial-to-mesenchymal transition in cancer progression', *British Journal of Cancer*, 99(9), pp. 1375–1379. Available at: https://doi.org/10.1038/sj.bjc.6604662.

Potente, M. and Carmeliet, P. (2017) 'The Link Between Angiogenesis and Endothelial Metabolism', *Annual Review of Physiology*, 79(Volume 79, 2017), pp. 43–66. Available at: https://doi.org/10.1146/annurev-physiol-021115-105134.

Potente, M., Gerhardt, H. and Carmeliet, P. (2011) 'Basic and Therapeutic Aspects of Angiogenesis', *Cell*, 146(6), pp. 873–887. Available at: https://doi.org/10.1016/j.cell.2011.08.039.

Potente, M. and Mäkinen, T. (2017) 'Vascular heterogeneity and specialization in development and disease', *Nature Reviews Molecular Cell Biology*, 18(8), pp. 477–494. Available at: https://doi.org/10.1038/nrm.2017.36.

Pradella, D. *et al.* (2021) 'A ligand-insensitive UNC5B splicing isoform regulates angiogenesis by promoting apoptosis', *Nature Communications*, 12(1), p. 4872. Available at: https://doi.org/10.1038/s41467-021-24998-6.

Presta, M. *et al.* (2005) 'Fibroblast growth factor/fibroblast growth factor receptor system in angiogenesis', *Cytokine & Growth Factor Reviews*, 16(2), pp. 159–178. Available at: https://doi.org/10.1016/j.cytogfr.2005.01.004.

Qian, C. *et al.* (2023) 'Targeting vascular normalization: a promising strategy to improve immune–vascular crosstalk in cancer immunotherapy', *Frontiers in Immunology*, 14. Available at: https://doi.org/10.3389/fimmu.2023.1291530.

Qian, C. *et al.* (2025) 'Broadening horizons: molecular mechanisms and disease implications of endothelial-to-mesenchymal transition', *Cell Communication and Signaling*, 23(1), p. 16. Available at: https://doi.org/10.1186/s12964-025-02028-y.

Qiu, L. *et al.* (2023) 'ChIP-seq identifies McSLC35E2 as a novel target gene of McNrf2 in Mytilus coruscus, highlighting its role in the regulation of oxidative stress response in marine

mollusks', *Frontiers in Physiology*, 14, p. 1282900. Available at: https://doi.org/10.3389/fphys.2023.1282900.

Quinlan, A.R. (2014) 'BEDTools: The Swiss-Army Tool for Genome Feature Analysis', *Current Protocols in Bioinformatics*, 47(1). Available at: https://doi.org/10.1002/0471250953.bi1112s47.

Quinlan, A.R. and Hall, I.M. (2010) 'BEDTools: a flexible suite of utilities for comparing genomic features', *Bioinformatics*, 26(6), pp. 841–842. Available at: https://doi.org/10.1093/bioinformatics/btq033.

R Core Team (2024) 'R: A Language and Environment for Statistical Computing', *R Foundation for Statistical Computing* [Preprint], (Vienna, Austria). Available at: https://www.R-project.org/.

Rahman, H.S. *et al.* (2020) 'An Overview of In Vitro, In Vivo, and Computational Techniques for Cancer-Associated Angiogenesis Studies', *BioMed Research International*, 2020(1), p. 8857428. Available at: https://doi.org/10.1155/2020/8857428.

Rai, A. and Cross, J.C. (2014) 'Development of the hemochorial maternal vascular spaces in the placenta through endothelial and vasculogenic mimicry', *Developmental Biology*, 387(2), pp. 131–141. Available at: https://doi.org/10.1016/j.ydbio.2014.01.015.

Ramírez, F. *et al.* (2016) 'deepTools2: a next generation web server for deep-sequencing data analysis', *Nucleic Acids Research*, 44(W1), pp. W160-165. Available at: https://doi.org/10.1093/nar/gkw257.

Ramos, J., Felty, Q. and Roy, D. (2020) 'Integrated Chip-Seq and RNA-Seq Data Analysis Coupled with Bioinformatics Approaches to Investigate Regulatory Landscape of Transcription Modulators in Breast Cancer Cells', in P. Keohavong, K.P. Singh, and W. Gao (eds) *Molecular Toxicology Protocols*. New York, NY: Springer US, pp. 35–59. Available at: https://doi.org/10.1007/978-1-0716-0223-2_3.

Ranchoux, B. *et al.* (2018) 'Endothelial dysfunction in pulmonary arterial hypertension: an evolving landscape (2017 Grover Conference Series)', *Pulmonary Circulation*, 8(1), p. 2045893217752912. Available at: https://doi.org/10.1177/2045893217752912.

Rashbrook, V.S., Brash, J.T. and Ruhrberg, C. (2022) 'Cre toxicity in mouse models of cardiovascular physiology and disease', *Nature cardiovascular research*, 1, pp. 806–816. Available at: https://doi.org/10.1038/s44161-022-00125-6.

Rauff, A. *et al.* (2019) 'Imaging the Dynamic Interaction Between Sprouting Microvessels and the Extracellular Matrix', *Frontiers in Physiology*, 10, p. 1011. Available at: https://doi.org/10.3389/fphys.2019.01011.

Raza, Q. *et al.* (2024) 'Notch signaling regulates UNC5B to suppress endothelial proliferation, migration, junction activity, and retinal plexus branching', *Scientific Reports*, 14(1), p. 13603. Available at: https://doi.org/10.1038/s41598-024-64375-z.

Rebholz-Schuhmann, D., Oellrich, A. and Hoehndorf, R. (2012) 'Text-mining solutions for biomedical research: enabling integrative biology', *Nature Reviews Genetics*, 13(12), pp. 829–839. Available at: https://doi.org/10.1038/nrg3337.

Reid, E. *et al.* (2018) 'Preclinical Evaluation and Optimization of a Cell Therapy Using Human Cord Blood-Derived Endothelial Colony-Forming Cells for Ischemic Retinopathies', *Stem Cells Translational Medicine*, 7(1), pp. 59–67. Available at: https://doi.org/10.1002/sctm.17-0187.

Ren, B. (2018) 'FoxO1 transcriptional activities in VEGF expression and beyond: a key regulator in functional angiogenesis?', *The Journal of Pathology*, 245(3), pp. 255–257. Available at: https://doi.org/10.1002/path.5088.

Ren, J. *et al.* (2023) 'Single-cell sequencing reveals that endothelial cells, EndMT cells and mural cells contribute to the pathogenesis of cavernous malformations', *Experimental & Molecular Medicine*, 55(3), pp. 628–642. Available at: https://doi.org/10.1038/s12276-023-00962-w.

Ren, K. *et al.* (2014) 'KCTD10 Is Involved in the Cardiovascular System and Notch Signaling during Early Embryonic Development', *PLOS ONE*, 9(11), p. e112275. Available at: https://doi.org/10.1371/journal.pone.0112275.

Rennel, E.S. *et al.* (2008) 'The endogenous anti-angiogenic VEGF isoform, VEGF165b inhibits human tumour growth in mice', *British Journal of Cancer*, 98(7), pp. 1250–1257. Available at: https://doi.org/10.1038/sj.bjc.6604309.

Ricard, N. *et al.* (2021) 'The quiescent endothelium: signalling pathways regulating organ-specific endothelial normalcy', *Nature Reviews. Cardiology*, 18(8), pp. 565–580. Available at: https://doi.org/10.1038/s41569-021-00517-4.

Risau, W. (1997) 'Mechanisms of angiogenesis', *Nature*, 386(6626), pp. 671–674. Available at: https://doi.org/10.1038/386671a0.

Risau, W. and Flamme, I. (1995) 'Vasculogenesis', *Annual Review of Cell and Developmental Biology*, 11(Volume 11, 1995), pp. 73–91. Available at: https://doi.org/10.1146/annurev.cb.11.110195.000445.

Robertson, G. *et al.* (2007) 'Genome-wide profiles of STAT1 DNA association using chromatin immunoprecipitation and massively parallel sequencing', *Nature Methods*, 4(8), pp. 651–657. Available at: https://doi.org/10.1038/nmeth1068.

Rodrigues, S.F. and Granger, D.N. (2015) 'Blood cells and endothelial barrier function', *Tissue Barriers*, 3(1–2), p. e978720. Available at: https://doi.org/10.4161/21688370.2014.978720.

Rohlenova, K. *et al.* (2020) 'Single-Cell RNA Sequencing Maps Endothelial Metabolic Plasticity in Pathological Angiogenesis', *Cell Metabolism*, 31(4), pp. 862-877.e14. Available at: https://doi.org/10.1016/j.cmet.2020.03.009.

Rosmaninho, P. *et al.* (2018) 'Zeb1 potentiates genome-wide gene transcription with Lef1 to promote glioblastoma cell invasion', *The EMBO Journal*, 37(15), p. e97115. Available at: https://doi.org/10.15252/embj.201797115.

Ross, M. *et al.* (2023) 'Exercise-induced skeletal muscle angiogenesis: impact of age, sex, angiocrines and cellular mediators', *European Journal of Applied Physiology*, 123(7), pp. 1415–1432. Available at: https://doi.org/10.1007/s00421-022-05128-6.

Ruan, Y. *et al.* (2021) 'REXO4 acts as a biomarker and promotes hepatocellular carcinoma progression', *Journal of Gastrointestinal Oncology*, 12(6), pp. 3093–3106. Available at: https://doi.org/10.21037/jgo-21-819.

Ruhrberg, C. *et al.* (2002) 'Spatially restricted patterning cues provided by heparin-binding VEGF-A control blood vessel branching morphogenesis', *Genes & Development*, 16(20), pp. 2684–2698. Available at: https://doi.org/10.1101/gad.242002.

Rust, R. *et al.* (2019) 'A Revised View on Growth and Remodeling in the Retinal Vasculature', *Scientific Reports*, 9(1), p. 3263. Available at: https://doi.org/10.1038/s41598-019-40135-2.

Rust, R. (2020) 'Insights into the dual role of angiogenesis following stroke', *Journal of Cerebral Blood Flow & Metabolism*, 40(6), pp. 1167–1171. Available at: https://doi.org/10.1177/0271678X20906815.

Rutkowski, J.M., Davis, K.E. and Scherer, P.E. (2009) 'Mechanisms of Obesity and Related Pathologies: The Macro- and Microcirculation of Adipose Tissue', *The FEBS journal*, 276(20), pp. 5738–5746. Available at: https://doi.org/10.1111/j.1742-4658.2009.07303.x.

Saint-Geniez, M. and D'Amore, P.A. (2004) 'Development and pathology of the hyaloid, choroidal and retinal vasculature', *The International Journal of Developmental Biology*, 48(8–9), pp. 1045–1058. Available at: https://doi.org/10.1387/ijdb.041895ms.

Salaudeen, M.A. *et al.* (2024) 'Understanding the Pathophysiology of Ischemic Stroke: The Basis of Current Therapies and Opportunity for New Ones', *Biomolecules*, 14(3), p. 305. Available at: https://doi.org/10.3390/biom14030305.

Sánchez-Duffhues, G., García de Vinuesa, A. and ten Dijke, P. (2018) 'Endothelial-to-mesenchymal transition in cardiovascular diseases: Developmental signaling pathways gone awry', *Developmental Dynamics*, 247(3), pp. 492–508. Available at: https://doi.org/10.1002/dvdy.24589.

Sandoo, A. *et al.* (2010) 'The Endothelium and Its Role in Regulating Vascular Tone', *The Open Cardiovascular Medicine Journal*, 4, pp. 302–312. Available at: https://doi.org/10.2174/1874192401004010302.

Sangwung, P. *et al.* (2017) 'KLF2 and KLF4 control endothelial identity and vascular integrity', *JCI Insight*, 2(4), p. e91700. Available at: https://doi.org/10.1172/jci.insight.91700.

Šarić, J. *et al.* (2006) 'Extraction of regulatory gene/protein networks from Medline', *Bioinformatics*, 22(6), pp. 645–650. Available at: https://doi.org/10.1093/bioinformatics/bti597.

Sauer, B. and Henderson, N. (1988) 'Site-specific DNA recombination in mammalian cells by the Cre recombinase of bacteriophage P1', *Proceedings of the National Academy of Sciences*

of the United States of America, 85(14), pp. 5166–5170. Available at: https://doi.org/10.1073/pnas.85.14.5166.

Sayers, E. (2022) 'A General Introduction to the E-utilities', in *Entrez Programming Utilities Help [Internet]*. National Center for Biotechnology Information (US). Available at: https://www.ncbi.nlm.nih.gov/books/NBK25497/ (Accessed: 30 April 2024).

Schindelin, J. *et al.* (2012) 'Fiji: an open-source platform for biological-image analysis', *Nature Methods*, 9(7), pp. 676–682. Available at: https://doi.org/10.1038/nmeth.2019.

Schmidt, A., Brixius, K. and Bloch, W. (2007) 'Endothelial Precursor Cell Migration During Vasculogenesis', *Circulation Research*, 101(2), pp. 125–136. Available at: https://doi.org/10.1161/CIRCRESAHA.107.148932.

Schoors, S. *et al.* (2014) 'Partial and Transient Reduction of Glycolysis by PFKFB3 Blockade Reduces Pathological Angiogenesis', *Cell Metabolism*, 19(1), pp. 37–48. Available at: https://doi.org/10.1016/j.cmet.2013.11.008.

Schoors, S. *et al.* (2015) 'Fatty acid carbon is essential for dNTP synthesis in endothelial cells', *Nature*, 520(7546), pp. 192–197. Available at: https://doi.org/10.1038/nature14362.

Schwab, A. *et al.* (2024) 'Zeb1 mediates EMT/plasticity-associated ferroptosis sensitivity in cancer cells by regulating lipogenic enzyme expression and phospholipid composition', *Nature Cell Biology*, 26(9), pp. 1470–1481. Available at: https://doi.org/10.1038/s41556-024-01464-1.

Selvam, S., Kumar, T. and Fruttiger, M. (2018) 'Retinal vasculature development in health and disease', *Progress in Retinal and Eye Research*, 63, pp. 1–19. Available at: https://doi.org/10.1016/j.preteyeres.2017.11.001.

Semenza, G.L. (2003) 'Targeting HIF-1 for cancer therapy', *Nature Reviews Cancer*, 3(10), pp. 721–732. Available at: https://doi.org/10.1038/nrc1187.

Seo, S.H. *et al.* (2022) 'Hypoxia-induced ELF3 promotes tumor angiogenesis through IGF1/IGF1R', *EMBO reports*, 23(8), p. e52977. Available at: https://doi.org/10.15252/embr.202152977.

Shah, A.V., Birdsey, G.M. and Randi, A.M. (2016) 'Regulation of endothelial homeostasis, vascular development and angiogenesis by the transcription factor ERG', *Vascular Pharmacology*, 86, pp. 3–13. Available at: https://doi.org/10.1016/j.vph.2016.05.003.

Shannon, P. *et al.* (2003) 'Cytoscape: A Software Environment for Integrated Models of Biomolecular Interaction Networks', *Genome Research*, 13(11), pp. 2498–2504. Available at: https://doi.org/10.1101/gr.1239303.

Shi, Z. *et al.* (2023) 'Research progress on the mechanism of angiogenesis in wound repair and regeneration', *Frontiers in Physiology*, 14, p. 1284981. Available at: https://doi.org/10.3389/fphys.2023.1284981.

Shu, D.Y., Butcher, E. and Saint-Geniez, M. (2020) 'EMT and EndMT: Emerging Roles in Age-Related Macular Degeneration', *International Journal of Molecular Sciences*, 21(12), p. 4271. Available at: https://doi.org/10.3390/ijms21124271.

Siemann, D.W. (2011) 'The Unique Characteristics of Tumor Vasculature and Preclinical Evidence for its Selective Disruption by Tumor-Vascular Disrupting Agents', *Cancer treatment reviews*, 37(1), pp. 63–74. Available at: https://doi.org/10.1016/j.ctrv.2010.05.001.

Siemerink, M.J. *et al.* (2013) 'Endothelial Tip Cells in Ocular Angiogenesis', *Journal of Histochemistry and Cytochemistry*, 61(2), pp. 101–115. Available at: https://doi.org/10.1369/0022155412467635.

Silvestre, J.-S., Smadja, D.M. and Lévy, B.I. (2013) 'Postischemic Revascularization: From Cellular and Molecular Mechanisms to Clinical Applications', *Physiological Reviews*, 93(4), pp. 1743–1802. Available at: https://doi.org/10.1152/physrev.00006.2013.

Simantov, R. and Silverstein, R.L. (2003) 'CD36: a critical anti-angiogenic receptor', *Frontiers in Bioscience: A Journal and Virtual Library*, 8, pp. s874-882. Available at: https://doi.org/10.2741/1168.

Simillion, C. *et al.* (2017) 'Avoiding the pitfalls of gene set enrichment analysis with SetRank', *BMC Bioinformatics*, 18(1), p. 151. Available at: https://doi.org/10.1186/s12859-017-1571-6.

Singh, B. *et al.* (2024) 'Elucidating the crosstalk between endothelial-to-mesenchymal transition (EndoMT) and endothelial autophagy in the pathogenesis of atherosclerosis', *Vascular Pharmacology*, 155, p. 107368. Available at: https://doi.org/10.1016/j.vph.2024.107368.

Skene, P.J. and Henikoff, S. (2017) 'An efficient targeted nuclease strategy for high-resolution mapping of DNA binding sites', *eLife*. Edited by D. Reinberg, 6, p. e21856. Available at: https://doi.org/10.7554/eLife.21856.

Slenders, L. *et al.* (2023) 'Identification of endothelial-to-mesenchymal transition gene signatures in single-cell transcriptomics of human atherosclerotic tissue'. bioRxiv, p. 2023.07.18.549599. Available at: https://doi.org/10.1101/2023.07.18.549599.

Sokol, L. *et al.* (2023) 'Prioritization and functional validation of target genes from single-cell transcriptomics studies', *Communications Biology*, 6(1), pp. 1–13. Available at: https://doi.org/10.1038/s42003-023-05006-7.

Sörensen, I., Adams, R.H. and Gossler, A. (2009) 'DLL1-mediated Notch activation regulates endothelial identity in mouse fetal arteries', *Blood*, 113(22), pp. 5680–5688. Available at: https://doi.org/10.1182/blood-2008-08-174508.

Souilhol, C. *et al.* (2018) 'Endothelial–mesenchymal transition in atherosclerosis', *Cardiovascular Research*, 114(4), pp. 565–577. Available at: https://doi.org/10.1093/cvr/cvx253.

Spaderna, S. *et al.* (2008) 'The transcriptional repressor ZEB1 promotes metastasis and loss of cell polarity in cancer', *Cancer Research*, 68(2), pp. 537–544. Available at: https://doi.org/10.1158/0008-5472.CAN-07-5682.

Sripathy, S., Lee, M. and Vasioukhin, V. (2011) 'Mammalian Llgl2 Is Necessary for Proper Branching Morphogenesis during Placental Development ▿ ', *Molecular and Cellular Biology*, 31(14), pp. 2920–2933. Available at: https://doi.org/10.1128/MCB.05431-11.

Steucke, K.E. *et al.* (2015) 'Vascular smooth muscle cell functional contractility depends on extracellular mechanical properties', *Journal of biomechanics*, 48(12), pp. 3044–3051. Available at: https://doi.org/10.1016/j.jbiomech.2015.07.029.

Strasser, G.A., Kaminker, J.S. and Tessier-Lavigne, M. (2010) 'Microarray analysis of retinal endothelial tip cells identifies CXCR4 as a mediator of tip cell morphology and branching', *Blood*, 115(24), pp. 5102–5110. Available at: https://doi.org/10.1182/blood-2009-07-230284.

Stratman, A.N. *et al.* (2017) 'Interactions between mural cells and endothelial cells stabilize the developing zebrafish dorsal aorta', *Development (Cambridge, England)*, 144(1), pp. 115–127. Available at: https://doi.org/10.1242/dev.143131.

Su, N. *et al.* (2024) 'Identification and clinical validation of the role of anoikis-related genes in diabetic foot', *International Wound Journal*, 21(3), p. e14771. Available at: https://doi.org/10.1111/iwj.14771.

Su, W. *et al.* (2017) 'Long noncoding RNA ZEB1-AS1 epigenetically regulates the expressions of ZEB1 and downstream molecules in prostate cancer', *Molecular Cancer*, 16(1), p. 142. Available at: https://doi.org/10.1186/s12943-017-0711-y.

Subbalakshmi, A.R. *et al.* (2023) 'The ELF3 transcription factor is associated with an epithelial phenotype and represses epithelial-mesenchymal transition', *Journal of Biological Engineering*, 17(1), p. 17. Available at: https://doi.org/10.1186/s13036-023-00333-z.

Subramani, S. *et al.* (2015) 'HPIminer: A text mining system for building and visualizing human protein interaction networks and pathways', *Journal of Biomedical Informatics*, 54, pp. 121–131. Available at: https://doi.org/10.1016/j.jbi.2015.01.006.

Suh, J.W. *et al.* (2023) 'Promoting angiogenesis and diabetic wound healing through delivery of protein transduction domain-BMP2 formulated nanoparticles with hydrogel', *Journal of Tissue Engineering*, 14, p. 20417314231190641. Available at: https://doi.org/10.1177/20417314231190641.

Sun, J.-X. *et al.* (2021) 'Notch activation promotes endothelial quiescence by repressing MYC expression via miR-218', *Molecular Therapy Nucleic Acids*, 25, pp. 554–566. Available at: https://doi.org/10.1016/j.omtn.2021.07.023.

Sung, H.-K. *et al.* (2013) 'Adipose Vascular Endothelial Growth Factor Regulates Metabolic Homeostasis through Angiogenesis', *Cell Metabolism*, 17(1), pp. 61–72. Available at: https://doi.org/10.1016/j.cmet.2012.12.010.

Sweet, D.R. *et al.* (2023) 'Krüppel-Like Factors Orchestrate Endothelial Gene Expression Through Redundant and Non-Redundant Enhancer Networks', *Journal of the American Heart Association: Cardiovascular and Cerebrovascular Disease*, 12(4), p. e024303. Available at: https://doi.org/10.1161/JAHA.121.024303.

Swift, M.R. and Weinstein, B.M. (2009) 'Arterial-venous specification during development', *Circulation Research*, 104(5), pp. 576–588. Available at: https://doi.org/10.1161/CIRCRESAHA.108.188805.

Tahergorabi, Z. and Khazaei, M. (2012) 'A Review on Angiogenesis and Its Assays', *Iranian Journal of Basic Medical Sciences*, 15(6), pp. 1110–1126.

Takeda, A. *et al.* (2019) 'Single-Cell Survey of Human Lymphatics Unveils Marked Endothelial Cell Heterogeneity and Mechanisms of Homing for Neutrophils', *Immunity*, 51(3), pp. 561-572.e5. Available at: https://doi.org/10.1016/j.immuni.2019.06.027.

Tan, C.M.J. *et al.* (2021) 'Proteomic Signature of Dysfunctional Circulating Endothelial Colony-Forming Cells of Young Adults', *Journal of the American Heart Association*, 10(15), p. e021119. Available at: https://doi.org/10.1161/JAHA.121.021119.

Tarasov, A. *et al.* (2015) 'Sambamba: fast processing of NGS alignment formats', *Bioinformatics (Oxford, England)*, 31(12), pp. 2032–2034. Available at: https://doi.org/10.1093/bioinformatics/btv098.

Tarbell, J.M. and Cancel, L.M. (2016) 'The glycocalyx and its significance in human medicine', *Journal of Internal Medicine*, 280(1), pp. 97–113. Available at: https://doi.org/10.1111/joim.12465.

The Gene Ontology Consortium *et al.* (2023) 'The Gene Ontology knowledgebase in 2023', *Genetics*, 224(1), p. iyad031. Available at: https://doi.org/10.1093/genetics/iyad031.

Thiery, J.P. and Sleeman, J.P. (2006) 'Complex networks orchestrate epithelial–mesenchymal transitions', *Nature Reviews Molecular Cell Biology*, 7(2), pp. 131–142. Available at: https://doi.org/10.1038/nrm1835.

Thomsen, M.S., Routhe, L.J. and Moos, T. (2017) 'The vascular basement membrane in the healthy and pathological brain', *Journal of Cerebral Blood Flow & Metabolism*, 37(10), pp. 3300–3317. Available at: https://doi.org/10.1177/0271678X17722436.

Timmermans, F. *et al.* (2009) 'Endothelial progenitor cells: identity defined?', *Journal of Cellular and Molecular Medicine*, 13(1), pp. 87–102. Available at: https://doi.org/10.1111/j.1582-4934.2008.00598.x.

Timmons, J.A., Szkop, K.J. and Gallagher, I.J. (2015) 'Multiple sources of bias confound functional enrichment analysis of global -omics data', *Genome Biology*, 16(1), p. 186. Available at: https://doi.org/10.1186/s13059-015-0761-7.

Tombor, L.S. *et al.* (2021) 'Single cell sequencing reveals endothelial plasticity with transient mesenchymal activation after myocardial infarction', *Nature Communications*, 12(1), p. 681. Available at: https://doi.org/10.1038/s41467-021-20905-1.

Tonnesen, M.G., Feng, X. and Clark, R.A.F. (2000) 'Angiogenesis in Wound Healing', *Journal of Investigative Dermatology Symposium Proceedings*, 5(1), pp. 40–46. Available at: https://doi.org/10.1046/j.1087-0024.2000.00014.x.

del Toro, R. *et al.* (2010) 'Identification and functional analysis of endothelial tip cell–enriched genes', *Blood*, 116(19), pp. 4025–4033. Available at: https://doi.org/10.1182/blood-2010-02-270819.

Trimm, E. and Red-Horse, K. (2023) 'Vascular endothelial cell development and diversity', *Nature Reviews Cardiology*, 20(3), pp. 197–210. Available at: https://doi.org/10.1038/s41569-022-00770-1.

Tung, J.J., Tattersall, I.W. and Kitajewski, J. (2012) 'Tips, Stalks, Tubes: Notch-Mediated Cell Fate Determination and Mechanisms of Tubulogenesis during Angiogenesis', *Cold Spring Harbor Perspectives in Medicine*, 2(2), p. a006601. Available at: https://doi.org/10.1101/cshperspect.a006601.

Ueda, C. *et al.* (2025) 'Endothelial activating transcription factor 3 promotes angiogenesis and vascular repair in the mouse retina', *iScience*, 28(1). Available at: https://doi.org/10.1016/j.isci.2024.111516.

Unoki, N. *et al.* (2010) 'SDF-1/CXCR4 Contributes to the Activation of Tip Cells and Microglia in Retinal Angiogenesis', *Investigative Ophthalmology & Visual Science*, 51(7), pp. 3362–3371. Available at: https://doi.org/10.1167/iovs.09-4978.

Urbich, C. and Dimmeler, S. (2004) 'Endothelial Progenitor Cells', *Circulation Research*, 95(4), pp. 343–353. Available at: https://doi.org/10.1161/01.RES.0000137877.89448.78.

Vandewalle, C., Van Roy, F. and Berx, G. (2009) 'The role of the ZEB family of transcription factors in development and disease', *Cellular and Molecular Life Sciences*, 66(5), pp. 773–787. Available at: https://doi.org/10.1007/s00018-008-8465-8.

Vannier, C. *et al.* (2013) 'Zeb1 Regulates E-cadherin and Epcam (Epithelial Cell Adhesion Molecule) Expression to Control Cell Behavior in Early Zebrafish Development', *The Journal of Biological Chemistry*, 288(26), pp. 18643–18659. Available at: https://doi.org/10.1074/jbc.M113.467787.

Wälchli, T. *et al.* (2024) 'Single-cell atlas of the human brain vasculature across development, adulthood and disease', *Nature*, 632(8025), pp. 603–613. Available at: https://doi.org/10.1038/s41586-024-07493-y.

Wallez, Y. and Huber, P. (2008) 'Endothelial adherens and tight junctions in vascular homeostasis, inflammation and angiogenesis', *Biochimica et Biophysica Acta (BBA) - Biomembranes*, 1778(3), pp. 794–809. Available at: https://doi.org/10.1016/j.bbamem.2007.09.003.

Wang, X. *et al.* (2016) 'Bach1 Induces Endothelial Cell Apoptosis and Cell-Cycle Arrest through ROS Generation', *Oxidative Medicine and Cellular Longevity*, 2016, p. 6234043. Available at: https://doi.org/10.1155/2016/6234043.

Wang, Y. *et al.* (2015) 'KLF4 Promotes Angiogenesis by Activating VEGF Signaling in Human Retinal Microvascular Endothelial Cells', *PLoS ONE*, 10(6), p. e0130341. Available at: https://doi.org/10.1371/journal.pone.0130341.

Wässle, H. (2004) 'Parallel processing in the mammalian retina', *Nature Reviews. Neuroscience*, 5(10), pp. 747–757. Available at: https://doi.org/10.1038/nrn1497.

Watson, E.C., Grant, Z.L. and Coultas, L. (2017) 'Endothelial cell apoptosis in angiogenesis and vessel regression', *Cellular and Molecular Life Sciences: CMLS*, 74(24), pp. 4387–4403. Available at: https://doi.org/10.1007/s00018-017-2577-y.

Wautier, J.-L. and Wautier, M.-P. (2022) 'Vascular Permeability in Diseases', *International Journal of Molecular Sciences*, 23(7), p. 3645. Available at: https://doi.org/10.3390/ijms23073645.

Weinstein, N., Mendoza, L. and Álvarez-Buylla, E.R. (2020) 'A Computational Model of the Endothelial to Mesenchymal Transition', *Frontiers in Genetics*, 11, p. 40. Available at: https://doi.org/10.3389/fgene.2020.00040.

Weitzman, M., Bayley, E.B. and Naik, U.P. (2008) 'Robo4', *Cell Adhesion & Migration*, 2(4), pp. 220–222.

Welch-Reardon, K.M. *et al.* (2014) 'Angiogenic sprouting is regulated by endothelial cell expression of Slug', *Journal of Cell Science*, 127(Pt 9), pp. 2017–2028. Available at: https://doi.org/10.1242/jcs.143420.

Welch-Reardon, K.M., Wu, N. and Hughes, C.C.W. (2015) 'A role for partial endothelial-mesenchymal transitions in angiogenesis?', *Arteriosclerosis, thrombosis, and vascular biology*, 35(2), pp. 303–308. Available at: https://doi.org/10.1161/ATVBAHA.114.303220.

Wellner, U. *et al.* (2009) 'The EMT-activator ZEB1 promotes tumorigenicity by repressing stemness-inhibiting microRNAs', *Nature Cell Biology*, 11(12), pp. 1487–1495. Available at: https://doi.org/10.1038/ncb1998.

Whyte, W.A. *et al.* (2013) 'Master Transcription Factors and Mediator Establish Super-Enhancers at Key Cell Identity Genes', *Cell*, 153(2), pp. 307–319. Available at: https://doi.org/10.1016/j.cell.2013.03.035.

Wickham, H. (2009) *ggplot2: Elegant Graphics for Data Analysis*. New York, NY: Springer. Available at: https://doi.org/10.1007/978-0-387-98141-3.

Wiktorska, M., Sacewicz-Hofman, I. and Niewiarowska, J. (2023) 'The endothelial-to-mesenchymal transition changes the focal adhesion site proteins levels and the SLRP-lumican level in HMEC-1 cell line', *Experimental Cell Research*, 430(1), p. 113692. Available at: https://doi.org/10.1016/j.yexcr.2023.113692.

Wilhelm, K. *et al.* (2016) 'FOXO1 couples metabolic activity and growth state in the vascular endothelium', *Nature*, 529(7585), pp. 216–220. Available at: https://doi.org/10.1038/nature16498.

Williamson, K., Stringer, S. and Alexander, Y. (2012) 'Endothelial Progenitor Cells Enter the Aging Arena', *Frontiers in Physiology*, 3. Available at: https://doi.org/10.3389/fphys.2012.00030.

Wolff, T. *et al.* (2012) 'FACS-purified myoblasts producing controlled VEGF levels induce safe and stable angiogenesis in chronic hind limb ischemia', *Journal of Cellular and Molecular Medicine*, 16(1), pp. 107–117. Available at: https://doi.org/10.1111/j.1582-4934.2011.01308.x.

Woolard, J. *et al.* (2004) 'VEGF165b, an inhibitory vascular endothelial growth factor splice variant: mechanism of action, in vivo effect on angiogenesis and endogenous protein expression', *Cancer Research*, 64(21), pp. 7822–7835. Available at: https://doi.org/10.1158/0008-5472.CAN-04-0934.

Wu, H.-T. *et al.* (2020) 'Oncogenic functions of the EMT-related transcription factor ZEB1 in breast cancer', *Journal of Translational Medicine*, 18(1), p. 51. Available at: https://doi.org/10.1186/s12967-020-02240-z.

Xiao, F. *et al.* (2022) 'ZNF395 facilitates macrophage polarization and impacts the prognosis of glioma', *American Journal of Cancer Research*, 12(9), pp. 4312–4325.

Xiao, P. *et al.* (2023) 'Impaired angiogenesis in ageing: the central role of the extracellular matrix', *Journal of Translational Medicine*, 21(1), p. 457. Available at: https://doi.org/10.1186/s12967-023-04315-z.

Xiong, J. *et al.* (2018) 'A Metabolic Basis for Endothelial-to-Mesenchymal Transition', *Molecular Cell*, 69(4), pp. 689-698.e7. Available at: https://doi.org/10.1016/j.molcel.2018.01.010.

Xu, J. *et al.* (2017) 'Vascular CXCR4 Expression Promotes Vessel Sprouting and Sensitivity to Sorafenib Treatment in Hepatocellular Carcinoma', *Clinical Cancer Research: An Official Journal of the American Association for Cancer Research*, 23(15), pp. 4482–4492. Available at: https://doi.org/10.1158/1078-0432.CCR-16-2131.

Xu, Q. *et al.* (2021) 'Knockdown of growth factor receptor bound protein 7 suppresses angiogenesis by inhibiting the secretion of vascular endothelial growth factor A in ovarian cancer cells', *Bioengineered*, 12(2), pp. 12179–12190. Available at: https://doi.org/10.1080/21655979.2021.2005225.

Xue, L. *et al.* (2025) 'Key mechanisms of angiogenesis in the infarct core: association of macrophage infiltration with venogenesis', *Molecular Brain*, 18, p. 12. Available at: https://doi.org/10.1186/s13041-025-01182-1.

Yamashiro, Y. *et al.* (2023) 'Partial endothelial-to-mesenchymal transition mediated by HIF-induced CD45 in neointima formation upon carotid artery ligation', *Cardiovascular Research*, 119(7), pp. 1606–1618. Available at: https://doi.org/10.1093/cvr/cvac190.

Yancopoulos, G.D. *et al.* (2000) 'Vascular-specific growth factors and blood vessel formation', *Nature*, 407(6801), pp. 242–248. Available at: https://doi.org/10.1038/35025215.

Yang, J.-X. *et al.* (2018) 'Endothelial progenitor cells in age-related vascular remodeling', *Cell Transplantation*, 27(5), pp. 786–795. Available at: https://doi.org/10.1177/0963689718779345.

Yau, J.W., Teoh, H. and Verma, S. (2015) 'Endothelial cell control of thrombosis', *BMC Cardiovascular Disorders*, 15(1), p. 130. Available at: https://doi.org/10.1186/s12872-015-0124-z.

Yoshimatsu, Y. and Watabe, T. (2022) 'Emerging roles of inflammation-mediated endothelial–mesenchymal transition in health and disease', *Inflammation and Regeneration*, 42(1), p. 9. Available at: https://doi.org/10.1186/s41232-021-00186-3.

Yoshitomi, Y. *et al.* (2021) 'Emerging Role of AP-1 Transcription Factor JunB in Angiogenesis and Vascular Development', *International Journal of Molecular Sciences*, 22(6), p. 2804. Available at: https://doi.org/10.3390/ijms22062804.

You, N. *et al.* (2025) 'Reconceptualizing Endothelial-to-mesenchymal transition in atherosclerosis: Signaling pathways and prospective targeting strategies', *Journal of Advanced Research* [Preprint]. Available at: https://doi.org/10.1016/j.jare.2024.12.049.

Yu, G. *et al.* (2012) 'clusterProfiler: an R Package for Comparing Biological Themes Among Gene Clusters', *OMICS: A Journal of Integrative Biology*, 16(5), pp. 284–287. Available at: https://doi.org/10.1089/omi.2011.0118.

Yu, G., Wang, L.-G. and He, Q.-Y. (2015) 'ChIPseeker: an R/Bioconductor package for ChIP peak annotation, comparison and visualization', *Bioinformatics*, 31(14), pp. 2382–2383. Available at: https://doi.org/10.1093/bioinformatics/btv145.

Yu, Q.C. *et al.* (2022) 'Activation of Wnt/β-catenin signaling by Zeb1 in endothelial progenitors induces vascular quiescence entry', *Cell Reports*, 41(8), p. 111694. Available at: https://doi.org/10.1016/j.celrep.2022.111694.

Yurchenco, P.D. (2011) 'Basement Membranes: Cell Scaffoldings and Signaling Platforms', *Cold Spring Harbor Perspectives in Biology*, 3(2), p. a004911. Available at: https://doi.org/10.1101/cshperspect.a004911.

Yusoff, F.M. *et al.* (2021) 'Bach1 plays an important role in angiogenesis through regulation of oxidative stress', *Microvascular Research*, 134, p. 104126. Available at: https://doi.org/10.1016/j.mvr.2020.104126.

Zarkada, G. *et al.* (2021) 'Specialized endothelial tip cells guide neuroretina vascularization and blood-retina-barrier formation', *Developmental Cell*, 56(15), pp. 2237-2251.e6. Available at: https://doi.org/10.1016/j.devcel.2021.06.021.

Zeng, K. *et al.* (2023) 'USP22 upregulates ZEB1-mediated VEGFA transcription in hepatocellular carcinoma', *Cell Death & Disease*, 14(3), pp. 1–15. Available at: https://doi.org/10.1038/s41419-023-05699-y.

Zhang, L. *et al.* (2022) 'Single cell meta-analysis of EndMT and EMT state in COVID-19', *Frontiers in Immunology*, 13, p. 976512. Available at: https://doi.org/10.3389/fimmu.2022.976512.

Zhang, M. *et al.* (2019) 'The BD2 domain of BRD4 is a determinant in EndoMT and vein graft neointima formation', *Cellular Signalling*, 61, pp. 20–29. Available at: https://doi.org/10.1016/j.cellsig.2019.05.005.

Zhang, P., Sun, Y. and Ma, L. (2015) 'ZEB1: at the crossroads of epithelial-mesenchymal transition, metastasis and therapy resistance', *Cell Cycle (Georgetown, Tex.)*, 14(4), pp. 481–487. Available at: https://doi.org/10.1080/15384101.2015.1006048.

Zhang, Q., Cannavicci, A. and Kutryk, M.J.B. (2022) 'Exploring Endothelial Colony-Forming Cells to Better Understand the Pathophysiology of Disease: An Updated Review', *Stem Cells International*, 2022, p. 4460041. Available at: https://doi.org/10.1155/2022/4460041.

Zhang, X. *et al.* (2015) 'RNA-Seq and ChIP-Seq Reveal SQSTM1/p62 as a Key Mediator of JunB Suppression of NF-κB-Dependent Inflammation', *Journal of Investigative Dermatology*, 135(4), pp. 1016–1024. Available at: https://doi.org/10.1038/jid.2014.519.

Zhang, X. *et al.* (2018) 'ZEB1 confers chemotherapeutic resistance to breast cancer by activating ATM', *Cell Death & Disease*, 9(2), pp. 1–15. Available at: https://doi.org/10.1038/s41419-017-0087-3.

Zhang, Y. *et al.* (2008) 'Model-based Analysis of ChIP-Seq (MACS)', *Genome Biology*, 9(9), p. R137. Available at: https://doi.org/10.1186/gb-2008-9-9-r137.

Zhang, Y. *et al.* (2019) 'The roles of ZEB1 in tumorigenic progression and epigenetic modifications', *Biomedicine & Pharmacotherapy*, 110, pp. 400–408. Available at: https://doi.org/10.1016/j.biopha.2018.11.112.

Zhang, Y.E. (2009) 'Non-Smad pathways in TGF-β signaling', *Cell Research*, 19(1), pp. 128–139. Available at: https://doi.org/10.1038/cr.2008.328.

Zhang, Z. *et al.* (2025) 'Endothelial-to-mesenchymal transition in cardiovascular diseases', *Trends in Molecular Medicine* [Preprint]. Available at: https://doi.org/10.1016/j.molmed.2025.05.002.

Zhao, G. *et al.* (2021) 'Single-Cell Transcriptomics Reveals Endothelial Plasticity During Diabetic Atherogenesis', *Frontiers in Cell and Developmental Biology*, 9, p. 689469. Available at: https://doi.org/10.3389/fcell.2021.689469.

Zhao, P. *et al.* (2021) 'Single-cell RNA-seq reveals a critical role of novel pro-inflammatory EndMT in mediating adverse remodeling in coronary artery–on–a–chip', *Science Advances*, 7(34), p. eabg1694. Available at: https://doi.org/10.1126/sciadv.abg1694.

Zhong, J. *et al.* (2025) 'Dissecting endothelial cell heterogeneity with new tools', *Cell Regeneration*, 14, p. 10. Available at: https://doi.org/10.1186/s13619-025-00223-3.

Zhong, T.P. *et al.* (2001) 'Gridlock signalling pathway fashions the first embryonic artery', *Nature*, 414(6860), pp. 216–220. Available at: https://doi.org/10.1038/35102599.

Zhu, F. *et al.* (2015) 'Protein interaction network constructing based on text mining and reinforcement learning with application to prostate cancer', *IET Systems Biology*, 9(4), pp. 106–112. Available at: https://doi.org/10.1049/iet-syb.2014.0050.

Zhu, L.J. *et al.* (2010) 'ChIPpeakAnno: a Bioconductor package to annotate ChIP-seq and ChIP-chip data', *BMC Bioinformatics*, 11(1), p. 237. Available at: https://doi.org/10.1186/1471-2105-11-237.